1990

The Synthesis, Characterization, and Reactivities of Metal Tetratertiaryphosphine Complexes.

Scott Anthony Laneman
Louisiana State University and Agricultural & Mechanical College

INFORMATION TO USERS

The most advanced technology has been used to photograph and reproduce this manuscript from the microfilm master. UMI films the text directly from the original or copy submitted. Thus, some thesis and dissertation copies are in typewriter face, while others may be from any type of computer printer.

The quality of this reproduction is dependent upon the quality of the copy submitted. Broken or indistinct print, colored or poor quality illustrations and photographs, print bleedthrough, substandard margins, and improper alignment can adversely affect reproduction.

In the unlikely event that the author did not send UMI a complete manuscript and there are missing pages, these will be noted. Also, if unauthorized copyright material had to be removed, a note will indicate the deletion.

Oversize materials (e.g., maps, drawings, charts) are reproduced by sectioning the original, beginning at the upper left-hand corner and continuing from left to right in equal sections with small overlaps. Each original is also photographed in one exposure and is included in reduced form at the back of the book.

Photographs included in the original manuscript have been reproduced xerographically in this copy. Higher quality 6" x 9" black and white photographic prints are available for any photographs or illustrations appearing in this copy for an additional charge. Contact UMI directly to order.

U·M·I

University Microfilms International
A Bell & Howell Information Company
300 North Zeeb Road. Ann Arbor, MI 48106-1346 USA
313/761-4700 800/521-0600

Order Number 9112244

The synthesis, characterization, and reactivities of metal tetratertiaryphosphine complexes

Laneman, Scott Anthony, Ph.D.

The Louisiana State University and Agricultural and Mechanical Col., 1990

U·M·I
300 N. Zeeb Rd.
Ann Arbor, MI 48106

THE SYNTHESIS, CHARACTERIZATION, AND REACTIVITIES OF METAL TETRATERTIARYPHOSPHINE COMPLEXES.

A Dissertation

Submitted to the Graduate Faculty of the
Louisiana State University and
Agricultural and Mechanical College
in partial fulfillment of the
requirement for the degree of
Doctor of Philosophy

in

the Department of Chemistry

by
Scott Anthony Laneman
B.S., Southeast Missouri State University, 1985
August, 1990

Acknowledgements

The author would like to thank the many people contributing to his experience and education which have culminated in this thesis especially: Dr. George Stanley, whose patience and guidance made this collection of work seem like a collaboration instead of a graduate research project; Dr. Mark McLaughlin and his chemical background which made the "chalk-talks" enjoyable and educational; Dr. Andrew Maverick, for his presence and helpful discussions in German; Dr. Frank Fronczek, whose expertise was very much appreciated with the X-ray diffraction studies and in left field; Marcus Nauman, whose friendship and NMR expertise are always available; Jeff Crow and all those who helped me prepare this thesis; all the committee members for their time spent reading this thesis; the newly formed Stanley group for aiding me with experiments; Robie Smith, whose friendship and assistance will never be forgotten; Timmie, for her attention during all the seminar rehearsals; my family for their encouragement; and most importantly, Mimi, for her love and support which made everything possible.

To Moo.

Table of Contents

List of Tables

List of Figures

List of Schemes

List of Abbreviations

MeCN	acetonitrile
cm^{-1}	wavenumber
d	doublet (NMR)
dd	doublet of doublets (NMR)
Et	ethyl, $-CH_2CH_3$
Et_2O	diethyl ether
Hz	Hertz, sec^{-1}
IR	infrared
L	a generic, unidentate ligand
m	medium (IR), multiplet (NMR)
M	a generic metal
Me	methyl, $-CH_3$
NMR	nuclear magnetic resonance
Ph	phenyl, $-C_6H_5$
q	quartet (NMR)
R	a generic alkyl group
s	strong (IR), singlet (NMR)
t	triplet (NMR)
THF	tertahydrofuran
w	weak (IR)
X	a counteranion

Abstract

The synthesis of the binucleating tetratertiary phosphine ligand $R_2PCH_2CH_2(Ph)PCH_2P(Ph)CH_2CH_2PR_2$ (R = Et, Ph), (LTTP), is described and several new bimetallic systems have been characterized. LTTP ligand design features include the combination of bis(phosphino)methane bridge with bis(phosphino)ethane chelating units. These merging functionalities can coordinate two transition metal centers and allow bimetallic reactivity from intramolecular interactions. eLTTP (R = Et) contains electron-rich alkyl-phosphines which also strongly coordinate and discourage fragmentation of the metal complex. Another class of tetratertiaryphosphines, where the central methylene groups is replaced by a central propylene (eLTTP-pr) and/or *p*-xylylene group (eLTTP-*p*-xyl), are synthesized and characterized along with three bisphosphines, $Et_2PCH_2CH_2P(Ph)Me$, $Et_2PCH_2CH_2PPh_2$, $Et_2PCH_2CH_2PEt_2$ for monometallic model studies.

The reaction of two equivalents of $NiCl_2{\cdot}6H_2O$ with the ethyl-substituted version of LTTP (eLTTP) in EtOH produces both meso- and racemic-diastereomeric forms of Ni_2Cl_4(eLTTP), which readily crystallizes from THF to produce THF-solvated crystals. Single crystal X-ray structure analyses of *meso*-Ni_2Cl_4(eLTTP) and *rac*-Ni_2Cl_4(eLTTP) are presented.

The reaction of $[(CO)_2RhCl]_2$ with eLTTP yields the rhodium(I) eLTTP dimer $Rh_2Cl_2(CO)_2$(eLTTP). Reaction of $[Rh(NBD)_2]BF_4$ (NBD = 1,5-norbornadiene) with the above tetraphosphine and bisphosphine ligands mentioned above produces square-planar cationic rhodium(I) complexes of type $[Rh_n(NBD)_{2n}P_2]^{n+}(BF_4^-)_n$ (P_2 = a chelate bisphosphine when n = 1; P_2 = a single tetraphosphine ligand forming two separate five-membered chelate rings when n =

2). These metal complexes were identified with $^{31}P\{^{1}H\}$ and ^{1}H NMR.

Homobimetallic rhodium complexes based on the electron-rich binucleating tetratertiaryphosphine eLTTP are remarkably active and selective hydroformylation catalysts. Initial rates of 740/hr and high selectivities (ratios of linear to branched aldehyde products of 25-30:1) at 80°C/80 psi have been seen for 1-hexene. The increase in catalytic activation is believed to be due to bimetallic cooperativity via intramolecular hydride transfer. This proposal has been tested by comparison with monometallic model systems and bimetallic systems with ligands that increase the distance between the two metal centers. Together, these results are the most dramatic examples of homobimetallic cooperativity observed for a catalytic process.

Chapter 1 Introduction

The use of monometallic complexes in catalysis has been well documented largely because these systems appear to be much more efficient homogeneous catalysts than dimer and cluster systems. However, multimetallic systems potentially possess several advantages over monometallic complexes, which include:

1) The ability to form multi-centered metal to ligand bonds with a substrate, thus assisting in the activation of that species toward further reaction.
2) The capacity to favor multi-electron transfers by acting as an electron reservoir.
3) The utilization of weak metal-metal bonds as reactive sites in which a substrate can directly insert without prior ligand dissociation.
4) The availability of mixed metal systems that may selectively activate different substrates.

Despite these potential advantages, there are few examples of homogeneous polymetallic catalysts to date that have activities approaching or surpassing those of monometallic systems.[1] However, when one considers all the possible combinations of oxidation states, coordination frameworks, and electronic factors from a wide variety of metals and ligands, the area of polymetallic systems is far from being fully explored. Recently two examples have surfaced which provide strong justification for continuing work in this area. Adams and coworkers reported a

unique polymetallic osmium cluster which could catalyze transalkylation of amines, a reaction which is currently unknown for monometallic systems.[2a] Ojima[2b] reported a polymetallic cluster of two rhodium and cobalt metal centers. The cluster was capable of hydroformylsilyation of alkynes with $HSiR_3$. Similar to hydroformylation, which is the conversion of alkenes into aldehydes, hydroformylsilylation forms aldehydes in the form $R'CH_2C(SiR_3)=CHCHO$.

The theory of polymetallic catalysts is fine on paper, but in practice a number of problems arise. First, the synthesis of clusters and dimers in high yield can be difficult; and second, these complexes may fragment under catalytic conditions. In recent years a variety of techniques have improved the preparation of polymetallic complexes.[3] The general trend is to use a ligand template which can be designed to systematically assemble the polymetallic framework, preferably in a step-wise fashion. The problems associated with the fragmentation of clusters may be inhibited by employing a strong metal-metal bond or bridging ligand. Since M-M bond breaking is one of the possible advantages stated previously, our strategy has been to use bridging ligands which will play the primary role in preventing fragmentation. The bridging ligand should keep two metal centers in close proximity until a new M-M bond can be restored at the end of the catalytic cycle. In order for the ligand to be effective, it must be able to strongly coordinate to the metal, otherwise; the possibility of fragmentation would increase as the catalytic conditions become more severe.

The use of phosphines as ligands has long been studied in coordination chemistry and homogeneous catalysis.[4] Phosphines are versatile ligands when used as ancillary ligands, particularly in stabilizing low-valent later transition metal complexes. Bisphosphines, like bis(diphenylphosphino)ethane,

$Ph_2PCH_2CH_2PPh_2$, are capable of forming five-membered chelate rings with transition metals to further stabilize the metal coordination relative to monodentate phosphines. Changing the substituents attached to the phosphine to vary the amount of electron donation is a powerful tool for tuning the electronic factors within metal complexes. For example, in metal complexes with coordinated phosphine ligands, the phosphines generally act as σ-donors. Changing the substituent from aryl groups to more electron donating alkyl groups will considerably increase the electron donating ability of the phosphine. The changes in the electron density on the metal can often substantially change the reactivity of the metal.

One method of maintaining close M-M proximity involves the use of bridging phosphine ligands. Bridging ligands such as bis(diphenylphosphino)methane, $Ph_2PCH_2PPh_2$, are capable of linking two metals while allowing some flexibility at the central methylene carbon. The lone pairs of these bridging phosphines are aligned parallel with a separation sufficient to span two adjacent metal centers (Figure 1). There are several examples of bimetallic complexes bridged by such phosphines in the literature.[5]

The problems with the synthesis and fragmentation of polymetallic complexes can now be avoided by the preparation of a specially designed bridging ligand template composed of bridging, chelating, and electron-rich phosphines.

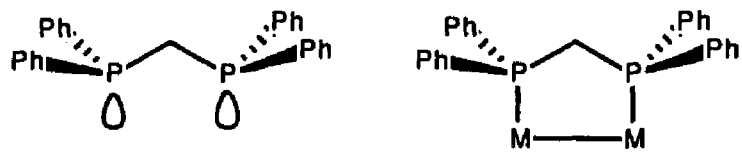

Figure 1: The bis(diphenylphosphino)methane ligand (dppm) as an uncoordinated ligand and as a bridging ligand.

This new ligand can easily coordinate two metal centers and keep them in proximity allowing M-M bond breakage and reformation, while the electron-rich strongly coordinating phosphines inhibit dissociation and fragmentation of the polymetallic complex.

The first binucleating ligand system that combined these bridging and chelating functions with alkylphosphine donors, $(Et_2PCH_2CH_2)_2PCH_2P(CH_2CH_2PEt_2)_2$,[6] eHTP (ethyl substituted **HexaTertiary Phosphine**) was synthesized in high yield in 1985 by Askham and Stanley in these laboratories. This ligand was designed with four diethylphosphinoethyl linkages capable of forming four chelate rings along with the two internal phosphines to two transition metals. The internal phosphines are designed to act as bridging phosphines to ideally keep both metals in close proximity. Ethyl substituents on the terminal phosphines were used instead of phenyl substituents to increase the electron-donor ability of the phosphines and to decrease the chances of ligand dissociation and increase the solubility of its metal complexes in less polar solvents. In addition, ethyl groups on the terminal phosphine are not as sterically demanding as phenyl groups and allow a wider variety of coordination preferences about the metal atom.

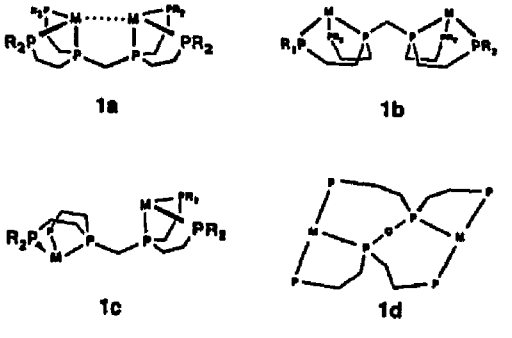

Figure 2: The possible rotational isomers of M_2(eHTP) complexes.

Metal complexation of eHTP is easily accomplished by the addition of two equivalents of a wide variety of metals; however, the expected closed-mode geometry, **1a** (with a M-M bond present) was generally not the final product. Instead, a variety of open-mode geometries, **1b-1c**, were usually found. The addition of two equivalents of $CrCl_3(THF)_3$ to eHTP was expected to form *fac,fac*-Cr_2Cl_6(eHTP) with a geometry similar to **1b**, but instead formed the unexpected *mer*-multibridged product **1d** (Figure 2).[7]

Further studies with bimetallic eHTP complexes of Group VI and Group VIII transition metals showed that the ligand was too sterically encumbered making these bimetallic complexes catalytically non-reactive. Van der Waals energy studies using the SYBYL molecular graphics/mechanics program package showed that bimetallic square planar four coordinate eHTP complexes could not easily form the closed mode (**1a**) it was designed for. Also, the eHTP ligand takes up three coordination sites on a single metal atom and stabilizes the metal centers all too well. Four coordinate square planar metal geometries are very common in catalysis and unless the metals can approach one another there can be no "bimetallic

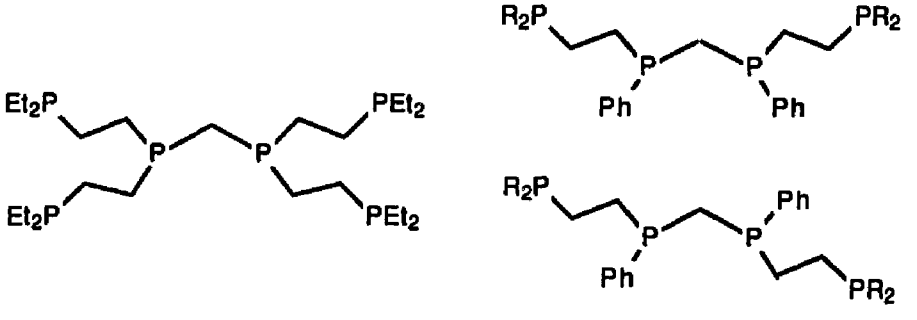

Figure 3: The polyphosphine ligand eHTP (left) and the new LTTP diastereomeric ligands (right).

cooperativity".[8]

The basis of this thesis, therefore, is the synthesis, characterization, metal complexation, and reactivities of a new, less sterically demanding binucleating ligand ligand. The same general concepts that went into the design of eHTP are present including bridging phosphines for keeping metals in proximity and chelation for added metal stability. This new ligand, called LTTP for Linear TetraTertiary Phosphine, was specifically designed to relieve the steric hindrances observed in eHTP. Although LTTP has two arms removed from the internal phosphines, it still behaves as a strong binucleating polyphosphine ligand (Figure 3).

Chapter 2 Synthesis of LTTP

The combination of a bis(phosphino)methane bridge with bis(phosphino)-ethane chelating units in eHTP proved to be a unique environment well suited for the formation of bimetallic species. eHTP, however, was impractical for studying bimetallic cooperativity due to the tridentate, bis-chelate nature of the ligand which blocked too many coordination sites and because of considerable internal steric factors. A new ligand was designed to alleviate these problems and still maintain strong metal coordination and steric accessibility for bimetallic assisted reaction.

One approach to solve both of the above problems was to simply remove a bis(diethylphosphino)ethyl linkage ($-CH_2CH_2PEt_2$) off each internal phosphine on eHTP and create a linear tetratertiary phosphine (LTTP)[9] of the general type $R_2PCH_2CH_2(R')PCH_2P(R')CH_2CH_2PR_2$. This new ligand would still have the bridging and chelating framework of eHTP, yet provide a considerably more open environment about the metal centers for reactions to occur. The removal of the two extra chelate arms renders the internal phosphines chiral generating a pair of diastereomers: the racemic (*R*,*R* and *S*,*S*) and the meso (*R*,*S*) diastereomers.

The preparation of a ligand similar to LTTP was reported by Stelzer and coworkers, who synthesized the tetratertiaryphosphine complex $i\text{-}Pr_2PCH_2CH_2\text{-}CH_2(i\text{-}Pr)PCH_2P(i\text{-}Pr)PCH_2CH_2CH_2P\text{-}i\text{-}Pr_2$.[10] This complex contained both bridging bis(phosphino)methane and two (phosphino)propylene arm linkages similar to LTTP. The conversion of the overall synthesis for Stelzer's tetraphosphine from $Cl_2PCH_2PCl_2$ was very low (10-15% yield), and transition metal complexes based on this ligand have not as yet been reported.

The synthetic procedure for preparing the LTTP ligand is shown in Scheme

Scheme 1

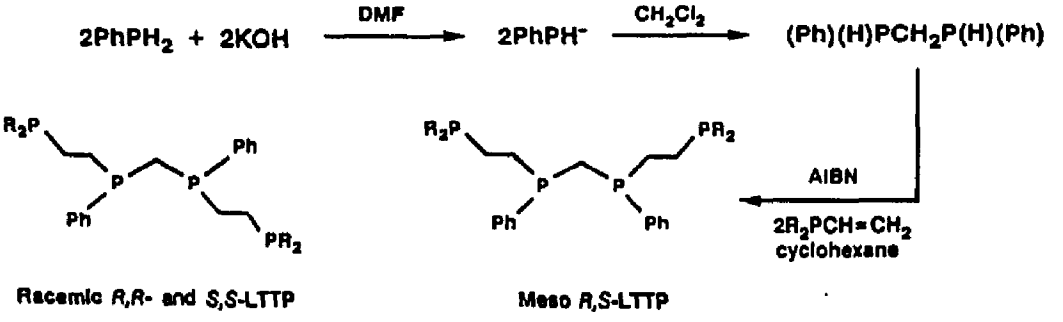

1. The first step was the synthesis of the central bis(phosphino)methane unit, Ph(H)PCH_2P(H)Ph, by a procedure developed by Langhans and Stelzer.[11] Phenylphosphine ($PhPH_2$) and CH_2Cl_2 are placed in a reaction vessel with DMF as the solvent. The phosphide is generated *in situ* from $PhPH_2$ by the slow addition of a 56% aqueous solution of KOH. The phosphide reacts further with CH_2Cl_2 to form Ph(H)PCH_2P(H)Ph.[12]

The Ph(H)PCH_2P(H)Ph is then treated with two equivalents of $R_2PCH{=}CH_2$ under AIBN free-radical-catalyzed conditions[13] to produce a 1:1 mixture of both diastereomers of LTTP in very high yields. Unlike Stelzer's linear tetratertiary phosphine, synthesis which involves the use of propylene-linked groups which are rather difficult to synthesize (*vide supra*), the ethylene-linked terminal phosphines groups are much easier to build (88-92% isolated yield based on Ph(H)PCH_2P-(H)Ph, 39-40% yield based on $PhPH_2$).[9b]

As stated in the introduction, ligands are designed for a variety of reasons. The phenyl groups that replaced the two -$CH_2CH_2PEt_2$ arms from the internal phosphines of eHTP were used in order to help facilitate crystallization of the transition metal complexes of these ligands. Two substituents (R = Et, Ph) of LTTP were synthesized to vary the basicity of the external phosphine so that differ-

ences in reactivities of transition metal complexes in catalysis could be studied. The primary ligand of choice is when R is the electron-rich ethyl group since electron-rich alkylated phosphines will strongly coordinate to transition metal centers and be far more effective at inhibiting ligand dissociation or fragmentation.

Although the internal phosphine has a single phenyl substituent, the phosphine is still considered to be electron-rich because of the saturated carbon chains that make up the backbone of the ligand. The internal phosphine with a single phenyl group is more electron-rich relative to a phosphine with 2 phenyl substituents.

The ligands eLTTP and phLTTP were isolated by the vacuum distillation (0.1 torr) of all impurities at 170° C and 210°C, respectively, leaving behind pure ligand as a viscous liquid in the distillation pot. Both ligands were fully characterized by ^{31}P and ^{1}H NMR, elemental analysis, and x-ray crystallography (of transition metal complexes containing these ligands). The phLTTP ligand is air stable while eLTTP slowly oxidizes to phosphine oxide over a period of months.

The expanded $^{31}P\{^{1}H\}$ NMR spectra of both ligands are presented in Figure 4. The spectra were recorded at 40.48 MHz (100 MHz ^{1}H equivalent) and 161.92 MHz (400 MHz ^{1}H equivalent). The differences between the spectra at different magnetic field strengths appear to be quite dramatic. In the 40.48 MHz case, the coupling of the internal phosphine of eLTTP would appear to be centered at -25.85 ppm (upper right) as an 8-line pattern, but the 161.92 MHz spectrum shows a distinct pair of doublets of doublets (directly below). The resonance from the lower field strength spectrum is actually two overlapping signals from both internal phosphines of each diastereomer separated by 0.7 ppm. The same reasoning exists for the resonance at -18.4 ppm (upper left). In the 40.48 MHz the signals for the

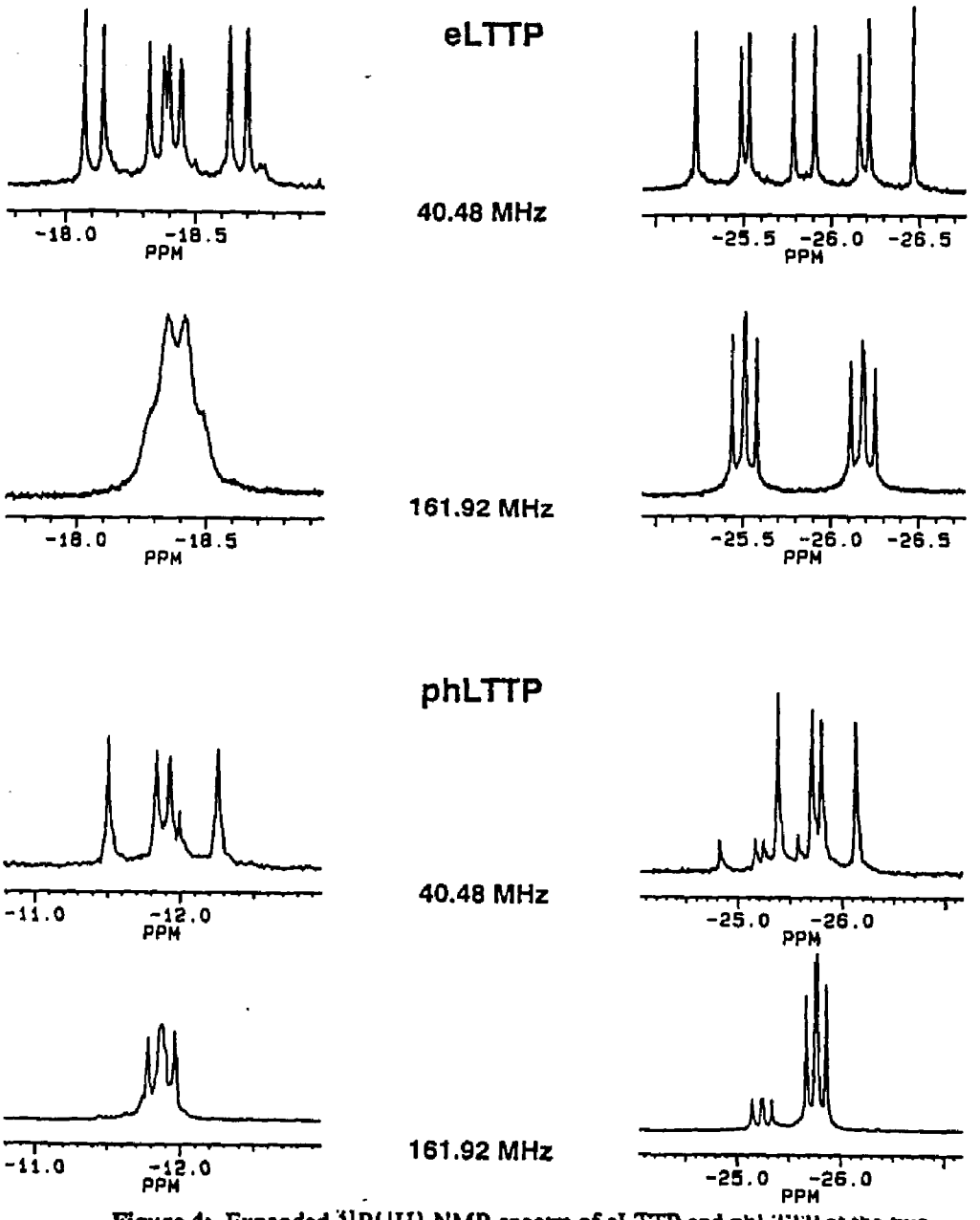

Figure 4: Expanded $^{31}P\{^{1}H\}$ NMR spectra of eLTTP and phLTTP at the two different field strengths indicated. The lower field is equivalent to a ^{1}H resonance frequency of 100 MHz, while the higher field corresponds to 400 MHz.

external phosphine appear to be a complex coupling pattern, but are actually just two doublets of doublets (dd) that are overlapping. The centers of the overlapping resonances are separated by only 0.3 ppm. The chemical shift and coupling arguments of phLTTP are exactly the same as in eLTTP except that the center of each resonance is shifted by less than 0.5 ppm for the internal phosphines and 0.1 ppm for the external phosphines.

The P-P couplings and spin systems are identical for each sample at different field strengths. The couplings of each spectra were reproduced by the Bruker NMR simulation program PANIC using an AXX'A' spin system. The simulations produced a simple doublet of doublets pattern for the internal and external phosphorus atoms with the following coupling: $J_{Pint\text{-}Pext}$ = 22.5 Hz and $J_{Pint\text{-}Pint}$ = 109.5 Hz for eLTTP; $J_{Pint\text{-}Pext}$ = 29.9 Hz and $J_{Pint\text{-}Pint}$ = 107.6 Hz for phLTTP.

The differences in coupling patterns and line widths of the resonances from low to high field strengths are mainly due to the Hz/ppm ratio of each spectrometer. The Hz/ppm ratio of the 161.92 MHz spectrometer is four times higher than the 40.48 MHz spectrometer. This effect can both benefit and complicate spectral identifications. As the Hz/ppm ratio decreases, the width of the spin coupling pattern of a resonance will increase. As the Hz/ppm ratio increases, the line width of the resonance begins to broaden because the coupling pattern begins to collapse within itself (see the external phosphine resonances at 161.92 Hz for both ligands in Figure 4). The higher field, however, can clearly separate and show the relative proportions of the meso and racemic diastereomers of eLTTP and phLTTP (see the internal resonances for phLTTP at 161.92 MHz.).

The diastereomers of eLTTP can be separated into pure racemic-eLTTP and meso-eLTTP through a route that utilizes a bimetallic nickel complex. More details

describing the diastereomer separation is described in Section 3.3.

Chapter 3 Nickel Complexes of eLTTP

Section 3.1 Introduction

Nickel complexes can exhibit a high activity toward the dimerization of ethylene and propylene.[14] Wilke and others[15] postulate that cyclooctatetraene is produced through bimetallic nickel intermediates. Originally, nickel complexes of eLTTP were synthesized to study C-C bond formation reactions, but other uses of the nickel eLTTP complexes have surfaced which will be discussed further.

eLTTP is prepared as a mixture of racemic and meso diastereomers. The literature contains many examples in which diastereomers can be separated via nickel complexation and fractional crystallization.[16] The nickel can be readily extracted from the complex leaving a pure diastereomer. Nickel complexes of eLTTP have served this function.

Section 3.2 *rac*- and *meso*-Ni_2Cl_4(eLTTP)[9b]

The reaction of two equivalents of $NiCl_2 \cdot 6H_2O$ with eLTTP in EtOH produces Ni_2Cl_4(eLTTP) in nearly quantitative yield. The product can be isolated as a yellow-orange solid that is air-stable in both solution and solid state. The $^{31}P\{^1H\}$ NMR shows the presence of both diastereomers of Ni_2Cl_4(eLTTP) in roughly equal amounts as determined by peak heights and integrations. There are no resonances upfield in the negative ppm region that would indicate an uncoordinated tertiary-phosphine. Both diastereomers of Ni_2Cl_4(eLTTP) crystallize from a THF solution as large, well-shaped THF-solvated crystals. Both crystals are orange-red with different morphologies. Upon removal from THF one crystal type rapidly loses its THF solvent of crystallization and turns opaque, while the other set of crystals maintain the THF solvent and remain clear. The crystals can then be easily separat-

ed using the Pasteur method.

X-ray analysis on each type of crystal confirmed that a single diastereomer of the eLTTP ligand is coordinated to two nickel atoms. The crystal that lost its THF solvent molecule was crystallographically identified as *meso*-Ni_2Cl_4(eLTTP). The ORTEP plots from the structural determination of both *rac*- and *meso*-Ni_2Cl_4-(eLTTP) are shown in Figures 5 and 6. Selected bond distances and angles are listed in Table I. Each Figure displays the molecule in two perspectives; parallel and perpendicular to the central P1···P3 vector. The two perspectives allow a clear viewing of the rotational orientation of the molecule. In each case, the nickel atoms have an oxidation state of +2 with a d^8 electron configuration. Since d^8 Ni(II) atoms do not generally form Ni-Ni bonds,[17] the open mode eLTTP rotational orientation was expected. Both systems have square-planar geometries about the metal center with eLTTP coordinating in the expected bridging/chelating manner. The local coordination geometry about each nickel is similar to that seen in the monometallic $NiCl_2$(dppe) (dppe = 1,2-bis(diphenylphosphino)ethane).[18] The dppe ligand also forms a 5-membered chelate ring with nickel.

In the past anti and syn nomenclature has been used for the hexaphosphine M_2(eHTP) complexes that exist in a variety of rotational geometries.[8,19] This nomenclature will continue to be used to designate the general rotational orientation of each half of the complex with respect to the central methylene bridge hydrogen atoms. In the syn conformation, the metal atom is on the same side of the eLTTP ligand as the central methylene group hydrogen atoms; anti indicates that the metal atom is on the opposite side. An anti-anti conformer, for example, would be a rotational conformation in which there is a M-M bond or the metal atoms are proximate. The anti-anti structure is loosely referred to as a closed-mode complex, while syn-

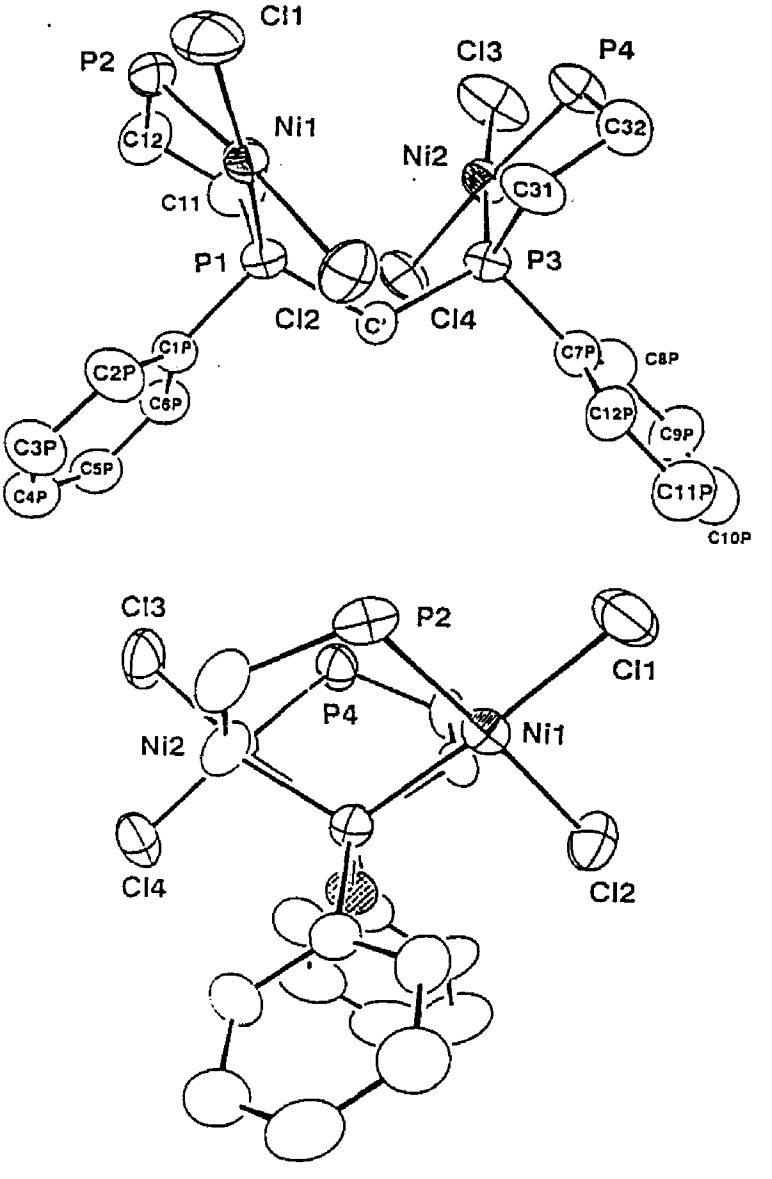

Figure 5: ORTEP plots of *rac*-Ni_2Cl_4(eLTTP) oriented parallel and perpendicular to the central P1···P3 vector to illustrate the rotational orientation. The ethyl groups of the external phosphorus atoms have been omitted for clarity. The central methylene carbon has been hatched in the perpendicular view to highlight its position. Thermal ellipsoids are shown at the 33% level.

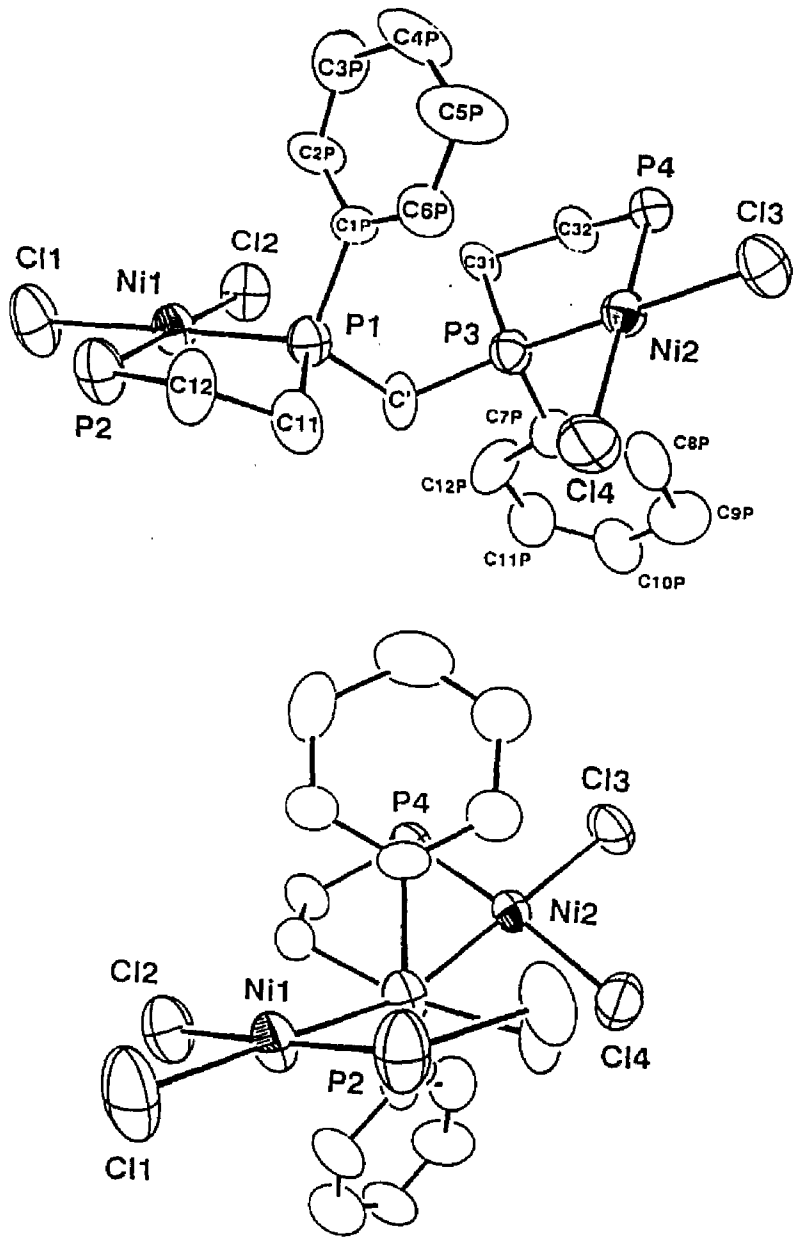

Figure 6: ORTEP plots of *meso*-Ni_2Cl_4(eLTTP) orientated parallel and perpendicular to the central P1--P3 vector to illustrate the rotational orientation. The ethyl groups on the external phosphorus atom have been omitted for clarity. Thermal ellipsoid are shown at the 33% probability level.

Table I: Selected bond distances (Å) and angles (deg) of both *rac*- and *meso*-diastereomers of Ni_2Cl_4(eLTTP).[a]

	racemic	meso
Ni1-Ni2	6.272 (1)	5.417 (1)
Ni1-Cl1	2.195 (2)	2.194 (2)
Ni1-Cl2	2.208 (2)	2.205 (2)
Ni1-P1	2.139 (2)	2.134 (2)
Ni1-P2	2.144 (2)	2.153 (2)
Ni2-Cl3	2.187 (2)	2.173 (2)
Ni2-Cl4	2.209 (2)	2.215 (2)
Ni2-P3	2.136 (2)	2.131 (2)
Ni2-P4	2.160 (2)	2.141 (2)
P1-C'	1.852 (7)	1.838 (6)
P3-C'	1.824 (7)	1.854 (6)
Cl1-Ni1-Cl2	95.17 (8)	94.90 (8)
Cl1-Ni1-P1	175.55 (9)	174.26 (8)
Cl1-Ni1-P2	88.06 (9)	87.86 (8)
Cl2-Ni1-P1	90.27 (8)	90.25 (7)
Cl2-Ni1-P2	176.75 (9)	175.63 (8)
P1-Ni1-P2	86.50 (8)	86.86 (8)
Cl3-Ni2-Cl4	94.13 (8)	95.89 (9)
Cl3-Ni2-P3	175.07 (9)	173.48 (9)
Cl3-Ni2-P4	89.79 (8)	86.74 (9)
Cl4-Ni2-P3	89.58 (8)	90.46 (8)
Cl4-Ni2-P4	175.30 (9)	175.9 (1)
P3-Ni2-P4	86.37 (7)	86.84 (8)
Ni1-P1-C'	115.0 (2)	122.1 (2)
Ni2-P3-C'	121.5 (2)	120.7 (2)
P1-C'-P3	121.7 (4)	119.3 (3)

[a]Numbers in parentheses are estimated standard deviations in the least significant digits.

anti or syn-syn conformations are called open-mode structures.

In terms of the syn and anti nomenclature, the structure of *rac*-Ni_2Cl_4-(eLTTP) is anti-anti with the two nickel atoms symmetrically splayed apart, very similar to structures seen for *rac*-$Rh_2Cl_2(CO)_2$(eLTTP)[9a] (*vide infra*) and the eHTP complexes $M_2Cl_2(eHTP)^{2+}$ (M = Pd, Pt)[17a,b] and $M_2(CO)_6(eHTP)$ (M = Cr, Mo, W).[19c] The Ni1-P1···P3-Ni2 torsional angle for the racemic complex is 106° with a Ni-Ni separation of 5.417 (1) Å. The torsional angles of $M_2Cl_2(eHTP)^{2+}$ (M = Pd, Pt) and $M_2(CO)_6(eHTP)$ (M = Cr, Mo, W) with the hexaphosphine ligand eHTP, which range from 58° to 102°, are smaller than that seen for *rac*-Ni_2Cl_4-(eLTTP). The smaller torsional angles in the bimetallic hexaphosphine eHTP complexes might imply that there are fewer intramolecular steric interactions relative to eLTTP. This would be disturbing since eLTTP was designed to be <u>less</u> bulky that eHTP. In order to properly assess the intramolecular steric interactions, it is more meaningful to compare the P-CH_2-P angles. *rac*-Ni_2Cl_4(eLTTP), for example, has a P-CH_2-P angle of 119.3 (3)° which can be contrasted to the considerably larger P-CH_2-P angles in the hexaphosphine complexes $M_2Cl_2(eHTP)^{2+}$: 126.6 (4)° for Pd and 129.7 (9)° for Pt. These eHTP complexes (M = Pd, Pt) are generally comparable to *rac*-Ni_2Cl_4(eLTTP) because of the symmetrically splayed partially closed mode configurations that appear in the x-ray structures.

meso-Ni_2Cl_4(eLTTP) has a syn-anti rotational conformation with a considerably larger Ni1-P1···P3-Ni2 torsional angle of 160° and a Ni-Ni separation of 6.272 (1) Å. The metal-ligand bond distances and angles are essentially the same as those in the racemic system. The major difference between the two structures is the rotational orientation about the central methylene bridge. The syn-anti conformation in *meso*-Ni_2Cl_4(eLTTP) is somewhat asymmetric relative to the symmetrically splayed

structure of *rac*-Ni_2Cl_4(eLTTP). This is most apparent in the two Ni-P_{int}-C' bond angles. The meso complex has Ni1-P1-C' and Ni2-P3-C' angles of 115.0 (2)° and 121.5 (2)°, respectively, compared to 122.1 (2)° and 120.7 (2)°, respectively, for the racemic complex. In the syn-anti structure half of the bimetallic complex the Ni2 side in the meso complex experiences a more crowded steric environment, this allows the M-P_{int}-C' bond angle on the less crowded side of the complex to relax to a greater extent relative to the angle on the more sterically encumbered half of the complex.

The ^1H NMR spectra for *rac*- and *meso*-Ni_2Cl_4(eLTTP) are shown in Figure 7. Two-dimensional ^1H *J*-correlated NMR experiments aided in the identification of chemical shifts and coupling of all the protons in these systems. This method allows the separation of resonances and their $J_{H\text{-}H}$ and $J_{P\text{-}H}$ constants that overlap in the conventional one dimension spectrum. The detailed ^1H NMR assignments and coupling constants are listed in Table II.

The main ^1H NMR difference between the racemic and meso diastereomers lies in the fact that the protons of the central methylene bridge in the meso diastereomer are magnetically inequivalent. This difference causes significantly different and distinct resonances for each diastereomer. In the ^1H NMR of the racemic system, the triplet at $\delta = 3.27$ ppm results from coupling of the two equivalent internal phosphorus atoms to the two equivalent protons on the central methylene bridge. In the meso system two resonances are present due to asymmetry that exists within the complex. Two quartets appear at $\delta = 3.21$ and 3.64 ppm, in which each quartet actually consists of an overlapping pair of doublets of triplets. The doublet is from geminal coupling between the inequivalent protons, and the triplet is from the two equivalent internal phosphorus atoms. Coupling constants are

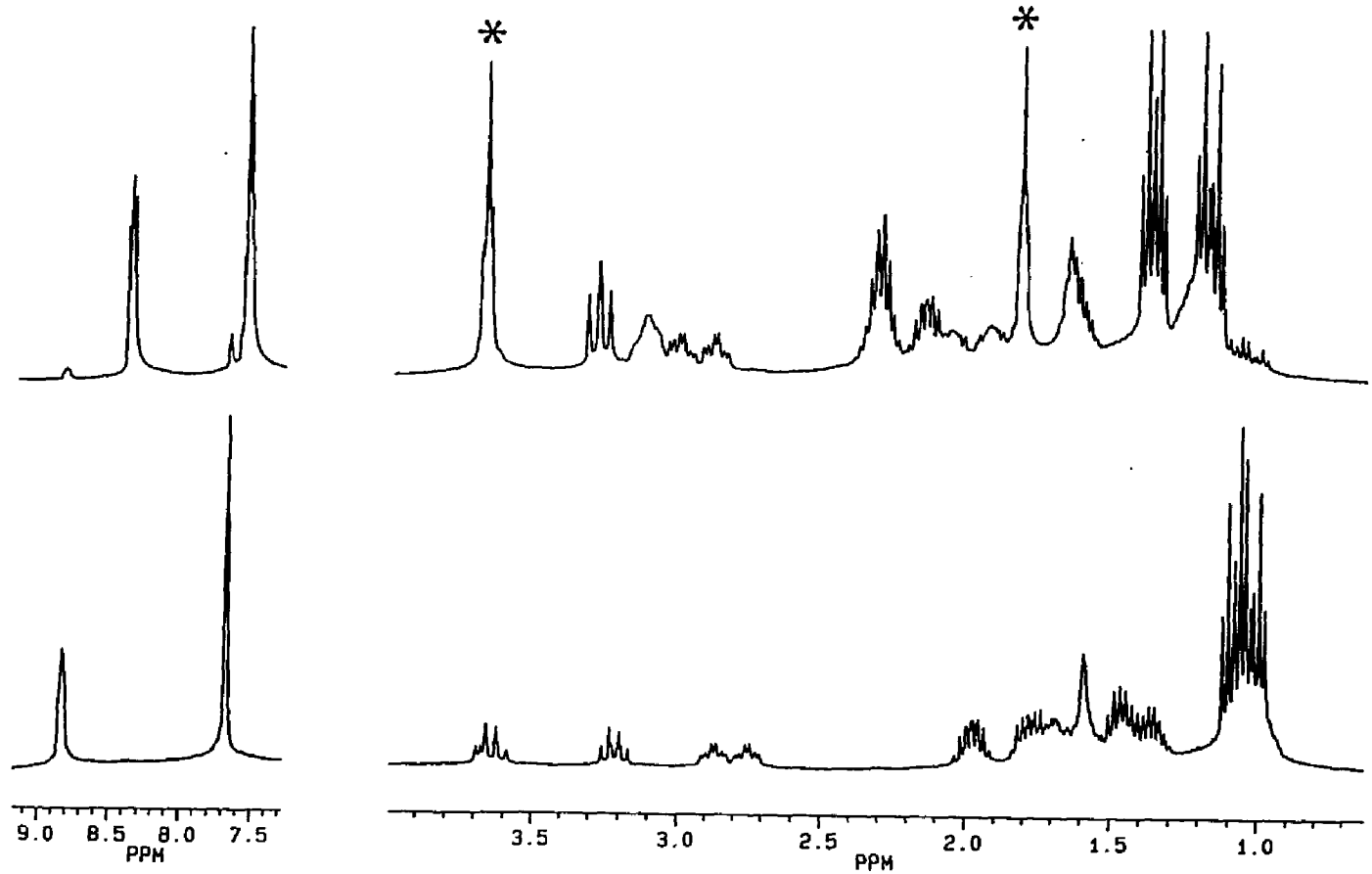

Figure 7: The ^1H NMR of rac- (top) and meso- (bottom) Ni_2Cl_4(eLTTP) in CD_2Cl_2 (400.13 MHz). Asterisked peaks are THF solvent impurities.

Table II: ^{1}H NMR Data for *meso*- and *rac*-Ni_2Cl_4(eLTTP)

	meso			racemic		
Proton	δ, ppm	$J(^{1}H\text{-}^{1}H)$, Hz	$J(^{1}H\text{-}^{31}P)$, Hz	δ, ppm	$J(^{1}H\text{-}^{1}H)$, Hz	$J(^{1}H\text{-}^{31}P)$, Hz
P-CH_2-CH_3	1.01	7.7 (t)	20.0 (d)	1.16	7.8 (t)	20.0 (d)
	1.07	7.7 (t)	17.2 (d)	1.36	7.8 (t)	17.2 (d)
P-CH_2-CH_3	1.35	7.4 (q)	15.6 (d)	1.61	7.7 (q)	14.8 (d)
	1.46	7.8 (q)	9.2 (d)	2.13	7.8 (q)	10.0 (d)
	1.77	1.2 (d)	11.2 (d)	2.26	7.7 (q)	8.8 (d)
		7.8 (q)		2.23	7.8 (q)	11.2 (d)
	1.97	8.0 (q)	10.0 (d)			
P-CH_2-CH_2-P	1.57	2.0 (d)	12.0 (d)	1.91	2.0 (d)	11.6 (d)
		6.8 (d)			7.0 (d)	
		14.8 (d)			13.5 (d)	
	1.68	7.0 (d)	6.4 (d)	2.05	1.9 (d)	10.8 (d)
		8.0 (d)			7.0 (d)	
		15.0 (d)			15.1 (d)	
	2.67	2.6 (d)	15.6 (d)	2.87	2.0 (d)	14.8 (d)
		6.4 (d)			6.5 (d)	
		12.8 (d)			15.5 (d)	
	2.74	2.0 (d)	15.6 (d)	2.99	2.0 (d)	14.0 (d)
		6.2 (d)			6.5 (d)	
		13.0 (d)			15.5 (d)	
P-CH_2-P	3.21	14.2 (d)	11.6 (t)	3.27		14.8 (t)
	3.64	14.2 (d)	14.0 (t)			
P-*Ph*	7.66	3.3 (t)		7.54	1.9 (d)	*a*
					3.3 (t)	
	8.82	3.0 (d)	12.0 (d)	8.37	1.8 (d)	12.0 (d)
		5.7 (d)			8.2 (d)	

[a] $J_{P\text{-}H}$ was present but unresolvable.

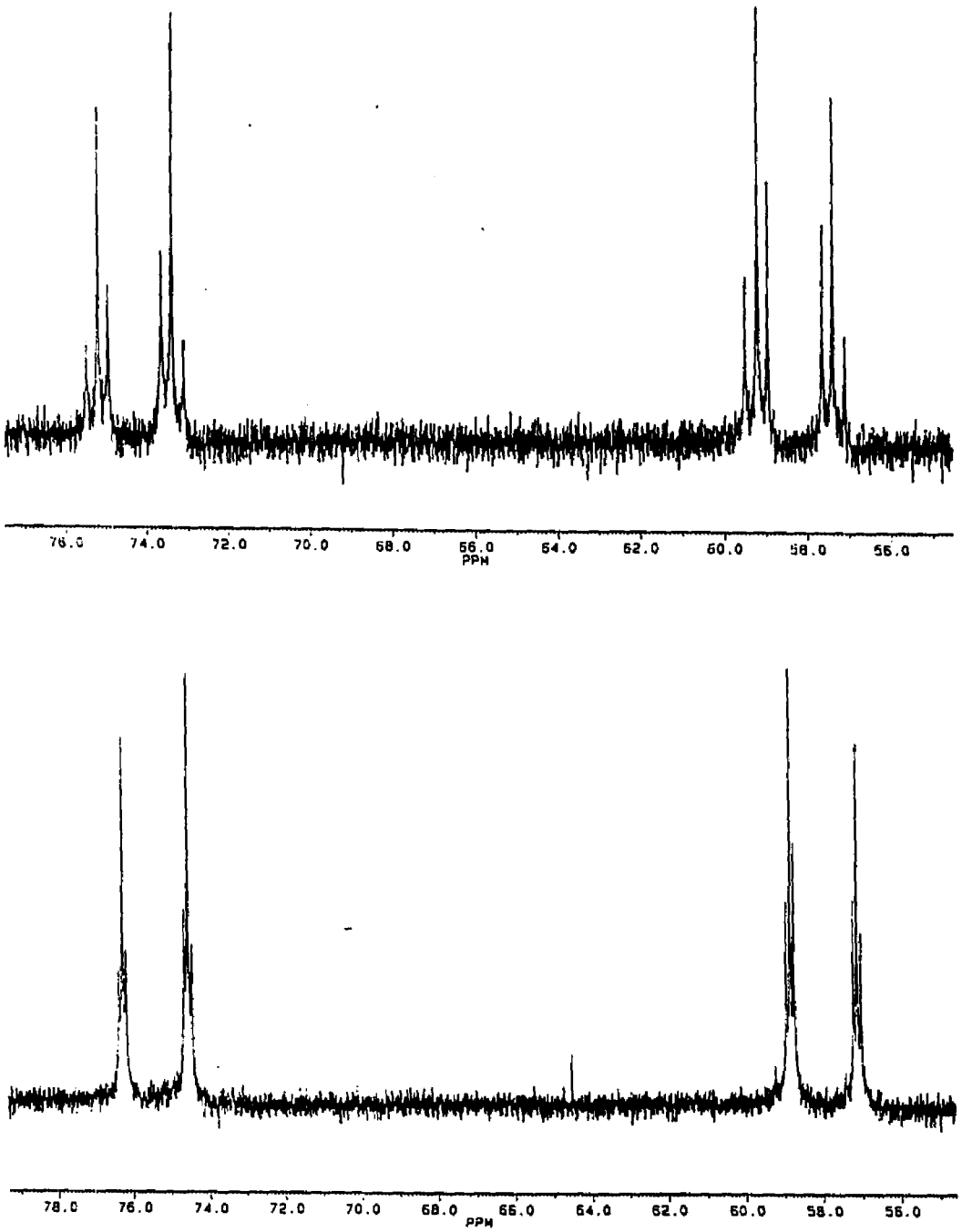

Figure 8: The $^{31}P\{^{1}H\}$ of *meso*- (top) and *rac*- (bottom) Ni_2Cl_4(eLTTP) in CD_2Cl_2 (40.48 MHz).

listed in Table II.

The differences between the Ni_2Cl_4(eLTTP) diastereomers can also be seen in the $^{31}P\{^1H\}$ NMR (Figure 8). The resonances of the internal and external phosphorus atoms are present for each diastereomer. The racemic complex has two doublets of triplets at δ = 75.41 ppm (external phosphorus, $J_{P\text{-}P}$ = 69.0 and 3.9 Hz) and δ = 57.97 ppm (internal, $J_{P\text{-}P}$ = 69.0 and 3.9 Hz), and the meso complex has two doublets of triplets at δ = 74.28 ppm (external, $J_{P\text{-}P}$ = 72.8 and 10.8 Hz) and δ = 58.32 ppm (internal, $J_{P\text{-}P}$ = 72.8 and 10.8 Hz). In each diastereomer a doublet coupling exists from a two bond pathway through the metal from the external phosphorus atom to the internal atom because a three bond $J_{P\text{-}P}$ coupling through the ethylene chain would not produce a coupling constant this large. The strong coupling between the two internal phosphorus atoms of the free ligand suggests that both internal phosphorus atoms in the nickel complex may also strongly couple. Both strongly coupled internal phosphorus atoms now couple to a single external phosphorus atom thus generating the triplet pattern. The differences between the diastereomers show up in this coupling. The racemic complex has a triplet coupling of $J_{P_{int}\text{-}P_{ext}}$ = 3.9 Hz compared to $J_{P_{int}\text{-}P_{ext}}$ = 10.8 Hz in the meso complex.

Elemental analyses of both diastereomers of Ni_2Cl_4(eLTTP) with agreed satisfactorily well with the theoretical values. The values obtained are listed in the experimental section.

Section 3.3 eLTTP Extractions and *rac*, trans-$Ni(CN)_2(\eta^2$-eLTTP)

The reaction of two equivalents of $NiCl_2 \cdot 6H_2O$ with eLTTP produces a mixture of *meso-* and *racemic-* $NiCl_4$(eLTTP) in very good yields (85-90%). On

evaporating a THF solution, two air-stable crystal morphologies are produced. The first crystal is red-orange and readily loses its THF solvent of crystallization and turns opaque, while the second red-orange crystal maintains its THF solvent and remains clear. These two crystals can be separated by the Pasteur method. X-ray analysis performed on each type of crystal proved that they are the two different eLTTP diastereomers of Ni_2Cl_4(eLTTP) with the opaque morphology being the meso diastereomer.[9b]

The separation of both diastereomers of Ni_2Cl_4(eLTTP) allows a potential method for obtaining diastereomerically pure free eLTTP ligand. If the free ligand can be decomplexed from the diastereomerically pure bimetallic nickel complex, then a considerable amount of time and effort in chromatographic work can be saved. There was precedent for the decomplexation of phosphines from Ni(II) by treatment with excess cyanide.[16,20] Refluxing a H_2O/benzene mixture with *rac*-Ni_2Cl_4(eLTTP) and excess NaCN displaced *rac*-eLTTP with 45% recovery. The yield indicated incomplete decomplexation and a yellow side product was isolated. The large cubic red-orange crystals grown from THF were composed of a 5-coordinated monometallic nickel complex determined by x-ray crystallography to be the *rac*, trans- Ni(CN)$_2$(η^2-eLTTP) complex as shown in Figure 9.

One way to address the problem of low ligand recovery is to consider the formation of the impurity species trans-Ni(CN)$_2$(η^2-eLTTP). As the cyanide ion is attacking Ni_2Cl_4(eLTTP) in the aqueous layer there is a buildup of the partially liberated ligand in the form of *trans*-Ni(CN)$_2$(η^2-eLTTP). *trans*-Ni(CN)$_2$(η^2-eLTTP) escapes further attack of cyanide ion by dissolving into the non-polar benzene phase. By changing the nature of the non-polar solvent, one can avoid this problem. Following the same procedure with heptane instead of benzene gives a

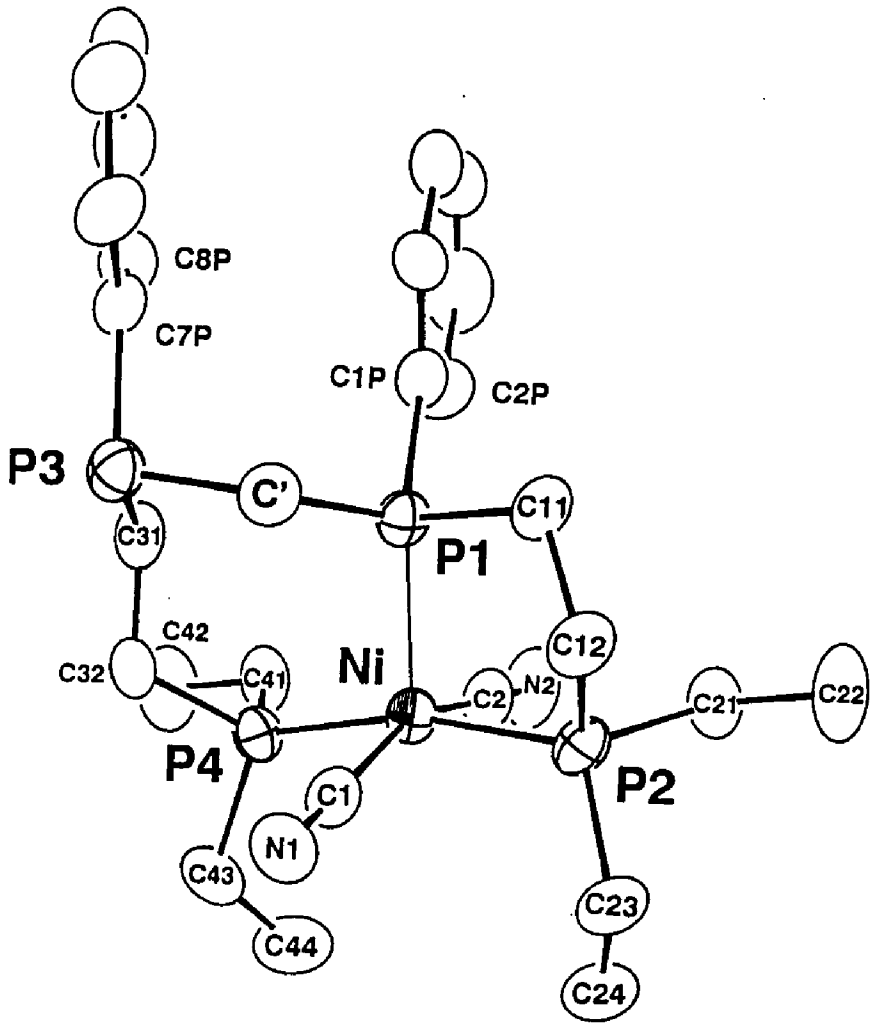

Figure 9: The ORTEP of *rac*, trans-$Ni(CN)_2(\eta^2$-eLTTP).

Table III. Bond distances (Å) for *rac,trans*-$Ni(CN)_2(\eta^2$-eLTTP).[a]

Ni-P1	2.395 (2)	C11-C12	1.542 (8)
Ni-P2	2.183 (2)	C21-C22	1.52 (1)
Ni-P4	2.186 (2)	C23-C24	1.50 (1)
Ni-C1	1.876 (7)	C31-C32	1.543 (9)
Ni-C2	1.859 (7)	C41-C42	1.52 (1)
P1-C'	1.827 (6)	C43-C44	1.50 (1)
P1-C11	1.850 (6)	C1P-C2P	1.378 (8)
P1-C1P	1.812 (6)	C1P-C6P	1.390 (9)
P2-C12	1.819 (7)	C2P-C3P	1.41 (1)
P2-C21	1.814 (7)	C3P-C4P	1.35 (1)
P2-C23	1.825 (6)	C4P-C5P	1.34 (1)
P3-C'	1.858 (6)	C5P-C6P	1.36 (1)
P3-C31	1.843 (6)	C7P-C8P	1.382 (8)
P3-C7P	1.827 (6)	C7P-C12P	1.407 (9)
P4-C32	1.829 (6)	C8P-C9P	1.37 (1)
P4-C41	1.821 (6)	C9P-C10P	1.39 (1)
P4-C43	1.812 (7)	C10P-C11P	1.40 (1)
N1-C1	1.164 (7)	C11P-C12P	1.357 (9)
N2-C2	1.156 (7)		

[a]Numbers in parentheses are estimated standard deviations in the least significant digits.

Table IV: Bond angles (deg) for *rac,trans*-$Ni(CN)_2(\eta^2$-eLTTP).[a]

P1-Ni-P2	87.54 (7)	P2-C12-C11	110.4 (4)
P1-Ni-P4	105.67 (7)	P2-C21-C22	115.0 (5)
P1-Ni-C1	94.6 (2)	P2-C23-C24	113.5 (5)
P1-Ni-C2	107.3 (2)	P3-C31-C32	111.0 (4)
P2-Ni-P4	165.48 (8)	P4-C32-C31	114.3 (4)
P2-Ni-C1	85.6 (2)	P4-C41-C42	114.9 (5)
P2-Ni-C2	91.9 (2)	P4-C43-C44	115.2 (6)
P4-Ni-C1	87.3 (2)	P1-C1P-C2P	118.4 (6)
P4-Ni-C2	89.9 (2)	P1-C1P-C6P	122.3 (5)
C1-Ni-C2	157.9 (3)	C2P-C1P-C6P	119.2 (6)
C'-P1'C11	102.3 (3)	C1P-C2P-C3P	119.3 (8)
C'-P1-C1P	105.0 (3)	C2P-C3P-C4P	120.1 (9)
C11-P1-C1P	99.9 (3)	C3P-C4P-C5P	119.8 (9)
C12-P2-C21	106.2 (3)	C4P-C5P-C6P	122.4 (9)
C12-P2-P23	105.6 (3)	C1P-C6P-C5P	119.1 (7)
C21-P2-C23	105.3 (3)	P3-C7P-C8P	125.5 (6)
C'-P3-C31	103.3 (3)	P3-C7P-C12P	116.8 (5)
C'-P3-C7P	101.9 (3)	C8P-C7P-C12P	117.8 (6)
C31-P3-C7P	102.6 (3)	C7P-C8P-C9P	121.6 (7)
C32-P4-C41	104.8 (3)	C8P-C9P-C10P	119.8 (7)
C32-P4-C43	102.3 (3)	C9P-C10P-C11P	119.7 (7)
C41-P4-C43	105.4 (3)	C10P-C11P-C12P	119.3 (7)
P1-C'-P3	122.1 (3)	C7P-C12P-C11P	121.7 (7)
P1-C11-C12	111.3 (5)		

[a]Numbers in parentheses are estimated standard deviations in the least significant digits.

quantitative extraction of pure eLTTP from Ni_2Cl_4(eLTTP).

The structure of *rac,trans*-Ni(CN)$_2$(η^2-eLTTP) obtained from x-ray analysis shows that the monometallic complex has two cyano ligands trans to one another on a Ni(II) metal center. The other two coordination sites are occupied by the external phosphorus atoms of eLTTP. The bond distances and angles of *rac,trans*-Ni(CN)$_2$(η^2-eLTTP) are listed in Tables III and IV. The molecule, *rac,trans*-Ni-(CN)$_2$(η^2-eLTTP), is described as a partially liberated complex in which the cyanide anions have only displaced the less basic internal phosphine portion of eLTTP.

Several interesting structural features are found in *rac*, trans-Ni(CN)$_2$(η^2-eLTTP). The geometry about the metal center is slightly distorted from square planar toward square pyramidal (SPy) with P2-Ni-P4 and C1-Ni-C2 angles of 165.48 (8)° and 157.9 (3)°, respectively. The distortion arises from a weak interaction of the internal phosphine's lone pair with the empty p_z orbital of the nickel at the axial position. The Ni-P_{ext} bond distances are 2.183 (2) Å and 2.186 (2) Å, which fall in the range of normal Ni-P bonds. A distance of 2.395 (2) Å from the nickel to the internal phosphorus atom (P1) suggests a weak but definite interaction. Axial interactions in Ni(II) complexes with phosphine ligands have been reported before by several groups.[21]

Power and coworkers, for example, reported a similar penta-coordinated nickel complex, *trans*-Ni(CN)$_2$(P(CH$_2$OH)Ph$_2$)$_3$.[22] The geometry about the metal was, once again, SPy. The distances of the basal Ni-P bonds were 2.231 (4) and 2.244 (3) Å, with an apical Ni-P bond of 2.400 (3) Å. They also reported that trans-Ni(CN)$_2$(P(CH$_2$OH)Ph$_2$)$_3$ represented the closest approach to a Ni-P_{axial} dissociation while maintaining overall structural integrity for several reasons: (i) the

apical Ni-P bond is the longest seen in a Ni(II) phosphine complex, (ii) the difference between the apical and the basal Ni-P bonds are the largest reported (ca. 0.16 Å), (iii) the geometry about the metal is closer to SPy than other penta-coordinated $Ni(CN)_2P_3$ complexes (The authors argue that SPy is structurally nearer to square planar geometry and more likely to be a precursor for dissociation than a trigonal bipyramidal geometry), and (iv) $P(CH_2OH)Ph_2$ is one of the largest phosphine ligands known in a penta-coordinated nickel complex, $Ni(CN)_2P_3$.

Until *rac,trans*-$Ni(CN)_2(\eta^2$-eLTTP), *trans*-$Ni(CN)_2(P(CH_2OH)Ph_2)_3$ was considered the closest reported approach to a Ni-L_{axial} dissociation while maintaining overall penta-coordinate structural integrity. While the apical Ni-P bond is longer (2.400 (3) Å) in Power's system than in *rac,trans*-$Ni(CN)_2(\eta^2$-eLTTP) (2.359 (2) Å), the basal Ni-P bonds in Power's system are also considerably longer compared to *rac,trans*-$Ni(CN)_2(\eta^2$-eLTTP) (*vide supra*). The longer Ni-P_{basal} distances in *trans*-$Ni(CN)_2(P(CH_2OH)Ph_2)_3$ are due to poor σ-donor character of $P(CH_2OH)Ph_2$ relative to eLTTP. Comparison of the basal P-Ni-P and C-Ni-C angles shows that *rac,trans*-$Ni(CN)_2(\eta^2$-eLTTP) is closer to square planar geometry about the metal (165.48 (8)° and 157.9 (3)° of *rac,trans*-$Ni(CN)_2(\eta^2$-eLTTP) compared to 164.0 (3)° and 144.1 (1)° for Brown's complex). Additionally, the difference between the apical and basal Ni-P bond lengths in *rac,trans*-Ni $(CN)_2$-$(\eta^2$-eLTTP) are larger (ca. 0.21 Å).

In the solid state, *rac,trans*-$Ni(CN)_2(\eta^2$-eLTTP) contains four inequivalent phosphorus nuclei; however, this is not the case in the solution $^{31}P\{^1H\}$ NMR spectrum. In the $^{31}P\{^1H\}$ NMR at room temperature, the *rac,trans*-$Ni(CN)_2(\eta^2$-eLTTP) complex contains only two sharp singlets. The singlets are produced from a temperature-dependent fluxional process in solution. Apparently in solution, the

apical Ni-P is very weak and easily broken by dissociation. At room temperature the ligand on the molecule is actually wagging in solution so both internal phosphorus atoms are interacting with the metal center. The exchange process occurs rapidly on the NMR timescale which causes singlets for both internal and external phosphorus atoms. Variable temperature $^{31}P\{^{1}H\}$ NMR studies of this system down to -80 °C were only slightly helpful. The exchange between each internal phosphorus atoms can be slowed down, but not stopped, by lowering the temperature. New resonances can be observed in the $^{31}P\{^{1}H\}$ NMR at lower temperatures, but the coupling constants could not be obtained due to broadening. The broadening may be brought on by either one or all the following reasons: (i) broadening that occurs when decreasing the temperature, (ii) intermediate freezing of the fluxional process, (iii) or formation of paramagnetic intermediates during the freezing of the fluxional process.

The IR (KBr) of *rac,trans*-$Ni(CN)_2(\eta^2$-eLTTP) has a strong absorption at 2100 cm^{-1} characteristic of a -CN stretch. Also present is a small shoulder at 2119 cm^{-1} which may indicate the slight presence of the meso diastereomer of the ligand.

Chapter 4 Rhodium Complexations of eLTTP

Section 4.1 $Rh_2Cl_2(CO)_2(eLTTP)$[9a]

The reaction of $[Rh(CO)_2Cl]_2$ with bisphosphines such as bis(diphenylphosphino)ethane commonly produces $Rh(CO)ClP_2$ (P_2 = a bisphosphine that forms a chelate ring with the metal center).[23] However, the reaction of $[(CO)_2RhCl]_2$ with eLTTP produces $Rh_2Cl_2(CO)_2(eLTTP)$ in only 40-65% yield along with a red-brown precipitate that has remained unidentified. Only 15-20% of isolated crystalline $Rh_2Cl_2(CO)_2(eLTTP)$ can be obtained.

The $^{31}P\{^1H\}$ NMR (Figure 10) demonstrates that $[Rh(CO)Cl]_2$ has reacted with eLTTP. ^{31}P and ^{103}Rh nuclei have spins of 1/2 and are 100% abundant. The solution $^{31}P\{^1H\}$ NMR of a pure crystalline sample gave rise to a dd at 83.8 ppm and a doublet of multiplets (dm) at 56.2 ppm. The resonance at 83.8 ppm is the external phosphorus atom coupling to the rhodium atom ($J_{Rh\text{-}P}$ = 149 Hz) and the internal phosphorus atom ($J_{P\text{-}P}$ = 31 Hz). The coupling pattern of the internal phosphorus atom at 56.2 ppm is more difficult to decipher. The large doublet arises from rhodium coupling ($J_{Rh\text{-}P}$ = 139 Hz), but the phosphorus-phosphorus coupling is more complex. The multiplet is the result of various coupling pathways between the two phosphorus atoms, especially if there is a 5-membered chelate ring. Phosphorus atoms can couple through the carbon backbone of a chelate ring or through metal-phosphorus bonds. In metal phosphine complexes, such as in $Rh_2Cl_2(CO)_2$-(eLTTP), there is the usual two bond P-P coupling that has a pathway through the metal. Four-bond coupling between P_{ext} and P'_{int} on the other half of the molecule in $Rh_2Cl_2(CO)_2(eLTTP)$ can also occur, which produces a multiplet instead of the expected doublet from a single two-bond coupling pathway. The four-bond coupling pathway goes through the rhodium metal and then through the central

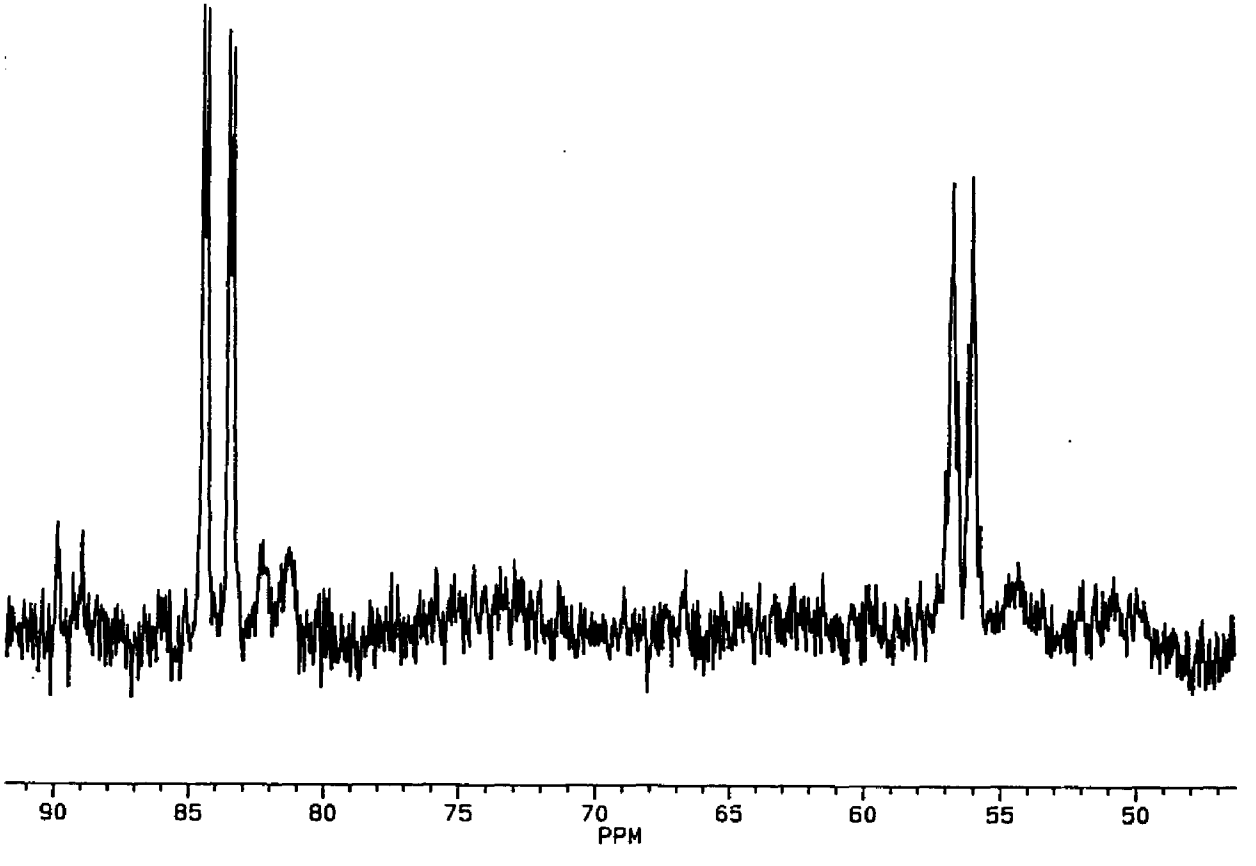

Figure 10: The $^{31}P\{^{1}H\}$ NMR of $Rh_2Cl_2(CO)_2$(eLTTP) obtained from crystallization in d_4-MeOH (161.92 MHz).

methylene carbon. Generally, four bond P-P coupling is very small (< 1 Hz) and considered negligible. The strong coupling between two internal phosphines through the central methylene carbon in eLTTP, however, acts as a conductor and allows coupling of the distant P atom.

When rhodium is coordinated to both Cl and CO ligands, more than two resonances in the $^{31}P\{^{1}H\}$ NMR are expected due to the possibilities of each phosphorus atom being trans to either a Cl ligand or a CO ligand. In fact, the $^{31}P\{^{1}H\}$ NMR of a crude powdered sample of a distereomeric mixture of $Rh_2Cl_2(CO)_2$(eLTTP) before crystallization shows such resonances. In the $^{31}P\{^{1}H\}$ NMR of the crystalline sample, the Cl ligand is trans to P_{ext}, while the CO is trans to P_{int}. When Cl is trans to P_{int}, the resonance shifts upfield from 77.65 ppm (dd) to 64.73 ppm (dm, $J_{Rh\text{-}P}$ = 164.8 Hz) (Figure 11). When CO is trans to P_{ext}, the resonance shifts downfield from 48.65 ppm (dm) to 61.52 ppm (dd, $J_{Rh\text{-}P}$ = 120.15 Hz, $J_{P\text{-}P}$ = 32.8 Hz). These shifts are relatively common and can occur when phosphorus atoms are trans to Cl and CO ligands in monometallic $MCl(CO)P_2$ complexes.[24]

The ^{1}H NMR was performed in CD_2Cl_2 and showed a variety of multiplets due to various H-H and P-H couplings. The presence of two diastereomers of eLTTP and CO/Cl ligand isomers (*vide supra*) creates a large number of overlapping proton resonances which complicate the ^{1}H NMR spectra. There was little difference, for example, observed in the ^{1}H NMR of the crystalline and the powder samples of $Rh_2Cl_2(CO)_2$(eLTTP). The chemical shifts of the multiplets are listed in the experimental section and will not be discussed further.

Crystals of $Rh_2Cl_2(CO)_2$(eLTTP) can be obtained by the slow evaporation of THF or toluene. An X-ray structure of red-orange crystals from either solvent

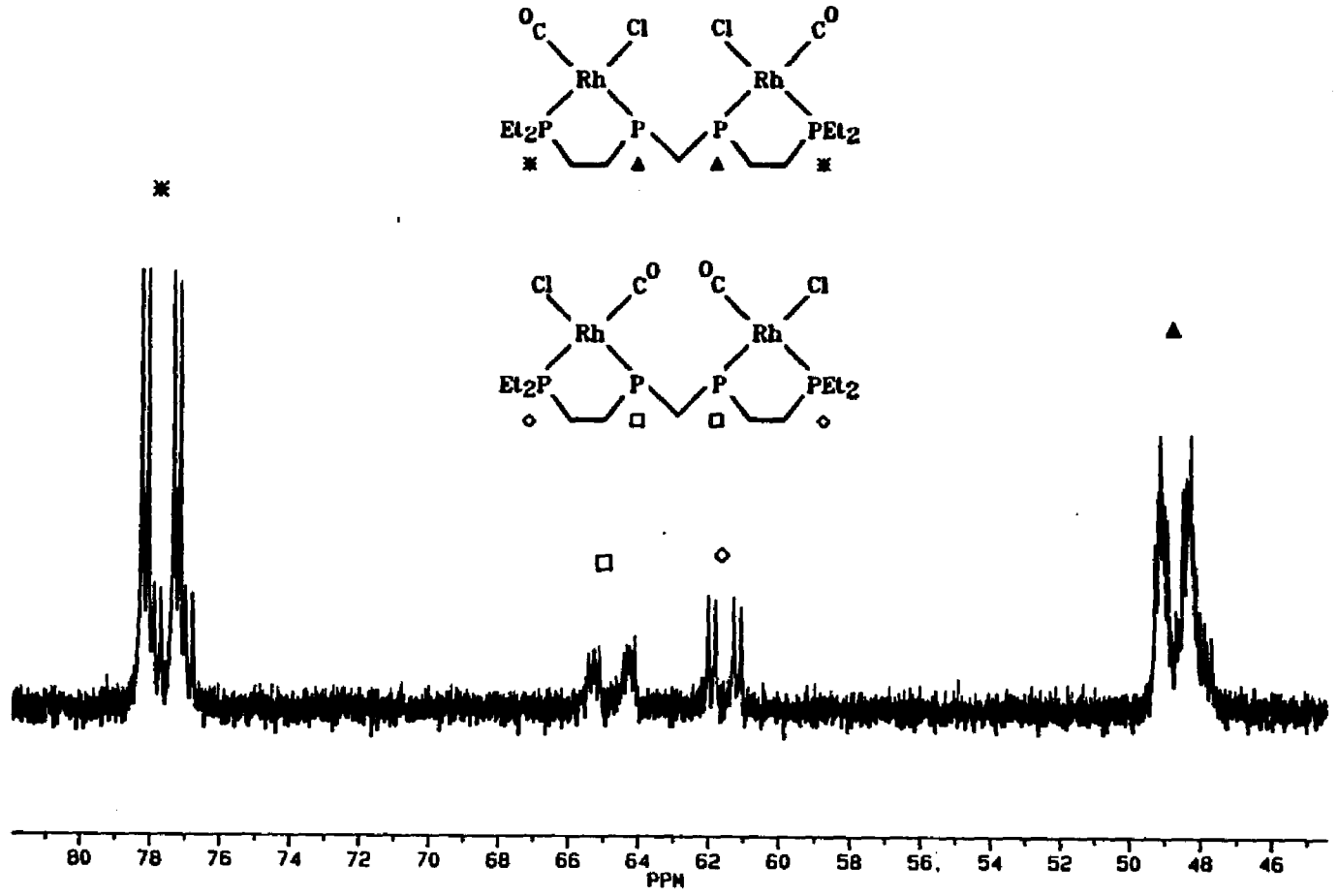

Figure 11: The $^{31}P\{^{1}H\}$ NMR of a powder sample of $Rh_2Cl_2(CO)_2$(eLTTP) in CD_2Cl_2 (161.92 MHz).

reveals that the racemic *R,R*- and *S,S*- diastereomers are present and have indeed coordinated to two Rh(I) metal centers. The ORTEP diagrams as well as the selected bond lengths and angles of $Rh_2Cl_2(CO)_2$(eLTTP)·THF are shown in Figure 12 and Table V, respectively. The structure of $Rh_2Cl_2(CO)_2$(eLTTP), which was grown from toluene, was very similar and will not be shown; however, the bond lengths and angles are listed in Table V. Each bimetallic unit lies on a 2-fold rotation axis that passes through the central methylene carbon of the eLTTP ligand. The crystals grown from THF contain a single THF solvent of crystallization. The coordination about the metal center is square planar with minor distortions away from ideal due to puckering of the 5-membered chelate ring. This is the first reported crystal structure of any $MX(CO)P_2$ moiety (M = Rh, Ir; X = halide; P_2 = five-membered ring chelating bistertiaryphosphine) whether they exist as a dimer bridged by a central methylene carbon or just as a monometallic unit.

$Rh_2Cl_2(CO)_2$(eLTTP) adopts an open mode conformation, formally an anti-anti rotational conformation, in which both $RhCl(CO)P_2$ moieties are symmetrically splayed apart by rotations about the central methylene carbon. The Rh-Rh separation is 5.813 (2) Å with a Rh-P1···P1'-Rh' torsional angle of 123° when crystals are grown from THF. The crystals grown from toluene have a structure very similar to that which was grown from THF except in the rotational conformation. for this system the Rh-Rh separation is 5.496 (8) Å with a Rh-P1···P1'-Rh' torsional angle of 110°.[9a] The rotation angle can be seen in the lower portion of Figure 12 which shows a view looking down the P1-P1' axis. These orientations are similar to those seen for some eHTP binuclear systems which have symmetrically splayed M1-P···P-M2 torsional angles ranging form 58° to 102°.[19a,c] A major difference between $Rh_2Cl_2(CO)_2$(eLTTP) and the $M_2Cl_2(eHTP)^{2+}$ hexaphosphine complexes

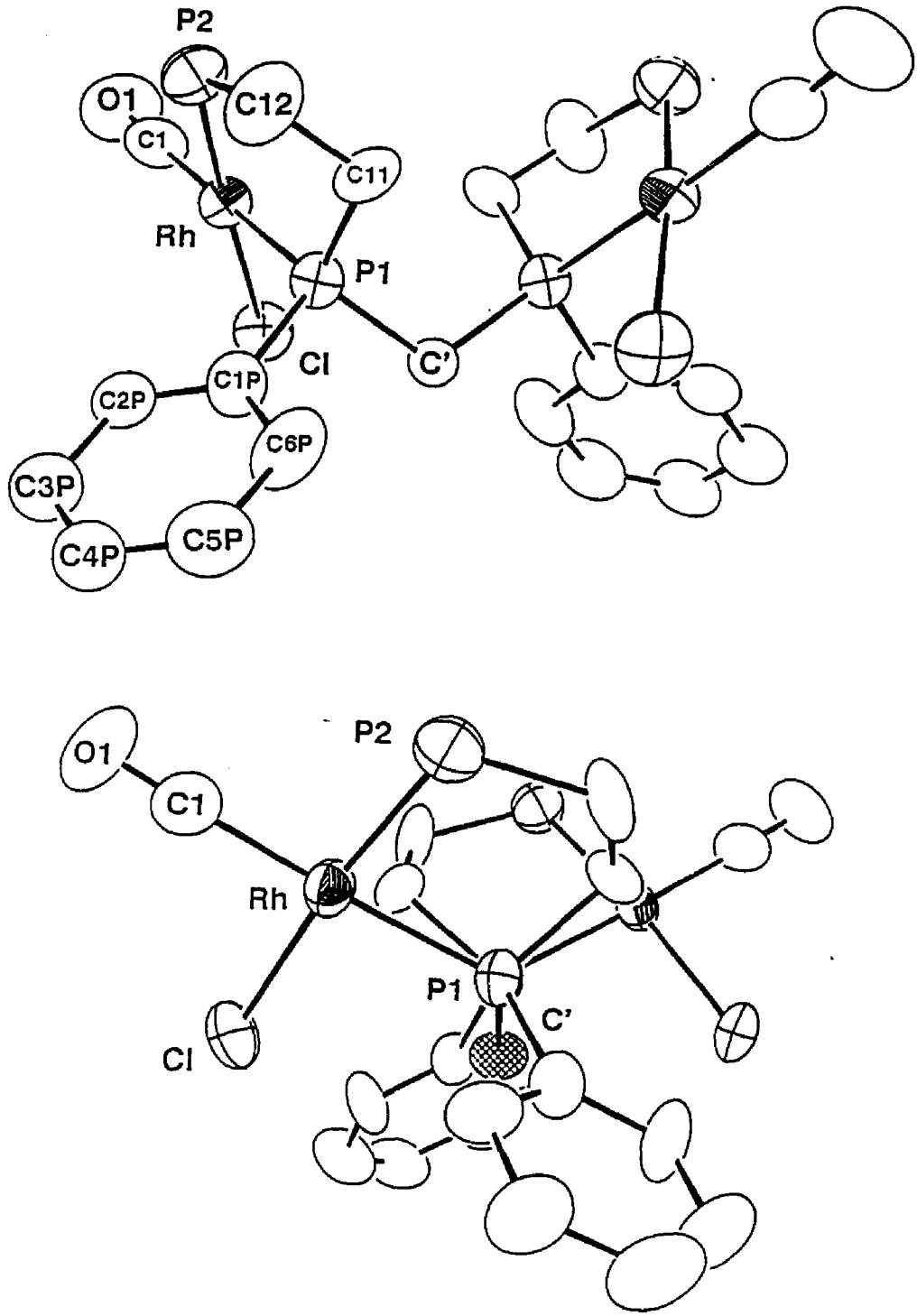

Figure 12: Parallel and perpendicular views of *rac*-$Rh_2Cl_2(CO)_2$(eLTTP)·THF. Ethyl groups have been omitted for clarity.

Table V. Selected bond distances (Å) and angles (deg) for *rac*-$Rh_2Cl_2(CO)_2$-(eLTTP)·THF and *rac*-$Rh_2Cl_2(CO)_2$(eLTTP).[a]

	$Rh_2Cl_2(CO)_2$(eLTTP)·THF	$Rh_2Cl_2(CO)_2$(eLTTP)
Rh-Rh'	5.813 (2)	5.4960 (8)
Rh-Cl	2.382 (4)	2.385 (1)
Rh-P1	2.289 (4)	2.309 (1)
Rh-P2	2.229 (5)	2.225 (1)
Rh-C1	1.87 (2)	1.872 (6)
P1-C'	1.87 (1)	1.827 (4)
P1-C11	1.86 (1)	1.828 (6)
P1-C1P	1.84 (2)	1.827 (5)
P2-C12	1.88 (2)	1.830 (6)
O1-C1	1.11 (2)	1.130 (7)
C11-C12	1.46 (2)	1.531 (8)
Cl-Rh-P1	89.7 (1)	88.47 (5)
Cl-Rh-P2	173.1 (2)	170.69 (6)
Cl-Rh-C1	93.5 (6)	95.4 (2)
Rh-C1-O1	178. (6)	178.6 (6)
P1-Rh-P2	83.4 (2)	83.96 (5)
P1-Rh-C1	176.8 (6)	175.5 (2)
P2-Rh-C1	93.4 (6)	92.4 (2)
P1-C'-P1'	113. (1)	116.6 (4)
Rh-P1-C'	118.2 (2)	118.0 (1)
C'-P1-C1P	100.8 (7)	103.1 (3)
C'-P1-C11	109.0 (6)	108.8 (2)
C11-P1-C1P	103.1 (7)	102.8 (3)
P1-C11-C12	105. (1)	105.3 (4)
P2-C12-C11	113. (1)	109.5 (4)
Rh-P···P'-Rh' (Dihedral Angle)	123	110

[a]Numbers in parentheses are estimated standard deviations in the least significant digits.

is that the central P-CH_2-P angle is considerably smaller. $M_2Cl_2(eHTP)^{2+}$ complexes have P-CH_2-P angles that range between 126.6 (4)° for $Pd_2Cl_2(eHTP)^{2+}$ and 129.7 (9)° for $Pt_2Cl_2(eHTP)^{2+}$ [19a,b], but the same angle in the two structures of $Rh_2Cl_2(CO)_2(eLTTP)$ are only 113 (1)° and 116.6 (4)°. This result definitely implies that these eLTTP systems have significantly less steric interactions between each half of the ligand system and strongly suggests that rotations about the central methyl bridge should be more facile than in eHTP complexes. The different rotational conformations observed in the crystal structures of $Rh_2Cl_2(CO)_2(eLTTP)$ result from weak crystal packing forces. This implies that rotations about the central methylene bridge are very facile and probably allow the bimetallic eLTTP complexes to easily rotate to a conformation that would allow bimetallic cooperativity for the activation or reaction of a substrate.

To further study to study the rotational flexibility about the central methylene bridge in $Rh_2Cl_2(CO)_2(eLTTP)$, a van der Waals (VDW) energy study was performed. Using the SYBYL molecular mechanics program, one can study the steric interactions within a molecule by calculating the VDW energies of the atoms in the complex by rotating about the two central P_{int}-C (central methylene carbon) bonds. The atomic coordinates of *rac*-$Rh_2Cl_2(CO)_2(eLTTP)$·THF obtained from our X-ray analysis were used as a starting point in the study. The VDW energies were calculated at 5° intervals about the two central P-CH_2-P bonds. The compiled results of the VDW energy study form a two dimensional contour map that is summarized in Figure 12.

The VDW energy map of $Rh_2Cl_2(CO)_2(eLTTP)$ shows a larger area of low-lying energy regions compared to previous VDW studies involving $M_2(eHTP)$ hexaphosphine complexes[8,19] which, once again, signifies greater rotational flexi-

bility and less steric interactions within the molecule. Each axis represents the rotation about a P_{int}-C bond. Contour values are in units of kcal/mole and are separated by different schemes of shading which include: less than 1 kcal/mole; less than 5 kcal/mole; and less than 20 kcal/mole. Values higher than 20 kcal/mole are not listed for clarity. Labels A through D mark the positions of various low energy rotational conformations. The global minimum (relative "0" energy) is at the position marked at A, which is nearly coincident with the rotational conformation shown in the two crystal structures of $Rh_2Cl_2(CO)_2$(eLTTP). Most importantly, there is a low-lying energy region at the origin (Region D) which was <u>not</u> present in previous hexaphosphine M_2(eHTP) VDW studies. This corresponds to a closed-mode rotational conformation in which the metals are in next to one another. Bimetallic complexes with eLTTP as the ligand are now capable of forming M-M bonds, while analogous square planar eHTP ligated complexes <u>cannot</u> form M-M bonds due to severe intramolecular steric interaction. This, of course, was the

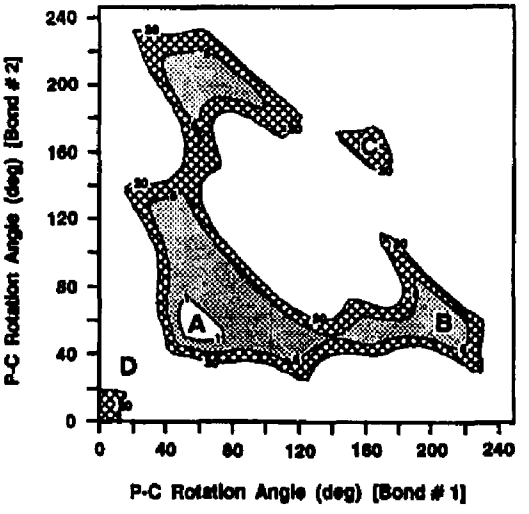

Figure 13: An expanded portion of the full 360°x360° van der Waals energy rotation map of *rac*-$Rh_2Cl_2(CO)_2$(eLTTP)·THF.

primary reason for designing eLTTP. $Rh_2Cl_2(CO)_2$(eLTTP) was also characterized by IR spectroscopy . There are strong absorption bands characteristic of a carbonyl ligand and eLTTP (see experimental section).

Section 4.2 $[Rh_2(NBD)_2(eLTTP)](BF_4)_2$

The low isolated yields (40-47%) of $Rh_2Cl_2(CO)_2$(eLTTP) were considered unacceptable, so new routes for making Rh_2(eLTTP)-type compounds were explored. Another reason for not using $Rh_2Cl_2(CO)_2$(eLTTP) is that the Cl ligand is a strong inhibitor in hydroformylation catalysis - a reaction that we were quite interested in studying. The use of π-coordinated alkene ligands appeared attractive since they are relatively labile and would not compete for coordination sites at the rhodium metal during catalysis.

The addition eLTTP to two equivalents of $[Rh(NBD)_2]BF_4$ (NBD = norbornadiene)[20] made $[Rh_2(NBD)_2(eLTTP)](BF_4)_2$ in 80-90% isolated yields. The final complex is isolated as a red solid which is soluble in CH_2Cl_2, MeCN, MeOH, and acetone. The solid contains a mixture of both ligand diastereomers. One norbornadiene molecule on $Rh(NBD)_2^+$ is displaced by half of the eLTTP ligand so that the tetraphosphine ligand can form two 5-membered chelate rings with the rhodium atoms. The rhodium atoms have a +1 oxidation state, which is a d^8 system, and prefer square planar geometries when bonded to four ligands. The PCH_2CH_2P portion of eLTTP, because it can form a 5-membered ring, occupies two cis coordination sites on the metal with the two π-bonds of the norbornadiene ligand completing the square-planar bonding arrangement.

The eLTTP complex $[Rh_2(NBD)_2(eLTTP)](BF_4)_2$ can be compared to a similar bimetallic rhodium complex based on the TETRAPHOS ligand, $Ph_2PCH_2CH_2P$-

$(Ph)CH_2CH_2P(Ph)CH_2CH_2PPh_2$, prepared by Brown and Canning.[25] They propose the same general coordination geometry for $[Rh_2(COD)_2(TETRAPHOS)](BF_4)_2$ (COD = 1,5-cyclooctadiene) that we assign to $[Rh_2(NBD)_2(eLTTP)](BF_4)_2$. The TETRAPHOS complex is considerably less stable toward H_2 and decomposes at ambient conditions to form a η^4-TETRAPHOS monometallic rhodium complex and metallic rhodium shown in Figure 14. $[Rh_2(NBD)_2(eLTTP)](BF_4)_2$ is stable toward H_2 up to 150° C where only a small amount of decomposition is observed.

The authors propose that decomposition occurs when MeOH displaces the COD ligands. As the MeOH solvent molecules coordinate to the metal, they displace an internal phosphine on the first metal center. The uncoordinated internal phosphine can quickly form a 5-membered chelate ring with the second metal center. Afterwards, the first rhodium atom dissociates completely and the uncoordinated phosphine of TETRAPHOS can swing around to the second rhodium atom forming the final 5-membered chelate ring.

The use of electron rich phosphines which coordinate more strongly than aryl phosphines should inhibit the initial Rh-P dissociation. In fact, only partial decom-

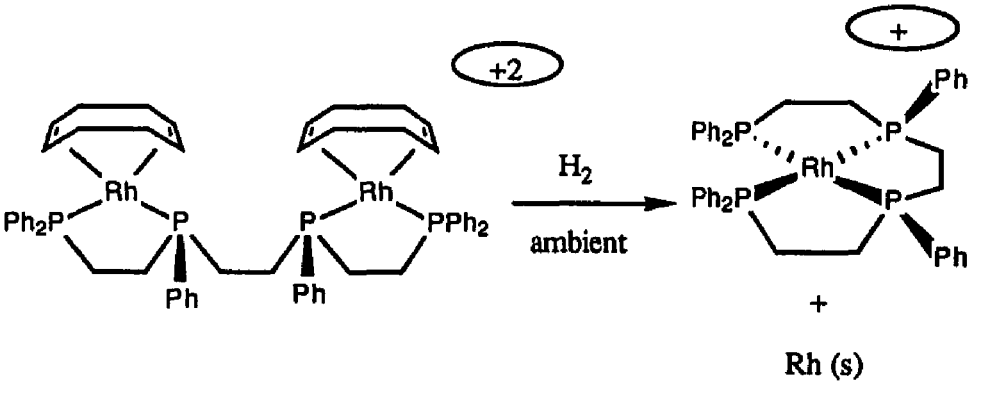

Figure 14: The decomposition of $[Rh_2(COD)_2(TETRAPHOS)](BF_4)_2$ with hydrogen.

position was observed at 100°C and 250 psi H_2 using our $[Rh_2(NBD)_2(eLTTP)](BF_4)_2$ complex. These conditions are considerably more severe than Brown's (ambient) providing clear evidence of the much stronger coordinating ability of electron-rich phosphines.

During the reaction workup for $[Rh_2(NBD)_2(eLTTP)](BF_4)_2$, a red oil is obtained and dissolved in CH_2Cl_2. The CH_2Cl_2 solution is vacuum evaporated to dryness to leave a red solid. Crystals of $[Rh_2(NBD)_2(eLTTP)](BF_4)_2$ can be grown from the mother liquor at -40°C. The crystals are not, as of yet, of x-ray quality and rapidly desolvate losing their crystalline appearance. $[Rh_2(NBD)_2(eLTTP)](BF_4)_2$ is not air sensitive in the solid state, but solutions of $[Rh_2(NBD)_2(eLTTP)](BF_4)_2$ do decompose in minutes on exposure to air.

$[Rh_2(NBD)_2(eLTTP)](BF_4)_2$ has been characterized by $^{31}P\{^1H\}$ NMR and ^1H NMR. The $^{31}P\{^1H\}$ NMR of the red solid shows two dd from the external phosphorus atoms of each diastereomer at 60.00 and 60.50 ppm (Figure 15). The dd pattern arises from $J_{Rh\text{-}P}$ = 151.6 Hz and $J_{P\text{-}P}$ = 23.5 Hz and $J_{Rh\text{-}P}$ = 151.7 Hz and $J_{P\text{-}P}$ = 23.3 Hz , respectively. At 49.00 and 49.70 ppm is a dm from the diastereotopic internal phosphorus atoms. The doublet coupling comes from $J_{Rh\text{-}P}$ = 158.1 and 153.8 Hz, respectively. Similar to $Rh_2Cl_2(CO)_2(eLTTP)$, various coupling pathways between the phosphorus atoms exist that cause extra coupling which makes the resonance appear as a multiplet. Usually, electron-rich phosphines coordinated to metal centers have resonances farther upfield than less electron-rich phosphines. In $[Rh_2(NBD)_2(eLTTP)](BF_4)_2$ the more electron-rich external phosphorus atom Et_2P- should be shifted upfield the most; however, the internal phosphorus atoms are furthest upfield. We are not sure about the reasons for the change in chemical shift.

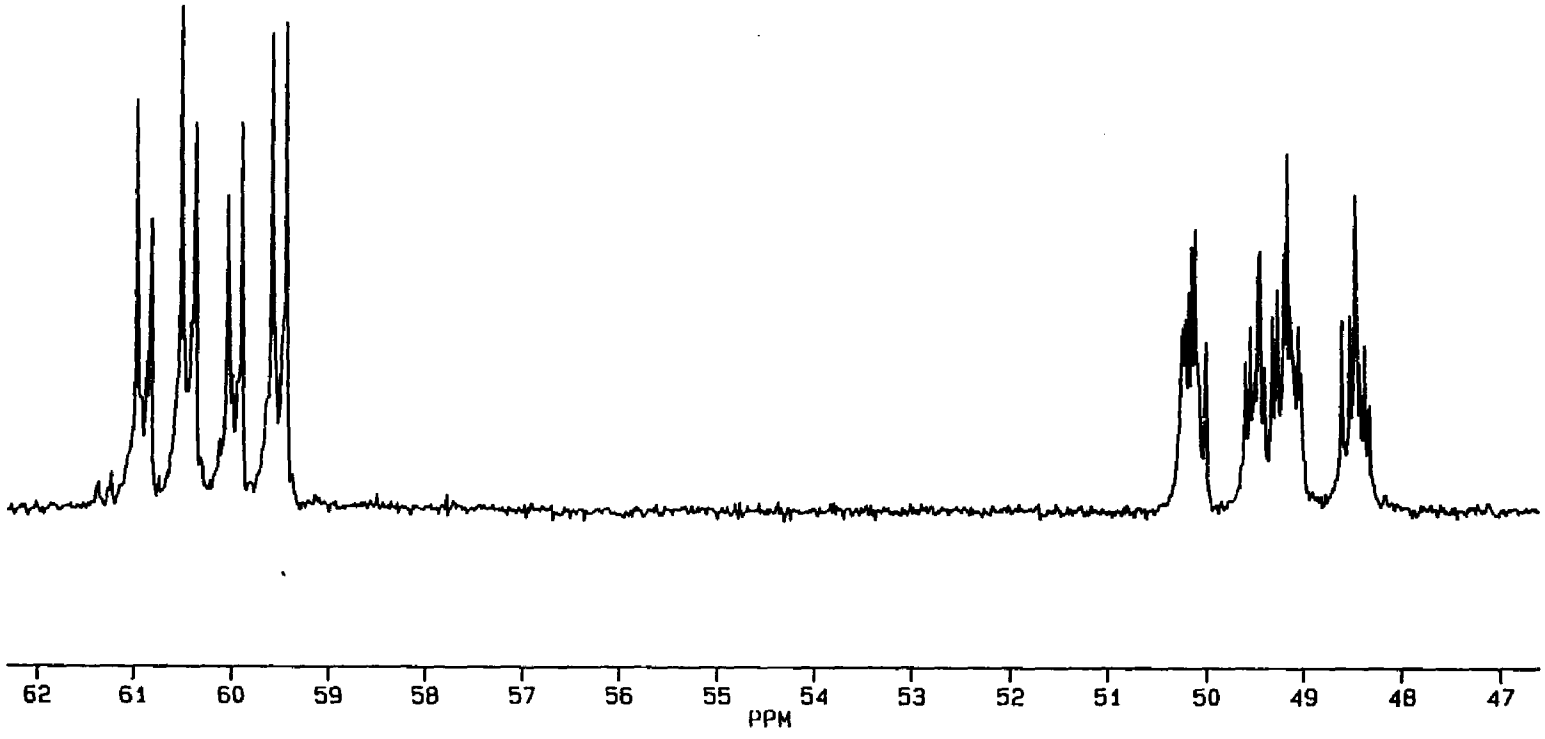

Figure 15: The $^{31}P\{^{1}H\}$ NMR of the diastereomeric mixture of $[Rh_2(NBD)_2(eLTTP)](BF_4)_2$ in CD_2Cl_2 (40.48 MHz).

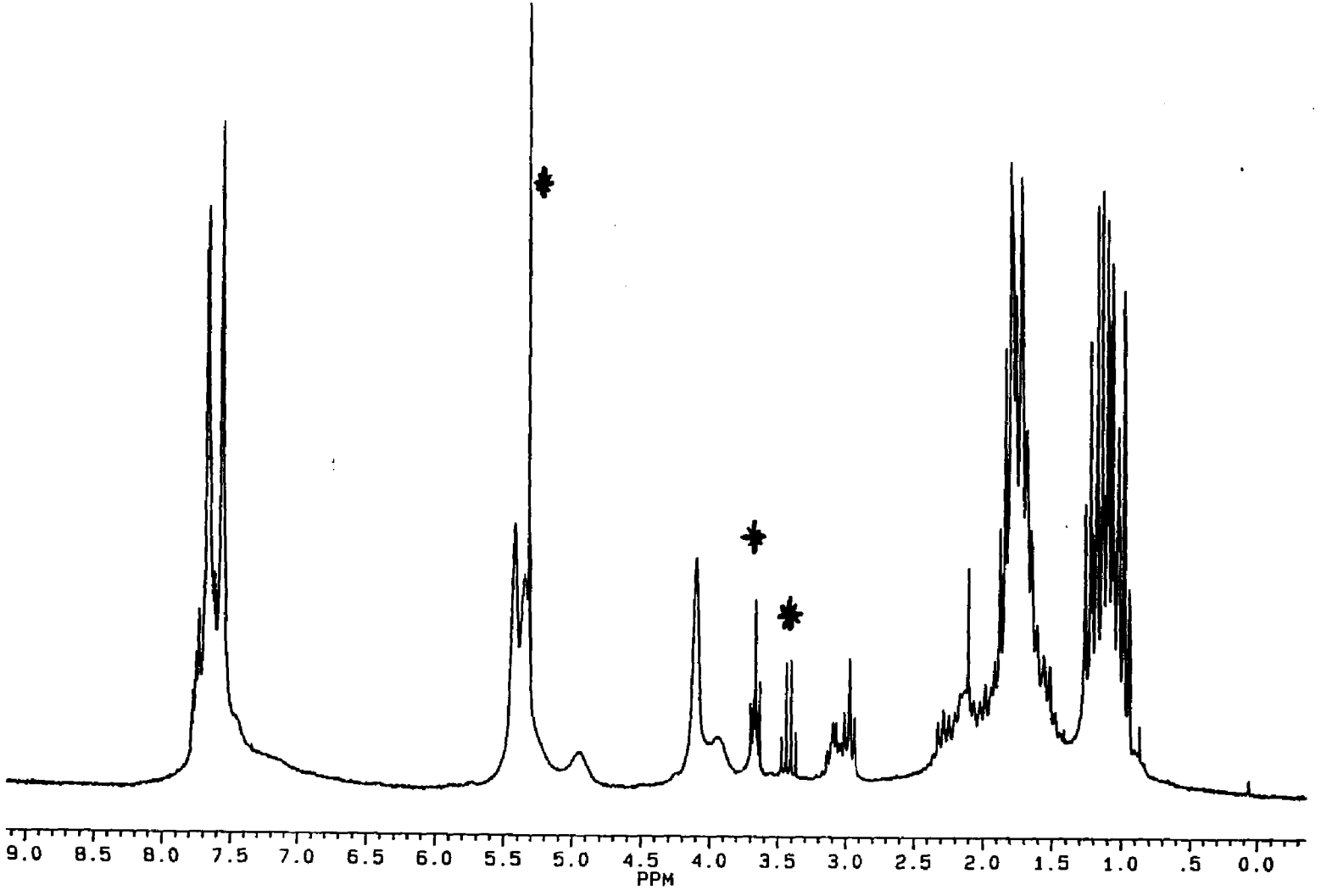

Figure 16: The ^1H NMR of the diastereomeric mixture of $[Rh_2(NBD)_2(eLTTP)](BF_4)_2$ in CD_2Cl_2 (200.13 MHz). Asterisked peaks are solvent impurities.

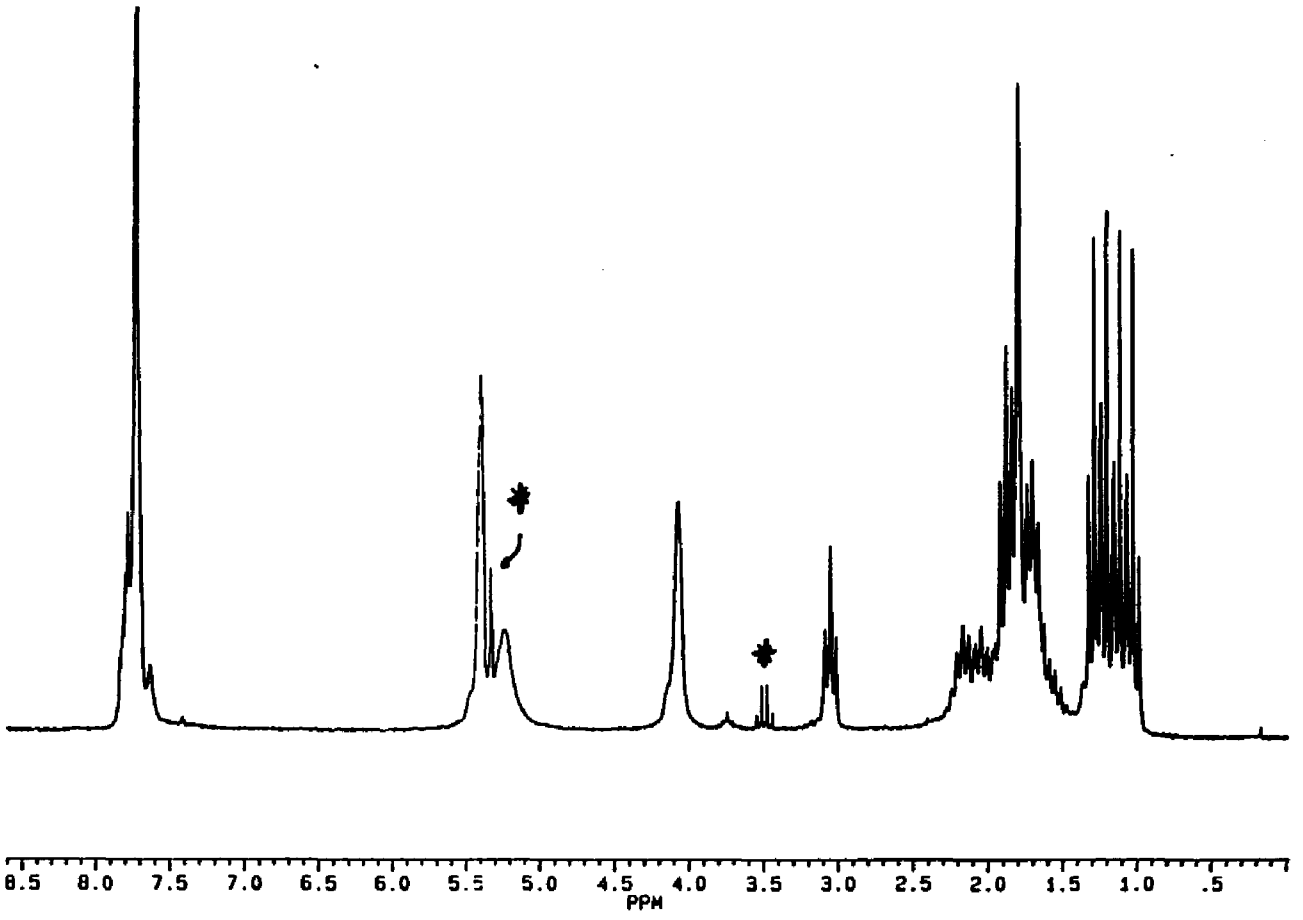

Figure 17: The ^1H NMR of the racemic diastereomer of $[Rh_2(NBD)_2(eLTTP)](BF_4)_2$ in CD_2Cl_2 (200.13 MHz). Asterisked peaks are solvent impurities.

In the ^1H NMR of $[Rh_2(NBD)_2(eLTTP)](BF_4)_2$, the spectra consist of a variety of multiplets. The chemical shifts of these multiplets are consistent with other bimetallic complexes based on eHTP and eLTTP including the broad singlets from norbornadiene. The protons of the ethylene bridge of the chelate ring and the methylene group of the terminal ethyl substituents are multiplets as well as the aromatic protons of the phenyl group on the internal phosphine. The chemical shifts are summarized in the experimental section.

The NBD ligands are seen by their resonances in the ^1H NMR (Figure 16). Resonances from the olefinic protons of NBD at δ = 5.22, 5.38 and 5.40 ppm (from *rac*- and *meso*- diastereomers of the ligand) appear as a broad singlets due to rotation of the ligand. At room temperature, the olefinic resonances on NBD appear to be near the coalescence temperature. An increase in temperature would increase the energy of the fluxional process, thus increasing the rotation of the NBD ligand about the rhodium atom on the NMR time-scale. The increased rotation should cause the olefinic protons to become equivalent which in turn will collapse the two broad singlets into a single sharp singlet.

The protons on the tertiary sp^3-hybridized carbons of NBD appear as a broad singlet at δ = 4.08 ppm. The signal is coincident for both diastereomers. The two protons on the secondary sp^3-hybridized carbon of norbornadiene appear as a broad singlet at δ = 1.75 (*meso*-) and 1.80 (*rac*-) ppm. The resonances are broad again due to fluxional ligand (NBD) rotation.

In $Ni_2Cl_4(eLTTP)$, the protons on the central methylene carbon are magnetically different for the two diastereomeric forms[9b] (See Section 3.2). The ^1H NMR of $[Rh_2(NBD)_2(eLTTP)](BF_4)_2$ shows coupling patterns of the central methylene protons very similar to those of the nickel system. In the *rac*-$[Rh_2(NBD)_2$-

(eLTTP)]$(BF_4)_2$ complex, the resonance is a triplet (δ = 3.27 ppm, $J_{P\text{-}H}$ = 7.42 Hz) due to the coupling of two equivalent internal phosphorus atoms. The protons of the central methylene carbon are magnetically inequivalent for the *meso*-[Rh_2-$(NBD)_2$(eLTTP)]$(BF_4)_2$ complex resulting in a closely spaced doublet of triplets (δ = 3.10 ppm, $J_{P\text{-}H}$ = 7.72 Hz and $J_{H\text{-}H}$ = 3.99 Hz).

The ^1H NMR of crystalline [$Rh_2(NBD)_2$(eLTTP)]$(BF_4)_2$ (Figure 17, previous page) shows that only the racemic diastereomer is present. Resonances resulting from a meso diastereosmer are not observed in this spectrum, and the only resonance seen is a triplet pattern for the protons of the central methylene carbon. There are no resonances from the protons on the central methylene carbon of the meso diastereomer. Small amounts of the pure racemic diastereomer of [Rh_2-$(NBD)_2$(eLTTP)]$(BF_4)_2$ can be obtained by careful crystallization.

Elemental analysis of [$Rh_2(NBD)_2$(eLTTP)]$(BF_4)_2$ was performed and in view of other experimental evidence agreed satisfactorily with the theoretical value (listed in the experimental section).

Chapter 5 Hydroformylation studies

Section 5.1 Introduction

Hydroformylation is the transition metal catalyzed conversion of olefins into aldehydes by the addition of synthesis gas (H_2/CO). Two aldehyde products can typically be formed during the hydroformylation of terminal olefins: the linear straight chain aldehyde (normal) and the branched aldehyde product (iso) as shown in Scheme 2 (next page). The ratio of linear aldehyde versus the branched aldehyde is called the selectivity . Hydroformylation is the second largest homogeneous process in the world in which over 10 billion pounds of aldehydes are produced every year. Aldehydes are important intermediates in a variety of processes such as the production of alcohols, lubricants, detergents, and plasticizers.

A number of transition metal complexes can be used to homogeneously catalyze hydroformylation; however, cobalt and rhodium have been extensively used and studied based on their reactivities and selectivities. Cobalt, which was the first transition metal used industrially, is still used today. The unmodified cobalt process uses no ligands, aside from H_2 and CO, and the active catalyst is $HCo(CO)_4$ which can be easily produced from $Co_2(CO)_8$, cobalt salts (e.g. cobalt acetate), or cobalt metal. Relatively severe reaction conditions of 120-180° C (high temperatures needed to maintain a reasonable rate) and 250-350 atmospheres of H_2/CO (high pressures needed to keep the hydride and carbonyl ligands coordinated on the metal) are required to stabilize the hydrido cobalt carbonyl species. The product mixture of this process starting with terminal olefins contains *ca.* 80% aldehydes with a selectivity of 3-4:1 linear to branched ratio, *ca.* 10% alcohols, *ca.* 1% alkanes, and *ca.* 9% other products based on 0.1-1.0% metal concentration (relative to alkene). Isomerization of the olefin is prevalent during the reaction. In fact the

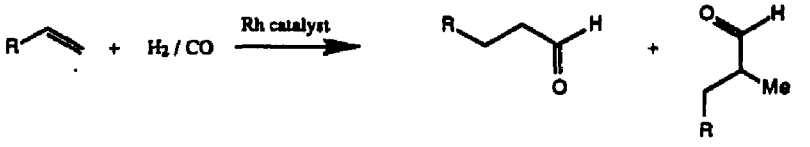

Scheme 2: The general reaction of hydroformylation.

same product ratios are obtained when using 3-hexene as the starting feedstock.[26]

The ligand modified cobalt catalyst (the Shell process) system containing an alkyl tertiaryphosphine, e.g. PBu_3, is more stable than the unmodified system. Slighly different reaction conditions are equired: H_2/CO pressures ranging from 50-100 atmospheres at temperatures of 160-200° C are typical. Higher selectivities in the range 6-8:1 linear to branched are also found relative to the unmodified system. However, the products produced are mainly alcohols (*ca.* 80%), alkanes (*ca.* 15%), and other products (*ca.* 5%). A decrease in activity of the ligand modified system is another drawback. At 145° C hydroformylation for the unmodified $HCo(CO)_4$ system is five times faster than the ligand modified system at 180° C.[26]

Ligand modified rhodium systems have been found to be very active hydroformylation catalysts. Several tertiary-phosphine rhodium precursors can be used to form the active catalyst $HRh(CO)_2L_2$ (L = PBu_3 or PPh_3). The Rh/PPh_3 catalyst system is commercially used today and is licensed by Union Carbide. The rhodium systems are both more stable and active than the related cobalt systems and require very mild reaction conditions (H_2/CO in the range of 1-25 atm at 25-120° C) and low catalyst concentrations (10^{-2}-10^{-3} % metal/olefin). Although rhodium is approximately 3500 times more expensive than cobalt, the cost of rhodium is compensated by its higher activity (10^3-10^4) and selectivities (10-14:1). Aldehydes are

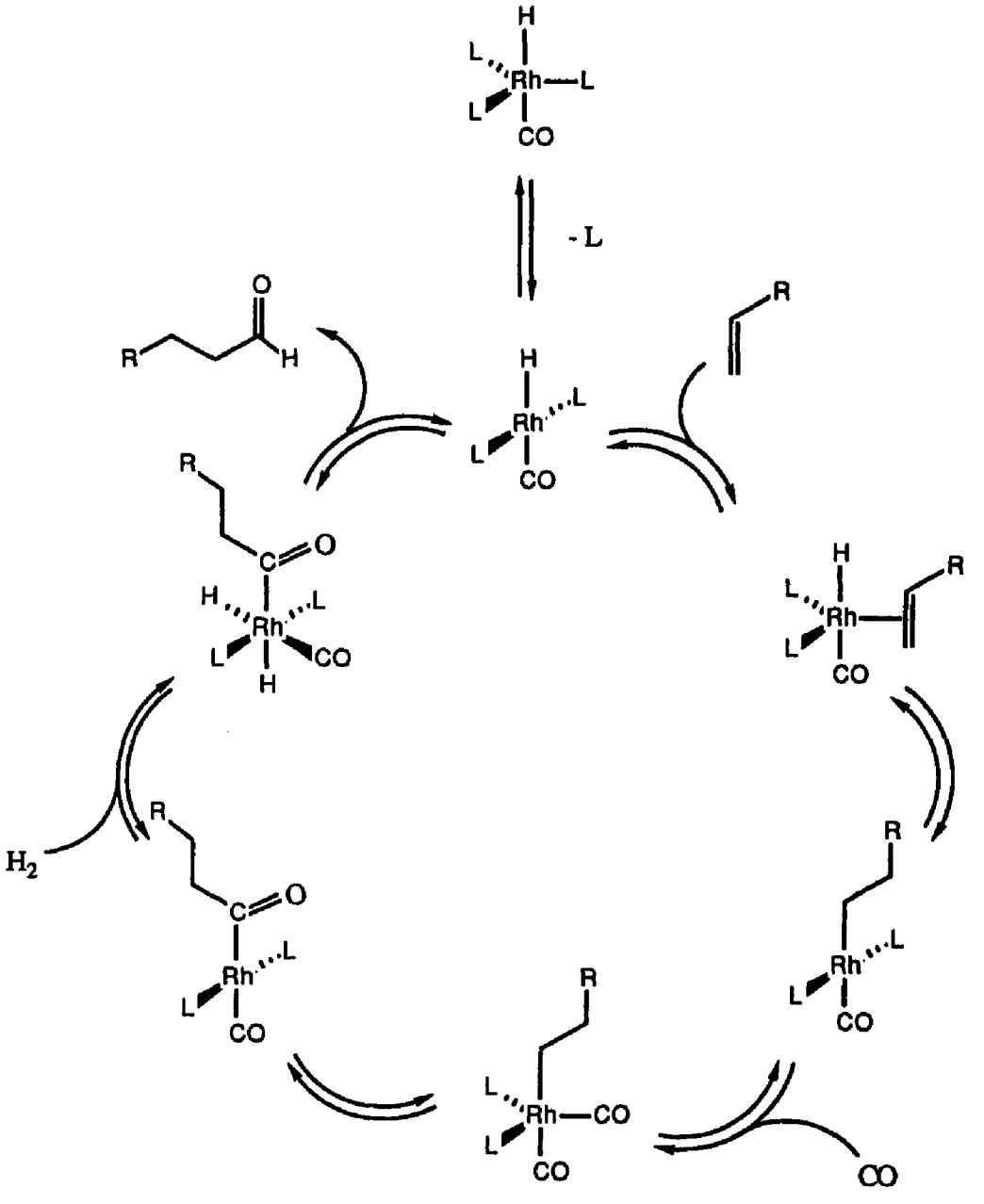

Figure 18: Mechanism of hydroformylation of a terminal olefin by a rhodium-phosphine catalyst (L = triphenylphosphine) showing the production of a linear aldehyde.

very selectively produced (ca. 96%) with little or no side products (alcohols, 0%; alkanes, 2%, other products 2%).[26]

The mechanism of hydroformylation , which has been studied thoroughly, contains all intermediate steps in equilibrium (Figure 18). The process begins by the initial π coordination of the olefin. A hydride on the metal can transfer to either carbon atom of the olefin to form an alkyl-metal intermediate. A carbon monoxide ligand can coordinate and insert into the alkyl-metal bond forming an acyl group on the metal. Oxidative addition of H_2 followed by the reductive elimination of one of the hydride ligands and acyl group leads to the formation of aldehyde product. Since all intermediates are in equilibrium, isomerization of a terminal olefin to an internal olefin can occur by a number of steps: initial hydride transfer to the α-carbon of the olefin to form the branched alkyl-metal intermediate which can now form an internal olefin by ß-elimination of a hydrogen atom from the γ-carbon, or by back-reaction of the aldehyde (the reverse of the catalytic cycle).[26]

The hydroformylation mechanism in Figure 18 only involves a single metal center. However, several examples in the literature suggest that hydroformylation of alkenes may also occur through a bimetallic reductive elimination of the aldehyde.[26c] Heck and Breslow, for example, proposed a mechanism[27] shown in Figure 19 using $HCo(CO)_4$ system to propose two possible routes for the final reductive/elimination of the product aldehyde from the catalyst. The first route consisted of the traditional oxidative addition of H_2 to the cobalt-acyl complex to form the dihydride metal complex, which then goes on to form an aldehyde and $HCo(CO)_3$ by reductive elimination. The second route uses a second mole of $HCo(CO)_4$ as the hydrogen source, in which the aldehyde is formed by an intermolecular hydride transfer reductive elimination, and formation of a Co-Co bond. The

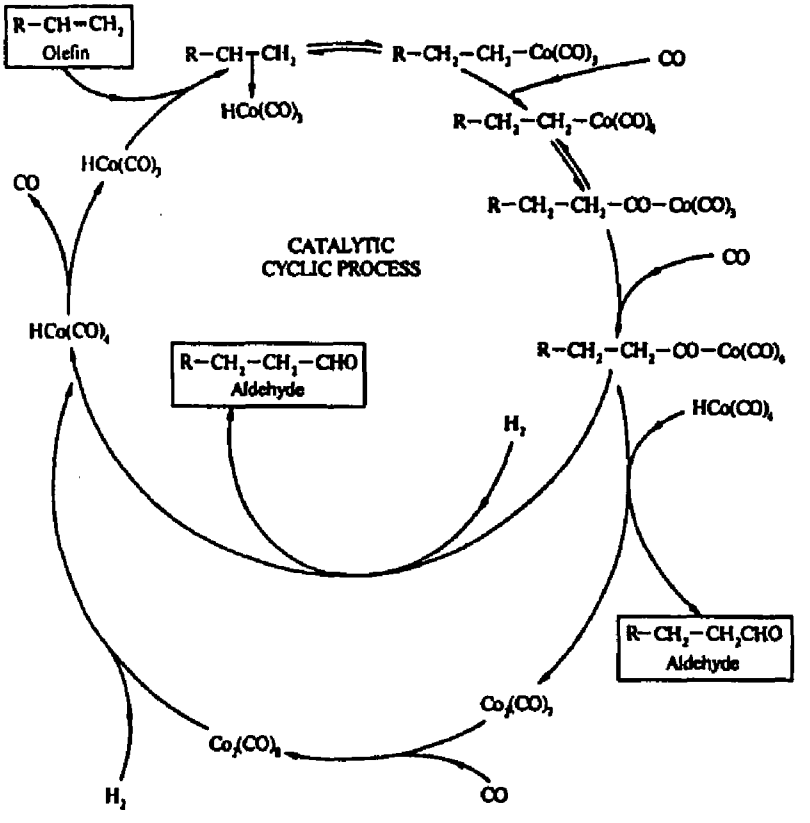

Figure 19: The Heck-Breslow mechanism of hydroformylation based on a cobalt carbonyl system.

catalytic cycle is completed upon the addition of H_2 to break apart $Co_2(CO)_8$ to form two moles of $HCo(CO)_4$. There have also been several reports on the effects of heterobimetallic homogeneous catalysts on the rate and selectivity of hydroformylation reactions.[28] Marko and coworkers have proposed that the rate-limiting step in their mechanistic study of the $HCo(CO)_4/HMn(CO)_5$ stoichiometric system is the bimolecular reaction of an unsaturated cobalt acyl with the manganese hydride to give a binuclear elimination of the aldehyde product.[29] Bimetallic eLTTP complexes could be well suited for the study of bimetallic cooperativity in hydroformylation.

Section 5.2 Hydroformylation of 1-Hexene

Initial studies using $Rh_2Cl_2(CO)_2$(eLTTP) show that it can act as a hydroformylation catalyst. Many hydroformylation results of $Rh_2Cl_2(CO)_2$(eLTTP) appear similar to those observed in related chelated-bisphosphine monometallic Rh(I) complexes. Hydroformylation studies with 1-hexene showed that $Rh_2Cl_2(CO)_2$-(eLTTP) has catalytic activity, although it is quite slow (< 0.05 turnovers/hr at ambient conditions). The catalyst activity can be increased by the abstraction of two chloride ligand using $TlPF_6$ (0.48 turnovers/hr at ambient conditions). Increasing the pressure and temperature further increases the catalytic activity of $Rh_2Cl_2(CO)_2$-(eLTTP). The Cl^- abstracted-$Rh_2(CO)_2(eLTTP)^{2+}$ system complex converted 48.3% of 1-hexene into aldehyde (59.1 turnovers/hr) in 14.5 hrs at 80 °C and 350 psi H_2/CO. Most surprisingly, the normal/iso ratio of the aldehyde product was found to be 18:1. This selectivity surpasses that of the vast majority of monometallic $HRh(CO)L_3$ catalysts with mono and bisphosphine ligands typically which give linear/branched ratios in the range of 1.3-16:1.[30]

The presence of the chloride ligand in $Rh_2Cl_2(CO)_2$(eLTTP) decreases the rate of hydroformylation compared to the complex from which Cl^- has been abstracted. This is consistent with other Rh-based hydroformylation catalyst in which halide ligands are well known to strongly inhibit the hydroformylation reaction.[26a] The presence of the chloride ligand in $Rh_2Cl_2(CO)_2$(eLTTP), coupled with low synthetic yields, led us to the synthesis of $[Rh_2(NBD)_2(eLTTP)](BF_4)_2$, which was found to be an excellent hydroformylation catalyst precursor.

This new norbornadiene substituted eLTTP-based bimetallic rhodium cation complex readily converted 1-alkenes into aldehydes. In our preliminary studies, the reaction conditions were varied in order to find the optimum rates and selectivities for linear aldehyde formation. At this time the majority of the reactions in this study were performed at 80 °C and 80 psi (of a 1:1 mixture of H_2/CO) for comparison with other systems that have been reported.

The hydroformylation of 1-alkenes with $[Rh_2(NBD)_2(eLTTP)](BF_4)_2$ was studied using the apparatus in Figure 20. The reactions were carried out in 450 mL or 600 mL glass-lined Parr autoclaves. Each autoclave was connected to a pressure regulator and a one liter external gas reservoir. The regulator maintains a constant pressure in the autoclave at all times. The external gas reservoirs are initially charged from a large gas cylinder containing a 1:1 mixture of H_2/CO. A computerized controller supplied by Parr controlled, monitored and recorded the following variables: the temperature and pressure of the gas in the one liter external gas reservoir and the temperature and the stirring rate (RPM's) of the autoclave. The data recorded by the controller were then transferred to a personal computer in which reaction rates were calculated. The turnover rates were calculated by converting the gas consumption into moles of aldehyde produced over a given period of time using the

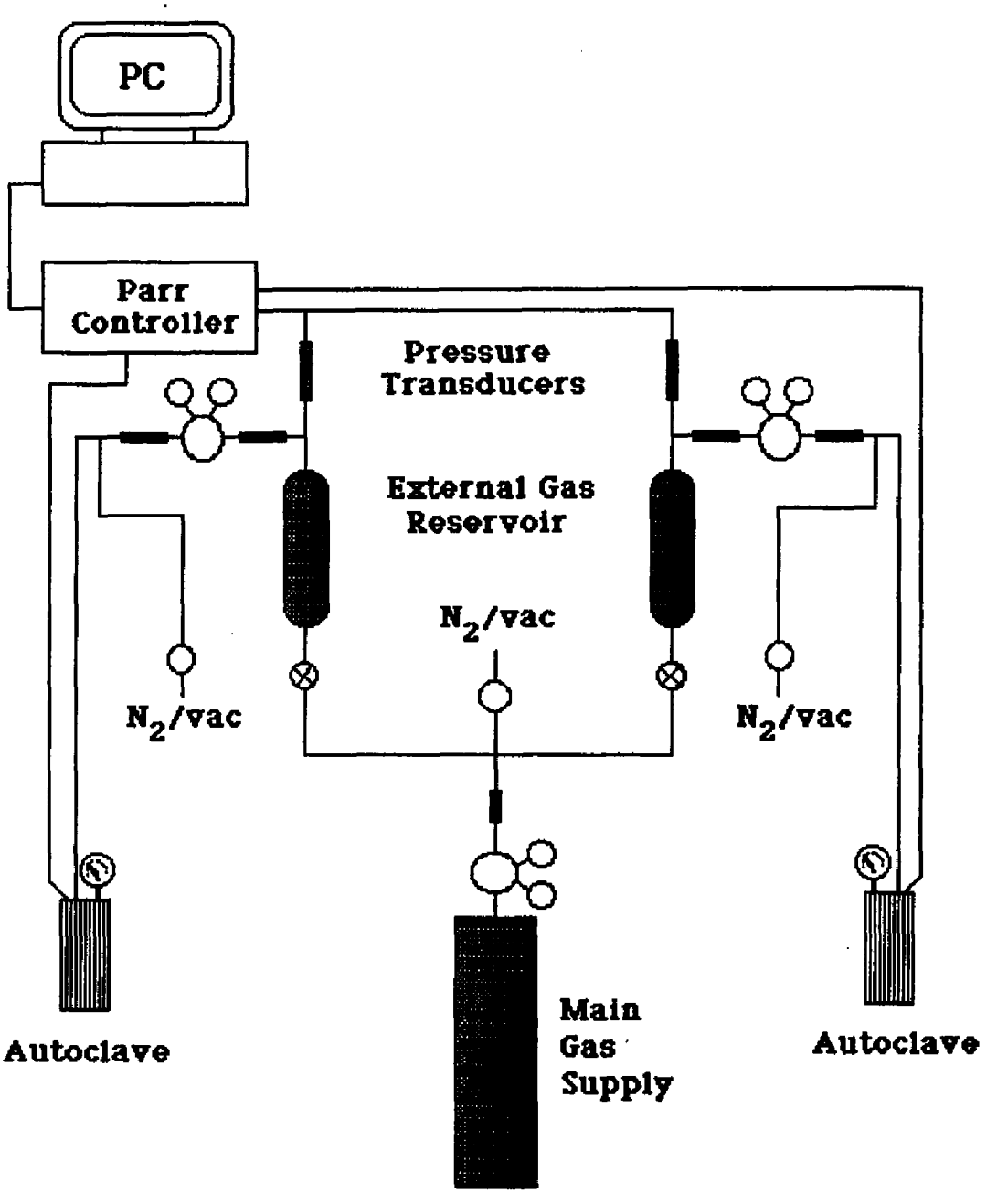

Figure 20: Schematic view of laboratory apparatus to perform hydroformylation reaction.

ideal gas law. The reaction products were analyzed by ^1H NMR spectroscopy and GC analysis. Further experiments with $[Rh_2(NBD)_2(eLTTP)](BF_4)_2$ are clearly needed to fully understand and optimize the hydroformylation conditions for this new bimetallic catalyst. The data presented here are preliminary.

At 80 °C and 80 psi $[Rh_2(NBD)_2(eLTTP)]2BF_4$ was an excellent catalyst for hydroformylating 1-hexene with acetone as the solvent. The initial rate of hydroformylation under these conditions was 735 turnovers/hr.[31] As olefin is being consumed the reaction rate naturally drops off as aldehyde is produced in a closed system. The increasing aldehyde concentration also begins to effectively compete with the olefin for coordination sites at the metal. The aldehyde can re-enter the catalytic cycle by back reaction (oxidative addition) onto the metal.

The selectivity of the aldehydes produced is remarkably high. Initially at 80° C and 80 psi $[Rh_2(NBD)_2(eLTTP)](BF_4)_2$ has a linear to branched ratio of 30:1! The selectivity of the catalyst drops to about 24-28:1 in the latter stages of the run. The cause for this drop in selectivity will be discussed later. Along with the aldehydes being produced, isomerization of the terminal olefin to an internal olefin can occur. $[Rh_2(NBD)_2(eLTTP)](BF_4)_2$ produces only a 5-14% of isomerized alkenes at 80°C and 80 psi. No alcohol or alkane products are observed which is consistent with that seen in other Rh(I) hydroformylation systems.[34]

Isomerization to an internal alkene can occur since the hydroformylation mechanism can proceed forward or backwards due to the equilibration of all intermediates (Fig. 18). At high concentrations of aldehyde, the equilibrium can shift to favor decarbonylation in which the metal complex reacts with the aldehyde to form the acyl-metal hydride complex. The rate-determining step in the hydroformylation mechanism based on $RhH(CO)(PPh_3)_3$ is believed to be the final hydride transfer

Table VI: The effects of temperature and pressure in hydroformylation catalysis of 1-hexene using $[Rh_2(NBD)_2(eLTTP)]^{2+}$ with a 1:1 mixture of H_2:CO.

Temp.(°C)	Pressure (psi)	TO/hr[a]	l/b (% isom.)[b]
25	80	11	3:1 (3%)
60	80	150	30:1 (4-8%)
70	80	450	25:1 (14%)
80	80	740	30:1 (8-14%)
90	80	930	30:1 (24%)
100	80	520	13:1 (75%)
80	40	160	13:1 (25%)
80	60	470	23:1 (15%)
80	80	780	30:1 (8-14%)
80	100	570	20:1 (8%)
80	120	530	15:1 (9%)
80	160	320	10:1 (12%)
80	200	240	7:1 (71%)
80	240	220	7:1 (37%)

[a] Initial turnover number (TO) for catalytic run on a per mole basis, calculated for the first 1-2 hours once the reaction begins. Solvent for all runs was acetone.
[b] Ratio of linear to branched aldehyde products and the amount of alkene isomerization (%-isom.), observed at the end of the run is given in parentheses, were determined from an average of three GC and ^1H NMR runs.

to form the aldehyde.[32,33] Since the other steps in the mechanism are believed to be faster, all intermediates are quickly produced upon decarbonylation of the aldehyde.[34]

The rate of hydroformylation depend strongly on temperature, as shown in Table VIII. As is with most systems, an increase in temperature will increase the turnover rate of the catalyst. At 25 °C and 80 psi $[Rh_2(NBD)_2(eLTTP)](BF_4)_2$ had an initial turnover rate of 11 turnovers/hr and only 2% aldehyde conversion after 36 hours. Not only was the aldehyde production low, but the amount of alkene isom-

erization was also low. After 36 hours, there was only 3% isomerization to the internal alkene. The selectivity of the aldehydes formed at room temperature was a poor 3:1 linear to branched. Brown and coworkers[35] reported that the branched product is favored at low temperatures.

As the temperature is increased (with the pressure held constant at 80 psi) from 60° to 70°C, the initial rate increases nearly threefold to 450 turnovers/hr, while the selectivity remains nearly unchanged. At a temperature of 90 °C the initial rate peaks at 930 turnovers/hr then begins to drop at 100 °C to 450 turnovers/hr due to competition with alkene isomerization. The general trend of rate increase and then decrease with increasing temperature is generally consistent other monometallic hydroformylation systems.[36]

The amount of alkene isomerization also increased with temperature. Both hydroformylation and isomerization are possible catalytic routes, however, at lower temperatures hydroformylation is faster than isomerization seen in Table VI. As the temperature increased to 90 °C, the rate of hydroformylation increased faster than isomerization. Above 90 °C, however, the rate for alkene isomerization, in general, becomes faster than the rate of hydroformylation as seen in the percentage of internal alkene isomerization, which increased from nearly 0 to 75% when the temperature increased from 25 to 100 °C. One problem related to the increase in isomerization may be to the lack of sufficient stirring. An excess of CO in solution is favored by poor stirring because CO is more soluble in solvents than H_2. If H_2 is not available to add to the metal-acyl (thus continuing the catalytic cycle), then rapid rearrangement of the acyl group on the metal back to an internal olefin can occur since the previous steps in the mechanism are fast and reversible.

The rate of hydroformylation also depends on H_2/CO pressure. At 80 °C

the pressure of the 1:1 H_2/CO mixture was varied from 40 to 240 psi which is also shown in Table VIII. The optimum pressure was between 80-200 psi. A pressure of 80 psi was chosen initially as the optimum since (*i*) the selectivity of the aldehyde produced is high and (*ii*) a comparison can be made between this system and other systems previously published.[32,36] Increased pressure caused the hydroformylation rate to decrease which is consistent with other studies involving a variety of rhodium catalysts. When the partial pressure of CO is increased there is a shift in equilibrium to favor $HRh(CO)_2P_2$ (P = a tertiary phosphine) which is now a saturated 18 electron complex. In order for catalysis to continue, either a CO or a phosphine ligand must dissociate to allow the coordination of the alkene. The high partial pressure of CO will retard any CO dissociation and thus slow the rate of hydroformylation and allow isomerization to dominate.

The turnover rate and selectivity of $[Rh_2(NBD)_2(eLTTP)](BF_4)_2$ compares well to other systems. Currently the Union Carbide Rh/PPh_3 catalyst is the dominant Rh-based hydroformylation process. Trial hydroformylation runs of 1-hexene using the $Rh(CO)_2(acac)/PPh_3$ system were performed under the same conditions as those used for $[Rh_2(NBD)_2(eLTTP)](BF_4)_2$ (80° C, 80 psi of a 1:1 mixture H_2/CO, and acetone as the solvent). As in industrial conditions, the trial runs were performed with a 950 fold excess of triphenylphosphine, PPh_3, with respect to the metal.[37] The results obtained with this commercial monometallic system were 850 turnovers/hr, a selectivity of 14:1, and about 4% isomerization (Table VII).

In the commercial system, the active catalyst $RhH(CO)(PPh_3)_2$ needs a large excess of PPh_3 for two reasons: metal stabilization and selectivity enhancement of the aldehydes produced. The stabilization of the metal center during catalysis is

Table VII: Hydroformylation Catalysis for 1-hexene at 80° C and 80 psi of a 1:1 mixture of H_2:CO.

Catalyst	L/Rh[a]	TO/hr[b]	l/b (% isom.)[c]
$[Rh_2(NBD)_2(eLTTP)]^{2+}$	0.5:1	740	30:1 (8-14%)
$[Rh(NBD)(depmpe)]^{+}$ [d]	1:1	10	2-5:1 (80-90%)
$[Rh(NBD)(dedppe)]^{+}$ [e]	1:1	8	2-3:1 (80-90%)
$[Rh(NBD)(depe)]^{+}$ [f]	1:1	9	3-4:1 (40-60%)
$HRh(CO)(PPh_3)_3$ [g]	10:1	4900	4:1 (10%)
$HRh(CO)(PPh_3)_3$	950:1	850	14:1 (~4%)

[a] Phosphine ligand to rhodium ratio. [b] Initial turnover number (TO) for catalytic run on a per mole basis and calculated for the first 1-2 hours once the reaction begins. Solvent for all runs was acetone. [c] Ratio of linear to branched aldehyde products and the amount of alkene isomerization (%-isom.), observed at the end of the run is given in parentheses, were determined from an average of three GC and ^1H NMR runs. [d] depmpe = $Et_2PCH_2CH_2P(Me)Ph$. [e] dedppe = $Et_2PCH_2CH_2PPh_2$. [f] depe = $Et_2PCH_2CH_2PEt_2$. [g] Estimated from the work of Hughes and Unruh.

accomplished through the σ-donor ability (basicity) of the phosphine ligand. The basicity of arylphosphines is less than that of alkylphosphines due to the electron-withdrawing effect of the aromatic group which makes the ligand coordination facile. In conventional hydroformylation, rhodium complexes with aryl-phosphine ligands (and also phosphite ligands, which have similar or lower basicities relative to aryl-phosphines) are highly reactive compared to rhodium complexes with alkyl-phosphines due to facile dissociation of the aryl-phosphine. In fact, the electrophilic rhodium centers are so reactive that they can break P-C (aryl) bonds of a coordinated ligand. When a P-C (aryl) bond is broken, the phosphine ligand is converted into an anionic phosphide ligand which can form bonds with two transition metals (Figure 21). In the commercial process, a large excess of ligand is needed to stabilize the homogeneous catalyst inhibiting unreactive rhodium phosphide cluster

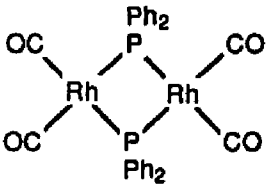

Figure 21: Possible complex of many unreactive polyphosphide rhodium products resulting from ligand degredation during hydroformylation.

formation which decreases the rate of hydroformylation.[32]

The use of electron-rich alkyl-phosphines, which coordinate strongly to the metal center, will increase the electron density on the rhodium atom decreasing its electrophilic character which should prevent ligand degradation reactions. The electron-rich alkyl-phosphines, unfortunately, also influence the reactivity of rhodium complexes in hydroformylation by making them poor catalysts. The hydroformylation rates become very slow with poor linear to branched ratios of 3-4:1 and increased olefin isomerization. The decrease in the rate is believed to result from the trapping of 16-electron intermediates in the catalytic cycle by coordination of CO. Dissociation of the CO will be slow because the increased electron density on the rhodium center will increase the Rh-CO bond strength by π^* backbonding. The initial interaction of the alkene with the electron-rich metal center to form a η^2-metal-olefin π-bond may also be slow because of the decreased electrophilic character of the metal.[32] In $HRh(CO)(PPh_3)_2$, the decrease in the electron donating ability of the aryl-phosphine ligands would enhance the electrophilic character of the catalyst making the initial coordination of the olefin faster.

PPh_3 is also a bulky ligand and the presence of two large PPh_3 ligands increases the steric interactions at the metal center enhancing the formation of the ster-

ically less encumbered linear alkyl intermediate which goes on to form the linear aldehyde product. Since PPh_3 is a facile ligand, a large excess of PPh_3 is needed to shift the equilibrium so that at least two ligands are coordinated for selectivity enhancement.

The practice of using excess ligand in catalysis for either improved stabilization or selectivity has its disadvantages. In the $HRh(CO)(PPh_3)_3$ system, the active and selective catalyst is proposed to be $HRh(CO)(PPh_3)_2$ which is formed in equilibrium by PPh_3 dissociation. Stabilization of the metal by increasing the concentration of the ligand will push the equilibrium toward the considerably less reactive $HRh(CO)(PPh_3)_3$. During a catalytic cycle substrates and ligands will always be in competition the for coordination sites of the metal center. High ligand concentrations with respect to the concentration of the substrate will cause a decrease in the overall rate due to the coordination site of the metal being blocked by a ligand. A decrease in the ligand to metal ratio should increase the rate of reaction. Hughes and coworkers[31] have shown that using $RhH(CO)(PPh_3)_3$ with a 10-fold molar excess of triphenylphosphine the initial rate is around 4900 turnovers/hr. This dramatic increase in rate is due to species such as $HRh(CO)_2(PPh_3)$ and $HRh(CO)_3$. Indeed, $HRh(CO)_3$ is an extremely active hydroformylation catalyst but only has a linear to branched selectivity of 1:1. The decreased ligand competition for coordination sites increases the rate of hydroformylation, but the selectivity of the aldehyde produced drops. The linear to branched ratio of the aldehydes in the case of 10:1 PPh_3:Rh was found to be 4:1, so for Rh/PPh_3 systems there is a trade-

$$HRh(CO)(PPh_3)_3 \underset{-PPh_3}{\overset{+CO}{\rightleftharpoons}} HRh(CO)_2(PPh_3)_2 \underset{-PPh_3}{\overset{+CO}{\rightleftharpoons}} HRh(CO)_3(PPh_3) \underset{-PPh_3}{\overset{+CO}{\rightleftharpoons}} HRh(CO)_4$$

off between high rates and high selectivities.

The reactivity of our bimetallic $[Rh_2(NBD)_2(eLTTP)](BF_4)_2$ catalyst precursor (740 turnover/hr) is similar to the commercial catalyst $RhH(CO)(PPh_3)_3$ (850 turnovers/hr), but the selectivity of our catalyst is higher (30:1 versus 14:1). The major differences between these two catalyst systems are ligand basicities and metal to ligand ratios. The commercial system requires an excess of triphenylphosphine to stabilize the catalyst and give good product selectivity, whereas $[Rh_2(NBD)_2(eLTTP)](BF_4)_2$ requires only one mole of the eLTTP tetratertiaryphosphine ligand. As mentioned previously, rhodium catalysts that use electron-rich alkyl-phosphines are almost always considered poor hydroformylation catalysts with low rates and selectivities. We are seeing quite the opposite with the eLTTP-based bimetallic $[Rh_2(NBD)_2(eLTTP)](BF_4)_2$ catalyst precursor. The high rate of hydroformylation using $[Rh_2(NBD)_2(eLTTP)](BF_4)_2$ is believed to be the direct result of bimetallic cooperativity between the two metal centers in the catalyst.

To determine if bimetallic cooperativity is occurring in our $[Rh_2(NBD)_2(eLTTP)](BF_4)_2$ system a comparison to an equal molar concentration (on a Rh basis) of a monometallic analog was done. In $[Rh_2(NBD)_2(eLTTP)](BF_4)_2$, the ligand is forming one five-membered chelate ring with each rhodium center with both halves bridged by a central methylene carbon. One can conceptually prepare an electronically analogous mono-metallic complex by simply breaking $[Rh_2(NBD)_2(eLTTP)](BF_4)_2$ in half. Replacing the central methylene carbon with a methyl

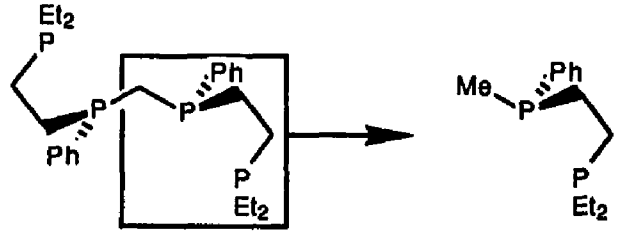

group creates a new bisphosphine monometallic complex that is electronically analogous to $[Rh_2(NBD)_2(eLTTP)](BF_4)_2$. The abbreviation for the new bisphosphine $Et_2PCH_2CH_2P(Ph)Me$ is depmpe for (diethylphosphino)(phenylmethylphosphino)ethane. The synthesis and characterization of the model ligands and their metal complexes are discussed in chapter 6.

Hydroformylation studies using the electronically analogous monometallic complex $[Rh(NBD)(depmpe)]BF_4$ showed that it is a very poor catalyst. When operating under the exact same conditions as the bimetallic complex $[Rh_2(NBD)_2$-$(eLTTP)](BF_4)_2$ (80° C, 80 psi, 1.95×10^{-5} moles of the Rh catalyst, acetone solvent), $[Rh(NBD)(depmpe)]BF_4$ had an initial rate of ~10 turnovers/hr and a selectivity of only 3.5:1 linear to branched aldehyde. The main problems with obtaining initial turnover rates in this system were a considerable induction period and large amounts of olefin isomerization. After 5 hours nearly 80% of 1-hexene is converted into 2- and 3-hexenes. These results obtained from [Rh(NBD)-(depmpe)]BF_4 are similar to other data for monometallic catalysts possessing electron-rich alkyl-phosphines.[32]

The low hydroformylation turnover rate and enhanced alkene isomerization of the other monometallic catalysts that contain electron-rich phosphines is probably caused by the coordination of an extra CO ligand to form the unreactive and stable 18 electron complex, $RhH(CO)_2P_2$ (P_2 = a five membered-chelate ring). The electron-rich metal strongly coordinates the CO ligands by π-backbonding which occupies a needed coordination site for hydroformylation. The oxidative addition of H_2 to form the acyl-metal dihydride complex is also believed to be a rate-determining step in hydroformylation.[33] If the decrease in electrophilicity due to alkylated phosphines can decrease the activity of the metal, then the formation of the dihydride

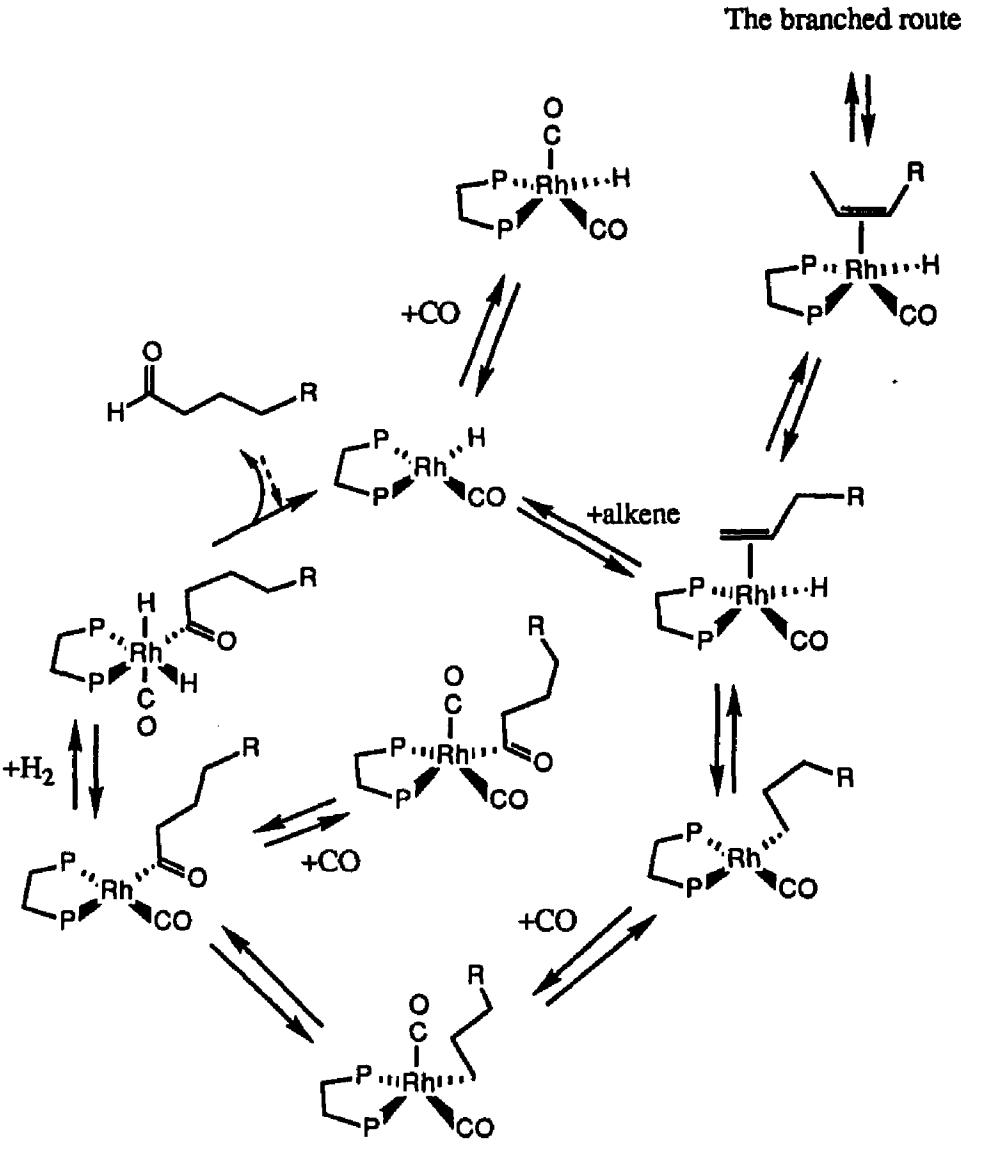

Figure 22: A hydroformylation mechanism for $HRh(CO)P_2$ (P_2 = a five-membered chelate bisphosphine) that includes 16-electon intermediates that are trapped by coordination of CO and an isomerization pathway that eventually leads to branched aldehyde product.

metal acyl complex would also be very slow (See Figure 22).[33]

Isomerization is a competing reaction during hydroformylation. At mild conditions, i.e. 80 °C and 80 psi, isomerization is slower than hydroformylation. Isomerization can dominate during hydroformylation if the rate of hydroformylation has decreased or stopped for the reasons described in the previous paragraph. Slow hydroformylation catalysts are usually fine isomerization catalysts due to the rapid and reversible steps in the hydroformylation mechanism.

The very low hydroformylation turnover rate of the monometallic complexes under identical conditions compared to $[Rh_2(NBD)_2(eLTTP)](BF_4)_2$ suggests that the increased activity of the bimetallic system is a direct result of bimetallic co-operation. Experiments with other monometallic analogs of $[Rh_2(NBD)_2$-$(eLTTP)](BF_4)_2$ such as $[Rh(NBD)(depe)]BF_4$ and $[Rh(NBD)(dedppe)]BF_4$ (where depe = $Et_2PCH_2CH_2PEt_2$, and dedppe = $Et_2PCH_2CH_2PPh_2$) clearly demonstrate that the metal is essentially deactivated and incapable of performing hydroformylation independently when a variety of alkyl-phosphines are used as ligands. Estimating the basicity of the internal phosphorus atom in $[Rh_2(NBD)_2$-$(eLTTP)]_2BF_4$ with respect to the monometallic model systems may be difficult. Therefore, a series of bisphosphine ligands, depe, depmpe, and dedppe, were synthesized and complexed with $[Rh(NBD)_2]BF_4$. This series constitutes a full spectrum of the basicities of the phosphine: from fully alkylated (very basic) to partially aromatic (less basic). The basicity of the internal phosphorus atom in eLTTP should fall somewhere in this series.

In order for $[Rh_2(NBD)_2(eLTTP)](BF_4)_2$ to behave as a bimetallic catalyst, the eLTTP ligand should be able to sterically access an anti-anti or partially closed-mode rotational orientation so that the metal atoms can be close together. VDW

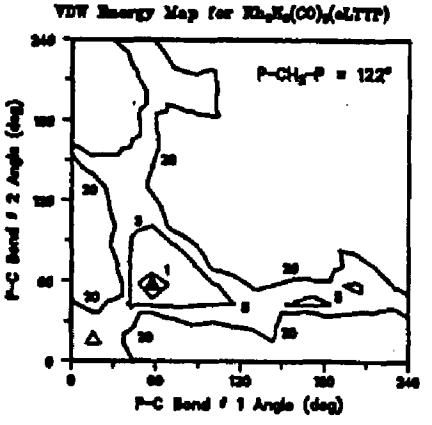

Figure 23: An expanded map of the van der Waals energy study of *rac*-$Rh_2H_2(CO)_2$(eLTTP). The solid triangle marks the global minimum of the study.

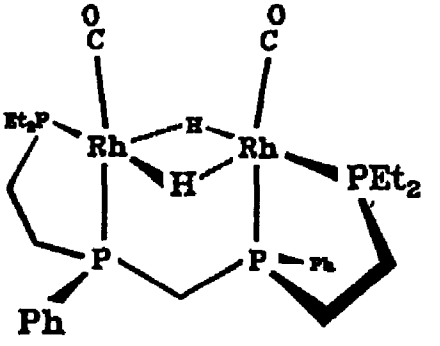

Figure 24: Computer generated *rac*-$Rh_2H_2(CO)_2$(eLTTP) similar to SYBYL open triangle conformation in Fig. 23.

energy studies using the coordinates of the $Rh_2Cl_2(CO)_2$(eLTTP) crystal structure have already provided evidence that a closed-mode rotational orientation is sterically accessible for square planar metal complexes. The active catalyst is proposed to be $Rh_2H_2(CO)_2$(eLTTP), which is produced from the precursor [Rh_2(NBD)$_2$-(eLTTP)](BF_4)$_2$. The modified crystal coordinates of $Rh_2Cl_2(CO)_2$(eLTTP) in which we substituted H for Cl (and used the correct Rh-H bond distance) were used for another VDW energy study.

The VDW energy study was performed as described for $Rh_2Cl_2(CO)_2$-(eLTTP) by calculating the VDW energies of the molecule at 5° rotational intervals of the two P_{int}-C bonds. The results of the VDW energy study of $Rh_2H_2(CO)_2$-(eLTTP) are shown in Figure 23. The VDW energy map shows a considerably larger area of low energy rotational conformations compared to the $Rh_2Cl_2(CO)_2$-(eLTTP) system (Figure 13, pg 39). This is not surprising since hydride is smaller than chloride. Most importantly, the hydride complex has a lower rotational energy

pathway to the closed mode conformer located at the origin of the VDW map.

Near the origin of the VDW energy contour map in Figure 23 an open triangle indicates a rotational geometry which possesses a local energy minimum. The structure of this rotational conformation can be calculated at this coordinate using SYBYL, and in this position the eLTTP ligand has rotated to allow the hydride on each rhodium atom to interact with the empty axial p_z orbital of the other rhodium center (Figure 24). This simple VDW energy study clearly indicates that the metal centers in $Rh_2H_2(CO)_2$(eLTTP) should be able to approach one another to do cooperative chemistry. Bridging hydrides have been well studied in the literature and are widely accepted both as ground state structures and as intermediates. The VDW energy calculation only measures the steric factors involved in rotations about the central methylene bridge and reveals nothing about the potential for forming chemical bonds between the hydrides and the empty p_z orbital of the neighboring metal atom. We have to use our chemical intuition to guide us in interpreting structure such as that shown in Figure 24.

The formation of a bridging hydride during the catalytic cycle is an important part of our proposed bimetallic cooperativity. Ligands such as hydrides and CO can be easily transferred from one metal to another. A proposed intermediate that

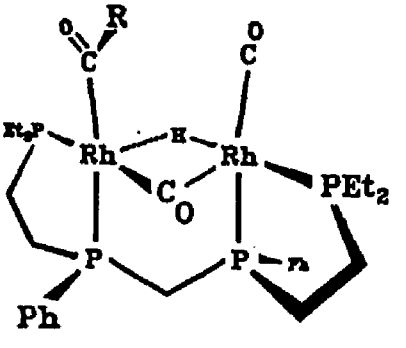

Figure 25: Proposed intemediate in the catalytic cycle.

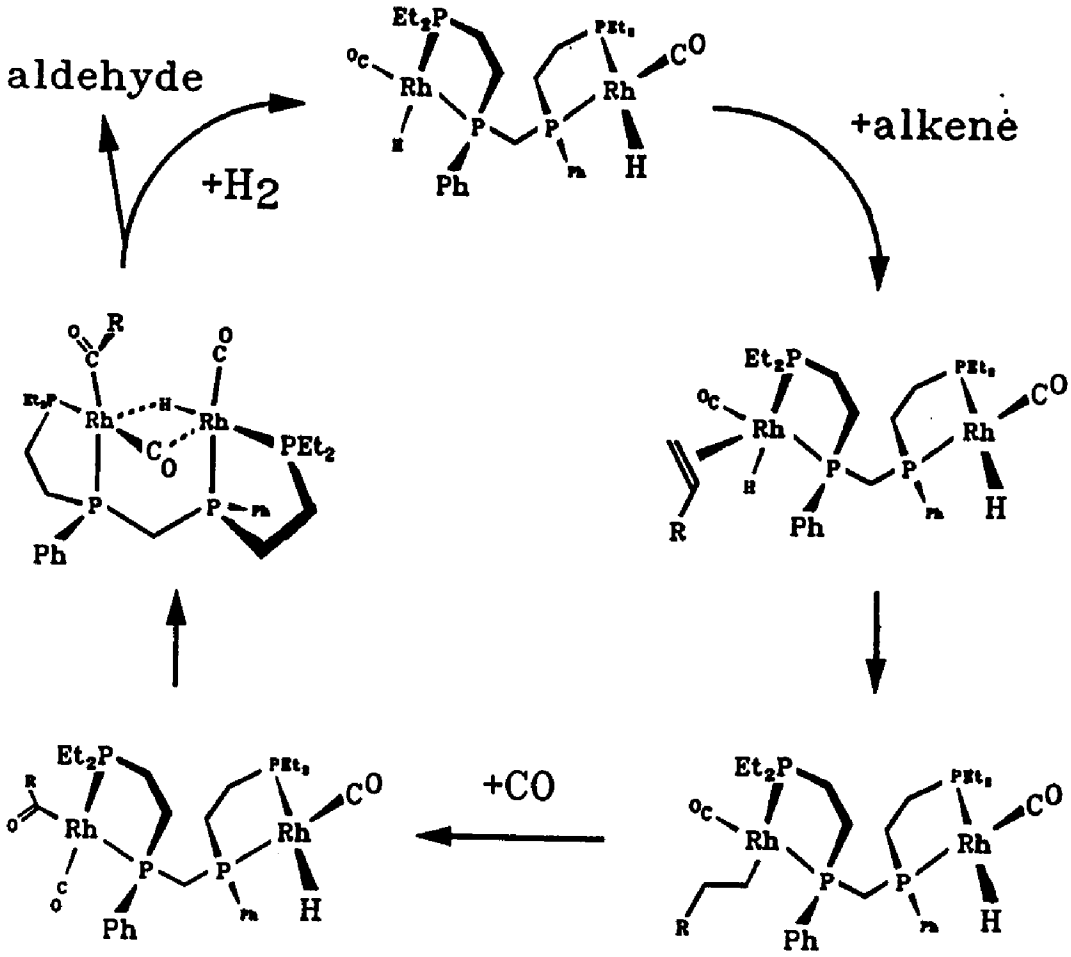

Figure 26: The full proposed bimetallic hydroformylation catalytic mechanism based on $Rh_2H_2(CO)_2$(eLTTP).

could exist in the Rh_2(eLTTP) hydroformylation cycle is shown in Figure 25. On one rhodium atom is an acyl group and a CO ligand produced from a traditional monometallic hydroformylation mechanism (see Fig. 18, p 30). The second rhodium atom contains a CO and a hydride ligand that is capable of bridging to the first metal center. Similar to the Heck-Breslow mechanism (Figure 19, lower cycle), a hydride can be transferred in an *intra*molecular fashion to drive the reductive elimination of the aldehyde product and the formation of a Rh-Rh bond. There is precidence of $[Rh_2(\mu\text{-}CO)_2(PPh_3)_4]$, which has two Rh(0) metal centers with a metal bond.[38] Following the Heck-Breslow mechanism, the Rh-Rh bond can be broken by the addition of H_2 thus completing the catalytic cycle to form the starting catalyst species $Rh_2H_2(CO)_2$(eLTTP) (Figure 26).

With the aid of an intramolecular hydride transfer, the bimetallic complex with electron-rich alkyl-phosphines is able to effectively perform hydroformylation catalysis. Without the cooperation of the second metal the turnover rates would be comparable with the poor rates seen in the monometallic model systems. Therefore, the turnover rates of the bimetallic system are calculated on a *per mole* basis of catalyst and not on a *per Rh atom* basis.

A simple structure-reactivity experiment can be performed to test the intramolecular hydride transfer idea. Increasing the distance between the two metals should eliminate the intramolecular hydride transfer step. Two new tetraphosphine ligands, eLTTP-pr and eLTTP-*p*-xyl, have been synthesized in order to increase the separation between the two rhodium atoms yet maintain the same basicity as eLTTP. The bimetallic rhodium complexes with the spacer group ligands, $[Rh_2(NBD)_2$(eLTTP-pr)$](BF_4)_2$ and $[Rh_2(NBD)_2$(eLTTP-*p*-xyl)$](BF_4)_2$ (discussed in chapter 6), were tested for hydroformylation.

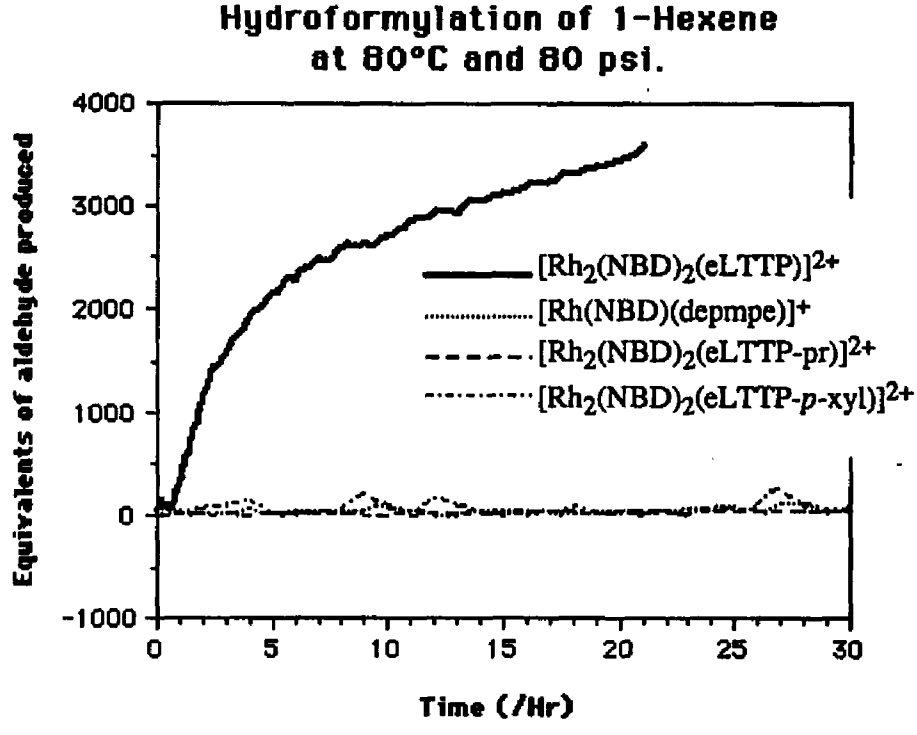

Figure 27: The hydroformylation of 1-hexene by several rhodium cationic phosphine complexes are graphed together by the number of equivalents of aldehyde produced per equivalent of catalyst versus time (/hours).

Figure 27 shows the number of equivalents of aldehyde produced by several hydroformylation catalysts employing electron-rich alkyl-phosphines: $[Rh_2(NBD)_2(eLTTP)](BF_4)_2$, the monometallic complex [Rh(NBD)(depmpe)]-BF_4, and bimetallic complexes with spacer-group ligands $[Rh_2(NBD)_2(eLTTP\text{-}pr)](BF_4)_2$ and $[Rh_2(NBD)_2(eLTTP\text{-}p\text{-}xyl)](BF_4)_2$. $[Rh_2(NBD)_2(eLTTP)](BF_4)_2$ is clearly the fastest catalyst. The bimetallic complexes with the spacer-group ligands and the monometallic complexes have very similar poor activities and selectivities.

The turnover rates, selectivities of aldehydes produced, and amount of alkene olefin isomerization are summarized in Table VIII (the following page). The

Table VIII: Qualitative structure reactivity analysis in Hydroformylation catalysis for 1-hexene at 80° C and 80 psi of a 1:1 mixture of H_2:CO.

Catalyst	TO/hr[a]	l/b (% isom.)[b]
$[Rh_2(NBD)_2(eLTTP)]^{2+}$	740	~30:1 (8-14%)
$[Rh(NBD)(depmpe)]^{+}$ [c]	10	2-5:1 (80-90%)
$[Rh_2(NBD)_2(eLTTP\text{-}pr)]^{2+}$	20	4:1 (94%)
$[Rh_2(NBD)_2(eLTTP\text{-}p\text{-}xyl)]^{2+}$	4	2:1 (95%)
$[Rh(NBD)(depe)]^{+}$ [d]	9	3-4:1 (40-60%)
$[Rh(NBD)(dedppe)]^{+}$ [e]	8	2-3:1 (80-90%)

[a] Initial turnover number (TO) for catalytic run on a per mole basis and calculated for the first 1-2 hours once the reaction begins. Solvent for all runs was acetone. [b] Ratio of linear to branched aldehyde products and the amount of alkene isomerization (%-isom.), observed at the end of the run is given in parentheses, were determined from an average of three GC and ^1H NMR runs. [c] depmpe = $Et_2PCH_2CH_2P(Me)Ph$. [d] depe = $Et_2PCH_2CH_2PEt_2$. [d] dedppe = $Et_2PCH_2CH_2PPh_2$.

initial turnover rate of $[Rh_2(NBD)_2(eLTTP\text{-}pr)](BF_4)_2$ has been calculated to be 20 turnovers/hr. This rate may seem high for a complex that is expected to behave similarly to other monometallic-type rhodium complexes that contain electron rich phosphines, but a very reasonable explanation to support this rate exists: the central propylene group can rotate to allow an orientation that may allow some intramolecular hydride transfers via bridging ligands to occur. These results are consistent with a trend reported by Sanger.[26c] By varying the concentration of a ligand $Ph_2P(CH_2)_nPPh_2$ (n = 4, 5) with respect to the metal (Rh, Co) an increase in hydroformylation activity was observed when the ligand to metal ratio was 0.5:1. Sanger suggests that the coincidence between the maximum activity and the L:M ratio is due to bimetallic cooperativity as a result of the ligand bridging two metals. Also, the ligand $Ph_2P(CH_2)_nPPh_2$, even with n = 3 which is similar to

$[Rh_2(NBD)_2(eLTTP\text{-}pr)](BF_4)_2$, is capable of obtaining a favorable rotational conformation so that the two metals are in proximity and can cooperate. In $[Rh_2(NBD)_2(eLTTP\text{-}pr)](BF_4)_2$, the turnover rate quickly decreases and isomerization dominates with a product aldehyde selectivity of 2:1 linear to branched.

As anticipated, $[Rh_2(NBD)_2(eLTTP\text{-}p\text{-}xyl)](BF_4)_2$ effectively separates the two metal centers and eliminates any possible intramolecular transfer as seen in the initial rate of 4 turnovers/hr. Essentially, each half of $[Rh_2(NBD)_2(eLTTP\text{-}p\text{-}xyl)](BF_4)_2$ is behaving as an isolated monometallic catalyst with electron-rich phosphines. The selectivity is 1.8:1, which is also very consistent with the monometallic model catalysts.

The rates and selectivities obtained from experiments involving the monometallic complexes and the bimetallic complexes with the spacer-group ligands were calculated in the early stages of each run. The amount of aldehyde produced after 24 hours is very small (<5%) and the majority of it is produced in the first 2 hours. Fast internal olefin isomerization processes (~50% conversion in 90 min.) consumes most of the terminal olefin. The results from the monometallic analogs, VDW energy studies, and the data obtained from experiments with the spacer-group ligands all strongly support the existence of a high level of bimetallic cooperativity in hydroformylation catalysis by our $[Rh_2(NBD)_2(eLTTP)](BF_4)_2$ complex.

Although the increase in turnover rate with the bimetallic catalyst was anticipated (but not to the extent observed!), the high product selectivity to linear aldehyde using $[Rh_2(NBD)_2(eLTTP)](BF_4)_2$ was not. In hindsight, however, the dramatic increase in linear aldehyde selectivity observed with $[Rh_2(NBD)_2(eLTTP)](BF_4)_2$ may results from intramolecular steric effects. It is generally well

recognized that steric factors are primarily responsible for the selectivity in monometallic hydroformylation catalysts. Two bisphosphine ligands developed by Union Carbide[34d] and Eastman Kodak[34c] create extremely crowded environments about the metal center (Figure 28). The selectivities using these ligands in the hydroformylation of propylene are 79:1 and 54:1, respectively.

The first step in the hydroformylation catalytic cycle is the olefin coordination to the metal. In a monometallic complex, as the olefin approaches the square-planar rhodium complex, the substituents will begin to distort away from square-planar to ideally form a trigonal-bipyramidal geometry. The hydride can then transfer to either the α- or ß-carbon of the coordinated olefin forming either linear or branched alkyl-metal intermediates which go on to form linear or branched aldehyde products.

In solution, the ground state rotational conformer for $Rh_2H_2(CO)_2$(eLTTP) (the presumed active catalyst) is probably an open-mode conformer as shown in Figure 29. This is supported by crystal structures on $Rh_2Cl_2(CO)_2$(eLTTP) and the VDW energy studies. As the olefin approaches one side of $Rh_2H_2(CO)_2$-

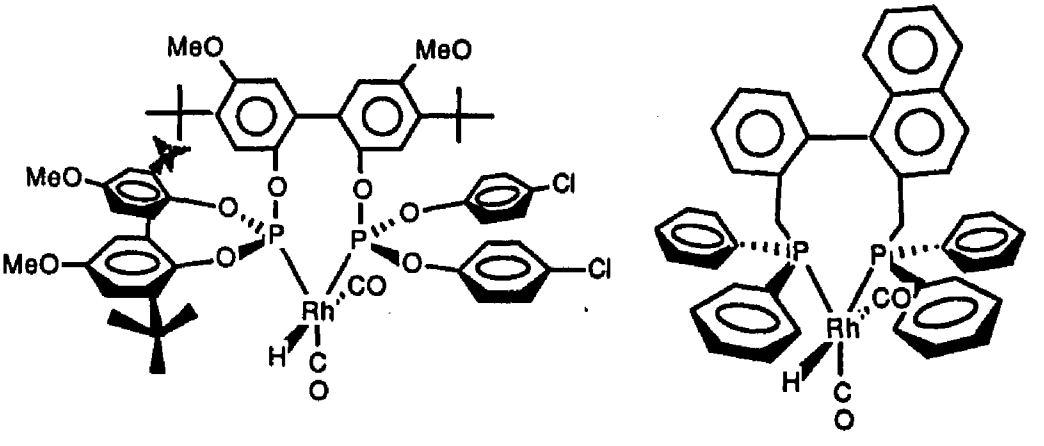

Figure 28: Rhodium hydroformylation complexes by Union Carbide (left) and Eastman Kodak (right) that use extremely bulky ligands to selectively produce linear aldehydes.

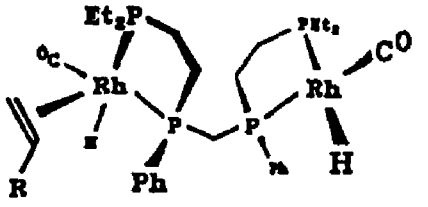

Figure 29: A possible rotational orientation as an olefin coordinates to the catalyst.

(eLTTP) the substituents on the metal center will also begin to distort away from square-planar geometry. The amount of distortion to trigonal bipyramidal, however, is limited due to the presence of the other half of the bimetallic complex. This maximizes the steric congestion about the rhodium center and forces the hydride to selectively transfer to the ß-carbon of the olefin, producing the sterically less encumbered linear alkyl-metal intermediate.

The high rates and selectivities of the aldehyde products make $[Rh_2(NBD)_2$-(eLTTP)$](BF_4)_2$ an attractive potential commercial hydroformylation catalyst. By using electron-rich alkylated phosphines to stabilize the metal center, high turnover rates were obtained without the use of excess phosphine in marked contrast to monometallic analogs such as $HRh(CO)(PPh_3)_3$. The true significance of these results lies in the possibility of preparing the first reactive and highly selective surface-supported hydroformylation catalyst. The central methylene carbon of $[Rh_2$-$(NBD)_2$(eLTTP)$](BF_4)_2$ can be functionalized and attached to a surface producing a surface-supported catalyst. This type of catalyst would be called a "heterogenized" homogeneous catalyst, and would allow highly selective hydroformylation catalysis to occur homogeneously while the surface-support allows for easy separation of the catalyst from the product mixture. This type of catalyst would have a profound effect in today's commercial processes by reducing or eliminating catalyst recovery problems and product/catalyst separations in the hydroformylation of higher olefins.

Chapter 6 Model ligands and Metal Complexes

Section 6.1 Introduction

The homobimetallic rhodium complex $[Rh_2(NBD)_2(eLTTP)](BF_4)_2$ has been found to be a highly active hydroformylation catalyst that produced exceptional turnover rates and selectivities. The increased activity of $[Rh_2(NBD)_2(eLTTP)]$-$(BF_4)_2$ is considerably higher than observed with other Rh(I) catalysts that contain electron-rich phosphines and is proposed to be the result of bimetallic cooperation. Simple structure-reactivity experiments were executed with similar Rh(I) model complexes in order to test the bimetallic cooperativity theory. This chapter is reserved for the discussion of the synthesis and characterization of these model ligands and their metal complexation used for the structure-reactivity experiments.

Section 6.2 eLTTP-pr and eLTTP-*p*-xyl

LTTP was designed to strongly coordinate to two metal centers by cis chelation while keeping them in proximity via a single central methylene carbon between the two internal phosphines. With this bonding arrangement two transition metals can potentially cooperate with each other during a catalytic cycle. In order to study bimetallic cooperativity, additional ligands must be designed and synthesized so that certain reaction steps are either enhanced or eliminated. By increasing the distance between the two transition metals in LTTP any bimetallic cooperativity effects should be reduced or eliminated (Figure 30). These ideas were the basis for designing LTTP analog ligands in which the central methylene carbon is replaced by a central propylene group, $Et_2PCH_2CH_2(Ph)PCH_2CH_2CH_2P(Ph)CH_2CH_2PEt_2$ (eLTTP-pr), or a p-xylylene group, $Et_2PCH_2CH_2(Ph)PCH_2$-*p*-C_6H_4-$CH_2P(Ph)$-$CH_2CH_2PEt_2$ (eLTTP-*p*-xyl).

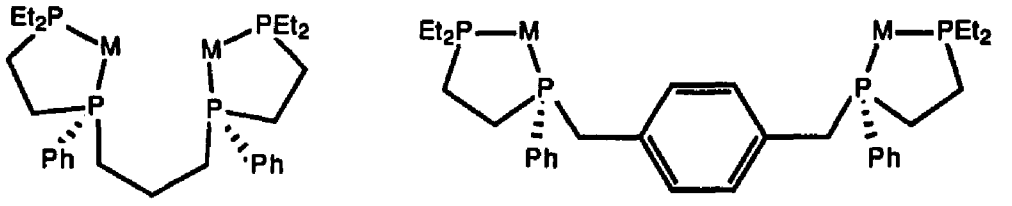

Figure 30: Metal complexes of eLTTP with spacer groups propylene (left) and p-xylylene (right).

The synthesis of eLTTP-pr is very similar to that of eLTTP. The starting material $Ph(H)PCH_2CH_2CH_2P(H)Ph$ can be purchased from Strem and treated with $Et_2PCH{=}CH_2$ under free-radical conditions (AIBN) in cyclohexane (Scheme 3). After refluxing overnight the solvent is stripped by rotory evaporation leaving a clear and colorless viscous liquid which contains product and an unidentified rearrangement product that contains a P-H bond. (P-H bonds are easily identifiable by their large coupling of ca. 206 Hz in the uncoupled ^{31}P and ^{1}H NMR experiment.)

The product can be purified by either vacuum distillation of the impurities up to 200° C , or by the addition of excess solid KH to a THF solution of the crude mixture. The distillation route removes the impurities and leaves pure product in the distillation pot. The KH route is less severe but takes longer. Solid KH is allowed to sit in a THF solution of the crude mixture for a week, which eventually turns

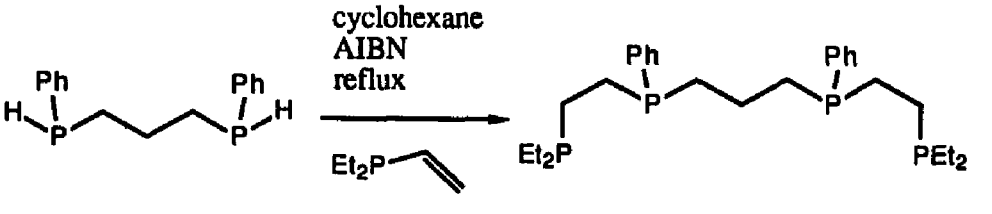

Scheme 3: Synthetic route of eLTTP-pr.

yellow then orange. The KH reacts with the P-H bond forming H_2 and a phosphide $R_2P^-K^+$. The solvent is stripped rotory evaporation and the solid is treated with hexane. The hexane is allowed to sit for two days to ensure complete extraction of the product. eLTTP-pr is obtained as a clear and colorless liquid when the hexane layer is decanted, eluted through an alumina column, and stripped via vacuum evaporation.

eLTTP-pr has been characterized by ^{31}P and ^{1}H NMR. In the $^{31}P\{^{1}H\}$ NMR shown in Figure 31 two doublet resonances appear at -18.6 ppm (external phosphorus atom) and -21.7 ppm (internal phosphorus atom) which are consistent for chemical shifts for these types of phosphorus atoms. The doublets of $J_{P\text{-}P}$ = 21.5 Hz arises from two inequivalent phosphorus nuclei of spin 1/2 coupling with each other through the ethylene linking group. There is no coupling observed between the internal phosphorus atoms unlike eLTTP which has a strong 109 Hz two bond coupling. eLTTP has a strong coupling between the two internal phosphorus atoms due to the fact that only two chemical bonds separate the nuclei, whereas in eLTTP-pr there are four bonds. The magnitude of the coupling between two phosphorus nuclei decreases as the number of bonds between them increases. The ^{1}H NMR contains many regions of unresolvable multiplets due to coupling from both neighboring H and P nuclei and overlapping resonances. The ^{1}H NMR spectrum is summarized in the experimental section and will not be discussed further.

The more rigid *p*-xylylene spacer group was also used to enforce the separation between the metal centers and stop any bimetallic cooperativity during a catalytic run (See Figure 30). 1,4-Benzene was not chosen as a spacer group because the internal phosphine would not have as similar a basicity as those found in eLTTP. The methylene groups of the *p*-xylylene should donate sufficient

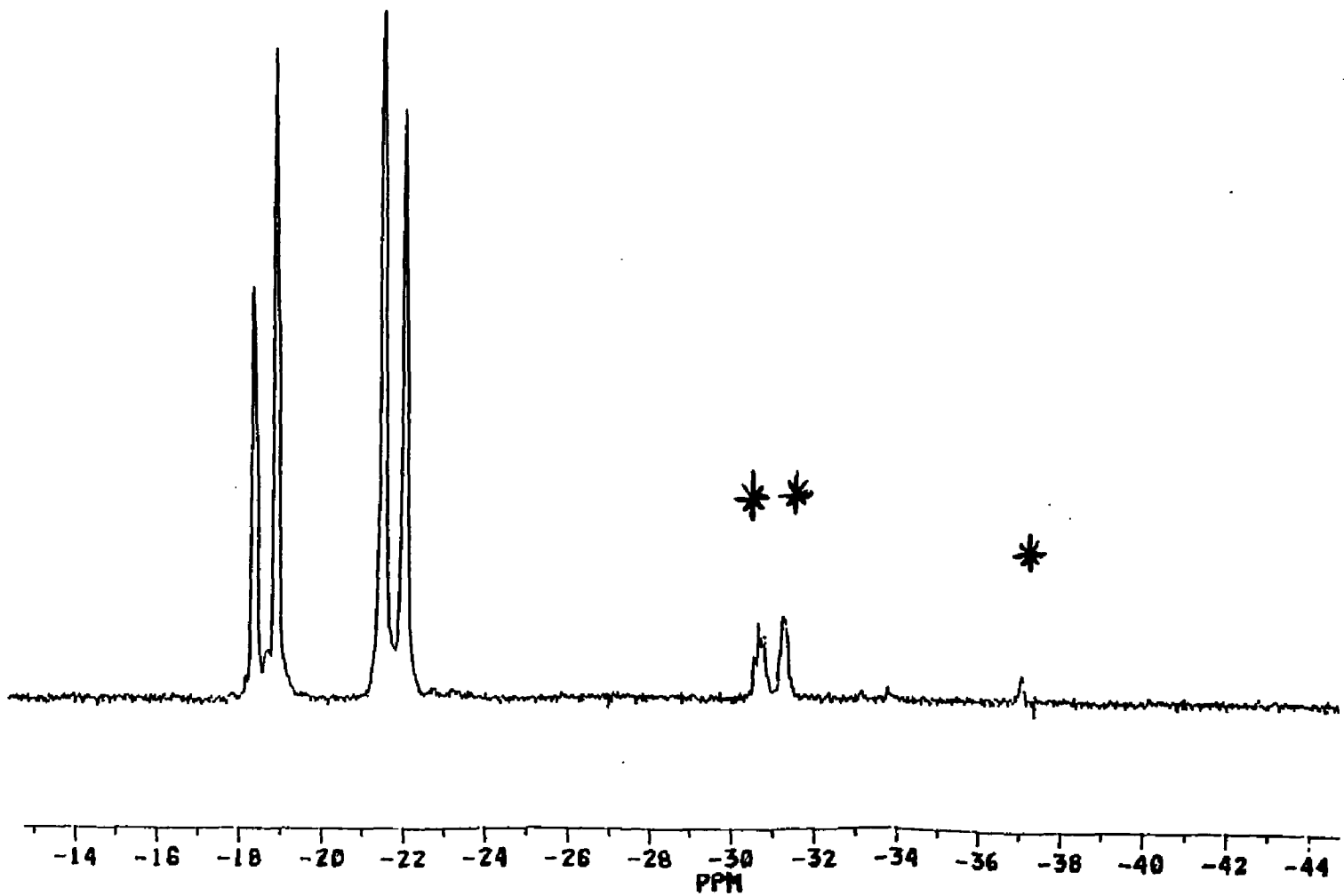

Figure 31: The $^{31}P\{^{1}H\}$NMR of eLTTP-pr in d_6-benzene (40.48 MHz). Astericked peaks are impurities.

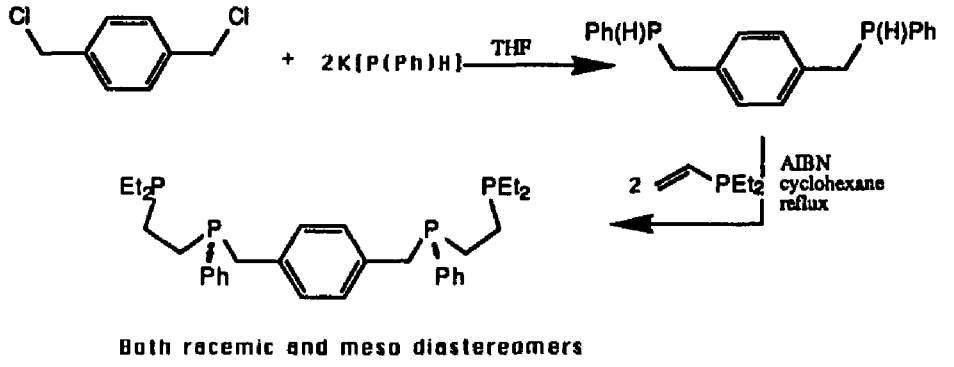

Scheme 4: Synthetic route to eLTTP-*p*-xyl.

electron density to make it similar to the central methylene group of eLTTP.

The first step in synthesizing eLTTP-*p*-xyl was to make the internal bisphosphine with the *p*-xylylene spacer group, $Ph(H)PCH_2$-*p*-C_6H_4-$CH_2P(H)Ph$. The S_N2 with two equivalents of K[P(H)Ph] to α,α'-dichloro-*p*-xylene in THF produces the diastereomeric mixture of $Ph(H)PCH_2$-*p*-C_6H_4-$CH_2P(H)Ph$. $Ph(H)PCH_2$-*p*-C_6H_4-$CH_2P(H)Ph$ is isolated as a white solid in 73% yield and can be converted in 53% yield to the final product $Et_2PCH_2CH_2P(Ph)$-*p*-C_6H_4-$P(Ph)CH_2CH_2PEt_2$, or eLTTP-*p*-xyl, by free-radical catalyzed addition of $Et_2PCH{=}CH_2$ by AIBN (see Scheme 4).

eLTTP-*p*-xyl has been characterized by ^{31}P and ^1H NMR. In the $^{31}P\{^1H\}$ NMR (Figure 32) two doublet resonances appear at -14.1 ppm (external phosphorus atom) and -11.5 ppm (internal phosphorus atom). The doublets of $J_{P\text{-}P}$ = 20.3 Hz (external) and $J_{P\text{-}P}$ = 22.0 Hz (internal) arises from two inequivalent phosphorus nuclei of spin 1/2 coupling with each other through the ethylene chain. As in eLTTP-pr, there is no coupling through the xylylene group observed between the internal phosphorus atoms.

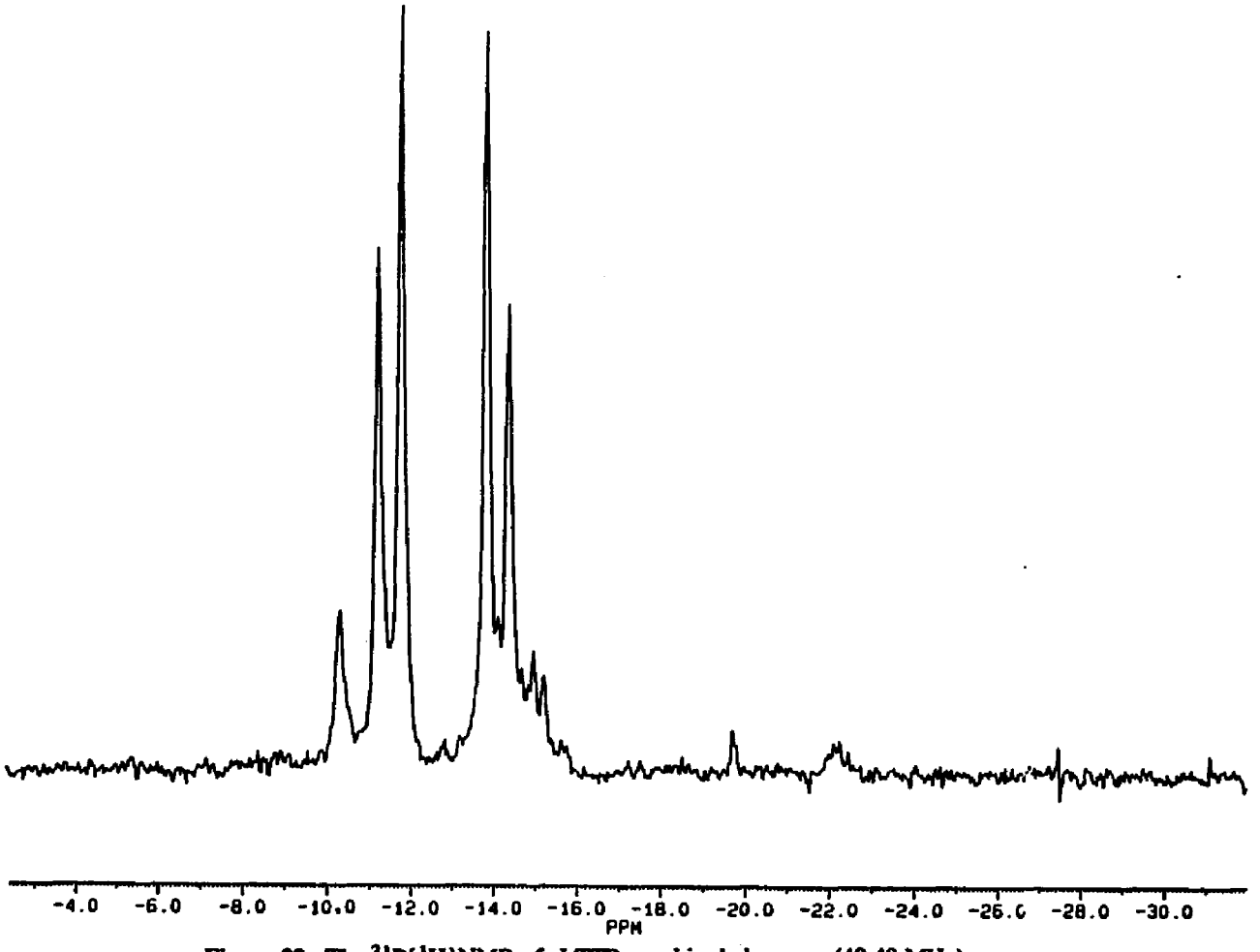

Figure 32: The $^{31}P\{^{1}H\}$NMR of eLTTP-*p*-xyl in d_6-benzene (40.48 MHz).

The ^1H NMR contains many regions of unresolvable multiplets due to coupling from both neighboring H and P nuclei and overlapping resonances. The ^1H NMR spectrum is summarized in the experimental section and will not be discussed further.

Section 6.3 $Et_2PCH_2CH_2P(Me)Ph$ and $Et_2PCH_2CH_2PPh_2$

The study of monometallic analogs of a M_2-eLTTP catalyst will call for new ligands that will contain phosphorus atoms of similar electron basicities and/or steric bulk. eLTTP can be viewed as two halves that can form 5-membered chelate rings with a transition metal that is bridged by a central methylene carbon. Dismantling the ligand at the central methylene carbon and substituting a methyl group, which has similar donor properties, would generate the bisphosphine $Et_2PCH_2CH_2P(Me)Ph$ (depmpe). This bisphosphine ligand is our first choice to fulfill the electronic requirements for a ligand to be used as a monometallic analog (Figure 33).

Ethylene bridged bisphosphines, $-PCH_2CH_2P-$, are very easily made by Meek's free radical addition of a vinylphosphine to a P-H bond.[13] PhP(Me)H, the P-H portion of Meek's reaction, is synthesized by the addition of MeI to a THF solution of K[PhP(H)]. $Et_2PCH{=}CH_2$ is added to PhP(Me)H in cyclohexane under

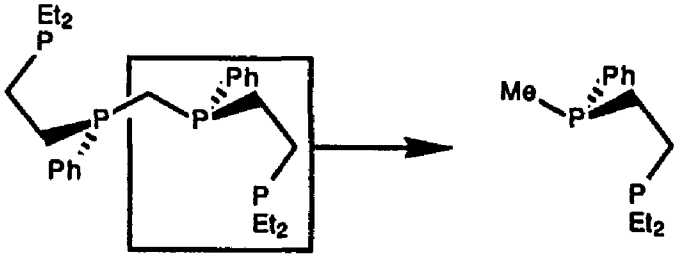

Figure 33: The dismantling of eLTTP to produce $Et_2PCH_2CH_2P(Me)Ph$, which is electronically analogous to eLTTP to study monometallic models.

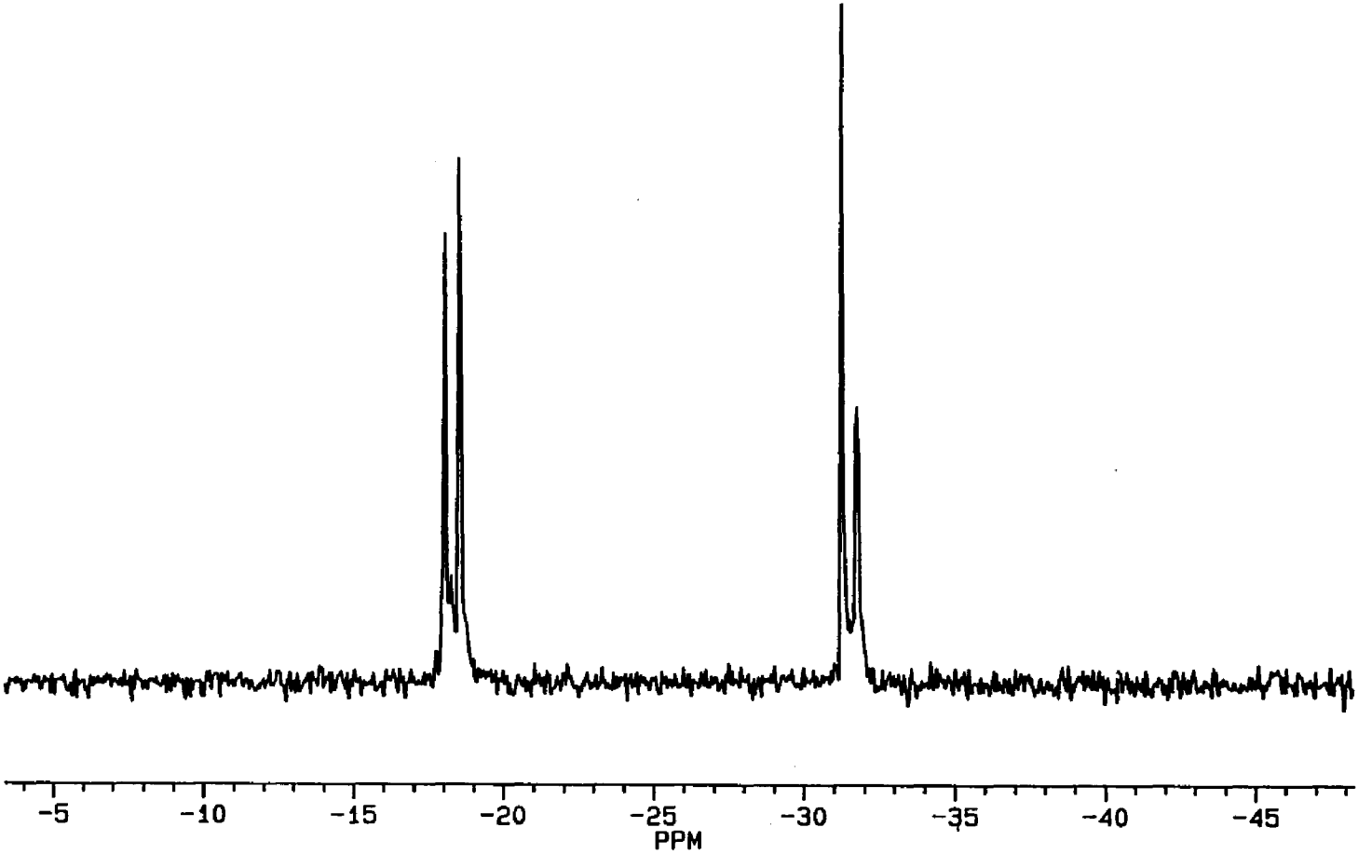

Figure 34: The $^{31}P\{^{1}H\}$NMR of $Et_2PCH_2CH_2P(Ph)Me$ in d_6-benzene (40.48 MHz).

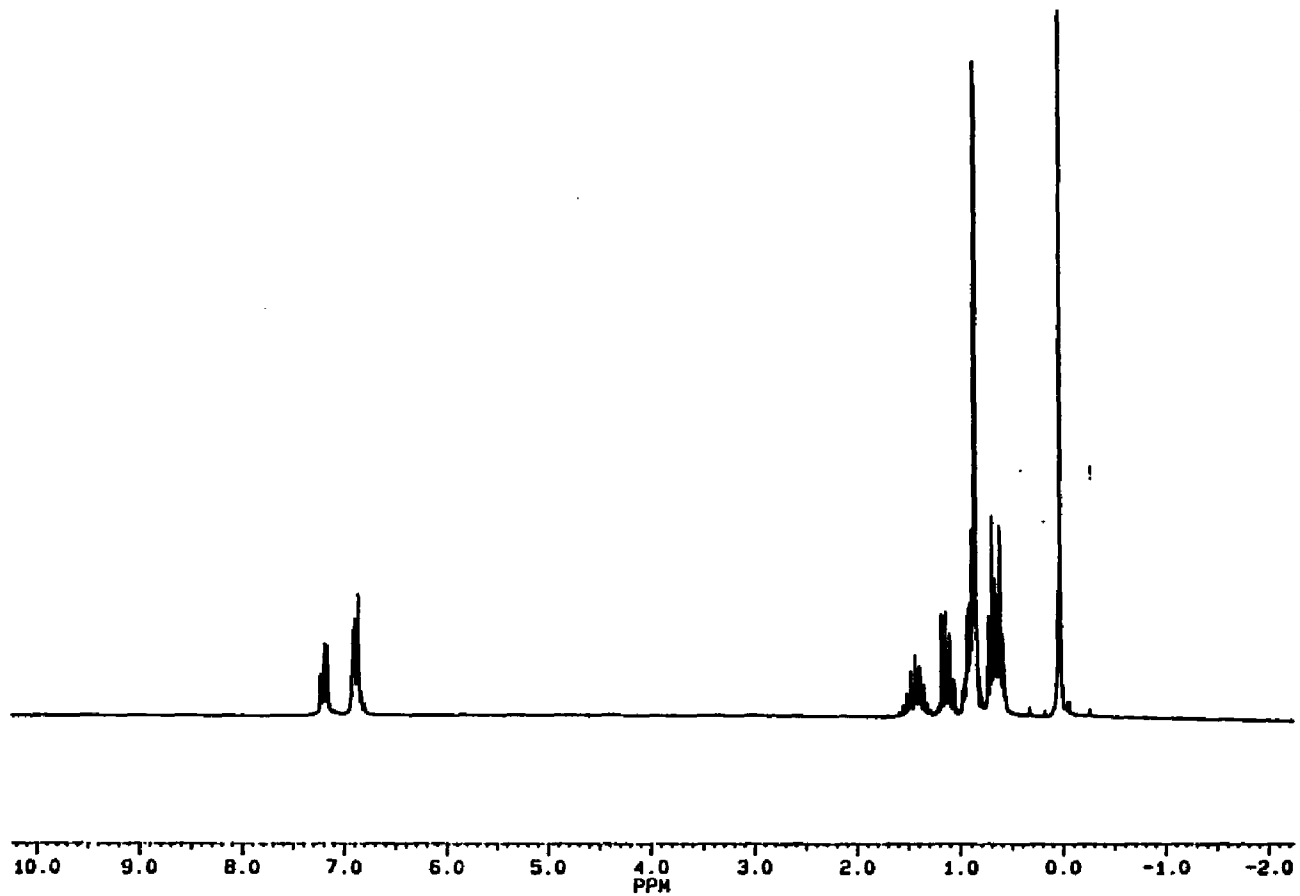

Figure 35: The ^1H NMR of $Et_2PCH_2CH_2P(Ph)Me$ in d_6-benzene (200.13 MHz).

free radical conditions to form $Et_2PCH_2CH_2P(Me)Ph$ with very good yield (80 %).

$Et_2PCH_2CH_2P(Me)Ph$ has been characterized by ^{31}P and ^{1}H NMR (Figures 34 and 35). In the $^{31}P\{^{1}H\}$ NMR two doublet resonances appear at -18.3 ppm (Et_2P-) and -31.5 ppm (Ph(Me)*P*-) which are consistent for chemical shifts for these types of phosphorus atoms. Each doublet has a coupling constant of $J_{P\text{-}P}$ = 20 Hz which arises from two inequivalent phosphorus nuclei of spin 1/2 interacting with each other. The ^{1}H NMR contains many regions of multiplets due to coupling from both neighboring H and P nuclei. The phenyl protons appear as two multiplets at 6.85-6.95 and 7.18-7.38 ppm, and the terminal methyl group of the Et_2P- section appears as multiplets at 0.55-0.80 ppm. The protons on the methyl group at 0.90 ppm are coupled into a doublet of $J_{P\text{-}H}$ = 4 Hz. The methylene protons of the terminal ethyl groups appear as a multiplet at 0.80-1.02 ppm. The resonances of the protons on the chelate ring exist as two multiplets at 1.05-1.20 and 1.29-1.60 ppm.

Similar to $Et_2PCH_2CH_2P(Me)Ph$, $Et_2PCH_2CH_2PPh_2$ (dedppe) was synthesized by Meek's free-radical pathway of Ph_2PH and $Et_2PCH{=}CH_2$ with AIBN in 34% yield. $Et_2PCH_2CH_2PPh_2$ is another ligand for monometallic analogs that will also examine the effects of basicity and increase in steric bulk on the catalytic reaction products. The clear and colorless liquid was characterized by ^{31}P and ^{1}H NMR (Figures 36 and 37). The $^{31}P\{^{1}H\}$ NMR provided two doublet resonances at -17.58 ppm (Et_2P-) and -11.71 ppm (-PPh_2) with coupling $J_{P\text{-}P}$ = 25.3 Hz. The two doublet resonances overlap with two smaller resonances with complex coupling due to an impurity from the free-radical step.[39] Similar to Et_2PCH_2-$CH_2P(Me)Ph$ the ^{1}H NMR of $Et_2PCH_2CH_2PPh_2$ contains many regions of multi-

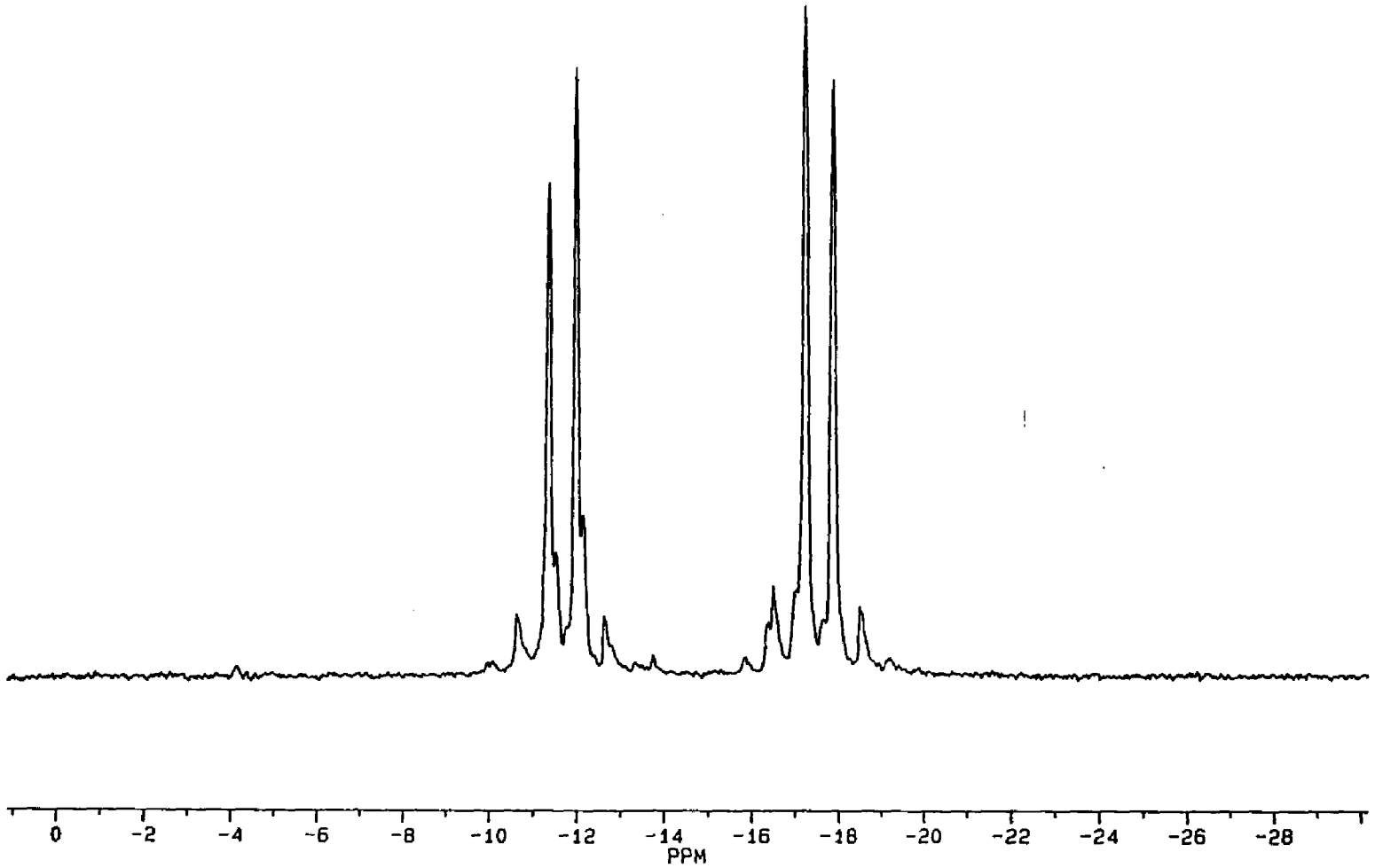

Figure 36: The $^{31}P\{^{1}H\}$NMR of $Et_2PCH_2CH_2PPh_2$ (with overlapping impurities) in d_6-benzene (40.48 MHz).

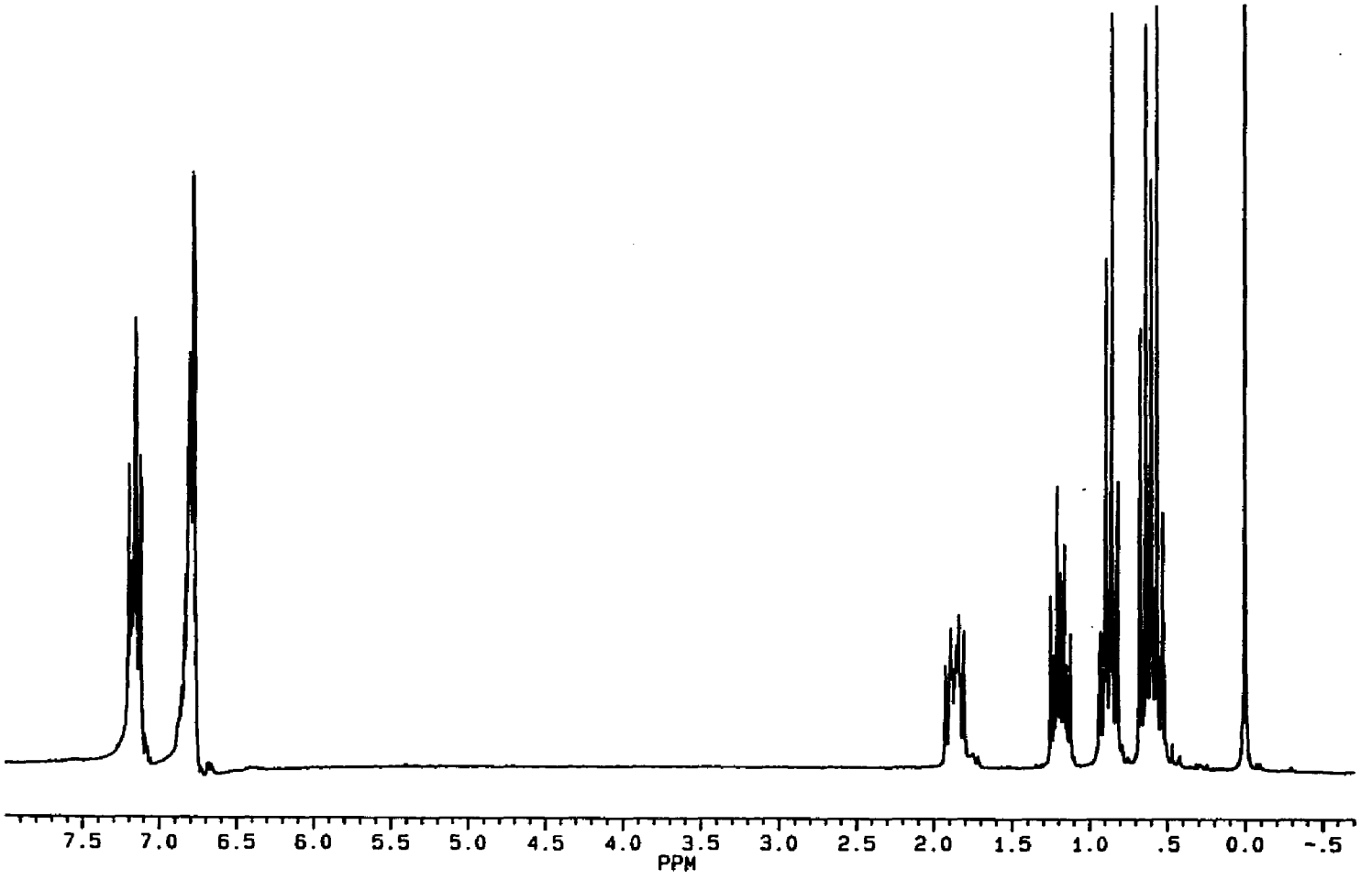

Figure 37: The ^{1}H NMR of $Et_2PCH_2CH_2PPh_2$ in d_6-benzene (200.13 MHz).

plets due to coupling from both neighboring H and P nuclei. The phenyl protons appear as two multiplets at 6.73-6.87 and 7.10-7.25 ppm. The terminal methyl group of the Et_2P- section appears as a multiplet at 0.55-0.71 ppm. The methylene protons of the terminal ethyl groups are a multiplet at 0.79-0.93 ppm. The resonances of the protons on the chelate ring exist as two multiplets at 1.11-1.36 and 1.78-1.93 ppm.

Section 6.4 $[Rh_2(NBD)_2(eLTTP\text{-}pr)](BF_4)_2$

Following the same synthetic procedure as $[Rh_2(NBD)_2(eLTTP)](BF_4)_2$, the addition of two equivalents of $[Rh(NBD)_2](BF_4)_2$ to eLTTP-pr afforded the bimetallic complex $[Rh_2(NBD)_2(eLTTP\text{-}pr)](BF_4)_2$ in 80% yield. Similar to $[Rh_2(NBD)_2(eLTTP)](BF_4)_2$, the oxidation state of the rhodium atoms are +1, and the geometry about the metal centers is square planar. All rhodium complexes discussed in this chapter will have the same oxidation state and square planar metal geometry.

$[Rh_2(NBD)_2(eLTTP\text{-}pr)](BF_4)_2$ is closely related to another complex by Brown and Canning. A TETRAPHOS ligand with a bridging propylene group instead of a ethylene group was used to make $[Rh_2(COD)_2(TETRAPHOS\text{-}pr)](BF_4)_2$.[25,40] The $^{31}P\{^1H\}$ NMR for $[Rh_2(COD)_2(TETRAPHOS\text{-}pr)](BF_4)_2$ (on a single diastereomer of unknown stereochemistry), for example, is reported to be a pair of dd at δ = 58.7 ppm ($J_{Rh\text{-}P}$ = 150 Hz, $J_{P\text{-}P}$ = 25 Hz, -PPh$_2$) and 50.7 ppm ($J_{Rh\text{-}P}$ = 148 Hz, $J_{P\text{-}P}$ = 25 Hz, -P(Ph)-). The $^{31}P\{^1H\}$ NMR of $[Rh_2(NBD)_2(eLTTP\text{-}pr)](BF_4)_2$ in Figure 38 shows that both diastereomers are present. The external phosphorus resonances of each diastereomer are a dd at δ = 60.1 ppm ($J_{Rh\text{-}P}$ = 153.5 Hz, $J_{P\text{-}P}$ = 24.4 Hz) and 60.6 ppm ($J_{Rh\text{-}P}$ = 153.3 Hz, $J_{P\text{-}P}$ = 24.5

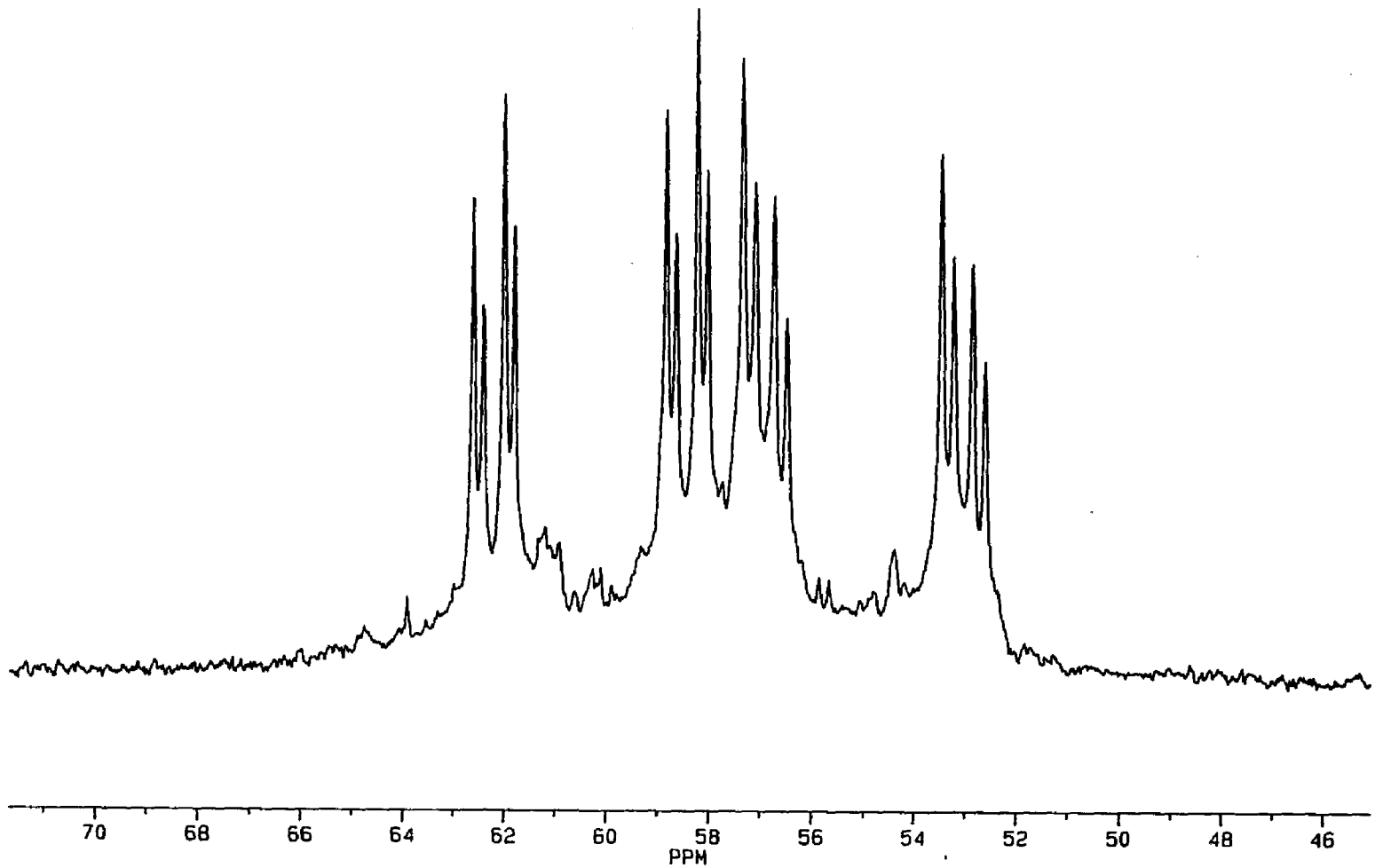

Figure 38: The $^{31}P\{^{1}H\}$ NMR of the diastereomeric mixture of $[Rh_2(NBD)_2(eLTTP\text{-}pr)](BF_4)_2$ in CD_2Cl_2 (40.48 MHz).

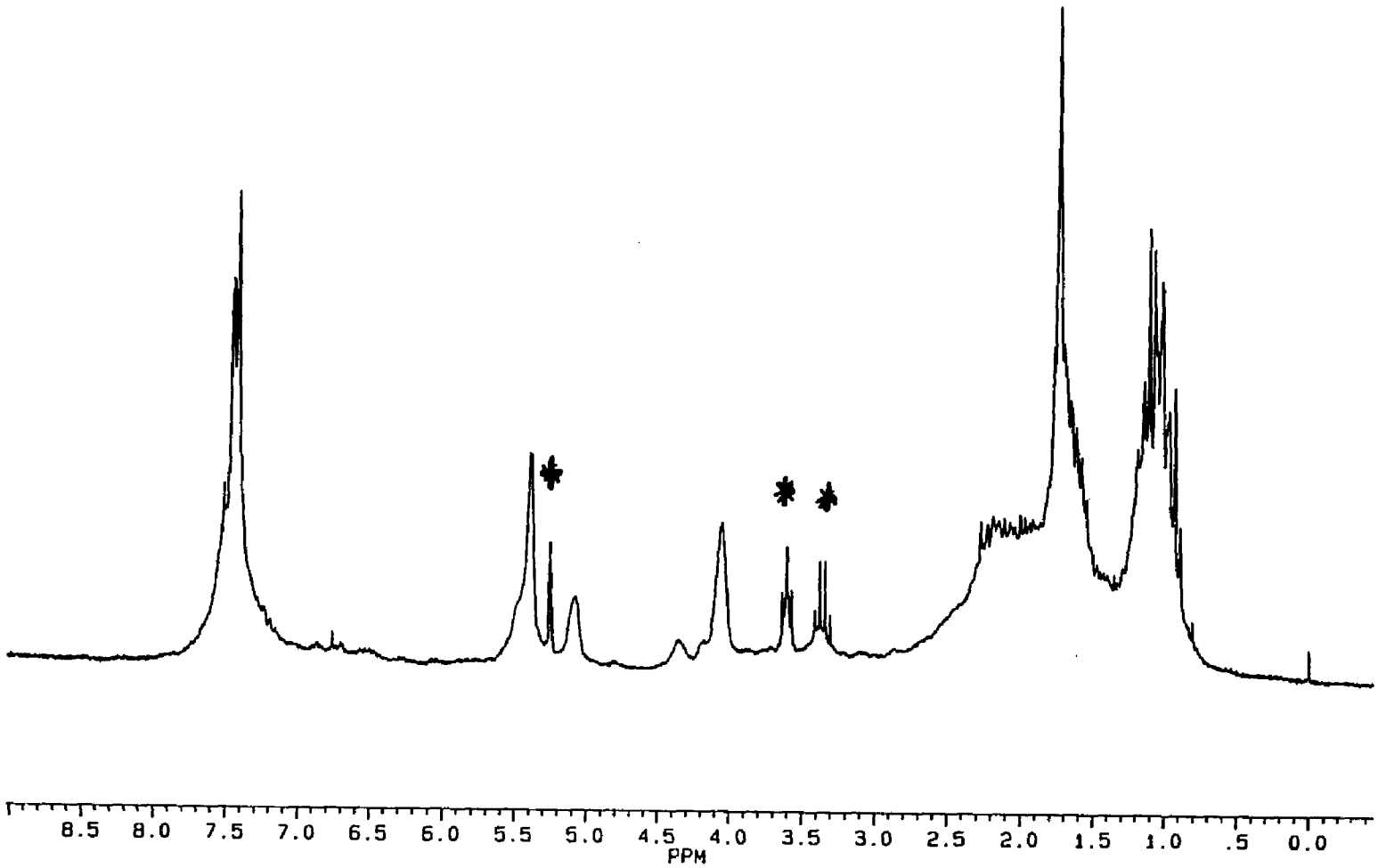

Figure 39: The ^1H NMR of the diastereomeric mixture of $[Rh_2(NBD)_2(eLTTP\text{-}pr)](BF_4)_2$ in CD_2Cl_2 (200.13 MHz). Asterisked peaks are solvent impurities.

Hz), while the internal phosphorus centers have resonances at δ = 54.7 ppm ($J_{Rh\text{-}P}$ = 157.1 Hz, $J_{P\text{-}P}$ = 24.4 Hz) and 55.3 ($J_{Rh\text{-}P}$ = 157.5 Hz, $J_{P\text{-}P}$ = 24.5 Hz). The chemical shift of the external phosphorus of $[Rh_2(NBD)_2\text{-}(eLTTP)](BF_4)_2$ is unexpectedly more downfield that of the external phosphorus of $[Rh_2(COD)_2$(TETRAPHOS-pr)$](BF_4)_2$. Although a higher electron density on an atom usually causes an upfield shift in the ^{31}P resonance, the Et_2P- group in eLTTP is observed at a lower field than the Ph_2P- group in phLTTP-pr. The same upfield shift is found for the internal phosphorus atoms of $[Rh_2(NBD)_2(eLTTP)](BF_4)_2$.

The usual multiplets occur at the same chemical shift in the ^1H NMR spectrum (Fig. 39) for both the eLTTP and eLTTP-pr metal complexes. All of the protons from the methylene groups of the terminal ethyl substituents and the protons on the ethylene and propylene bridges have similar chemical shifts thus generating a problem with overlapping signals. The ^1H spectrum of the ligand eLTTP-pr is summarized in the experimental section.

The olefinic protons of norbornadiene at δ = 5.10 and 5.40 ppm in the ^1H NMR appear as broad singlets due to facile rotation of the ligand. The proton on the tertiary sp^3-hybridized carbon of norbornadiene is a broad singlet at 4.08 ppm, and the two protons on the secondary sp^3-hybridized carbon of norbornadiene are a broad singlet at 1.78 ppm.

The CH_2Cl_2 solvent can be difficult to remove and can be seen in the ^1H NMR spectra at δ = 5.3 ppm. The presence of any solvent can interfere with an elemental analysis, so when the elemental analysis of $[Rh_2(NBD)_2(eLTTP\text{-}pr)](BF_4)_2$ was obtained, the amount of solvent present can be calculated from the experimental values. The values found agreed satisfactorily with the presence of one molecule of solvent and are given in the experimental section.

Section 6.5 $[Rh_2(NBD)_2(eLTTP\text{-}p\text{-}xyl)](BF_4)_2$

The same procedure for preparing $[Rh_2(NBD)_2(eLTTP)](BF_4)_2$ was used for the synthesis of $[Rh_2(NBD)_2(eLTTP\text{-}p\text{-}xyl)](BF_4)_2$, namely the addition of eLTTP-*p*-xyl to two equivalents of $[Rh(NBD)_2](BF_4)_2$. The product was isolated as a red-brown solid that was air stable.

$[Rh_2(NBD)_2(eLTTP\text{-}p\text{-}xyl)](BF_4)_2$ was characterized by $^{31}P\{^1H\}$ NMR shown in Figure 40. In $[Rh_2(NBD)_2(eLTTP)](BF_4)_2$, both diastereomers showed resonances in the $^{31}P\{^1H\}$ NMR shifted by a few tenths of a ppm. Only a single resonance is present for each phosphine in $[Rh_2(NBD)_2(eLTTP\text{-}p\text{-}xyl)](BF_4)_2$. The external phosphorus atom (δ = 61.2 ppm) is coupled to the rhodium atom ($J_{Rh\text{-}P}$ = 151.1 Hz) and the internal phosphorus atom ($J_{P\text{-}P}$ = 25.0 Hz). The internal phosphorus atom (δ = 54.9 ppm) is coupled to rhodium atom ($J_{Rh\text{-}P}$ = 161.7 Hz) and the external phosphorus atom ($J_{P\text{-}P}$ = 25.0 Hz). The presence of only one set of resonances implies that only one diastereomer of unknown stereochemistry is present, or that the resonances of each diastereomer are coincident. However, an overlapping dd pattern of low intensity at 61.2 ppm may indicate the small presence of one of the diastereomers. The chemical shifts and the $J_{Rh\text{-}P}$ and $J_{P\text{-}P}$ coupling constants are very similar to that of $[Rh_2(NBD)_2(eLTTP\text{-}pr)](BF_4)_2$.

The chemical shifts of the internal phosphorus atoms of the spacer-group ligands in the bimetallic rhodium complexes are downfield in comparison with the internal phosphorus atoms of $Rh_2(NBD)_2(eLTTP)](BF_4)_2$. Substitution of the propylene and *p*-xylene spacer-groups for the central methylene group eliminates the strong virtual coupling between the internal phosphorus atoms that was present in eLTTP and its bimetallic complexes.

In the ^1H NMR the presence of the eLTTP-*p*-xyl ligand in $[Rh_2(NBD)_2$-

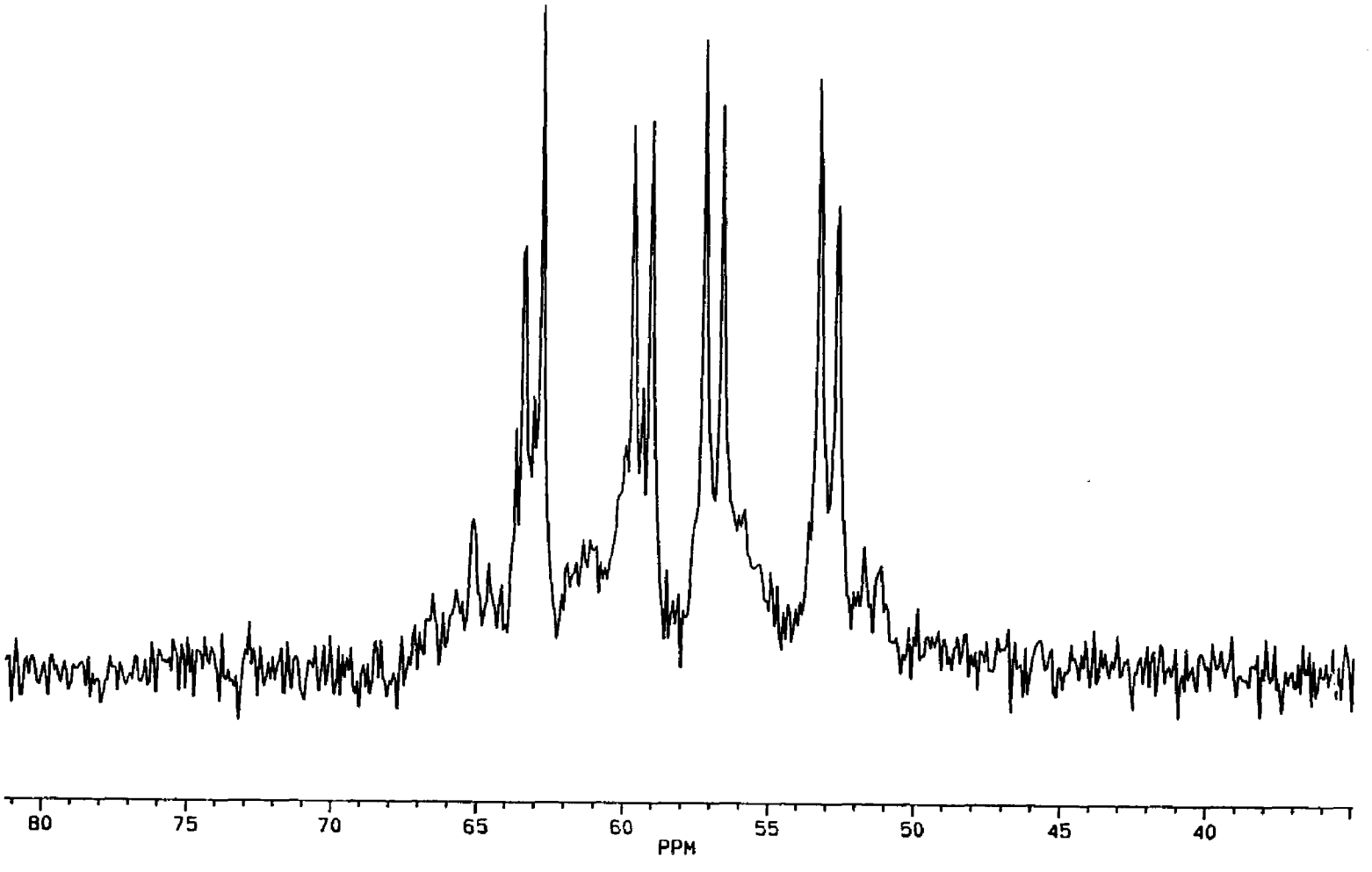

Figure 40: The $^{31}P\{^{1}H\}$ NMR of the diastereomeric mixture of $[Rh_2(NBD)_2(eLTTP\text{-}p\text{-}xyl)](BF_4)_2$ in CD_2Cl_2 (40.48 MHz).

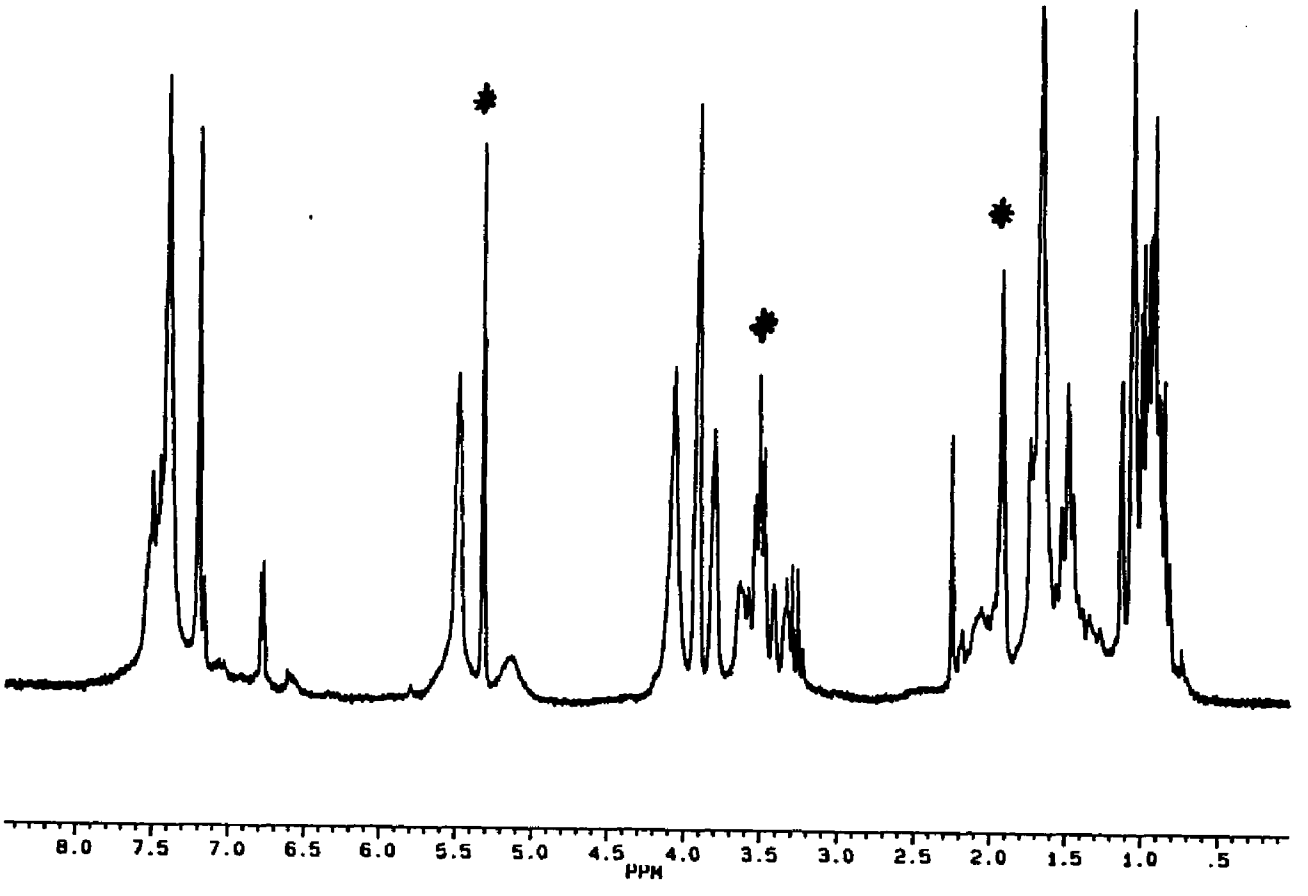

Figure 41: The ^{1}H NMR of the diastereomeric mixture of $[Rh_2(NBD)_2(eLTTP\text{-}p\text{-}xyl)](BF_4)_2$ in CD_2Cl_2 (200.13 MHz). Asterisked peaks are solvent impurities.

(eLTTP-*p*-xyl)]$(BF_4)_2$ is indicated by the aromatic protons of the *p*-xylylene spacer group (Fig. 41). All the aromatic protons on the *p*-xylylene spacer group are equivalent and do not couple with any other nuclei; therefore, they appear as a singlet at δ = 7.2 ppm. The protons on the methylene portion of the *p*-xylene spacer-group are multiplets at δ = 3.2-3.7 ppm. Again, we observe considerable signal overlap from regions 0.7-2.4 and 7.1-7.7 ppm due to all the NMR active nuclei in $[Rh_2(NBD)_2$-(eLTTP-*p*-xyl)]$(BF_4)_2$. The rest of the protons of the eLTTP-*p*-xyl are overlapping multiplets that have consistent chemical shifts relative to the other LTTP ligands studied here and are highly coupled with other protons and phosphorus atoms. The ^1H chemical shifts are summarized in the experimental section.

The olefinic protons of norbornadiene at δ = 5.1 and 5.5 ppm appear as a single broad singlet due to rotation of the ligand. The proton on the tertiary sp^3-hybridized carbon of norbornadiene is a broad singlet at δ = 3.8 and 4.1 ppm, and the two protons on the secondary sp^3-hybridized carbon of norbornadiene is a broad singlet at δ = 1.7 ppm. The identity of the broad singlet at δ = 3.8 ppm is unknown but may be a resonance from a NBD ligand of one diastereomer.

The presence of CH_2Cl_2 solvent can be seen in the ^1H NMR spectra at δ = 5.3 ppm. The elemental analysis of $[Rh_2(NBD)_2$(eLTTP-*p*-xyl)]$(BF_4)_2$ was obtained and the amount of solvent present was determined from the experimental values. The values found agreed satisfactorily with the presence of three molecules of solvent and are given in the experimental section.

Section 6.6 $[Rh(NBD)(Et_2PCH_2CH_2P(Ph)Me)]BF_4$

The addition of one equivalent of $Et_2PCH_2CH_2P(Ph)Me$ (depmpe) to one equivalent of $[Rh(NBD)_2]BF_4$ in CH_2Cl_2/THF/Hexane produces a red-brown solid

in 80-90% yield that has been characterized as [Rh(NBD)(depmpe)]BF_4 by ^{31}P and ^{1}H NMR and elemental analysis. Crystals can be obtained when the mother liquor of the reaction is placed in a -40° C freezer.

The $^{31}P\{^{1}H\}$ NMR spectrum in Figure 42 shows only two resonances due to the two inequivalent phosphorus nuclei. The Et_2P- ^{31}P resonance is a doublet of doublets at $\delta = 65.7$ ppm from coupling with -P(Ph)Me ($J_{P\text{-}P} = 25.3$ Hz) and the metal center ($J_{Rh\text{-}P} = 153.03$ Hz). The other phosphorus resonance is also a dd at $\delta = 52.1$ ppm with the same coupling arguments ($J_{P\text{-}P} = 25.3$ Hz, $J_{Rh\text{-}P} = 159.6$ Hz). The chemical shift and coupling constants are consistent with that seen for bimetallic rhodium complexes with eLTTP-type ligands.

The olefinic protons of norbornadiene at $\delta = 5.0$ and 5.5 ppm appear as broad singlets in the ^{1}H NMR of [Rh(NBD)(depmpe)]BF_4 (Figure 43) due to rotation of the ligand. The protons on the tertiary sp^3-hybridized carbons of norbornadiene form a broad singlet at $\delta = 3.9$ ppm. The two protons on the secondary sp^3-hybridized carbon of norbornadiene also occur as a broad singlet at $\delta = 1.5$ ppm.

The resonances due to $Et_2PCH_2CH_2P(Ph)Me$ are present with the methyl group -P(Ph)*Me* appearing at $\delta = 1.6$ ppm as a doublet ($J_{P\text{-}H} = 13.3$ Hz) due to coupling with the phosphorus atom. The ethyl groups, phenyl group, and the protons in the ethylene chain appear as multiplets with chemical shift similar to that found in other rhodium norbornadiene complexes. The chemical shifts are summarized in the experimental section. Elemental analysis of [Rh(NBD)(depmpe)]-BF_4 was obtained and agreed very well with the theoretical (see experimental section) although CH_2Cl_2 was present in the ^{1}H NMR.

We consider [Rh(NBD)(depmpe)]BF_4 to be the best monometallic electronic analog of $[Rh_2(NBD)_2(eLTTP)](BF_4)_2$. In studying bimetallic cooperativity in

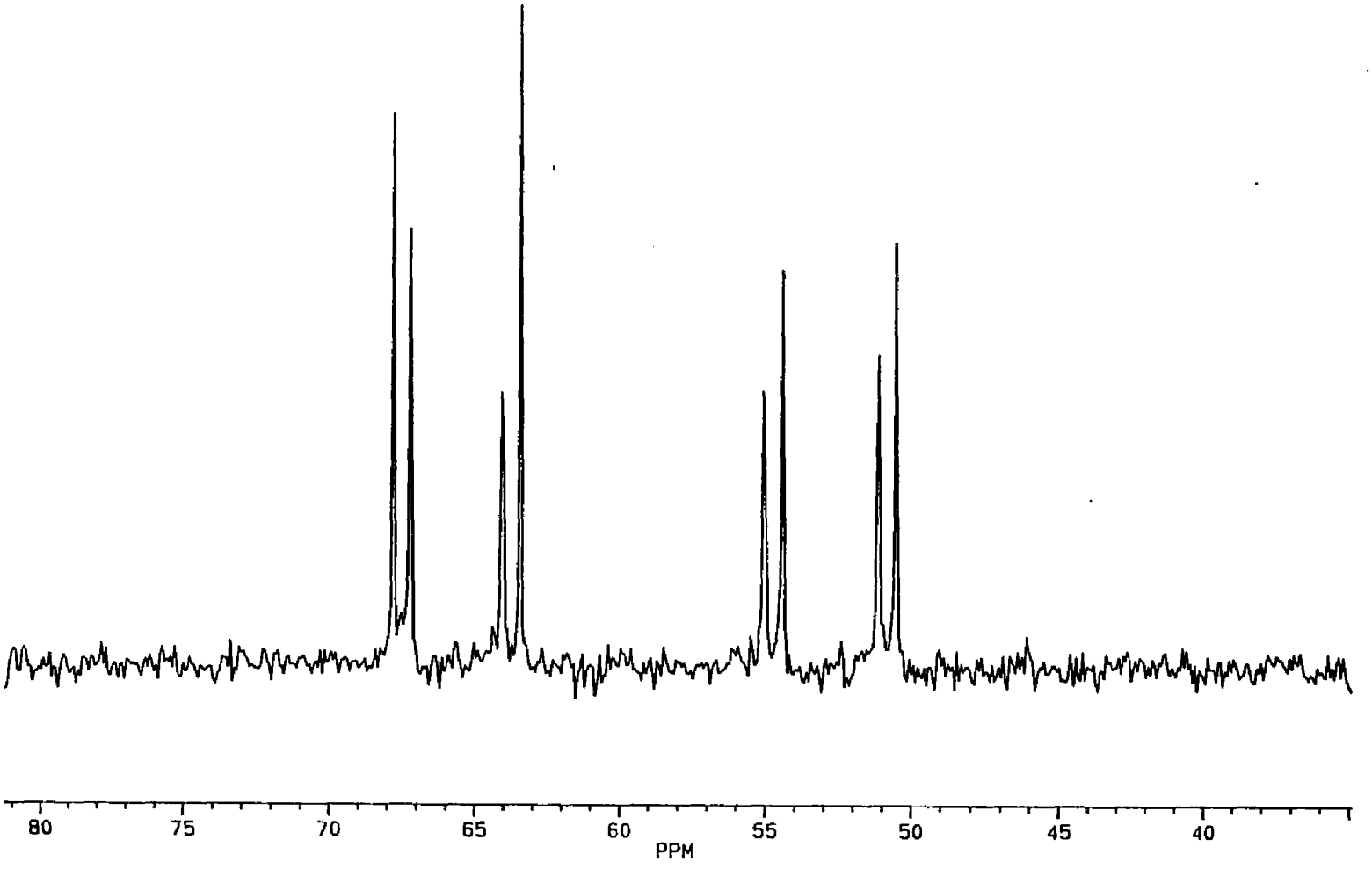

Figure 42: The $^{31}P\{^{1}H\}$ NMR of $[Rh(NBD)(Et_2PCH_2CH_2P(Ph)Me)]BF_4$ in d_6-acetone (40.48 MHz).

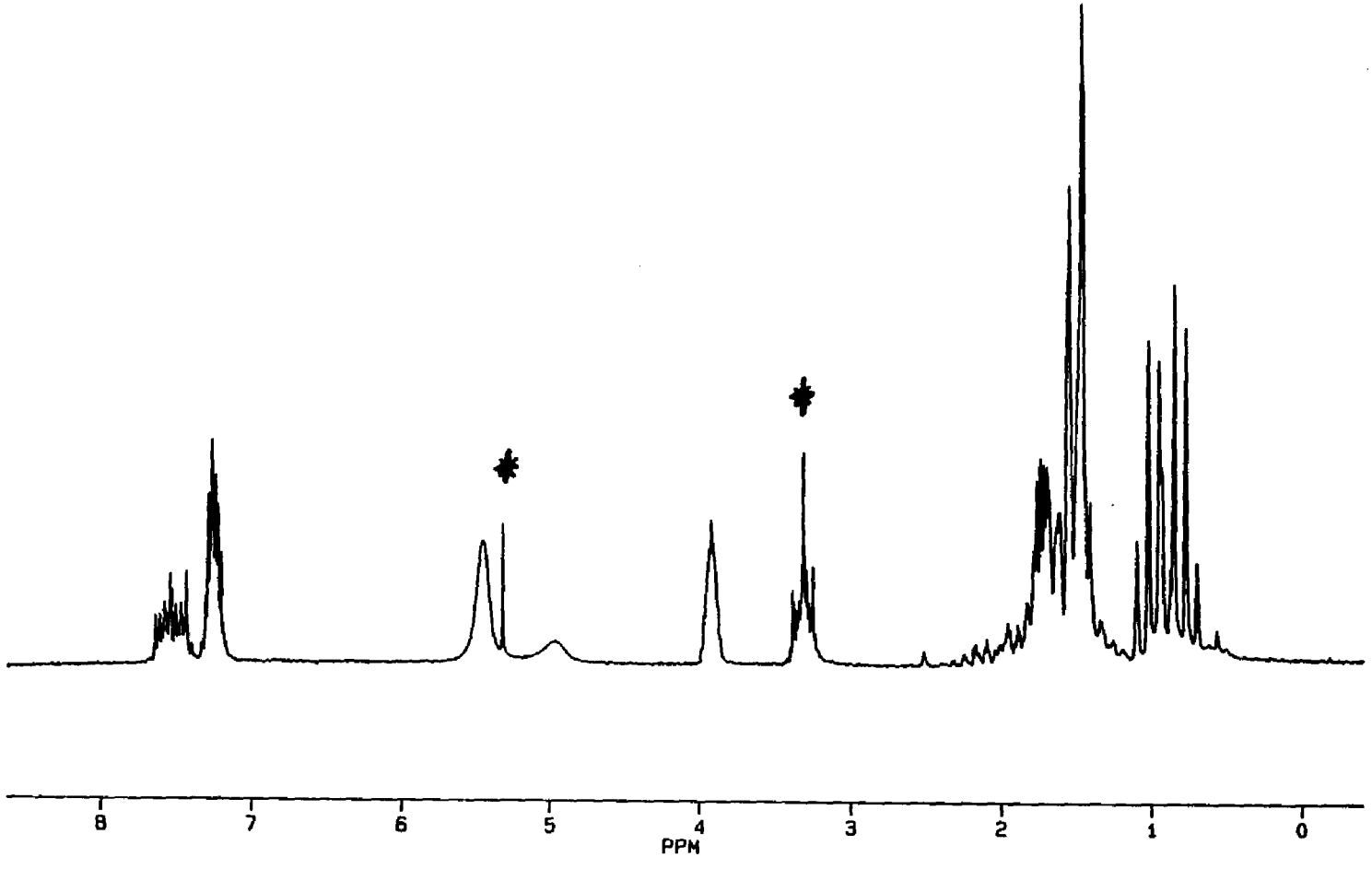

Figure 43: The ^1H NMR of $[Rh(NBD)(Et_2PCH_2CH_2P(Ph)Me)]BF_4$ in d_6-acetone (200.13 MHz). Asterisked peaks are solvent impurities.

homogeneous catalysis, monometallic models must be as identical as possible to their bimetallic counterpart either from a steric and/or electronic viewpoint. The substitution of the central methylene carbon that bridges both 5-membered chelate rings in eLTTP for a methyl group in $Et_2PCH_2CH_2P(Ph)Me$ is probably the closest analog in terms of basicity and donor abilities for the phosphorus centers.

Section 6.7 $[Rh(NBD)(Et_2PCH_2CH_2PPh_2)]BF_4$

$[Rh(NBD)(dedppe)]BF_4$ (dedppe = $Et_2PCH_2CH_2PPh_2$) was synthesized in the same fashion as the other rhodium complexes by adding $Et_2PCH_2CH_2PPh_2$ to $[Rh(NBD)_2]BF_4$ in CH_2Cl_2/THF/Hexane. A red-brown solid in 80-90% yield was obtained after workup which was found to be air-stable. X-ray quality crystals can be grown from the mother liquor of the reaction in a -40°C freezer.

$[Rh(NBD)(dedppe)]BF_4$ has been fully characterized by $^{31}P\{^1H\}$ NMR. Two resonances in Figure 44 are centered at δ = 60.47 and 60.50 ppm. Each resonance is a doublet pattern due to coupling with the rhodium atom with $J_{Rh\text{-}P}$ = 154 Hz and $J_{Rh\text{-}P}$ = 157 Hz. While the Et_2P- and -PPh_2 phosphorus atoms are clearly different, no coupling between the phosphorus atoms is observed. One explanation of the lack of coupling between the phosphorus atoms is that the overall coupling value averages out to be zero. Two coupling pathways exist; one through the metal center and the other through the carbon backbone of the chelate ring. Each coupling pathway can have a equal value of opposite sign which would cancel out the overall phosphorus coupling. The chemical shift of the -PPh_2 group shifts downfield near the resonance of the -PEt_2 group, which has consistently been around 60 ppm for other rhodium norbornadiene phosphine complexes.

The olefinic protons of norbornadiene at δ = 5.1 and 5.7 ppm appear as a

broad singlets in the ^1H NMR in Figure 45 due to rotation of the ligand. The protons on the tertiary sp^3-hybridized carbons of norbornadiene form a broad singlet at $\delta = 4.2$ ppm. The two protons on the secondary sp^3-hybridized carbon of norbornadiene occur as a broad singlet at 1.8 ppm that is overlapping resonances from the dedppe ligand.

The ^1H NMR has a multiplet in the aromatic region of the spectrum at $\delta =$ 7.5-7.6 ppm. The methyl protons of the terminal ethyl groups are present in the spectrum as a multiplet at 1.1-1.3 ppm. The methylene protons of the terminal ethyl group resonate as a multiplet at 1.7-1.9 ppm. The protons on the chelate ring are found in the range of 2.3-2.6 ppm as a multiplet. All proton coupling patterns are multiplets from coupling to both neighboring protons and phosphorus atoms.

X-ray quality crystals were grown from the mother liquor in a freezer at -40° C. The ORTEP diagram of the molecule is shown in Figure 46 and confirms the square-planar arrangement of the metal center with the bisphosphine coordinating in a chelating fashion and the cis-coordination of the NBD. The structure is considered to be a good representative of all the $Rh(NBD)P_2$ (P_2 = a bis-phosphine unit that forms a 5-membered chelate ring with the metal center) complexes discussed in this thesis since all the complexes were synthesized in the same fashion and have analogous ^1H and ^{31}P NMR spectra. Selected bond distances and angles are listed in Tables IX and X. After final refinements the R and R_w values are 0.060 and 0.068, respectively.

The norbornadiene ligand is coordinated to the metal center by the two π bonds. The Rh-C bond distances of the olefinic carbon atoms of the NBD ligand trans to the Et_2P- group are 2.219 (9) and 2.215 (9) Å, and the bond distances to the other Rh-C olefinic carbon atoms of NBD trans to the Ph_2P- group are 2.239

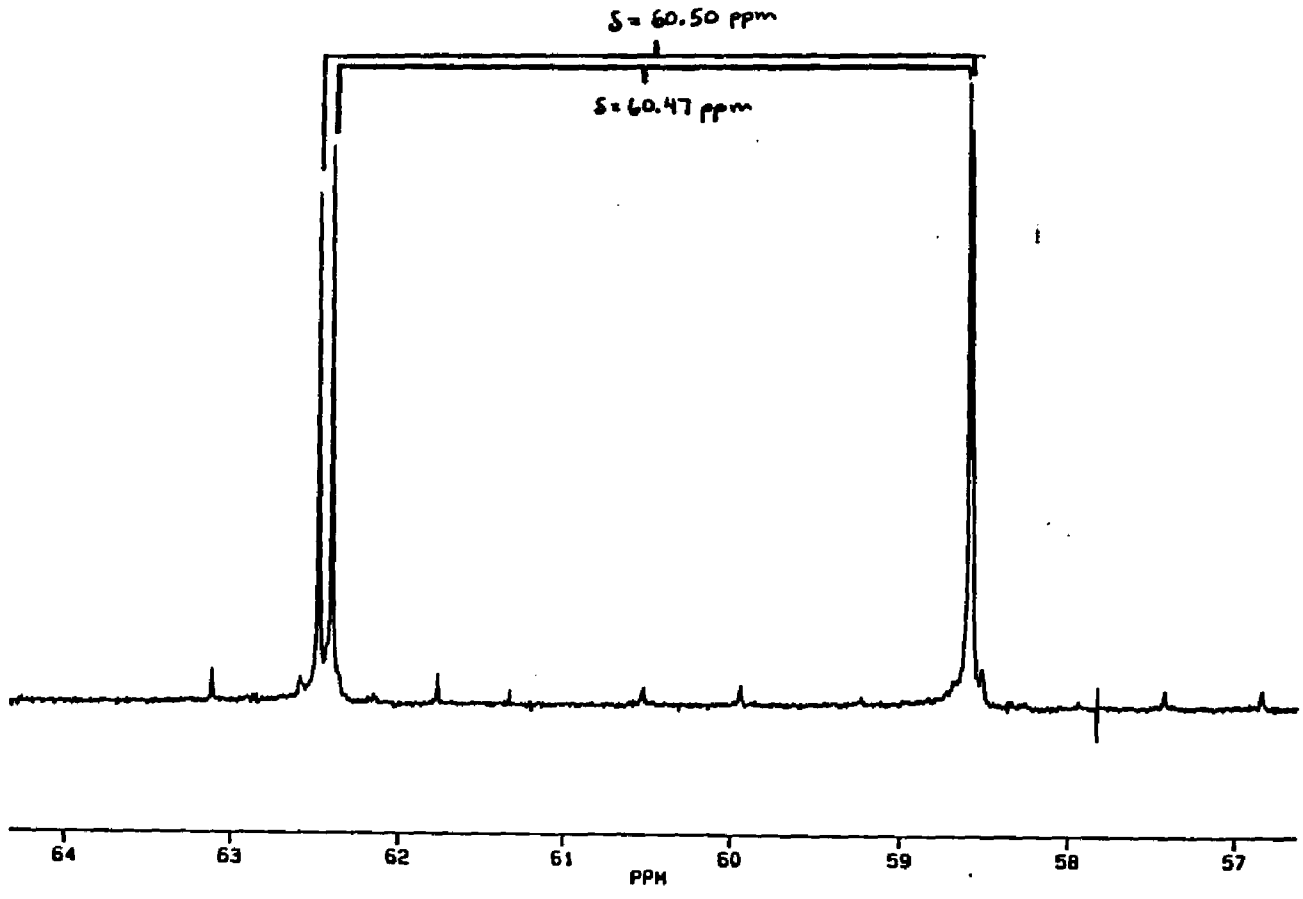

Figure 44: The $^{31}P\{^{1}H\}$ NMR of $[Rh(NBD)(Et_2PCH_2CH_2PPh_2)]BF_4$ in CD_2Cl_2 (40.48 MHz). The lines clarify the center of each resonance and its coupling pattern.

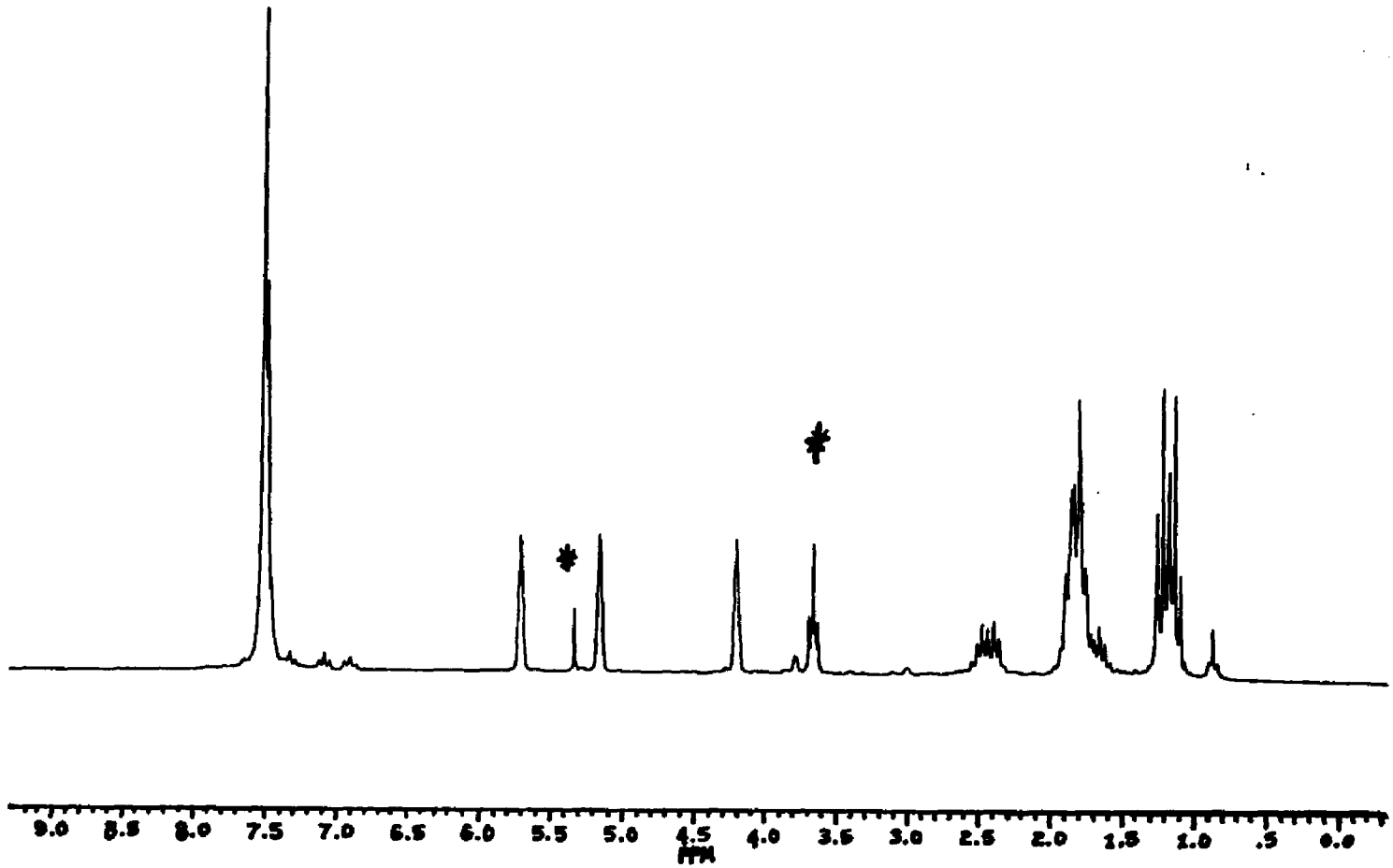

Figure 45: The ^1H NMR of $[Rh(NBD)(Et_2PCH_2CH_2PPh_2)]BF_4$ in CD_2Cl_2 (200.13 MHz). Asterisked peaks are solvent impurities.

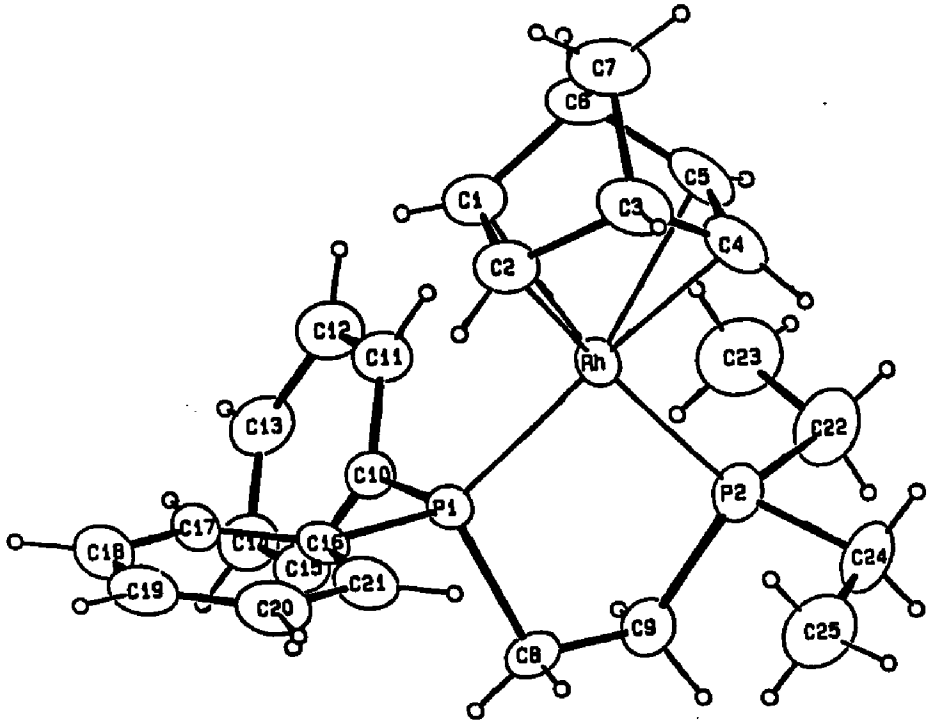

Figure 46: ORTEP of $[Rh(NBD)(Et_2PCH_2CH_2PPh_2)]BF_4$.

Table IX: Bond distances (Å) of $[Rh(NBD)(Et_2PCH_2CH_2PPh_2)]BF_4 \cdot 0.5CH_2Cl_2$.

Rh-P1	2.260 (2)	C10-C11	1.39 (2)
Rh-P2	2.292 (3)	C10-C15	1.42 (2)
Rh-C1	2.219 (9)	C11-C12	1.38 (2)
Rh-C2	2.215 (9)	C12-C13	1.41 (2)
Rh-C4	2.239 (9)	C13-C14	1.40 (2)
Rh-C5	2.23 (1)	C14-C15	1.38 (2)
P1-C8	1.85 (1)	C16-C17	1.37 (2)
P1-C10	1.82 (1)	C16-C21	1.41 (2)
P1-C16	1.83 (1)	C17-C18	1.41 (2)
P2-C9	1.87 (1)	C18-C19	1.37 (2)
P2-C22	1.84 (2)	C19-C20	1.41 (2)
P2-C24	1.83 (1)	C20-C21	1.41 (2)
C1-C2	1.39 (1)	C22-C23	1.55 (3)
C1-C6	1.56 (1)	C24-C25	1.52 (2)
C2-C3	1.58 (1)	Cl(1)-C1S	1.78 (2)
C3-C4	1.54 (1)	B-F1	1.37 (2)
C3-C7	1.59 (2)	B-F2	1.37 (2)
C4-C5	1.40 (2)	B-F3	1.32 (2)
C5-C6	1.53 (2)	B-F4a	1.33 (2)
C6-C7	1.57 (2)	B-F4b	1.27 (3)
C8-C9	1.53 (2)		

Table X: Bond angles (deg) in $[Rh(NBD)(Et_2PCH_2CH_2PPh_2)]BF_4 \cdot 0.5CH_2Cl_2$.

P1-Rh-P2	83.73 (8)	C9-P2-C24	105.5 (7)
P1-Rh-C1	101.7 (2)	C22-P2-C24	100.9 (8)
P1-Rh-C2	102.6 (2)	Rh-C1-C2	71.5 (5)
P1-Rh-C4	162.0 (3)	Rh-C1-C6	94.9 (7)
P1-Rh-C5	159.1 (4)	C2-C1-C6	106.6 (9)
P2-Rh-C1	163.7 (3)	Rh-C2-C1	71.8 (5)
P2-Rh-C2	157.5 (3)	Rh-C2-C3	94.9 (5)
P2-Rh-C4	101.2 (3)	C1-C2-C3	106.6 (8)
P2-Rh-C5	103.7 (4)	C2-C3-C4	103.2 (8)
C1-Rh-C2	36.7 (4)	C2-C3-C7	98.3 (9)
C1-Rh-C4	78.4 (4)	C4-C3-C7	100.6 (9)
C1-Rh-C5	66.1 (4)	Rh-C4-C3	95.1 (5)
C2-Rh-C4	66.5 (4)	Rh-C4-C5	71.5 (6)
C2-Rh-C5	78.1 (4)	C3-C4-C5	106 (1)
C4-Rh-C5	36.6 (4)	Rh-C5-C4	72.0 (6)
Rh-P1-C8	108.9 (4)	Rh-C5-C6	95.2 (7)
Rh-P1-C10	113.5 (3)	C4-C5-C6	107 (1)
Rh-P1-C16	118.0 (4)	C1-C6-C5	103 (1)
C8-P1-C10	103.9 (5)	C1-C6-C7	99 (1)
C10-P1-C16	106.6 (4)	C3-C7-C6	93 (1)
Rh-P2-C9	109.7 (4)	P1-C8-C9	106.8 (9)
Rh-P2-C22	117.4 (5)	P2-C9-C8	109.3 (8)
Rh-P2-C24	116.2 (5)	P1-C10-C11	119.5 (8)
C9-P2-C22	106.1 (7)	P1-C10-C15	120.5 (9)
C11-C10-C15	120. (1)	P2-C22-C23	113 (1)
C10-C11-C12	121. (1)	P2-C24-C25	112.3 (9)
C11-C12-C13	119. (1)	F1-B-F2	106 (1)
C12-C13-C14	120. (1)	F1-B-F3	120 (1)
C13-C14-C15	121. (1)	F1-B-F4a	105 (1)
C10-C15-C14	119. (1)	F1-B-F4b	102 (1)
P1-C16-C17	122.5 (9)	F2-B-F3	128 (1)
P1-C16-C21	115.5 (8)	F2-B-F4a	93 (1)
C17-C16-C21	122. (1)	F2-B-F4b	91 (1)
C16-C17-C18	120. (1)	F3-B-F4a	96 (1)
C17-C18-C19	119. (1)	F3-B-F4b	60 (1)
C18-C19-C20	122. (1)	F4a-B-F4b	151 (2)
C19-C20-C21	119. (1)		

(9) and 2.23 (1) Å. All the other bond distances and angles in this complex are normal and will not be discussed further. Elemental analysis of crystalline [Rh (NBD)-(dedppe)]BF_4·0.5CH_2Cl_2 is in good agreement with theoretical values (see experimental section).

The purpose of synthesizing [Rh(NBD)(dedppe)]BF_4 was to produce a monometallic model that contains one electron-rich alkyl-phosphine and one less basic aryl-phosphine. The results from catalytic studies using [Rh(NBD)-(dedppe)]BF_4 will be compared to monometallic rhodium systems that use more electron-rich alkyl-phosphines to examine the sensitivity of hydroformylation catalyst to phosphine-ligand electronic effects.

Section 6.8 [Rh(NBD)($Et_2PCH_2CH_2PEt_2$)]BF_4

This was the last of the monometallic models of [Rh(NBD)P_2]BF_4 using $Et_2PCH_2CH_2PEt_2$ (depe) obtained from Strem Chemical . Similar synthetic procedures used on all the previous rhodium norbornadiene complexes were implemented. [Rh(NBD)(depe)]BF_4 was isolated as a red solid in 80-90% yields. Rod-like crystals of [Rh(NBD)(depe)]BF_4 can be grown when the mother liquor is placed in a -40° C freezer.

[Rh(NBD)(depe)]BF_4 has been characterized by $^{31}P\{^1H\}$ NMR (Figure 47). The spectrum consists of only a doublet at δ = 67.0 ppm ($J_{Rh\text{-}P}$ = 157 Hz) since both phosphorus atoms of the ligand are equivalent. The chemical shift of the phos-phorus resonance seen here is consistent with other chemical shifts obtained from [Rh(NBD)P_2]BF_4-type molecules in this thesis.

The increased symmetry the complex contains is due to equivalent phosphorus atoms creating a decipherable coupling of the NBD ligand (figure 48). The

olefinic protons of NBD at $\delta = 5.4$ ppm appear as a broad quartet due to coupling of phosphorus (triplet, $J_{P\text{-}H} = 2.2$ Hz) and the two equivalent protons on the tertiary sp^3-carbon of NBD (triplet, $J_{H\text{-}H} = 2.2$ Hz). The protons on the tertiary sp^3-hybridized carbons of NBD are a broad multiplet at $\delta = 4.1$ ppm. The two protons on the secondary sp^3-hybridized carbon of NBD form a singlet at $\delta = 1.7$ ppm.

The ^1H NMR also gives evidence that $Et_2PCH_2CH_2PEt_2$ has coordinated to rhodium by the multiplet at $\delta = 1.0\text{-}1.2$ ppm which accounts for the methyl group of the terminal ethyl groups on the phosphorus atoms. Since the methylene protons of the terminal ethyl group and the protons on the chelate ring have similar environments, they resonate at a range of $\delta = 1.5\text{-}1.8$ as an overlapping multiplet caused by proton and phosphorus couplings.

The presence of CH_2Cl_2 solvent can be seen in the ^1H NMR spectra at $\delta =$ 5.3 ppm. The elemental analysis of $[Rh(NBD)(Et_2PCH_2CH_2PEt_2)]BF_4$ was obtained and the amount of solvent present was determined from the experimental values. The values found agreed satisfactorily with the presence of one molecule of solvent and are given in the experimental section.

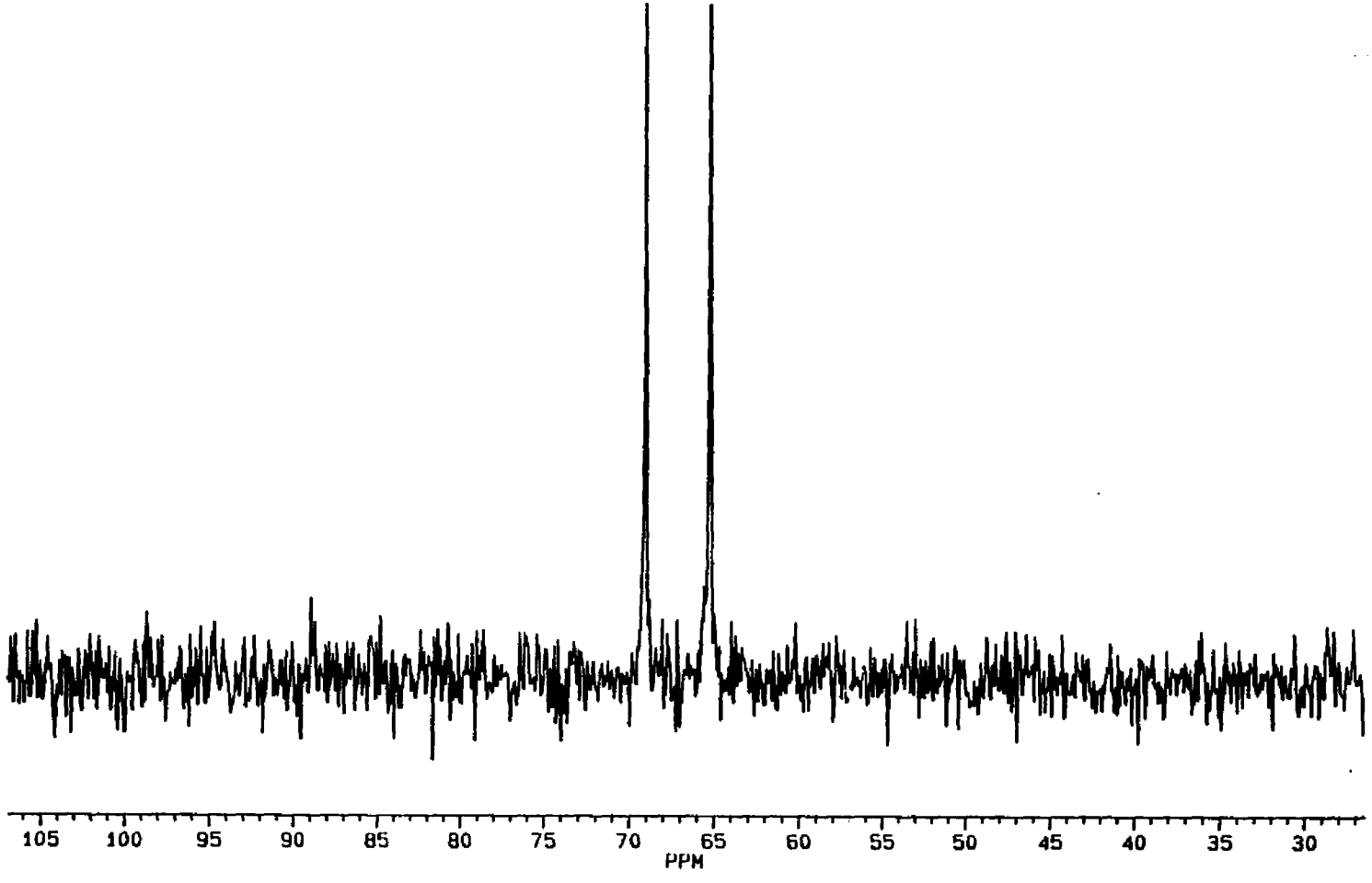

Figure 47: The $^{31}P\{^{1}H\}$ NMR of $[Rh(NBD)(Et_2PCH_2CH_2PEt_2)]BF_4$ in CD_2Cl_2 (40.48 MHz).

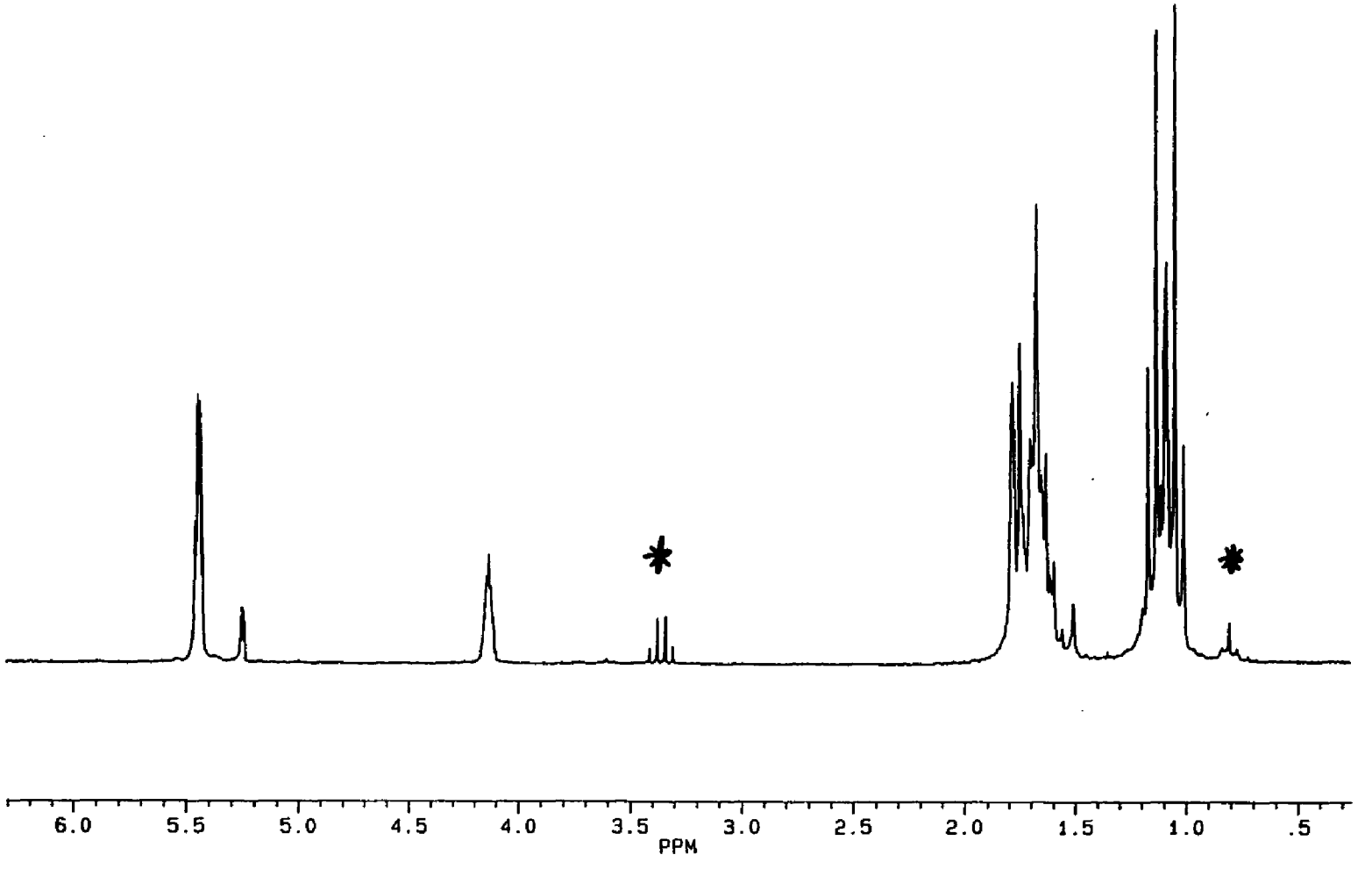

Figure 48: The ^{1}H NMR of $[Rh(NBD)(Et_2PCH_2CH_2PEt_2)]BF_4$ in CD_2Cl_2 (200.13 MHz). Asterisked peaks are solvent impurities.

Chapter 7 Conclusions

The new tetratertiary phosphine ligand, LTTP, can be synthesized from readily available starting materials in 39-40% yield. The combination of a bis(phosphino)methane bridge with bis(phosphino)ethane chelating units in eHTP has proven to be a unique environment well suited for the formation of bimetallic species. The bis(phosphino)methane unit keeps the metals in proximity while the metals are further stabilized by the 5-membered chelate ring formed by the bis(phosphino)ethane with the metal. The electron-rich ethyl substituent of LTTP, (eLTTP), can also strongly coordinate to the metal and inhibit any fragmentation.

Homobimetallic nickel complexes of eLTTP, *rac*- and *meso*-Ni_2Cl_4(eLTTP), can be easily separated their different crystal morphologies. The diastereomerically pure ligand can be liberated quantitatively from the pure diastereomer of each bimetallic nickel complex by refluxing an excess NaCN in a heptane/water mixture.

Homobimetallic rhodium complexes of eLTTP, $Rh_2Cl_2(CO)_2$(eLTTP) and $[Rh_2(NBD)_2(eLTTP)](2BF_4)_2$, can be used as homogeneous hydroformylation catalysts. High turnover rates (740/hr) and selectivities (30:1) of the linear aldehyde product are produced at 80 °C and 80 psi (H_2/CO) using $[Rh_2(NBD)_2(eLTTP)]$-$(2BF4)_2$ without the presence of excess phosphine. The rates and selectivities of $[Rh_2(NBD)_2(eLTTP)](2BF_4)_2$ comparisons favorably with the commercial process $HRh(CO)(PPh_3)_3$, which also has fast turnover rates (840/hr) and high selectivities (14:1); however, high amounts of PPh_3 are required to stabilize the catalyst.

The high catalytic activity of the electron-rich phosphine stabilized$[Rh_2$-$(NBD)_2(eLTTP)](2BF_4)_2$ is due to bimetallic cooperativity. Monometallic model complexes with electron-rich coordinating phosphines, $[Rh(NBD)(depmpe)]BF_4$, $[Rh(NBD)(dedppe)]BF_4$, and $[Rh(NBD)(depe)]BF_4$, have been used as hydrofor-

mylation catalyst in order to compare turnover rates. These rates for the monometallic model systems are only between 4-10 turnovers/hr and support the increase catalytic activity due bimetallic cooperativity.

VDW energy contour maps of $Rh_2H_2(CO)_2$(eLTTP) (proposed active catalyst) generated by SYBYL has shown that eLTTP can rotate to produce sterically accessible closed-mode conformation in which the metal are next to one another (the origin of the map). A computer generated conformation from a small low energy minimum near the origin shows that a rotational conformation with bridging hydrides are sterically possible. The high turnover rates of $Rh_2H_2(CO)_2$(eLTTP) are attributed to the formation of bridging hydrides.

Structure-reactivity analyses with second set of model complexes have been studied to test the relationship of bridging hydrides with respect to the high turnover rate of $Rh_2H_2(CO)_2$(eLTTP). Bimetallic rhodium complexes, $[Rh_2(NBD)_2$(eLTTP-pr)$](2BF_4)_2$, $[Rh_2(NBD)_2$(eLTTP-*p*-xyl)$](2BF_4)_2$, containing tetraphosphines that have been designed to increase the separation of the metals have been tested for hydroformylation. The rates of these complexes are 4-20 turnovers/hr. Increasing the distance of the metal dramatically reduces or eliminates the formation of a bridging hydride intermediate so that these complexes behave essentially as two independent monometallic catalysts.

This work represents the first dramatic example of homobimetallic cooperativity in catalysis and demonstrates that useful chemistry based on polymetallic system can be developed and should continued to be explored. Systems with more than one metal center can be designed to do some unique and exciting reactions that may not be possible with monometallic systems.

CHAPTER 8 Experimental

Section 8.1 Instrumentation

The NMR spectra were recorded on Bruker AC-100, AC-200, or AM-400 spectrometers at Louisiana State University or on a Varian CXP-300 FT spectrometer at Washington University in St.Louis. The NMR experiments were performed in either 5 or 10 mm tubes and were run at room temperature (25 °C) unless otherwise stated. NMR spectral simulations were performed on the Bruker instruments using the Bruker program PANIC. Infrared spectra were obtained from a Perkin-Elmer 283B spectrometer using either KBr or Nujol mull mediums. Mass spectra were performed on a Hewlett Packard 5985A GC/MS with electron impact (EI) and chemical ionization (CI) capabilities. Elemental analysis were performed by Galbraith Laboratories, Inc., Knoxville, Tennessee, and Oneida Research Laboratories, Inc., Whitesboro, New York.

X-ray crystallographic data was collected on Nicolet P3 (Washington Univ.) or Enraf-Nonias CAD4 (LSU) diffractometers at room temperature using MoKα radiation with a graphite crystal monochromator and the $\theta/2\theta$ scan data collection technique. Structure solving was performed on a VAX 11/780 (Washington Univ.) or MicroVAX II/3000 Series (LSU) computers using the Enraf-Nonius Structure Determination Package.

Section 8.2 General Procedures

Unless otherwise stated all manipulations were carried out under inert atmosphere (argon or nitrogen) using standard Schlenk line and glove box techniques. Solvents were redistilled under inert atmosphere from the appropriate drying agents as follows: diethyl ether, hexane, tetrahydrofuran (sodium/benzophenone); toluene

(sodium); dichloromethane and acetonitrile (calcium hydride); methanol and ethanol (magnesium). Distilled water was obtained from the chemistry building and degassed by purging with nitrogen gas for 15 minutes.

Reagents purchased were used without purification. $PhPH_2$, Et_2PCl, and $Ph_2PCH{=}CH_2$ were purchased from Strem Chemicals. Methyllithium, phenyllithium, cyclohexane, $CH_2{=}CHMgBr$, xylenes, sodium, and potassium were purchased from Aldrich. Alfa division of Morton Thiokol supplied the $NiCl_2{\cdot}6H_2O$, and Mallinckrodt supplied the N,N-dimethylformamide. The free radical initiator 2,2'-azobis(isobutyronitrile) was purchased from Pfaltz & Bauer, Inc. and recrystallized from methanol.

Gases purchased were used as received. Nitrogen used as the inert atmosphere gas was obtained from the "boil-off" of 150 liter liquid nitrogen dewars. Cylinders of nitrogen (used as a "purging gas" for the dry boxes), hydrogen, and argon were purchased from Liquid Carbonic. High purity (99.99%) synthesis gas of 50% carbon monoxide in hydrogen (1:1 H_2/CO) and 33.4% carbon monoxide in hydrogen (2:1 H_2/CO) were obtained from Liquid Carbonic.

The hydroformylation runs were performed in either a 450 mL or 600 mL stainless steel autoclave from Parr. The reactions were carried out using a glass insert and the progress of the reaction was observed by the gas uptake in a 1 liter reservoir that was connected to a two-stage regulator which delivered gas at a constant pressure. All information during the catalytic run was recorded onto a Parr Controller 4851 Controller.

Section 8.3 Ligand Synthesis

Section 8.3.1 eLTTP

In a 100 ml Schlenk flask was placed 3.84 g (0.017 moles) of $Ph(H)PCH_2P(H)Ph$[11] and 3.84 g (0.033 moles) of $Et_2PCH{=}CH_2$ in 50 mL of cyclohexane. A previously degassed reflux condenser with 0.0384 g of AIBN – (1/100th of the weight of the vinylphosphine) inside was attached to the Schlenk flask allowing the radical initiator to fall into the solution. The solution was refluxed overnight with stirring.

Afterwards, the solvent was vacuum evaporated leaving behind a colorless and cloudy viscous oil. The oil was taken up in 30 mL of ether and passed through a neutral alumina column to remove unreacted $Ph(H)PCH_2P(H)Ph$. The eluant was placed on a rotovap and stripped of its solvent via vacuum evaporation. A short-head distillation column was attached, and the oil was distilled under vacuum (0.1 torr). The temperature was slowly raised to 170° C and maintained for 20 minutes to distill impurities away. Liquid nitrogen placed under the receiving flask improved the purity of the final product. The residue in the distillation pot contained pure product appearing as a very cloudy colorless, very viscous liquid. Again, the oil was taken up in 30 mL of ether and passed through a neutral alumina column. The eluant was vacuum evaporated leaving behind 6.75 g of a cloudy colorless, very viscous liquid, eLTTP. (88% yield, typical isolated yields 75-90%)

Analysis: Calculated for $C_{25}H_{40}P_4$: C, 64.66; H, 7.91. Found C, 63.58; H, 7.91. $^{31}P\{^1H\}$NMR (C_6D_6, δ in ppm, H_3PO_4 reference): diastereotopic internal phosphorus atoms, -26.2 (1 P, dd $J_{P\text{-}P}$ = 10 Hz and $J_{P\text{-}P}$ = 12.2 Hz) and -25.5 (1 P, dd $J_{P\text{-}P}$ = 10.2 Hz and $J_{P\text{-}P}$ = 12.1 Hz); external phosphorus atoms, -18.37 (1 P, dd, $J_{P\text{-}P}$ = 10.3 Hz and $J_{P\text{-}P}$ = 12.5 Hz) and -18.31 (1 P, dd, $J_{P\text{-}P}$ = 10.4 Hz

and $J_{P\text{-}P}$ = 12.3 Hz). Computer-simulated coupling constants based on an AXX'A' spin system: $J_{P_{int}\text{-}P_{ext}}$ = 22.5 Hz and $J_{P_{int}\text{-}P_{int}}$ = 109.5 Hz. ^{1}H NMR (C_6D_6, δ in ppm, TMS reference): 0.49-0.70 (m, P-CH_2-CH_3), 0.78-0.91 (m, P-CH_2-CH_3), 0.91-1.23, 1.47-1.85 (m, P-CH_2-CH_2-P), 2.01-2.15 (m, P-CH_2-P), 6.50-6.97 and 7.05-7.47 (m, Ph).

Section 8.3.2 phLTTP

The procedure for preparing the phenylated version of LTTP was similar to that described for eLTTP above except that $Ph_2PCH{=}CH_2$ was used as the starting material in cyclohexane. The workup following the reaction, however, was different. After the cyclohexane was removed by vacuum evaporation, the very viscous liquid was dissolved in 20 ml of ether and placed in a -40° C freezer overnight. A white microcrystalline powder formed on the sides of the flask which was mainly composed (~80%) of the meso diastereomer (based on ^{31}P NMR). Further precipitations of the original viscous liquid decrease the purity of the microcrystalline powder. The ether solution was evaporated to give a very sticky solid from which the remaining impurities were removed by vacuum distillation up to 210° C (0.1 torr). The residue that remained was phLTTP (purity > 98%). Total isolated yield was 85-90%.

Analysis: Calculated for $C_{41}H_{40}P_4$: C, 75.00; H, 6.10. Found C, 75.22; H, 6.16. ^{31}P{^{1}H}NMR (C_6D_6, δ in ppm, H_3PO_4 reference): diastereotopic internal phosphorus atoms, -25.8 (1 P, dd $J_{P\text{-}P}$ = 13.3 Hz and $J_{P\text{-}P}$ = 17.0 Hz) and -25.2 (1 P, dd $J_{P\text{-}P}$ = 13.3 Hz and $J_{P\text{-}P}$ = 17.0 Hz); external phosphorus atoms, -11.9 (2 P, dd, $J_{P\text{-}P}$ = 13.3 Hz and $J_{P\text{-}P}$ = 17.0 Hz). Computer-simulated coupling constants based on an AXX'A' spin system: $J_{P_{int}\text{-}P_{ext}}$ = 29.9 Hz and $J_{P_{int}\text{-}P_{int}}$ =

107.6 Hz. ^{1}H NMR (C_6D_6, δ in ppm, TMS reference): 1.60-1.79, 1.79-1.93, 1.93-2.15 (m, P-C*H*$_2$-C*H*$_2$-P), 2.18 (t, P-C*H*$_2$-P), 6.90 and 7.20 (m, Ph).

Section 8.3.3 eLTTP-pr

The free-radical catalyzed addition of $Et_2PCH{=}CH_2$ (0.296 g, 2.552 mmoles) to $Ph(H)PCH_2CH_2CH_2P(H)Ph$ (0.661 g, 2.035 mmoles) with AIBN (0.003 g) was performed as described for eLTTP.

The solvent was vacuum evaporated and taken up in THF. Excess KH (1 g) was added and the mixture was hand-swirled occasionally. As the slurry stood unstirred for 1 week[41] a yellow color of the solution began to deepen. The solvent was stripped off, and the product was extracted with 20 mL of hexane. The slightly yellow solution was purified by passage through a neutral alumina. The solvent was stripped via vacuum evaporation leaving 0.766 g of eLTTP-pr (80 % yield) as a clear and colorless viscous liquid.

Analysis: $^{31}P\{^1H\}$NMR (C_6D_6, δ in ppm, H_3PO_4 reference): internal phosphorus atoms, -21.7 (1 P, dd, $J_{P\text{-}P} \approx 21.5$ Hz); external phosphorus atoms, -18.6 (1 P, dd, $J_{P\text{-}P} = 21.5$ Hz). ^{1}H NMR (C_6D_6, δ in ppm, TMS reference): 0.6-0.8 (m, CH_3CH_2P-); 0.9-1.0 (m, CH_3CH_2P-); 1.0-1.5 (overlapping m, -PC*H*$_2$C*H*$_2$P(Ph)C*H*$_2$C*H*$_2$C*H*$_2$P(Ph)C*H*$_2$C*H*$_2$P-); 6.8-7.0 and 7.0-7.3 (m, -(*Ph*)P-).

Section 8.3.4 *p*-$[HP(Ph)CH_2]_2C_6H_4$

K[(Ph)PH][42] (3.250 g, 21.959 mmoles) was added as a solid to a stirred solution of α,α'-dichloro-*p*-xylene (1.92 g, 10.980 mmoles) in THF in a glove box. As the yellow solid (K[(Ph)PH]) was added in portions to the clear and color-

less solution, the yellow color disappeared in seconds. As the addition of K[(Ph)PH] progressed (30 min) a white precipitate formed. When the addition was complete, the solution was a very pale yellow with a white solid present. The mixture was allowed to stir for 6-12 hours. The solvent was removed by rotary evaporation, leaving a white solid. The solid was extracted into 3 x 20 mL portions of warm freshly distilled toluene. The mixture was shaken vigorously during each extraction. The extracts were combined and vacuum evaporated leaving behind 2.580 g of product as a white solid (73 % yield).

Analysis: $^{31}P\{^{1}H\}$NMR (C_6D_6, δ in ppm, H_3PO_4 reference): diastereotopic phosphorus atoms, -40.53 (1 P, s). ^{1}H NMR (C_6D_6, δ in ppm, TMS reference): 4.25 (dt, $J_{P\text{-}H}$ = 209.4 Hz, $J_{H\text{-}H}$ = 7.30 Hz, Ph(*H*)P-); 3.10 and 3.12 (d, $J_{H\text{-}H}$ = 7.30 Hz, diastereomeric P-C*H*$_2$-p-xyl-); 6.95 (s, p-C$_6$*H*$_4$-); 7.36-7.54 (m, *Ph*(H)P-).

Section 8.3.5 eLTTP-*p*-xyl

p-[HP(Ph)CH$_2$]$_2$C$_6$H$_4$ (1.320 g, 4.099 mmoles) and Et$_2$PCH=CH$_2$ (0.951 g, 8.198 mmoles) in 80 mL of cyclohexane was added to a two neck Schlenk flask in a glove box. The flask was removed from the glove box and a degassed reflux condenser was attached. The mixture was warmed to near reflux before the addition of a 15 mL cyclohexane solution of AIBN (0.010 g) by cannula. The mixture refluxed for 4-5 hours before a second batch of AIBN was added in the same manner. The mixture refluxed for another 4-5 hours before the solvent was vacuum evaporated. The resulting oily solid (2.001 g) was dissolved in a minimal amount of CH_2Cl_2 and eluted through a neutral alumina column. The clear and colorless CH_2Cl_2 solution was placed in a -30° C freezer overnight which precipitated 0.168

g of white solid eLTTP-*p*-xyl in 10% yield whose 31P NMR showed some impurities.

An alternative route to this crystallization from CH_2Cl_2 (see Section 6.3.3) KH can be added to a THF solution containing the oily solid product. eLTTP-*p*-xyl (1.231 g, 57% yield) can be obtained from this alternate procedure. Purification of phosphines by KH addition is a better work-up technique compared to vacuum distillations at high temperatures. Although the KH route takes longer, the method is less severe and the isolated yields are higher.

Analysis: $^{31}P\{^1H\}$NMR (C_6D_6, δ in ppm, H_3PO_4 reference): external phosphorus atoms, -14.1 (1 P, d, $J_{P\text{-}H}$ = 20.3 Hz); internal phosphorus atoms, -11.5 (1 P, d, $J_{P\text{-}H}$ = 22.0 Hz). ^1H NMR (C_6D_6, δ in ppm, TMS reference): 0.75-1.0 (m, CH_3CH_2P-); 1.1-1.4 (m, CH_3CH_2P-); 1.5-1.8 (m, -PCH_2CH_2P-); 2.88 (s, P-CH_2-*p*-xyl-); 6.73 (s, *p*-C_6H_4-); 6.6-7.3 and 7.3-7.44 (m, -(*Ph*)P-).

Section 8.3.6 (Ph)P(Me)H

This product was originally reported by Stelzer and coworkers as a side product in the production of $Ph(H)PCH_2P(H)Ph$.[11] 2.615 g (17.67 mmoles) of K[(Ph)PH][43] was dissolved in50 mL of THF in a round bottom flask. A THF solution of MeI (2.509 g, 17.67 mmoles) was added very slowly via cannula to the yellow phosphide solution. After the yellow mixture stirred overnight a white precipitate of LiCl had formed and the mixture had lightened to a very pale yellow. Hexane was added to further precipitate additional LiCl and the mixture was filtered under a slight vacuum. The filtrate was distilled at ambient pressure to remove THF and hexane, from which 2.139 g of (Ph)P(Me)H was obtained (97% yield).

Analysis: $^{31}P\{^1H\}$NMR (C_6D_6, δ in ppm, H_3PO_4 reference): -70.50 (s).

^{1}H NMR (C_6D_6, δ in ppm, TMS reference): 1.2 (dd, PhP(*Me*)H, $J_{H\text{-}H}$ = 8.09 Hz, $J_{P\text{-}H}$ = 3.50 Hz); 4.0 (dq, PhP(Me)*H*, $J_{P\text{-}H}$ = 204.4 Hz, $J_{H\text{-}H}$ = 7.74 Hz); 7.25 (m, *Ph*P(Me)H)

Section 8.3.7 $Et_2PCH_2CH_2P(Ph)Me$

The free-radical catalyzed addition of $Et_2PCH{=}CH_2$[6] (1.472 g, 12.685 mmoles) to (Ph)P(Me)H (1.573 g, 12.685 mmoles) with AIBN (0.0147 g) was performed similar to the synthesis of eLTTP. Similar workup produces 2.434 g of a clear and colorless viscous liquid in 80% yield.

Analysis: $^{31}P\{^1H\}$NMR (C_6D_6, δ in ppm, H_3PO_4 reference): Et_2P-, -18.3 (1 P, d, $J_{P\text{-}P}$ = 20.4 Hz); Ph(Me)*P*-, -31.5 (1 P, d, $J_{P\text{-}P}$ = 20.7 Hz) ^{1}H NMR (C_6D_6, δ in ppm, TMS reference): 0.55-0.80 (m, P-CH_2-CH_3), 0.90 (d, Ph(*Me*)P-), 0.82-1.02 (m, P-CH_2-CH_3), 1.05-1.20, 1.29-1.60 (m, P-CH_2-CH_2-P), 6.85-6.95 and 7.18-7.28 (m, Ph).

Section 8.3.8 $Et_2PCH_2CH_2PPh_2$

The free-radical catalyzed addition of $Et_2PCH{=}CH_2$[6] (2.029 g, 17.49 mmoles) to Ph_2PH (3.232 g, 17.49 mmoles) with AIBN (0.020 g) was performed similar to the synthesis of eLTTP. The final product mixture is evaporated in vacuum at 130 °C which removes unreacted Ph_2PH (1.693 g) and $Et_2PCH{=}CH_2$. The residue left behind contains 1.803 g of $Et_2PCH_2CH_2PPh_2$ as a clear and colorless viscous liquid in 34 % yield (with approx 6% impurities).

Analysis: $^{31}P\{^1H\}$NMR (C_6D_6, δ in ppm, H_3PO_4 reference): Et_2P-, -17.58 (1 P, d, $J_{P\text{-}P}$ = 25.3 Hz); Ph_2P-, -11.71 (1 P, d, $J_{P\text{-}P}$ = 25.3 Hz) ^{1}H NMR (C_6D_6, δ in ppm, TMS reference): 0.55-0.71 (m, CH_3CH_2P-); 0.79-0.93

(m, CH_3CH_2P-); 1.11-1.36 and 1.78-1.93 (m, -PCH_2CH_2P-); 6.73-6.87 and 7.10-7.25 (m, Ph_2P-).

Section 8.4 Nickel Complexes

Section 8.4.1 Ni_2Cl_4(eLTTP)

A 25 ml EtOH solution of eLTTP (2.00 g, 4.31 mmole) was added to a stirred clear green solution of $NiCl_2 \cdot 6H_2O$ (2.50 g, 8.62 mmole) in 25 ml of EtOH. The solution turned red as the addition proceeded, with an orange precipitate forming near the end of the reaction. After the mixture was stirred overnight, the orange precipitate was collected by filtration and washed with three 10 ml portions of cold EtOH to give 1.42 g (45% yield) of mainly *meso*-Ni_2Cl_4(eLTTP). The filtrate was evaporated to give 1.25 g (40% yield) of mainly *rac*-Ni_2Cl_4(eLTTP) for an overall isolated yield of 85%. Typical overall isolated yields for this reaction ranged from 80-95%.

The orange solid was dissolved in a minimum volume of CH_2Cl_2 and evaporated to dryness, yielding a red solid (this procedure enhances the formation of crystals in the next step). The red solid was then dissolved in THF and allowed to gradually evaporate, giving rise to well-formed, medium to large crystals of *meso*-Ni_2Cl_4(eLTTP) and *rac*-Ni_2Cl_4(eLTTP)·THF. The orange-red crystals were air-stable, but one crystal type quickly desolvated to give opaque crystals. Thus the two types can be easily separated under a microscope. An X-ray structural determination has identified the crystal type that desolvated as *meso*-Ni_2Cl_4(eLTTP)-·1.5THF, while the other was composed of *rac*-Ni_2Cl_4(eLTTP)·THF. On a larger scale, the red solid isolated from evaporation of a CH_2Cl_2 solution can be dissolved in a minimal quantity of THF and allowed to stand for 1 hr. The reddish-orange

precipitate that forms was *rac*-Ni_2Cl_4(eLTTP) with only a trace of the meso-diastereomer present.

rac-Ni_2Cl_4(eLTTP). Analysis: Calculated for $C_{25}H_{40}Cl_4Ni_2P_4$ (after losing molecule of solvent): C, 41.49; H, 5.57. Found C, 42.14; H, 5.62. $^{31}P\{^1H\}$NMR (CD_2Cl_2, δ in ppm, H_3PO_4 reference): diastereotopic internal phosphorus atoms, 57.97 (1 P, dt $J_{P\text{-}P}$ = 69.0 Hz and $J_{P\text{-}P}$ = 3.9 Hz); external phosphorus atoms, 75.41 (1 P, dt, $J_{P\text{-}P}$ = 69.0 Hz and $J_{P\text{-}P}$ = 3.9 Hz. ^1H NMR (CD_2Cl_2, δ in ppm, TMS reference): See Table II on page 21.

meso-Ni_2Cl_4(eLTTP). Analysis: Calculated for $C_{25}H_{40}Cl_4Ni_2P_4$ (after losing molecule of solvent): C, 41.49; H, 5.57. Found C, 40.87; H, 5.46. $^{31}P\{^1H\}$NMR (CD_2Cl_2, δ in ppm, H_3PO_4 reference): internal phosphorus atoms, 58.32 (1 P, dt $J_{P\text{-}P}$ = 72.8 Hz and $J_{P\text{-}P}$ = 10.8 Hz); external phosphorus atoms, 74.21 (1 P, dt, $J_{P\text{-}P}$ = 72.8 Hz and $J_{P\text{-}P}$ = 10.8 Hz. ^1H NMR (CD_2Cl_2, δ in ppm, TMS reference): See Table II.

Section 8.4.2 *rac*, trans-$Ni(CN)_2(\eta^2$-eLTTP)

rac, trans-$Ni(CN)_2(\eta^2$-eLTTP) is a by-product of the eLTTP extraction of Ni_2Cl_4(eLTTP) in a benzene/H_2O/NaCN system described in Section 7.5.1.

Analysis: $^{31}P\{^1H\}$NMR (C_6D_6, δ in ppm, H_3PO_4 reference): internal phosphorus atoms, 43.0 (1 P, s); external phosphorus atoms, -14.7 (1 P, s). IR (KBr): ν_{CN} = 2100 cm^{-1} (sharp and strong), 2119 cm^{-1} (shoulder).

Section 8.5 eLTTP Ligand extractions

Section 8.5.1 Benzene/H_2O/NaCN system

rac-Ni_2Cl_4(eLTTP)[9b] (0.186 g, 0.257 mmole) and 0.75g (15.31 mmole) of

NaCN were placed in a flask with 20 mL of benzene in a glove box. The flask was sealed and removed from the glove box and connected to a Schlenk line where 20 mL of degassed water was added via syringe. A reflux condenser was attached and the stirred reaction mixture was heated to reflux for 30 min.

After cooling the stirring was stopped and two layers were allowed to separate. The yellow organic layer (top) was carefully removed via a cannula. Two additional extractions with 10 mL of benzene were performed. The organic layers were combined and brought into the glove box where they were vacuum evaporated leaving a viscous yellow oil. The yellow oil was dissolved in 2-3 mL of benzene and eluted through an neutral alumina column. The yellow impurity remained at the top of the column and the eLTTP ligand passed through the column. A clear and colorless viscous liquid was obtained after roto-evaporation (0.057 g, 48 % recovery).

The yellow impurity was removed from the neutral alumina column by eluting with THF. After slow evaporation of the solvent, crystals of *rac*,trans-Ni $(CN)_2(\eta^2$-eLTTP) were obtained. Spectroscopic data on *rac*,trans-Ni$(CN)_2(\eta^2$-eLTTP) is presented in Section 8.4.2.

Section 8.5.2 Heptane/H_2O/NaCN system

Ni_2Cl_4(eLTTP) (0.201 g, 0.278 mmole) and NaCN (0.650 g, 13.3 mmole) were added to a Schlenk flask in a glove box. Heptane (20 mL) was added to the flask which was then removed from the glove box. On a Schlenk line 20 mL degassed water was syringed into the flask. A reflux condenser was attached to the flask and the stirred mixture was heated to reflux for 1 hour.

After cooling the clear heptane layer (top) was removed via cannula. Two

addition extractions were performed with 10 mL of pentane. The organic layers were combined and vacuum evaporated. eLTTP was obtained as a clear and colorless viscous liquid (0.126 g, 98% recovery). The purity was confirmed by ^{31}P NMR.

Section 8.6 Rhodium Complexes

Section 8.6.1 $Rh_2Cl_2(CO)_2$(eLTTP)[9a]

eLTTP (0.0235 g, 0.51 mmole) in 25 mL of THF was gradually added via cannula to 0.197 g (0.51 mmole) of $Rh_2(\mu\text{-}Cl)_2(CO)_4$ in 25 mL of THF in a dry ice/ acetone bath under inert atmosphere conditions. The yellow Rh solution turned a golden-red color after the first drop of eLTTP. The solution was occasionally flushed with N_2 to remove CO released from the reaction. The reaction mixture was allowed to gradually warm to room temperature and left to stir overnight. A small amount of unidentified red-brown precipitate was separated by filtration. The red-orange filtrate was roto-evaporated to dryness and redissolved in ca. 20 mL of THF which deposited small X-ray quality orange-red crystals of a uniform morphology of *racemic*-Rh_2Cl_2-$(CO)_2$(eLTTP) diastereomer upon slow evaporation of solvent. X-ray quality crystals can also be grown from toluene by slow evaporation. Total isolated yield of crystalline $Rh_2Cl_2(CO)_2$(eLTTP), 15-20%.

Analysis: Calculated for $C_{27}H_{40}P_4Rh_2Cl_2O_2$: C, 40.68; H, 5.06. Found C, 39.53; H, 5.06. IR (KBr) 1970 cm^{-1} (carbonyl); 1419, 1441, and 1460 cm^{-1} (phosphine ligand). $^{31}P\{^1H\}$NMR (d_4-MeOH, δ in ppm, H_3PO_4 reference): internal phosphorus atoms, 56.2 (1 P, m, $J_{Rh\text{-}P}$ = 139 Hz); external phosphorus atoms, 83.8 (1 P, dd, $J_{P\text{-}P}$ = 31 Hz and $J_{Rh\text{-}P}$ = 149 Hz). ^1H NMR (CD_2Cl_2, δ in ppm, TMS reference): 0.8-1.25 (m, P-CH_2CH_3), 1.70-1.20 (m, PCH_2-CH_3),

1.19-1.33, 2.05-2.65 (m, P-CH_2-CH_2-P), 3.21 (t, *rac*-PCH_2-P), 3.39 and 3.62 (m, *meso*-P-CH_2-P), 7.32-7.60 and 7.85-8.10 (m, Ph).

Section 8.6.2 $[Rh_2(NBD)_2(eLTTP)](BF_4)_2$

A synthetic procedure similar to that of Bosnich and coworkers was followed.[20] $[Rh(NBD)_2]BF_4$ (0.154 g, 0.412 mmole) and eLTTP (0.096 g, 0.206 mmole) were weighed out and added to separate flasks in a glove box. Using a graduated cylinder 2.5 mL of CH_2Cl_2 and THF each was measured and combined. 3 mL of the CH_2Cl_2/ THF solution was added to the flask containing the $[Rh(NBD)_2]BF_4$ and 1 mL to the eLTTP flask. The ligand solution was quickly added dropwise to the $[Rh(NBD)_2]BF_4$/ CH_2Cl_2/ THF slurry while hand swirling the reaction flask. The reaction mixture rapidly turned to a clear red solution. The remaining CH_2Cl_2/ THF solution was used to rinse the eLTTP flask and was added rapidly to the reaction mixture. The reaction flask was swirled by hand for a few seconds. Hexane (3 mL) was measured with the graduated cylinder and poured into the reaction mixture resulting in a turbid solution. Again the reaction flask was swirled by hand until the reaction mixture turned clear red (at this point the reaction mixture may still contain precipitate). The mixture was allowed to stand, with occarional swirling, for 10 hours, during which time a dark red oil separated on the bottom of the flask. The CH_2Cl_2/ THF/hexane (not the red oil) was poured into a clean vial and placed into a -40° C freezer for crystallization. The dark red oil is pure $[Rh_2(NBD)_2(eLTTP)](BF_4)_2$. The oil is taken up in 1-2 mL of CH_2Cl_2 and the solvent is vacuum evaporated to give 0.212 g of a red-brown solid. Typical yields of this reaction range from 80-90%. $[Rh_2(NBD)_2(eLTTP)](BF_4)_2$ is soluble in CH_2Cl_2, acetone, and MeCN; slightly soluble in water; and unsoluble in THF, ethers, benzene, and

other non-polar solvents.

Red-orange crystals of *rac*-$[Rh_2(NBD)_2(eLTTP)](BF_4)_2$ (0.060 g) can grow from the vial that was placed in the -40°C freezer.

Analysis: Calculated for $C_{39}H_{56}P_4Rh_2B_2F_8$: C, 45.56; H, 5.49. Found C, 45.33; H, 5.03. $^{31}P\{^1H\}$NMR (CD_2Cl_2, δ in ppm, H_3PO_4 reference): internal phosphorus atoms, 49.00 (1P, dm, J_{Rh-P} = 158.1 Hz), and 49.70 (1P, dm, J_{Rh-P} = 153.8 Hz); external phosphorus atoms, 60.00 (1 P, dd, J_{P-P} = 23.5 Hz and J_{Rh-P} = 151.6 Hz), and 60.50 (1 P, dd, J_{P-P} = 23.3 Hz and J_{Rh-P} = 151.7 Hz). ^1H NMR (CD_2Cl_2, δ in ppm, TMS reference): 0.98-1.37 (m, P-CH_2-CH_3), 1.62-1.92 (m, P-CH_2-CH_3), 1.48-2.25 (m, P-CH_2-CH_2-P), 3.00 (t, J_{H-H} = 7.42 Hz, *rac*-P-CH_2-P), 3.10 (dt, J_{H-H} = 7.72 Hz, J_{H-H} = 3.99 Hz, *meso*-P-CH_2-P), 1.80 (br s, -CH_2- of NBD in *rac*-molecule), 1.75 (br s, -CH_2- of NBD in *meso*-molecule), 4.08 (br s, -C*H*- of NBD), 5.22, 5.38, and 5.40 (br s, -C*H*=C*H*- of NBD from combination of *rac*- and *meso*-molecules), 7.50-7.60 and 7.78-7.91 (m, Ph).

Section 8.6.3 $[Rh_2(NBD)_2(eLTTP\text{-}pr)](BF_4)_2 \cdot CH_2Cl_2$

$[Rh(NBD)_2]BF_4$ (0.204 g, 0.546 mmoles) and the ligand eLTTP-pr (0.134 g, 0.272 mmoles) are placed in separate 50 mL Erlenmeyer flasks along with 4 mL each of a 1:1 solution of CH_2Cl_2/THF in a glove box. The eLTTP-pr solution was added with occasional hand-swirling of the flask. The orange-red suspension turned into a deep red clear solution as the ligand was added. As 6 mL of hexane was added another suspension was formed, which virtually disappeared with more swirling. The flask was allowed to stand for 5 hours in which a red oil drops out of solution. The CH_2Cl_2/THF/hexane solution was decanted and the remaining red

oil was taken up in 2-5 mL of CH_2Cl_2. The red solution was vacuum evaporated to dryness giving 0.197 g of $[Rh_2(NBD)_2(eLTTP\text{-}pr)](BF_4)_2 \cdot CH_2Cl_2$ as a red-brown powder (96% yield).

Analysis: Calculated for $C_{42}H_{62}P_4Rh_2B_2F_8Cl_2$ (one CH_2Cl_2 solvent included): C, 44.36; H, 5.14. Found C, 44.62; H, 5.37. $^{31}P\{^1H\}$NMR (CD_2Cl_2, δ in ppm, H_3PO_4 reference): external phosphorus atoms, 60.6 (1 P, dd, $J_{P\text{-}P} = 24.5$ Hz and $J_{Rh\text{-}P} = 153.3$ Hz) and 60.1 (1 P, dd, $J_{P\text{-}P} = 24.4$ Hz and $J_{Rh\text{-}P} = 153.5$ Hz); internal phosphorus atoms, 55.3 (1 P, dd, $J_{P\text{-}P} = 24.5$ Hz and $J_{Rh\text{-}P} = 157.5$ Hz) and 54.7 (1 P, dd, $J_{P\text{-}P} = 24.4$ Hz and $J_{Rh\text{-}P} = 157.1$ Hz). ^1H NMR (CD_2Cl_2, δ in ppm, TMS reference): 0.89-1.28 (m, P-CH_2CH_3), 1.28-2.7 (overlapping m, $CH_3CH_2PCH_2CH_2P(Ph)CH_2CH_2CH_2P(Ph)CH_2CH_2PCH_2CH_3$), 1.78 (br s, -$CH_2$- of NBD), 4.08 (br s, -CH- of NBD); 5.10 and 5.40 (br s, -CH=CH- of NBD), 7.10-7.75 (m, -(*Ph*)P-).

Section 8.6.4 $[Rh_2(NBD)_2(eLTTP\text{-}p\text{-}xyl)](BF_4)_2 \cdot 3CH_2Cl_2$

$[Rh(NBD)_2]BF_4$ (0.390 g, 1.043 mmoles) is placed in a 50 mL Erlenmeyer flask along with 14 mL of a 1:1 solution of CH_2Cl_2/THF in a glove box. The ligand (0.168 g, 0.303 mmoles) was added as a solid with occasional hand-swirling of the flask. The orange-red suspension turned to a deep red clear solution as the ligand was added. As 9 mL of hexane was added another suspension was formed, which virtually disappeared with more swirling. The flask was allowed to stand for 5 hours from which a red oil dropped out of solution. The CH_2Cl_2/THF/hexane solution was decanted, and the remaining oil was taken up in 5-7 mL of CH_2Cl_2. The red solution was vacuum evaporated to dryness giving 0.390 g of $[Rh_2(NBD)_2(eLTTP\text{-}p\text{-}xyl)](BF_4)_2$ as a red-brown powder (96% yield).

Analysis: Calculated for $C_{37}H_{68}P_4Rh_2B_2F_8Cl_6$ (three CH_2Cl_2 solvent molecules included): C, 42.92; H, 4.85. Found C, 41.61; H, 4.87. $^{31}P\{^1H\}$NMR (CD_2Cl_2, δ in ppm, H_3PO_4 reference): internal phosphorus atoms, 61.2 (1 P, dd, $J_{P\text{-}P}$ = 25.0 Hz and $J_{Rh\text{-}P}$ = 151 Hz); external phosphorus atoms, 54.9 (1 P, dd, $J_{P\text{-}P}$ = 25.0 Hz and $J_{Rh\text{-}P}$ = 161.7 Hz). ^1H NMR (CD_2Cl_2, δ in ppm, TMS reference): 0.7-1.2 (m, P-CH_2-CH_3), 1.3-2.2 (overlapping m, P-CH_2CH_2-P-CH_2-CH_3), 1.7 (br s, -CH_2- of NBD); 3.9 and 4.1 (br s, -CH- of NBD); 5.1 and 5.5 (br s, -CH=CH- of NBD), 3.2-3.7 (m, diastereomeric P-CH_2-p-xyl-); 7.2 (s, p-C_6H_4-); 7.3-7.6 (m, (*Ph*)P-).

Section 8.6.5 $[Rh(NBD)(Et_2PCH_2CH_2P(Ph)Me)]BF_4$

$[Rh(NBD)_2]BF_4$ (0.225 g, 0.602 mmole) and $Et_2PCH_2CH_2P(Ph)Me$ (0.144 g, 0.600 mmole) were weighed out and placed in separate flasks in a glove box. Using a graduated cylinder 6 mL of CH_2Cl_2 and THF each was measured and combined. 3 mL of the CH_2Cl_2/ THF solution was added to the flask that contained $[Rh(NBD)_2]BF_4$ and 2 mL to the $Et_2PCH_2CH_2P(Ph)Me$ flask. See procedure and workup in previous section of $[Rh_2(NBD)_2(eLTTP)](BF_4)_2$. $[Rh(NBD)(Et_2PCH_2CH_2P(Ph)Me)]BF_4$ (0.190 g) was isolated as a red-brown solid. Typical yields of this reaction range from 80-90%.

Analysis: Calculated for $C_{20}H_{30}P_2RhBF_4$: C, 46.01; H, 5.79. Found C, 46.28; H, 5.89. $^{31}P\{^1H\}$NMR (d_6-acetone, δ in ppm, H_3PO_4 reference): Et_2P- phosphorus atom, 65.7 (1 P, dd, $J_{P\text{-}P}$ = 25.3 Hz and $J_{Rh\text{-}P}$ = 153.3 Hz); Me(Ph)P- phosphorus atom, 52.1 (1 P, dd, $J_{P\text{-}P}$ = 25.3 Hz and $J_{Rh\text{-}P}$ = 159.6 Hz). ^1H NMR (d_6-acetone, δ in ppm, TMS reference): 0.6-1.2 (m, CH_3CH_2P-); 1.5-1.8 (m, CH_3CH_2P-); 1.5-2.3 (overlapping m, PCH_2CH_2P); 1.6 (d, $J_{P\text{-}H}$ =

13.3 Hz, -P(*Me*)Ph) ; 1.5 (br s, -CH_2- of NBD); 3.9 (br s, -C*H*- of NBD); 5.0 and 5.4 (v br s, -C*H*=C*H*- of NBD); 7.1-7.2 and 7.3-7.6 (m, -P(Me)*Ph*).

Section 8.6.6 [Rh(NBD)($Et_2PCH_2CH_2PPh_2$)]BF_4·0.5CH_2Cl_2

[Rh(NBD)$_2$]BF_4 (0.081 g, 0.217 mmole) and $Et_2PCH_2CH_2PPh_2$ (0.065 g, 0.215 mmole) were weighed out and placed in separate flasks in a glove box. Using a graduated cylinder 2 mL of CH_2Cl_2 and THF each was measured and combined. 2 mL of the CH_2Cl_2/THF solution was added to the flask containing the [Rh(NBD)$_2$]BF_4 and 1 mL to the $Et_2PCH_2CH_2PPh_2$ flask. The ligand solution was quickly added dropwise to the [Rh(NBD)$_2$]BF_4/ CH_2Cl_2/ THF slurry while hand swirling the reaction flask. The reaction mixture became a clear red solution. The remaining CH_2Cl_2/ THF solution was used to rinse the $Et_2PCH_2CH_2PPh_2$ flask and was added rapidly to the reaction mixture. The reaction flask was swirled by hand for a few seconds. Hexane (3 mL) was poured into the reaction mixture causing turbidity. Again the reaction flask was swirled by hand until the reaction mixture turned clear red. The reaction was allowed to stand, with occasional swirling, for 10 hours, during which time a dark red oil separated on the bottom of the flask. The CH_2Cl_2/THF/hexane solution was decanted into a clean vial and the remaining red oil was taken up in 1-2 mL of CH_2Cl_2. The red solution is vacuum evaporated to dryness giving [Rh(NBD)($Et_2PCH_2CH_2PPh_2$)]BF_4 as a red-brown solid. Typical yields of this reaction range from 80-90%. The CH_2Cl_2/THF/ hexane solution which was poured off into a clean vial deposited a few crystals when placed into a -40° C freeze.

Analysis: Calculated for $C_{26.5}H_{31}P_2RhBF_4Cl$ (0.5 molecules of CH_2Cl_2 solvent present): C, 48.88; H, 5.31. Found C, 48.15; H, 5.21. $^{31}P\{^1H\}$NMR

(CD_2Cl_2, δ in ppm, H_3PO_4 reference): phosphorus atom, 60.47 (1 P, d, J_{Rh-P} = 154 Hz); phosphorus atom, 60.50 (1 P, d, J_{Rh-P} = 157 Hz). ^1H NMR (CD_2Cl_2, δ in ppm, TMS reference): 1.1-1.3 (m, CH_3CH_2P-); 1.7-1.9 (m, CH_3CH_2P-); 1.6-1.8 and 2.3-2.6 (m, PCH_2CH_2P); 1.8 (br s, -CH_2- of NBD); 4.2 (br s, -CH- of NBD); 5.1 and 5.7 (v br s, -CH=CH- of NBD); 7.5-7.6 (m, -PPh_2).

Section 8.6.7 $[Rh(NBD)(Et_2PCH_2CH_2PEt_2)]BF_4 \cdot CH_2Cl_2$

$[Rh(NBD)_2]BF_4$ (0.174 g, 0.834 mmole) and $Et_2PCH_2CH_2PEt_2$ (0.312 g, 0.834 mmole) were weighed out and added to separate flasks in a glove box. Using a graduated cylinder 2 mL of CH_2Cl_2 and THF each was measured and combined. 2 mL of the CH_2Cl_2/ THF solution was added to the flask that contained the $[Rh(NBD)_2]BF_4$ and 1 mL to the $Et_2PCH_2CH_2PEt_2$. The ligand solution was quickly added dropwise to the $[Rh(NBD)_2]BF_4$/ CH_2Cl_2/ THF slurry while hand swirling the reaction flask. The reaction mixture became a clear red solution. The remaining CH_2Cl_2/ THF solution was used to rinse the $Et_2PCH_2CH_2PEt_2$ flask and was added rapidly to the reaction mixture. The reaction flask was swirled by hand for a few seconds. Hexane (3 mL) was poured into the reaction mixture which causing turbidity. Again the reaction flask was swirled by hand until the reaction mixture was clear red. The reaction was allowed to stand with occasional swirling for 10 hours which deposited a dark red oil on the bottom of the flask. The CH_2Cl_2/THF/hexane solution was decanted into a clean vial and the remaining red oil was taken up in 1-2 mL of CH_2Cl_2. The red solution is vacuum evaporated to dryness giving 0.334 g of $[Rh(NBD)(Et_2PCH_2CH_2PEt_2)]BF_4$ as a red-brown solid (82% yield). Typical yields of this reaction range from 80-90%. Rod-like crystals deposited when the vial containing CH_2Cl_2/THF/hexane solution was

placed into a -40° C freezer.

Analysis: Calculated for $C_{18}H_{34}P_2RhBF_4Cl_2$ (one molecule of CH_2Cl_2 solvent present): C, 37.73; H, 5.98. Found C, 37.63; H, 6.05. $^{31}P\{^1H\}$NMR (CD_2Cl_2, δ in ppm, H_3PO_4 reference): phosphorus atom, 67.0 (d, J_{Rh-P} = 157 Hz); ^1H NMR (CD_2Cl_2, δ in ppm, TMS reference): 1.00-1.2 (m, CH_3CH_2P-); 1.5-1.9 (m, $CH_3CH_2PCH_2CH_2P$-), 1.7 (br s, -CH_2- of NBD); 4.1 (br s, -CH- of NBD); 5.4 (br dd, J_{P-P} = 2.2 Hz, J_{H-H} = 2.2 Hz, -CH=CH- of NBD).

Section 8.7 Typical Hydroformylation Run

$[Rh_2(NBD)_2(eLTTP)](BF_4)_2$ (0.020 g, 0.0195 mmole) was weighed in a glove box. Also weighed was roughly 4000 molar equivalents of 1-hexene, (6.4-7.5 g, 89.3 mmole). The acetone solvent was measured out using a graduated cylinder (40-45 mL). Small amounts of solvent were used to dissolve the catalyst in order to transfer it into a pear-shaped Schlenk flask. The rest of the solvent that was measured previously was poured into the Schlenk flask. The 1-hexene was then poured into the same Schlenk flask. The sealed Schlenk flask containing the catalyst and olefin was then brought out of the glove box.

With the Parr autoclave and gas lines degassed, the desired reaction temperature and stirring speed (730 rpm) were entered into the controller. The one liter external gas reservoir was filled with H_2/CO (1:1 mixture) to roughly 760 psi. The Schlenk flask containing the catalyst and olefin were added to the autoclave via cannula. The autoclave was partially filled with H_2/CO (20-40 psi less than desired reaction pressure) and closed off during the temperature ramp (usually 10 min). When the temperature of reaction was reached, additional H_2/CO was added if necessary, or an exhaust valve was opened briefly to obtain the desired pressure.

The gas line to the external reservoir was then fully opened.

Aliquots could be taken out at any time during the experiment via syringe through a septum. These aliquots were analyzed by NMR and GC to determine the percentages of aldehyde produced, aldehyde selectivity, isomerization of olefin, unreacted olefin, and any other possible by-products of hydroformylation.

The raw data recorded by the controller during the experiment were transferred to a computer, which included: pressure of the external reservoir, temperature of external reservoir, temperature of reaction, and elapsed time. The data were transformed into moles of gas consumption, aldehyde production (assuming all H_2/CO led to aldehyde production), and turnover rate.

Sources of error in the catalytic experiments can occur in weighing small samples of catalyst. The catalyst is weighed to the nearest milligram inside the glove box, however, vibrations of the glove box can cause an inaccurate weight of the catalyst with an error of at least 10%. Small discrepancies in weight can be cause large fluctuations in the turnover rate because of the small amounts of active catalyst needed. A possible solution of eliminating large errors in weighing catalyst may be done by increasing the amount of catalyst to be weight for a stock solution. However, the catalyst may decompose in a stock solution that has been not been used for a quite some time. Another source of error is the pressure gauge of the regulator on the autoclave. The smallest unit of precision on the gauge is 20 psi. The turnover rate and selectivities of pressure sensitive catalysts can be greatly affected by small deviations from the intended value. Finally, insufficient mixing of the catalyst and gases due to poor stirring can also affect the outcome of a hydroformylation experiment. These experiments were performed only with a stirring rate of 730 rpm (arbitrary choice). Turnover rates and selectivities were not optimized with respect to variations in stirring speed.

REFERENCES

1. (a) Muetterties, E.L.; Krause, M.J. *Angew. Chem. Int. Ed. Engl.* **1983**, *22*, 135.

   (b) Johnson, B.F.G. "*Transition Metal Clusters*", Wiley, New York, 1980.

2. (a) Adams, R.A.; Kim, H. S.; Wang, S. *J. Am. Chem. Soc.* **1985**, *107*, 6107.

   (b) Ojima, I. American Chemical Society 199th National Meeting, Boston, Mass., April 22-27, Symposium on New Science in Homogeneous Transition Metal Catalyzed Reactions, #44.

3. (a) Stone, F.G.A. *Angew. Chem. Int. Ed. Engl.* **1984**, *23*, 89.

   (b) Vahrenkamp, H. *Adv. Organomet. Chem.* **1983**, *22*, 169.

   (c) Richter, F.; Vahrenkamp, H. *Angew. Chem. Int. Ed. Engl.* **1979**, *18*, 531.

   (d) Osborn, J.A.; Stanley, G.G. *Angew. Chem. Int. Ed. Engl.* **1980**, *19*, 1025.

4. King, R.B. "Catalytic Aspects of Metal Phosphine Complexes", ACS Symp. Ser. **1982**, *196*, 312.

5. (a) Kubiak, C. P.; Eisenberg, R. *J. Am. Chem. Soc.* **1977**, *99*, 6129.

   (b) Sanger, A. R. *J. Chem. Soc., Dalton Trans.* **1977**, 1971.

(c) Mague J. T.; Sanger, A. R. *Inorg. Chem.* **1979**, *18*, 2060.

(d) DeLaet, D. L; del Rosario, R.; Fanwick, P. E.; Kubiak, C. P. *J. Am. Chem. Soc.* **1987**, *109*, 754.

(e) Berry, D. H.; Eisenberg, R. *Organometallics* , **1987**, 6, 1796.

(f) Wu, J.; Fanwick, P. E.; Kubiak, C. P. *J. Am. Chem. Soc.* **1988**, *110*, 1319.

6. Askham, F.R.; Stanley, G.G.; Marques, E.C. *J. Am. Chem. Soc.* **1985**, *107*, 7428.

7. Askham, F.R.; Maverick, A.W.; Stanley, G.G. *Inorg. Chem.* **1987**, *26*, 3963.

8. (a) Laneman, S.A.; Stanley, G.G. *Inorg. Chem.* **1987**, *26*, 1803.

(b) Saum, S.E.; Askham, F.R.; Fronczek, F.R.; Stanley, G.G. *Organometallics* , **1988**, *7*, 1409.

9. (a) Laneman, S.A.; Fronczek, F.R.; Stanley, G.G. *J. Am. Chem. Soc.* **1988**, *110*, 5585.

(b) Laneman, S.A.; Fronczek, F.R.; Stanley, G.G. *Inorg. Chem.* **1989**, *28*, 1872.

10. Hietkamp, S.; Sommer, H.; Stelzer, O. *Chem. Ber.* **1984**, *117*, 3414.

11. Langhans, K.P.; Stelzer, O. *Chem. Ber.* **1987**, *120*, 1707.

12. We have found in these laboratories that addition of reactants is crucial. Isslieb[39] and coworkers had shown that K[PhPH] does not react with CH_2Cl_2 to form $Ph(H)PCH_2P(H)Ph$, but Ph(H)P-P(H)Ph. We have shown that when K[PhPH] is added to CH_2Cl_2, not only is $Ph(H)PCH_2P(H)Ph$ formed but cyclic phosphines as well. (Laneman, S. A.; Fronczek, F. R.; Stanley, G. G. *Phosphorus, Sulfur, and Silicon*, **1989**, *42*, 97.)

13. DuBois, D. L.; Hyers, W. H.; Meek, D. W. *J. Chem. Soc., Dalton Trans.* **1975**, 1011.

14. Bogdanovic, B.; Spliethoff, B.; Wilke, G. *Angew. Chem. Int. Ed. Engl.* **1980**, *19*, 622.

15. (a) Wilke, G. *Pure Appl. Chem.* **1978**, *50*, 677.
    (b) Geibel, W.; Wilke, G.; Goddard, R.; Kruger, C.; Mynott, R. *J. Organomet. Chem.* **1978**, *160*, 139.
    (c) Knox, S. A. R.; Stansfield, R. F. D.; Stone, F. G. A.; Winter, M. J.; Woodward, P. J. *J. Chem. Soc., Chem. Commun.* **1978**, 221.
    (d) Green, M; Norman, N. C.; Orpen, A. G. *J. Am. Chem. Soc.* **1981**, *103*, 1269.

16. Allen, D. L.; Gibson, V. C.; Green, M. L. H.; Skinner, J. F.; Baskin, J.; Grebenik, P. D. *J. Chem. Soc., Chem. Commun.* **1983**, 895.

17. There are a few Ni(II) dimer systems that have short Ni-Ni separations (around 2.4-2.6 Å) which can be described as Ni=Ni double bonds. Cf.: (a) Fackler, J. P., Jr. *Prog. Inorg. Chem.* **1976**, *21*, 55. (b) Corbett, M.; Hoskins, B. F.; McLeod, N. *J. Aust. J. Chem.* **1975**, *28*, 2377.

18. Spek, A. L.; Van Eijck, B. P.; Jans, R. J. F.; Van Koten, G. *Acta Crystallogr., Sect. C: Cryst. Struct. Commun.* **1987**, *C43*, 1878.

19. (a) Saum, S.E.; Stanley, G.G. *Polyhedron*, **1987**, *6*, 1803.
(b) Saum, S. E.; Laneman, S. A.; Stanley, G. G. *Inorg. Chem.*, submitted for publication.
(c) Saum, S. E.; Askham, F. R.; Fronczek, F. R.; Stanley, G. G. *Organometallics* **1988**, *7*, 1409.

20. Schlenk, T. G.; Downes, J. M.; Milne, C. R. C.; Mackenzie, P. B.; Boucher, H.; Whalen, J.; Bosnich, B. *Inorg. Chem.* **1985**, *24*, 2334.

21. (a) Stalick, J. K.; Ibers, J. A. *Inorg. Chem.* **1969**, *8*, 1084.
(b) Stalick, J. K.; Ibers, J. A. *Inorg. Chem.* **1969**, *8*, 1090.
(c) Raymond, K. N.; Corfield, P. W. R.; Ibers, J. A. *Inorg. Chem.* **1968**, *7*, 1362. (d) Hirshfeld, F. L.; Hope, H. *Acta Crystallogr., Sect. B* **1980**, *B36*, 406.
(e) Allen, D. W.; Mann, F. G.; Millar, I. T.; Powell, H. M.; Watkins, D.

J. *J. Chem. Soc., Chem. Commun.* **1969**, 1004.

22. Hope, H.; Olmstead, M. M.; Power, P. P.; Viggiano, M. *Inorg. Chem.* **1984**, *23*, 326.

23. Sanger, A. R. *J. Chem. Soc. Dalton Trans.* **1977**, 120.

24. (a) Garrou, P. E. *Chem. Rev.* **1981**, *81*, 229.
(b) Slack, D. A.; Greveling, I.; Baird, M. C. *Inorg. Chem.* **1979**, *18*, 3125.

25. Brown, J. M.; Canning, L. R. *J. Organomet. Chem.* **1984**, *267*, 179.

26. (a) Masters, C. *Homogeneous Transition-metal Catalysis: A Gentle Art*, Chapman and Hall, New York, 1981, pp 102-135.
(b) Parshall, G. W. *Homogeneous Catalysis*, John Wiley and Sons, Inc., New York, 1980, pp 85-90.
(c) Sanger, A. R. *Homogeneous Catalysis with Metal Phosphine Complexes*; Pignolet, L. H. (ed.), Plenum, New York, 1983; pp 215-235.

27. Heck, R. F.; Breslow, D. D. *J. Am. Chem. Soc.* **1963**, *83*, 651.

28. (a) Gelmini, L; Stephan, D. W. *Organometallics* **1988**, *7*, 849.

(b) Hidai, M.; Fukoka, A.; Koyasu, Y.; Uchida, Y. *J. Chem. Soc., Chem. Commun.* **1984**, 516.

(c) Pino, P.; von Bezard, D. A. *Swiss Patent* 625,233, **1981.**

(d) Pino, P.; Consiglio, G. *Proceedings Symposium on Rhodium Homogeneous Catalysis*, Veszprem, 1978, p 98.

29. Kovacs, I.; Hoff, C. D.; Ungvary, F.; Marko, L. *Organometallics* **1985**, *4*, 1347

30. Hughes, R. O.; Unruh, J. D. *J. Mol. Catal.* **1981**, *12*, 71.

31. This turnover rate and selectivity is the average of five catalytic runs with standard deviations 740±40.

32. (a) Pruett, R. L.; Smith, J. A. *J. Org. Chem.* **1969**, *34*, 327.

(b) Masters, C. *Homogeneous Transition-metal Catalysis: A Gentle Art*, Chapman and Hall; New York, 1981; pp 121-127.

33. Tolman, C. A. and Faller, J. W. *Homogeneous Catalysis with Metal Phospine Complexes*; Pignolet, L. H. (ed.); Plenum; New York, 1983; pp 87-99.

34. Recent experiments have shown that some of 1-heptanal can be converted into internal olefins by $[Rh_2(NBD)_2(eLTTP)]_2BF_4$ under normal hydroformylation conditions (80° C and 80 psi H2/CO).

35. (a) Brown, J. M.; Canning, L. R.; Alexander, G. K.; Sidebottom, P. J. *J.*

Chem. Soc., Chem Commum. **1982**, 721. (b) Brown, J. M.; Alexander, G. K. *J. Chem. Soc., Chem Commum.* **1982**, 723.

36. (a) Evans, D.; Osborn, J. A.; Wilkinson, G. *J. Chem. Soc. (A)* **1968**, 3133.
(b) Paulik, F. E. *Catal. Rev.* **1972**, *6*, 49.
(c) U. S. Pat. 4,694,109 (**1986**).
(d) U. S. Pat. 4,748,261 (**1988**).

39. Typical industrial conditions use between 150-950 fold excess of PPh_3 relative to the metal. The selectivity (14:1) is about the same throughout this range.

38. Singh, P.; Dammann, C. B.; Hodgson, D. J. *Inorg. Chem.* **1973**, *12*, 1335.

39. A possible rearrangement product from the free-radical catalyzed reaction was characterized as a metal complex: $Ni(CNS)_2(Ph_2PCH_2CH_2P(Et)CH_2CH_2PPh_2)$. The uncoordinated free ligand, $Ph_2PCH_2CH_2P(Et)CH_2CH_2PPh_2$ may account for the additional resonances. Juma, B; Stanley, G.G, unpublished results.

40. TETRAPHOS-pr is used instead of the published name: 1,1,4,8,11,11-Hexaphenyl-1,4,8,11-tetraphosphaundecane.

41. Optimization of the reaction time with KH by either stirring or applying heat was not attempted.

42. Issleib, K.; Jacob, J. *Chem. Ber.* **1961**, *94*, 107.

APPENDIX 1

Crystallographic Data

Table A-I: Positional parameters for *rac*-Ni_2Cl_4(eLTTP)·THF

atom	*x*	*y*	*z*	*B*,[a] Å^2
Ni1	0.84885 (6)	0.19989 (8)	0.67459 (6)	3.92 (2)
Ni2	0.74388 (7)	-0.09454 (8)	0.86442 (7)	4.72 (3)
Cl1	0.9089 (2)	0.3401 (2)	0.7014 (2)	6.75 (7)
Cl2	0.7296 (1)	0.2646 (2)	0.6525 (2)	5.79 (6)
Cl3	0.8037 (2)	-0.1909 (2)	0.9573 (2)	9.96 (9)
Cl4	0.7348 (2)	-0.2035 (2)	0.7613 (2)	6.54 (6)
P1	0.8015 (1)	0.0583 (2)	0.6446 (1)	3.97 (5)
P2	0.9636 (1)	0.1310 (2)	0.6872 (2)	5.11 (6)
P3	0.6830 (1)	0.0109 (2)	0.7849 (1)	4.21 (5)
P4	0.7439 (2)	0.0128 (2)	0.9622 (2)	6.17 (7)
C'	0.7025 (5)	0.0207 (6)	0.6725 (5)	4.4 (2)
C11	0.8734 (6)	-0.0354 (7)	0.6858 (6)	6.1 (2)
C12	0.9552 (5)	0.0006 (7)	0.6605 (7)	6.3 (3)
C31	0.6964 (6)	0.1340 (6)	0.8307 (6)	5.8 (2)
C32	0.6866 (6)	0.1218 (6)	0.9268 (6)	5.6 (2)
C21	1.0367 (6)	0.1788 (9)	0.6198 (6)	7.1 (3)
C22	1.0070 (7)	0.182 (1)	0.5277 (7)	8.4 (3)
C23	1.0104 (6)	0.141 (1)	0.7972 (7)	11.4 (4)
C24	1.0847 (9)	0.143 (2)	0.8109 (9)	16.9 (6)
C41	0.730 (1)	-0.028 (2)	1.069 (1)	7.9 (6)*
C41'	0.676 (1)	-0.022 (1)	1.053 (1)	5.7 (4)*
C42	0.667 (2)	-0.087 (2)	1.066 (2)	11.1 (8)*
C42'	0.604 (1)	-0.060 (2)	1.033 (2)	9.1 (7)*
C43	0.851 (1)	0.080 (2)	0.984 (1)	7.4 (5)*
C43'	0.830 (1)	0.038 (2)	1.019 (1)	6.3 (5)*
C44	0.920 (2)	0.024 (2)	0.986 (2)	9.4 (7)*
C44'	0.884 (1)	0.091 (2)	0.951 (1)	7.0 (5)*
C1P	0.7912 (5)	0.0426 (6)	0.5308 (5)	4.2 (2)
C2P	0.7986 (6)	0.1218 (7)	0.4785 (6)	5.6 (2)
C3P	0.7961 (6)	0.1119 (8)	0.3917 (6)	6.9 (3)
C4P	0.7810 (5)	0.0186 (9)	0.3583 (6)	6.9 (3)

Table A-I (cont): Positional parameters for *rac*-Ni_2Cl_4(eLTTP)·THF

atom	*x*	*y*	*z*	*B*,[a] Å^2
C5P	0.7696 (5)	-0.0638 (8)	0.4083 (6)	5.9 (2)
C6P	0.7751 (5)	-0.0523 (7)	0.4969 (6)	5.2 (2)
C7P	0.5757 (5)	-0.0105 (8)	0.7777 (6)	5.6 (2)
C8P	0.5483 (6)	-0.1007 (8)	0.8078 (7)	7.2 (3)
C9P	0.4655 (6)	-0.120 (1)	0.8046 (8)	9.6 (4)
C10P	0.4154 (7)	-0.043 (1)	0.7667 (7)	11.0 (5)
C11P	0.4418 (7)	0.046 (1)	0.7364 (8)	10.4 (4)
C12P	0.5246 (6)	0.061 (1)	0.7423 (6)	8.0 (3)
C1S	0.516 (1)	0.344 (2)	0.061 (1)	11.4 (6)*
C2S	0.431 (1)	0.348 (2)	0.023 (1)	11.2 (6)*
C3S	0.437 (1)	0.340 (2)	0.060 (1)	10.3 (5)*
C4S	0.510 (2)	0.269 (2)	-0.072 (2)	14.7 (8)*
C5S	0.571 (1)	0.320 (2)	0.003 (2)	13.4 (7)*
C6S	0.537 (2)	0.397 (3)	0.038 (3)	8 (1)*
C7S	0.475 (2)	0.296 (3)	0.065 (2)	7.4 (9)*
C8S	0.540 (3)	0.253 (4)	0.016 (4)	13 (2)*
C9S	0.534 (2)	0.311 (3)	-0.078 (3)	7.9 (9)*
C10S	0.571 (3)	0.368 (4)	-0.035 (3)	10 (1)*

[a]Starred values indicate atoms were isotropically refined. Values for anisotropically refined atoms are given in the form of the isotropic equivalent displacement parameter defined as $4/3[a^2\beta(1,1) + b^2\beta(2,2) + c^2\beta(3,3) + ac(\cos\beta)\beta(1,3)$.

Table A-II: Positional parameters for *meso*-Ni_2Cl_4(eLTTP)·1.5THF

atom	*x*	*y*	*z*	B,[a] Å^2
Ni1	0.2835 (1)	0.08911 (8)	0.77115 (8)	3.85 (3)
Ni2	0.4903 (1)	0.40464 (8)	1.27041 (8)	3.54 (3)
Cl1	0.2177 (3)	-0.0456 (2)	0.6082 (2)	7.08 (9)
Cl2	0.2872 (3)	-0.0126 (2)	0.8588 (2)	5.17 (7)
Cl3	0.6305 (2)	0.5518 (2)	1.3996 (2)	5.18 (7)
Cl4	0.3717 (3)	0.4892 (2)	1.1859 (2)	5.73 (8)
P1	0.3484 (2)	0.2303 (2)	0.9226 (2)	3.59 (6)
P2	0.2849 (3)	0.1956 (2)	0.6949 (2)	5.13 (8)
P3	0.3547 (2)	0.2564 (2)	1.1549 (2)	3.56 (6)
P4	0.5921 (2)	0.3126 (2)	1.3490 (2)	3.57 (6)
C'	0.2673 (8)	0.2294 (7)	1.0115 (6)	4.0 (2)
C11	0.3157 (9)	0.3473 (6)	0.8931 (7)	4.6 (3)
C12	0.355 (1)	0.3367 (7)	0.7994 (7)	5.1 (3)
C31	0.4234 (8)	0.1429 (6)	1.1577 (6)	3.8 (2)
C32	0.4993 (9)	0.1714 (6)	1.2821 (7)	4.3 (3)
C21	0.373 (1)	0.1755 (9)	0.6106 (9)	9.9 (4)
C22	0.513 (1)	0.171 (1)	0.682 (1)	14.2 (6)
C23	0.117 (1)	0.189 (1)	0.606 (1)	10.8 (5)
C24	0.084 (2)	0.263 (1)	0.575 (2)	16.2 (7)
C41	0.7428 (8)	0.2984 (7)	1.3406 (7)	4.6 (3)
C42	0.849 (1)	0.3993 (8)	1.406 (1)	6.9 (4)
C43	0.621 (1)	0.3639 (8)	1.4937 (7)	5.3 (3)
C44	0.679 (1)	0.2927 (9)	1.5492 (8)	8.3 (4)
C1P	0.5203 (8)	0.2622 (6)	0.9986 (6)	3.5 (2)
C2P	0.5807 (9)	0.1786 (7)	0.9776 (7)	4.5 (3)
C3P	0.7121 (9)	0.2008 (7)	1.0282 (7)	5.0 (3)
C4P	0.7821 (9)	0.3090 (8)	1.0995 (8)	5.7 (3)
C5P	0.721 (1)	0.3903 (7)	1.1197 (8)	6.1 (3)
C6P	0.5877 (9)	0.3673 (7)	1.0695 (7)	4.8 (3)
C7P	0.2263 (8)	0.2398 (6)	1.1946 (6)	3.9 (2)
C8P	0.2328 (9)	0.3154 (8)	1.2945 (7)	4.9 (3)

Table A-II (cont): Positional parameters for *meso*-Ni_2Cl_4(eLTTP)·1.5THF

atom	*x*	*y*	*z*	*B*,[a] Å^2
C9P	0.136 (1)	0.3000 (8)	1.3254 (8)	5.9 (3)
C10P	0.0339 (9)	0.2132 (8)	1.2605 (8)	5.4 (3)
C11P	0.0252 (9)	0.1384 (8)	1.1585 (7)	5.5 (3)
C12P	0.1217 (8)	0.1521 (8)	1.1267 (7)	4.9 (3)
C1S	0.220 (2)	0.946 (2)	0.197 (1)	10.6 (6)*
C1S'	0.235 (7)	0.879 (6)	0.215 (5)	10 (2)*
C2S	0.223 (2)	1.002 (2)	0.306 (2)	10.8 (7)*
C2S'	0.192 (5)	0.914 (4)	0.319 (4)	11 (2)*
C3S	0.117 (2)	0.962 (2)	0.321 (2)	7.8 (7)*
C3S'	0.044 (3)	0.915 (3)	0.228 (3)	12 (1)*
C4S	0.026 (2)	0.843 (2)	0.208 (2)	18.1 (19)*
C5S	0.119 (2)	0.878 (2)	0.151 (2)	12.2 (8)*
C5S'	0.162 (6)	0.807 (5)	0.224 (5)	14 (2)*
C6S	0.991 (6)	0.495 (5)	0.917 (4)	10 (2)*
C7S	0.939 (4)	0.492 (4)	0.999 (4)	8 (1)*
C8S	1.025 (4)	0.447 (3)	1.034 (3)	7 (1)*
C9S	0.968 (5)	0.596 (4)	1.071 (4)	9 (1)*
C10S	1.034 (5)	0.447 (4)	0.882 (4)	8 (1)*

[a]Starred values indicate atoms were isotropically refined. Values for anisotropically refined atoms are given in the form of the isotropic equivalent displacement parameter defined as $(4/3)[a^2\beta(1,1) + b^2\beta(2,2) + c^2\beta(3,3) + ab(\cos\gamma)\beta(1,2) + ac(\cos\beta)\beta(1,3) + bc(\cos\alpha)\beta(2,3)]$.

Table A-III: Crystallographic data for *meso*- and *rac*-Ni_2Cl_4(eLTTP)·xTHF.

Crystal Parameters

	meso	racemic
formula	$Ni_2Cl_4P_4O_{1.5}C_{31}H_{52}$	$Ni_2Cl_4P_4OC_{29}H_{48}$
fw	831.86	795.83
crystal system	triclinic	monoclinic
space group	P1-bar	P21/c
a, Å	11.693 (6)	16.919 (2)
b, Å	13.830 (3)	13.656 (2)
c, Å	14.438 (3)	15.966 (6)
α, deg	111.87 (2)	90.00
β, deg	110.95 (2)	94.46 (2)
γ, deg	94.37 (2)	90.00
V, Å^3	1963 (1)	3678 (3)
Z	2	4
d_{calc}, g/ml	1.34	1.44
μ (Mo Kα), cm^{-1}	14.2	15.16
temperature, °C	21	22
cryst size, mm	0.38 x 0.28 x 0.19	0.32 x 0.25 x 0.23
cryst color	red-orange	orange-red

Data Collection and Structure Refinement

diffractometer	CAD4	CAD4
radiation	MoKα	MoKα
monochromator	graph. cryst.	graph. cryst.
attenuator	17.5	17.5
scan method	$\theta/2\theta$	$\theta/2\theta$
variable scan speed, deg/min	0.5-4	0.5-4
data limits, deg	$3 < 2\theta < 50$	$3 < 2\theta < 50$

Table A-III (cont): Crystallographic data for *meso*- and *rac*-Ni_2Cl_4-(eLTTP)·xTHF.

octants collcd	*h*, ±*k*, ±*l*	*h*, *k*, ±*l*
no. of reflcns	6894	6977
no. of unique data $F_o^2 > 3\sigma(F_o^2)$	3593	3533
weighting scheme	non-Poisson	non-Poisson
fudge factor, P	0.06	0.06
no. of params defined	372	352
data/param ratio	9.7	10.0
R[a]	0.058	0.062
R_w[b]	0.084	0.086
GOF[c]	1.88	1.88
largest final Fourier pk., e/Å^3	0.593	0.699
largest final shift/esd	0.07	0.05
abs cor	yes	yes
min transmission coefficient	0.8141	0.9498

---

[a] $R = \Sigma \mid |F_o| - |F_c| \mid / \Sigma |F_o|$. [b] $R_w = [\Sigma w (|F_o| - |F_c|)^2 / \Sigma w |F_o|^2]^{1/2}$; $w = 4F_o^2[\sigma 2(I) + (pF_o^2)^2]^{-1}$. [c] Goodness of fit = $[\Sigma w (|F_o| - |F_c|)^2/(N_{obs} - N_{param})]^{1/2}$.

Table A-IV: General displacement parameter expressions - B's for *rac*-Ni_2Cl_4(eLTTP).

Name	B(1,1)	B(2,2)	B(3,3)	B(1,2)	B(1,3)	B(2,3)	Beqv
Ni1	4.08 (4)	3.84 (4)	3.84 (4)	-0.35 (4)	0.38 (4)	-0.20 (4)	3.92 (2)
Ni2	6.23 (6)	3.69 (5)	4.23 (5)	0.62 (5)	0.41 (4)	-0.21 (4)	4.72 (3)
Cl1	7.7 (1)	5.4 (1)	6.9 (1)	-1.9 (1)	-0.6 (1)	-1.3 (1)	6.75 (7)
Cl2	4.9 (1)	4.9 (1)	7.7 (1)	1.00 (9)	1.2 (1)	1.2 (1)	5.79 (6)
Cl3	16.0 (2)	6.3 (1)	7.1 (2)	4.2 (2)	-2.5 (2)	0.2 (1)	9.96 (9)
Cl4	10.1 (2)	4.3 (1)	5.4 (1)	0.1 (1)	1.2 (1)	-0.8 (1)	6.54 (6)
P1	3.98 (9)	3.48 (9)	4.4 (1)	0.09 (8)	-0.09 (8)	0.23 (8)	3.97 (5)
P2	3.79 (9)	6.9 (1)	4.5 (1)	-0.3 (1)	-0.32 (9)	0.5 (1)	5.11 (6)
P3	4.6 (1)	3.8 (1)	4.2 (1)	-0.27 (9)	0.14 (8)	0.20 (9)	4.21 (5)
P4	9.1 (2)	5.0 (1)	4.2 (1)	1.4 (1)	-0.4 (1)	-0.8 (1)	6.17 (7)
C'	3.8 (3)	5.2 (4)	4.3 (4)	-1.1 (3)	0.8 (3)	0.1 (3)	4.4 (2)
C11	5.5 (4)	4.6 (4)	8.0 (6)	1.2 (4)	-0.9 (4)	1.7 (4)	6.1 (2)
C12	4.6 (4)	5.7 (5)	8.6 (6)	1.6 (4)	0.5 (4)	0.9 (5)	6.3 (3)
C31	8.5 (6)	3.5 (4)	5.1 (4)	0.5 (4)	-0.9 (4)	-1.1 (4)	5.8 (2)
C32	6.9 (5)	3.8 (4)	6.1 (5)	1.5 (4)	0.6 (4)	-0.4 (4)	5.6 (2)
C21	5.0 (4)	10.3 (7)	6.0 (5)	-0.3 (5)	1.1 (4)	1.4 (5)	7.1 (3)
C22	8.0 (6)	11.9 (9)	5.7 (5)	-0.3 (6)	2.2 (5)	0.3 (6)	8.4 (3)
C23	6.1 (5)	22 (1)	6.0 (6)	-4.7 (7)	-2.8 (4)	2.7 (7)	11.4 (4)
C24	13.7 (9)	28 (2)	8.1 (7)	-5.9 (9)	-5.9 (6)	6.1 (9)	16.9 (6)
C1P	4.0 (4)	4.6 (4)	4.0 (4)	-0.0 (3)	-0.0 (3)	-0.0 (3)	4.2 (2)
C2P	7.3 (5)	4.7 (4)	4.7 (4)	-0.2 (4)	-0.2 (4)	0.8 (4)	5.6 (2)
C3P	7.6 (6)	7.9 (6)	5.1 (5)	0.2 (5)	0.2 (4)	-0.6 (5)	6.9 (3)
C4P	4.8 (4)	10.2 (7)	5.5 (5)	-0.1 (5)	-0.1 (4)	-1.1 (5)	6.9 (3)
C5P	4.9 (4)	7.1 (6)	5.7 (5)	-0.1 (4)	-0.1 (4)	-0.7 (5)	5.9 (2)
C6P	5.0 (4)	4.7 (4)	5.8 (4)	0.1 (4)	0.1 (4)	-1.5 (4)	5.2 (2)
C7P	4.8 (4)	7.5 (6)	4.6 (4)	0.9 (4)	0.9 (3)	-0.4 (4)	5.6 (2)
C8P	6.8 (5)	7.6 (6)	7.2 (6)	1.2 (5)	1.2 (5)	-0.2 (5)	7.2 (3)
C9P	5.1 (5)	13.8 (9)	10.2 (8)	1.6 (6)	1.6 (5)	-2.6 (7)	9.6 (4)
C10P	6.7 (6)	19 (1)	7.0 (6)	1.8 (8)	1.8 (5)	-2.3 (8)	11.0 (5)
C11P	6.3 (6)	17 (1)	7.7 (7)	0.9 (8)	0.9 (5)	2.0 (8)	10.4 (4)
C12P	4.8 (5)	13.9 (9)	5.4 (5)	0.8 (5)	0.8 (4)	1.5 (6)	8.0 (3)

The form of the anisotropic displacement parameter is:
$\exp[-0.25\{h^2a^2B(1,1) + k^2b^2B(2,2) + l^2c^2B(3,3) + 2hkabB(1,2) + 2hlacB(1,3) + 2klbcB(2,3)\}]$ where a, b, c are reciprocal lattice constants.

Table A-V: General displacement parameter expressions - B's for *meso*-Ni_2Cl_4(eLTTP).

Name	B(1,1)	B(2,2)	B(3,3)	B(1,2)	B(1,3)	B(2,3)	Beqv
Ni1	4.65 (5)	2.73 (4)	3.34 (4)	0.40 (4)	1.17 (3)	1.01 (3)	3.85 (3)
Ni2	3.71 (4)	2.73 (3)	3.44 (4)	0.36 (3)	1.21 (3)	0.92 (3)	3.54 (3)
Cl1	11.0 (2)	3.6 (1)	3.7 (1)	1.1 (1)	1.1 (1)	0.54 (8)	7.08 (9)
Cl2	6.7 (1)	3.66 (8)	5.17 (8)	0.55 (8)	2.44 (8)	2.14 (6)	5.17 (7)
Cl3	5.4 (1)	3.26 (8)	4.63 (9)	-0.34 (8)	0.87 (9)	0.82 (7)	5.18 (7)
Cl4	6.1 (1)	4.21 (9)	5.8 (1)	1.86 (9)	1.3 (1)	2.02 (7)	5.73 (8)
P1	4.2 (1)	2.77 (7)	3.37 (7)	0.55 (7)	1.34 (7)	1.12 (6)	3.59 (6)
P2	7.8 (1)	3.60 (9)	3.48 (8)	1.38 (9)	1.71 (9)	1.55 (6)	5.13 (8)
P3	3.61 (9)	2.96 (8)	3.21 (8)	0.34 (7)	1.13 (7)	0.79 (6)	3.56 (6)
P4	3.8 (1)	3.39 (8)	3.11 (7)	0.41 (7)	1.24 (7)	1.19 (6)	3.57 (6)
C'	3.7 (4)	5.3 (4)	2.9 (3)	0.7 (3)	1.5 (2)	1.8 (2)	4.0 (2)
C11	6.9 (5)	2.9 (3)	3.6 (3)	1.6 (3)	1.7 (3)	1.3 (2)	4.6 (3)
C12	7.4 (5)	3.4 (3)	4.0 (3)	1.0 (3)	2.1 (3)	1.6 (2)	5.1 (3)
C31	3.8 (4)	3.0 (3)	3.7 (3)	0.7 (3)	1.1 (3)	1.1 (2)	3.8 (2)
C32	4.5 (4)	3.4 (3)	3.8 (3)	-0.0 (3)	1.0 (3)	1.2 (2)	4.3 (3)
C21	18.4 (9)	7.1 (6)	8.5 (4)	3.9 (6)	9.2 (4)	4.1 (4)	9.9 (4)
C22	16.6 (8)	13.0 (9)	22.2 (8)	6.1 (7)	15.3 (5)	9.6 (6)	14.2 (6)
C23	11 (1)	7.3 (6)	7.1 (6)	0.2 (6)	-3.7 (6)	3.8 (4)	10.8 (5)
C24	9 (1)	12.2 (7)	23 (1)	0.6 (7)	-1.9 (9)	11.8 (6)	16.2 (7)
C41	3.5 (4)	4.1 (3)	5.5 (4)	0.7 (3)	1.8 (3)	1.6 (3)	4.6 (3)
C42	4.3 (4)	4.7 (5)	9.1 (6)	-0.2 (4)	3.0 (4)	0.5 (4)	6.9 (4)
C43	7.2 (5)	5.8 (4)	3.2 (3)	2.0 (4)	2.5 (3)	1.8 (3)	5.3 (3)
C44	13.5 (8)	8.7 (5)	4.3 (4)	5.2 (5)	3.7 (4)	3.9 (3)	8.3 (4)
C1P	3.6 (3)	3.9 (3)	3.7 (3)	0.8 (3)	1.8 (2)	2.2 (2)	3.5 (2)
C2P	5.0 (4)	4.1 (3)	4.8 (3)	1.2 (3)	2.2 (3)	2.2 (2)	4.5 (3)
C3P	4.8 (4)	5.0 (4)	5.7 (4)	1.0 (3)	2.7 (3)	2.6 (3)	5.0 (3)
C4P	4.6 (5)	6.3 (4)	6.2 (4)	0.5 (4)	1.8 (3)	3.1 (3)	5.7 (3)
C5P	5.7 (5)	4.4 (4)	7.7 (5)	0.8 (4)	2.2 (4)	2.7 (3)	6.1 (3)
C6P	4.3 (4)	3.3 (3)	5.0 (4)	-0.3 (3)	1.0 (3)	1.1 (3)	4.8 (3)
C7P	3.5 (4)	3.2 (3)	3.9 (3)	0.1 (3)	1.3 (3)	0.8 (2)	3.9 (2)
C8P	4.0 (4)	5.2 (4)	4.1 (4)	0.6 (3)	1.8 (3)	0.8 (3)	4.9 (3)

Table A-V (cont): General displacement parameter expressions - B's for *meso*-Ni_2Cl_4(eLTTP).

Name	B(1,1)	B(2,2)	B(3,3)	B(1,2)	B(1,3)	B(2,3)	Beqv
C9P	4.65 (5)	2.73 (4)	3.34 (4)	0.40 (4)	1.17 (3)	1.01 (3)	3.85 (3)
C10P	3.71 (4)	2.73 (3)	3.44 (4)	0.36 (3)	1.21 (3)	0.92 (3)	3.54 (3)
C11P	11.0 (2)	3.6 (1)	3.7 (1)	1.1 (1)	1.1 (1)	0.54 (8)	7.08 (9)
C12P	6.7 (1)	3.66 (8)	5.17 (8)	0.55 (8)	2.44 (8)	2.14 (6)	5.17 (7)

The form of the anisotropic displacement parameter is:
$\exp[-0.25(h^2a^2B(1,1) + k^2b^2B(2,2) + l^2c^2B(3,3) + 2hkabB(1,2) + 2hlacB(1,3) + 2klbcB(2,3))]$ where a, b, c are reciprocal lattice constants.

Table A-VI: Positional parameters for *rac*-$Rh_2Cl_2(CO)_2$(eLTTP)·THF.

atom	*x*	*y*	*z*	*B*, Å^2
Rh	-0.21776 (9)	0.0248 (1)	0.24507 (7)	5.31 (3)
Cl1	-0.2037 (3)	0.2158 (5)	0.3481 (2)	7.1 (1)
P1	-0.1023 (3)	0.1372 (5)	0.1795 (2)	5.1 (1)
P2	-0.2177 (4)	-0.1391 (6)	0.1413 (3)	7.3 (1)
O1	-0.3682 (9)	-0.136 (1)	0.3234 (8)	13.0 (4)
C1	-0.314 (1)	-0.074 (2)	0.293 (1)	8.0 (5)
C'	0.000	0.247 (2)	0.250	5.2 (5)
C11	-0.042 (1)	0.003 (2)	0.1191 (9)	6.3 (4)
C12	-.0127 (1)	-0.083 (2)	0.0712 (9)	8.9 (5)
C21	-0.217 (3)	-0.335 (5)	0.162 (3)	10 (1)*
C21'	-0.141 (2)	-0.326 (3)	0.180 (2)	8.9 (8)*
C22	-0.140 (3)	-0.365 (5)	0.261 (2)	8 (1)*
C22'	-0.202 (3)	-0.386 (4)	0.235 (2)	12 (1)*
C23	-.330 (2)	-0.158 (3)	0.048 (2)	7.9 (7)*
C23'	-0.342 (3)	-0.236 (5)	0.082 (3)	9 (1)*
C24	-0.427 (3)	-0.158 (4)	0.069 (2)	12 (1)*
C24'	-0.384 (3)	-0.073 (4)	0.033 (2)	7 (1)*
C1P	-0.157 (1)	0.267 (2)	0.0935 (8)	5.6 (4)
C2P	-0.263 (1)	0.291 (2)	0.0797 (9)	6.5 (4)
C3P	-0.311 (1)	0.393 (2)	0.012 (1)	8.3 (5)
C4P	-0.247 (1)	0.459 (2)	-0.038 (1)	8.7 (5)
C5P	-0.144 (1)	0.434 (2)	-0.021 (1)	9.1 (6)
C6P	-0.095 (1)	0.337 (2)	0.0449 (8)	7.5 (5)
O1S	0.500	0.479 (3)	0.250	31 (2)
C1S	0.488 (2)	0.384 (3)	0.330 (1)	14.6 (8)
C2S	0.501 (2)	0.251 (2)	0.296 (1)	14.0 (8)

Starred atoms were refined isotropically. The terminal ethyl groups on P2 were disordered and sucessfully modeled and refined using isotropic thermal parameters. The primed set of carbon atoms (C21', C22', etc.) had 40% site ocupancy based on thermal parameter values. The site occupancies were not refined due to the limited data set. Atoms O1S, C1S and C2S belong to a THF solvent molecule lying on a crystallographic 2-fold axis. Anisotropically refined atoms are given in the form of the isotropic equivalent displacement parameter defined as: $(4/3)[a^2\beta(1,1) + b^2\beta(2,2) + c^2\beta(3,3) + ac(\cos\beta)\beta(1,3)]$.

Table A-VII: Positional parameters for *rac*-$Rh_2Cl_2(CO)_2$(eLTTP).

atom	*x*	*y*	*z*	*B*, Å^2
Rh	0.38071 (1)	0.04174 (4)	0.18442 (3)	2.664 (7)
Cl1	0.37788 (6)	0.2248 (2)	0.28458 (9)	4.36 (3)
P1	0.43969 (5)	0.1721 (1)	0.14528 (8)	2.65 (3)
P2	0.38318 (5)	-0.1034 (2)	0.0738 (1)	3.46 (3)
O1	0.3100 (2)	-0.1489 (5)	0.2347 (3)	6.7 (1)
C1	0.3361 (2)	-0.0759 (6)	0.2156 (4)	4.1 (1)
C'	0.500	0.2688 (7)	0.250	3.0 (2)
C11	0.4711 (2)	0.0627 (6)	0.0874 (4)	3.6 (1)
C12	0.4192 (2)	-0.0253 (7)	0.0096 (4)	4.4 (1)
C1P	0.3997 (2)	0.2985 (6)	0.0446 (3)	3.1 (1)
C2P	0.3398 (2)	0.3131 (7)	0.0026 (4)	4.6 (1)
C3P	0.3069 (3)	0.4021 (8)	-0.0795 (5)	5.9 (2)
C4P	0.3363 (3)	0.4753 (7)	-0.1171 (4)	5.4 (2)
C5P	0.3967 (3)	0.4638 (7)	-0.0757 (4)	5.1 (2)
C6P	0.4283 (2)	0.3731 (7)	0.0051 (4)	4.6 (1)
C21	0.3120 (2)	-0.1615 (8)	-0.0329 (4)	5.3 (2)
C22	0.2675 (3)	-0.0500 (9)	-0.08750 (5)	6.5 (2)
C23	0.4262 (3)	-0.2604 (7)	0.1239 (5)	5.8 (2)
C24	0.4103 (3)	-0.3477 (7)	0.1864 (6)	7.8 (2)

Anisotropically refined atoms are given in the form of the isotropic equivalent displacement parameter defined as:
$(4/3)[a^2ß(1,1) + b^2ß(2,2) + c^2ß(3,3) + ab(\cos\gamma)ß(1,2) + ac(\cos\beta)ß(1,3) + bc(\cos\alpha)ß(2,3)]$.

Table A-VIII: Crystallographic data for *rac*-$Rh_2Cl_2(CO)_2$(eLTTP)·THF and *rac*-$Rh_2Cl_2(CO)_2$(eLTTP).

	Crystal Parameters	
formula	$Rh_2Cl_2P_4O_3C_{31}H_{48}$	$Rh_2Cl_2P_4O_2C_{27}H_{40}$
fw	869.34	797.23
crystal system	monoclinic	monoclinic
space group	*P2/c*	*C2/c*
a, Å	13.419 (3)	26.148 (3)
b, Å	9.361 (2)	9.934 (3)
c, Å	15.574 (6)	15.031 (3)
β, deg	102.62 (3)	120.82 (2)
V, Å^3	1909 (1)	3349 (1)
Z	2	4
d_{calc}, g/ml	1.51	1.58
μ(Mo Kα), cm-1	23.84	13.43
temp, °C	23	21
cryst size, mm	.33 x.21 x .08	.39 x .29 x .21
cryst color	orange-red	orange-red
	Data Collection and Structure Refinement	
diffractometer	CAD4	CAD4
radiation; λ	Mo(Kα)	Mo(Kα)
attenuator	17.5	17.5
scan method	$\omega/2\theta$	$\omega/2\theta$
variable scan speed	0.5-5° /min	0.5-4° /min

Table A-VIII (cont): Crystallographic data for *rac*-$Rh_2Cl_2(CO)_2$(eLTTP)·THF and *rac*-$Rh_2Cl_2(CO)_2$(eLTTP).

data limits	$3° < 2\theta < 50°$	$3° < 2\theta < 50°$
octants collcd	$\pm h, k, \pm l$[a]	$h, k, \pm l$
reflcns collcd	5270	4404
unique data,		
$F_o^2 > 3\sigma(F_o^2)$	989	2270
weighting sheme	non-Poisson	non-Poisson
fudge factor, P	0.08	0.040
params refined	187	236
data/param ratio	5.3	9.6
R[b]	0.048	0.036
R_w[c]	0.062	0.042
GOF[d]	1.15	1.18
max final shift/esd	0.07	0.04
empirical abs cor	yes	yes
min transmiss. coef	0.9280	0.8735
max final diff.		
Fourier pk,. e/Å^3	0.44	0.60

---

[a] A hemisphere of data was collected up to $2\theta = 40°$ and a single quadrant between $2\theta = 41$-$50°$. The extra quadrant of data was collected and averaged to compensate for the small size of the crystal. [b] $R = \Sigma \| \, |F_o| - |F_c| \, | / \Sigma |F_o|$.

[c] $R_w = [\Sigma w (|F_o| - |F_c|)^2 / \Sigma w |F_o|^2]^{1/2}$; $w = 1 / \sigma^2 (|F_o|)$. [d] Goodness of fit = $[\Sigma w (|F_o| - |F_c|)^2 / (N_{obs} - N_{param})]1/2$

Table A-IX: Positional parameters for $[Rh(NBD)(Et_2PCH_2CH_2PPh_2)]BF_4 \cdot 0.5CH_2Cl_2$.

atom	*x*	*y*	*z*	*B*, Å^2
Rh	0.28770(5)	0.15148(4)	0.13328(2)	3.44(1)
P1	0.1727(2)	0.0933(1)	0.07082(7)	3.21(4)
P2	0.3026(2)	0.0023(2)	0.15846(8)	4.57(5)
C1	0.3180(7)	0.2885(6)	0.1061(3)	4.9(2)
C2	0.2426(7)	0.2975(6)	0.1325(3)	4.8(2)
C3	0.3004(8)	0.3165(7)	0.1856(4)	6.0(2)
C4	0.3565(8)	0.2256(8)	0.2008(3)	6.1(3)
C5	0.4316(9)	0.217(1)	0.1737(4)	5.8(3)
C6	0.4235(9)	0.301(1)	0.1417(5)	5.7(3)
C7	0.392(1)	0.376(1)	0.1748(5)	7.0(4)
C8	0.1231(9)	-0.0160(8)	0.0889(4)	4.5(3)
C9	0.216(1)	-0.0718(9)	0.1141(5)	5.1(3)
C10	0.2287(8)	0.0619(8)	0.0209(4)	3.5(2)
C11	0.3266(9)	0.0922(9)	0.0197(4)	4.3(3)
C12	0.374(1)	0.065(1)	-0.0161(5)	5.4(3)
C13	0.322(1)	0.0068(9)	-0.0523(5)	5.4(3)
C14	0.223(1)	-0.0236(9)	-0.0514(4)	5.0(3)
C15	0.1754(9)	0.0030(9)	-0.0154(4)	4.4(3)
C16	0.0577(8)	0.1610(8)	0.0462(4)	3.5(2)
C17	0.0344(9)	0.1903(8)	-0.0001(4)	4.5(3)
C18	-0.053(1)	0.245(1)	-0.0163(5)	5.6(3)
C19	-0.113(1)	0.2692(9)	0.0148(6)	6.2(4)
C20	-0.0907(9)	0.239(1)	0.0626(6)	6.0(4)
C21	-0.0034(9)	0.1843(9)	0.0788(5)	5.0(3)
C22	0.431(1)	-0.050(1)	0.1684(6)	8.0(4)
C23	0.483(1)	-0.036(1)	0.1257(7)	8.3(5)
C24	0.268(1)	-0.021(1)	0.2155(4)	6.7(4)
C25	0.158(1)	0.005(1)	0.2153(6)	8.0(5)
Cl(1)	0.0643(4)	0.2507(4)	0.2153(2)	9.9(1)
C1S	0.000	0.181(2)	0.250	8.0(7)
B	0.223(1)	0.336(1)	0.6632(5)	7.7(4)*
F1	0.1521(7)	0.3224(6)	0.6215(3)	11.7(2)*

Table A-IX (cont): Positional parameters for $[Rh(NBD)(Et_2PCH_2CH_2PPh_2)]BF_4 \cdot 0.5CH_2Cl_2$.

atom	*x*	*y*	*z*	*B*, Å^2
F2	0.2129(8)	0.2637(8)	0.6919(4)	15.0(3)*
F3	0.304(1)	0.388(1)	0.6638(5)	10.0(4)*
F4a	0.177(1)	0.394(1)	0.6878(5)	14.2(4)*†
F4b	0.303(2)	0.302(1)	0.6534(7)	14.1(6)*†

Starred atoms were refined isotropically.

The equivalent isotropic thermal parameter, for atoms refined anisotropically, is defined by the equation: $(4/3)[a^2ß_{11} + b^2ß_{22} + c^2ß_{33} + ac ß_{13}\cos\beta]$

† The occupancies of F4a and F4b are assigned a population of 1/2.

Table A-X: Crystallographic data for $[Rh(NBD)(Et_2PCH_2CH_2PPh_2)]BF_4 \cdot 0.5CH_2Cl_2$.

Crystal Parameters	
formula	$C_{26.5}H_{31}P_2RhBF_4Cl$
fw	612.6
crystal system	monoclinic
space group	*C2/c*
a, Å	13.346 (2)
b, Å	14.613 (4)
c, Å	28.787 (4)
β, deg	102.60 (1)
V, Å^3	5479 (2)
Z	8
d_{calc}, g/ml	1.48
μ(Mo Kα)	8.64
temp, °C	23
cryst size, mm	0.18 x 0.40 x 0.60
cryst color	red-orange

Data Collection and Structure Refinement	
diffractometer	CAD4
radiation	MoKα
attenuator	17.5
scan method	$\theta/2\theta$
variable scan speed	0.7-4.0° /min

Table A-X (cont): Crystallographic data for $[Rh(NBD)(Et_2PCH_2CH_2PPh_2)]BF_4 \cdot 0.5CH_2Cl_2$.

data limits	$3^\circ < 2\theta < 50^\circ$
octants collcd	$h, k, \pm l$
reflcns collcd	5239
unique data,	
$F_o^2 > 3\sigma(F_o^2)$	3662
weighting sheme	non-Poisson
fudge factor, P	0.02
params refined	246
data/param ratio	14.9
R[a]	0.060
R_w[b]	0.068
GOF[c]	5.75
max final shift/esd	0.12
empirical abs cor	yes
min transmiss. coef	0.8760
max final diff.	
Fourier pk,. e/Å^3	1.08

---

[a] $R = \Sigma \mid\mid F_o \mid - \mid F_c \mid\mid / \Sigma \mid F_o \mid$.

[b] $R_w = [\Sigma w (\mid F_o \mid - \mid F_c \mid)^2 / \Sigma w \mid F_o \mid^2]^{1/2}$; $w = 4F_o^2[\sigma 2(I) + (pF_o^2)^2]^{-1}$.

[c] Goodness of fit $= [\Sigma w (\mid F_o \mid - \mid F_c \mid)^2 / (N_{obs} - N_{param})]^{1/2}$.

Table A-XI: The General Displacement Parameter Expression - B's for $[Rh(NBD)(Et_2PCH_2CH_2PPh_2)]BF_4 \cdot 0.5CH_2Cl_2$.

Name	B(1,1)	B(2,2)	B(3,3)	B(1,2)	B(1,3)	B(2,3)	Beqv
Rh	3.55(2)	3.68(2)	2.84(2)	-0.33(2)	0.15(2)	-0.07(2)	3.44(1)
P1	3.35(7)	3.19(8)	2.97(7)	-0.47(7)	0.45(6)	-0.14(7)	3.21(4)
P2	4.8(1)	4.5(1)	4.32(9)	0.67(9)	0.70(8)	1.19(9)	4.57(5)
C1	5.8(4)	3.3(4)	5.5(4)	-1.1(3)	1.2(4)	-0.5(3)	4.9(2)
C2	5.6(4)	3.2(3)	5.7(4)	-0.5(3)	1.3(3)	-1.1(3)	4.8(2)
C3	6.2(4)	6.2(5)	5.8(5)	-1.9(4)	1.9(4)	-3.1(4)	6.0(2)
C4	5.9(5)	8.4(6)	3.5(4)	-2.5(4)	-0.2(4)	-2.0(4)	6.1(3)
C5	4.2(5)	7.8(7)	4.6(5)	-1.2(5)	-0.5(5)	-2.3(5)	5.8(3)
C6	5.1(5)	5.9(7)	6.4(6)	-2.0(5)	2.1(5)	-1.1(6)	5.7(3)
C7	7.8(7)	6.8(7)	7.0(7)	-2.7(6)	3.0(6)	-2.9(6)	7.0(4)
C8	5.7(6)	3.1(5)	4.7(5)	-1.2(4)	0.8(4)	0.7(4)	4.5(3)
C9	6.4(6)	3.8(5)	4.8(6)	-0.0(5)	0.5(5)	0.5(5)	5.1(3)
C10	3.9(4)	3.1(5)	3.4(4)	-0.2(4)	0.8(4)	0.1(4)	3.5(2)
C11	4.0(5)	4.1(6)	5.0(5)	-0.3(5)	1.4(4)	-0.3(5)	4.3(3)
C12	5.4(6)	4.8(6)	6.3(6)	-0.2(6)	2.0(5)	-0.5(6)	5.4(3)
C13	7.1(7)	4.0(6)	5.4(6)	-0.4(6)	2.1(5)	-0.2(5)	5.4(3)
C14	6.8(7)	4.2(6)	4.2(5)	-0.6(5)	1.6(5)	-0.9(5)	5.0(3)
C15	5.0(5)	4.1(5)	4.1(5)	-0.7(5)	1.0(4)	-0.4(5)	4.4(3)
C16	3.0(4)	3.3(5)	4.0(4)	-0.5(4)	0.3(4)	-0.5(4)	3.5(2)
C17	4.3(5)	4.0(5)	4.4(5)	-0.7(5)	-0.6(4)	0.6(5)	4.5(3)
C18	5.0(6)	4.8(6)	6.4(7)	-0.5(5)	-0.3(5)	0.4(6)	5.6(3)

Table A-XI (con't): The General Displacement Parameter Expression - B's for $[Rh(NBD)(Et_2PCH_2CH_2PPh_2)]BF_4 \cdot 0.5CH_2Cl_2$.

Name	B(1,1)	B(2,2)	B(3,3)	B(1,2)	B(1,3)	B(2,3)	Beqv
C19	4.0(5)	3.9(6)	9.7(8)	-0.4(5)	-0.4(6)	0.5(6)	6.2(4)
C20	3.9(5)	5.0(7)	9.2(8)	0.1(5)	1.5(5)	-0.5(7)	6.0(4)
C21	4.2(5)	5.1(6)	5.7(6)	-0.5(5)	1.1(4)	-1.0(5)	5.0(3)
C22	5.9(7)	7.8(8)	10(1)	2.8(6)	2.0(7)	3.9(7)	8.0(4)
C23	6.5(7)	8(1)	11(1)	1.8(7)	3.9(6)	0.6(9)	8.3(5)
C24	9.3(8)	6.5(8)	4.5(5)	0.3(7)	2.2(5)	1.9(5)	6.7(4)
C25	8.2(8)	9(1)	7.6(8)	-0.0(8)	4.1(6)	1.1(8)	8.0(5)
Cl(1)	9.0(3)	9.8(3)	11.1(3)	0.5(2)	3.1(2)	3.5(2)	9.9(1)
C1S	8(1)	7(1)	10(1)	0	4.2(9)	0	8.0(7)

The form of the anisotropic temperature factor is:

$\exp[-1/4\{h^2a^2B_{11} + k^2b^2B_{22} + l^2c^2B_{33} + 2(hkabB_{12} + hlacB_{13} + klbcB_{23})\}]$
where a, b, c are reciprocal lattice constants.

APPENDIX 2

Additional Spectra

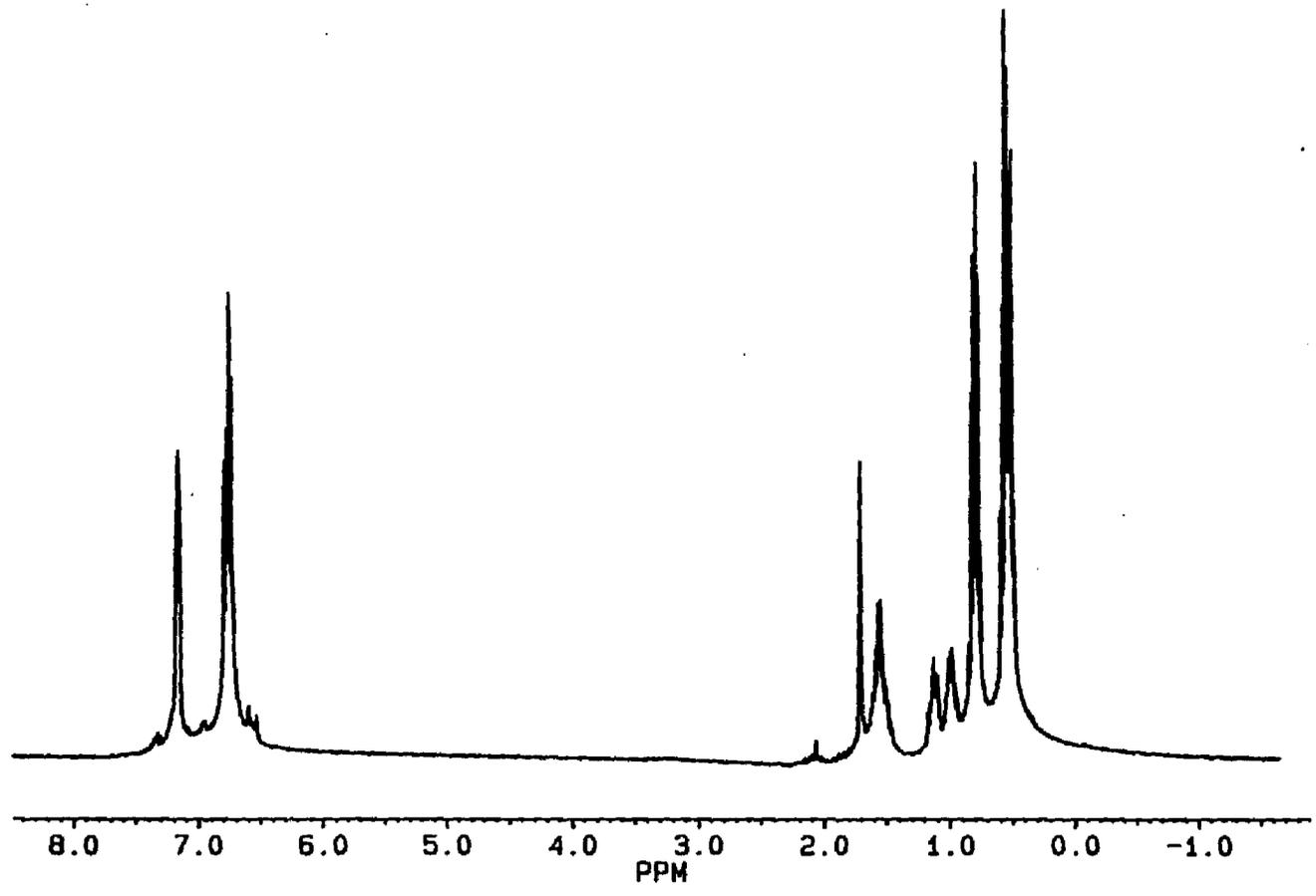

Figure B-1: The ^{1}H NMR of eLTTP in d_6-benzene (400.13 MHz).

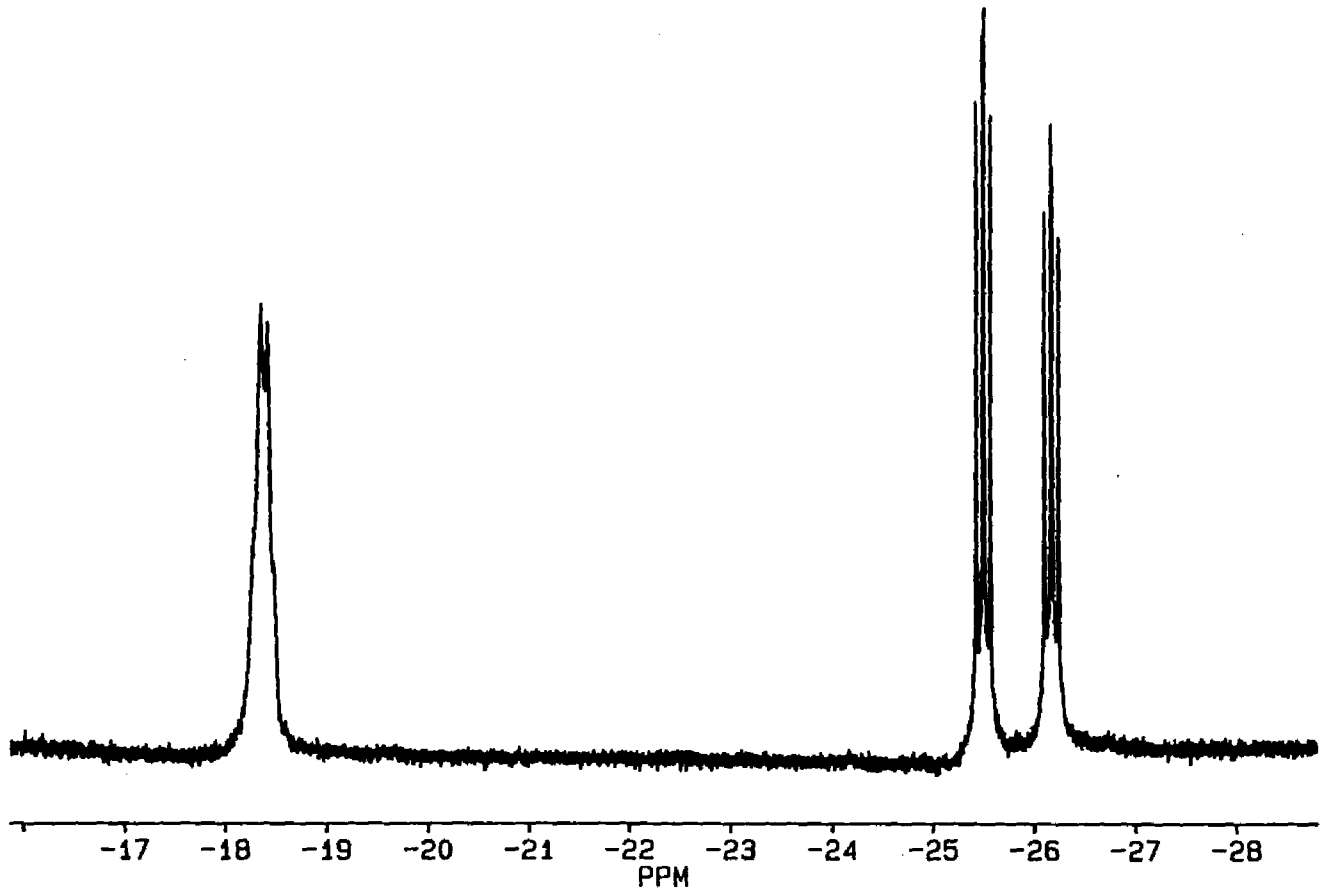

Figure B-2: The $^{31}P\{^{1}H\}$ NMR of eLTTP in d_6-benzene (400.13 MHz).

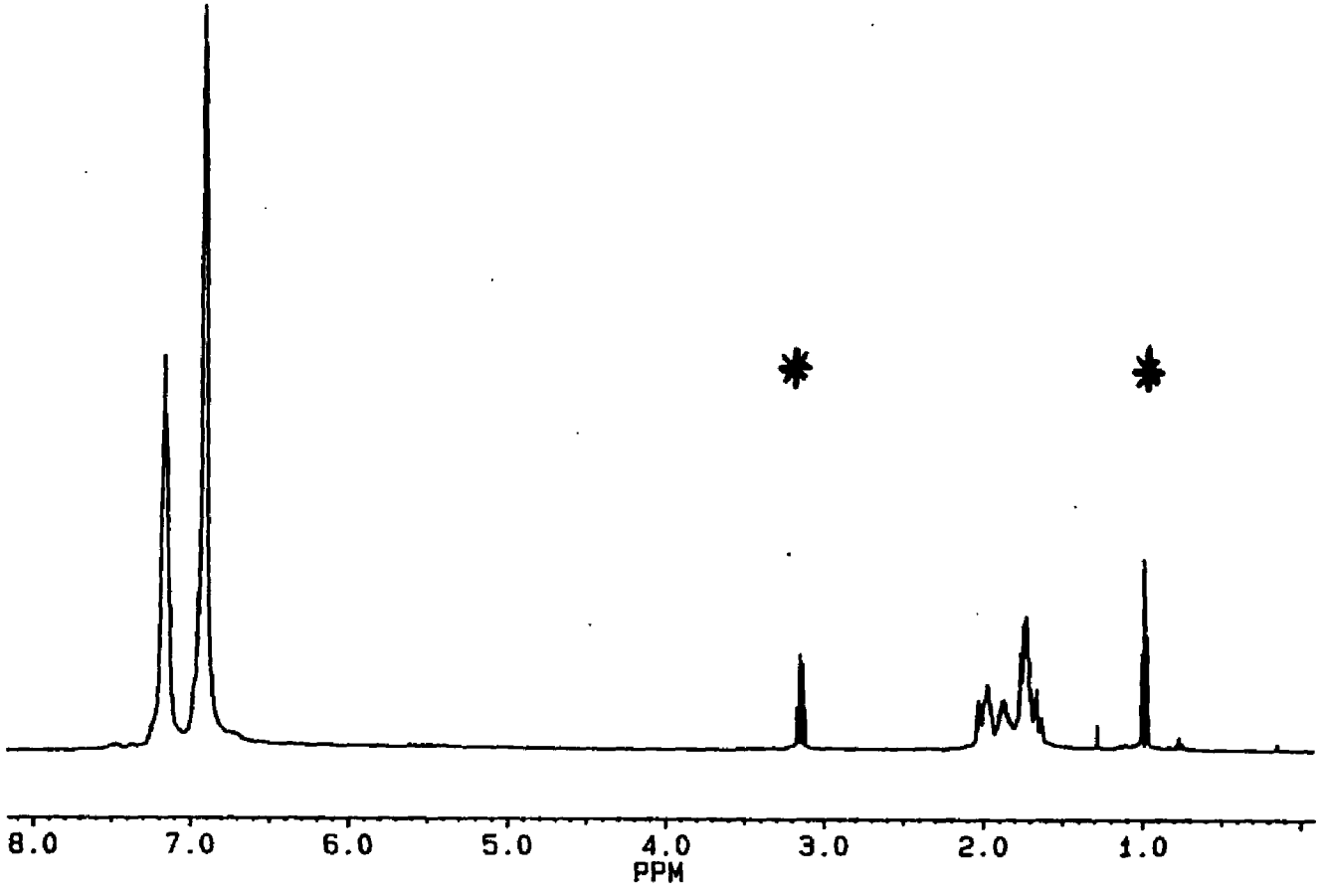

Figure B-3: The ^{1}H NMR of phLTTP in d_6-benzene (400.13 MHz). Astericked peaks are ether solvent.

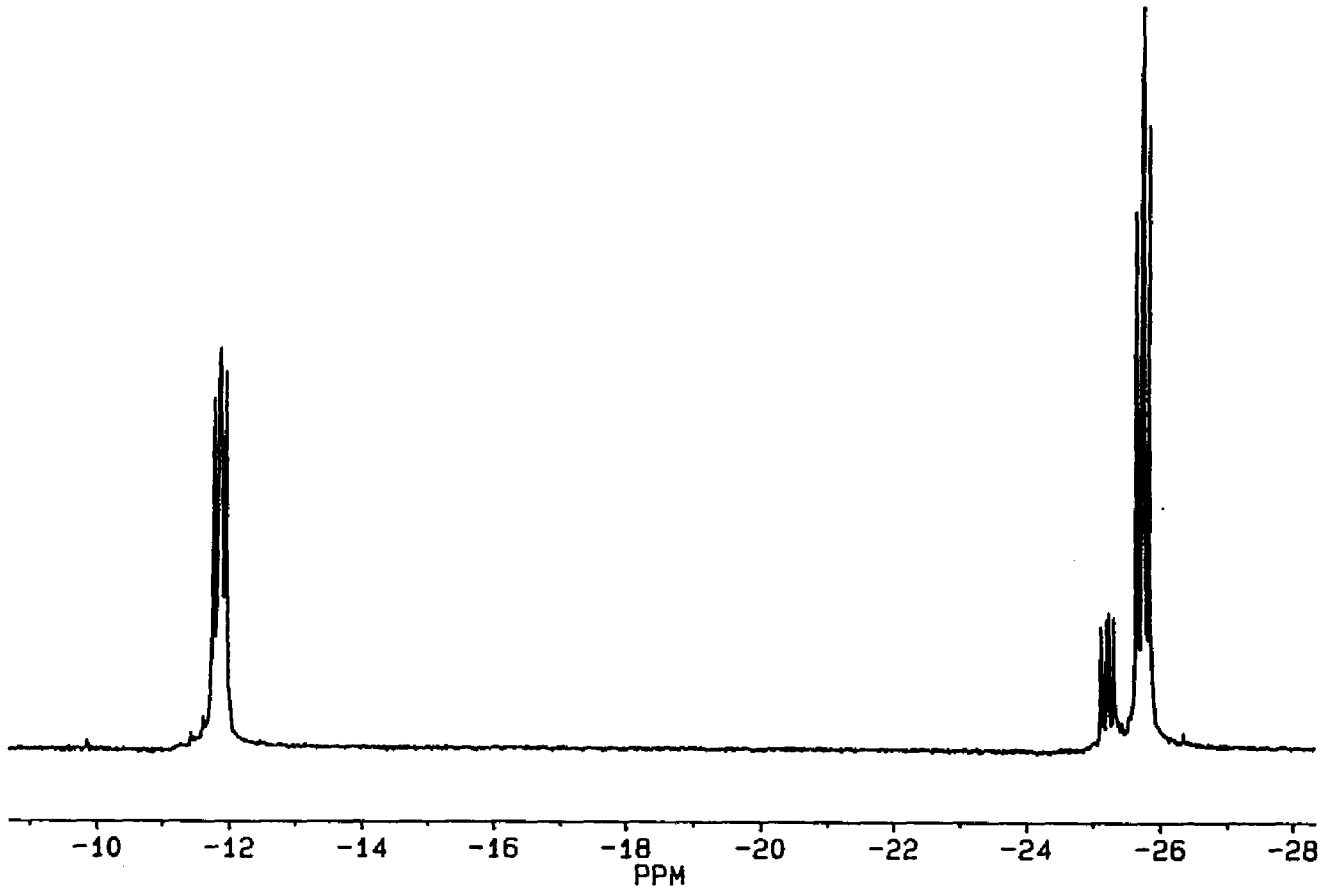

Figure B-4: The $^{31}P\{^{1}H\}$ NMR of phLTTP in d_6-benzene (400.13 MHz).

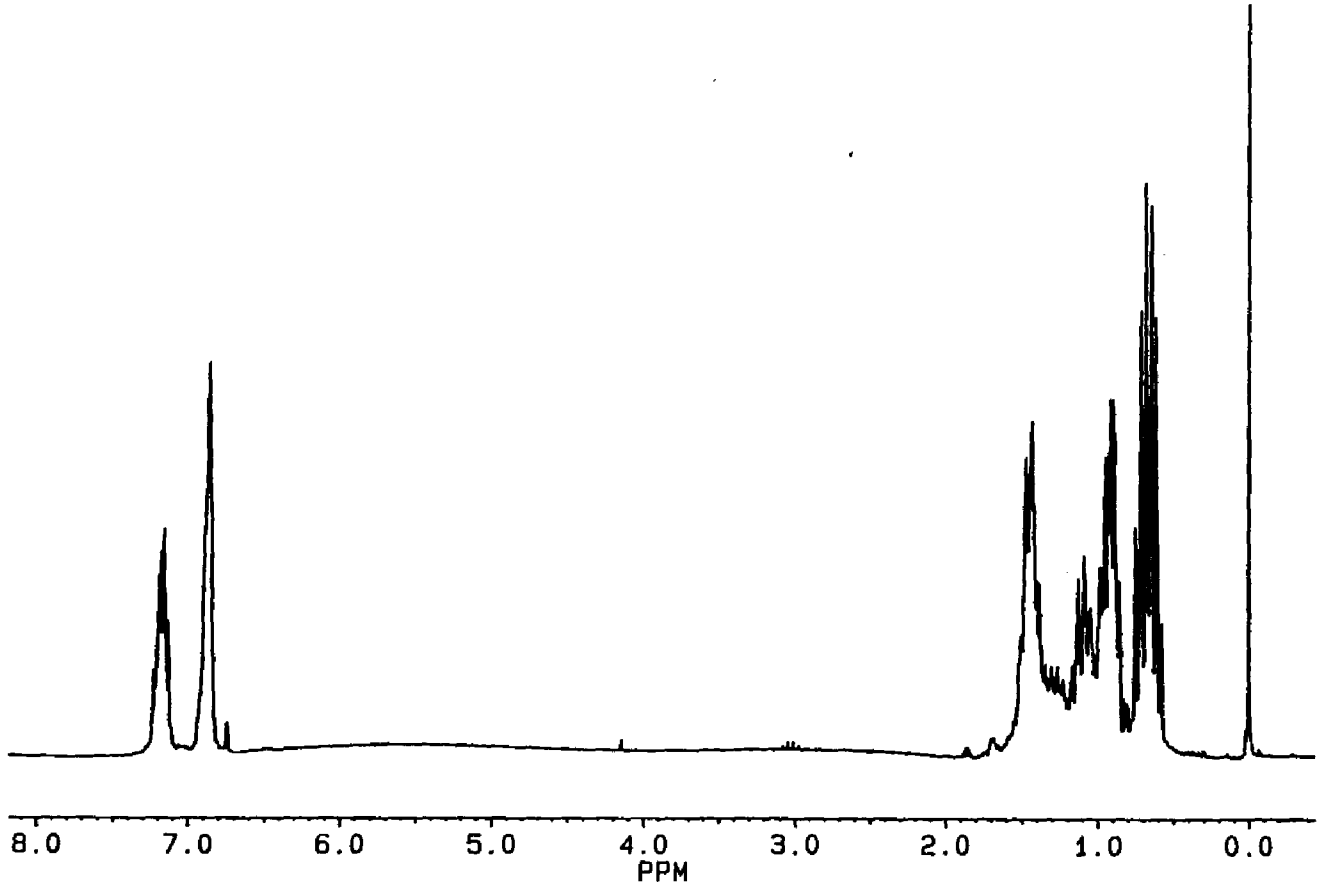

Figure B-5: The ^{1}H NMR of eLTTP-pr in d_6-benzene (200.13 MHz).

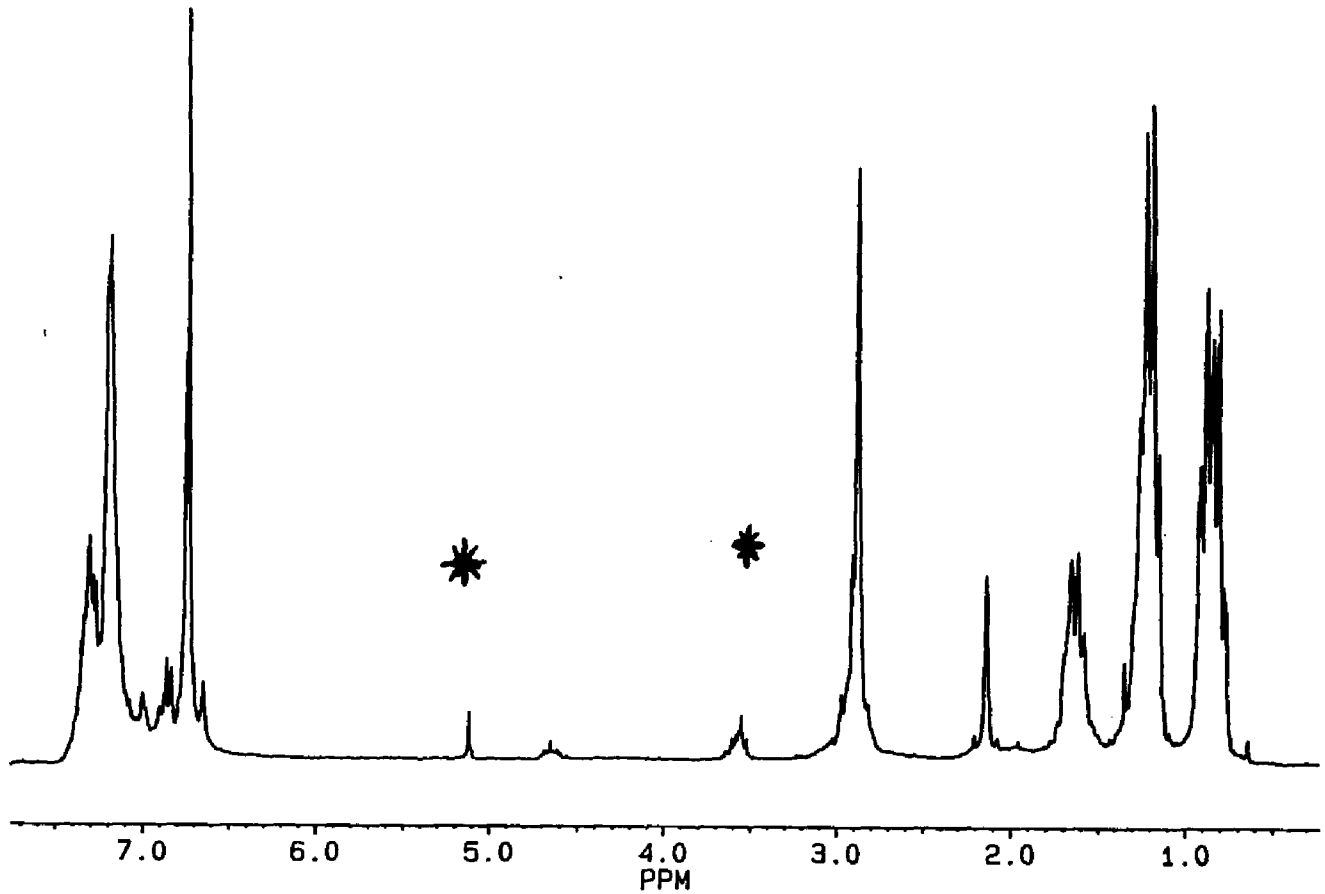

Figure B-6: The ^{1}H NMR of eLTTP-*p*-xyl in d_6-benzene (200.13 MHz). Astericked peaks are solvent impurities.

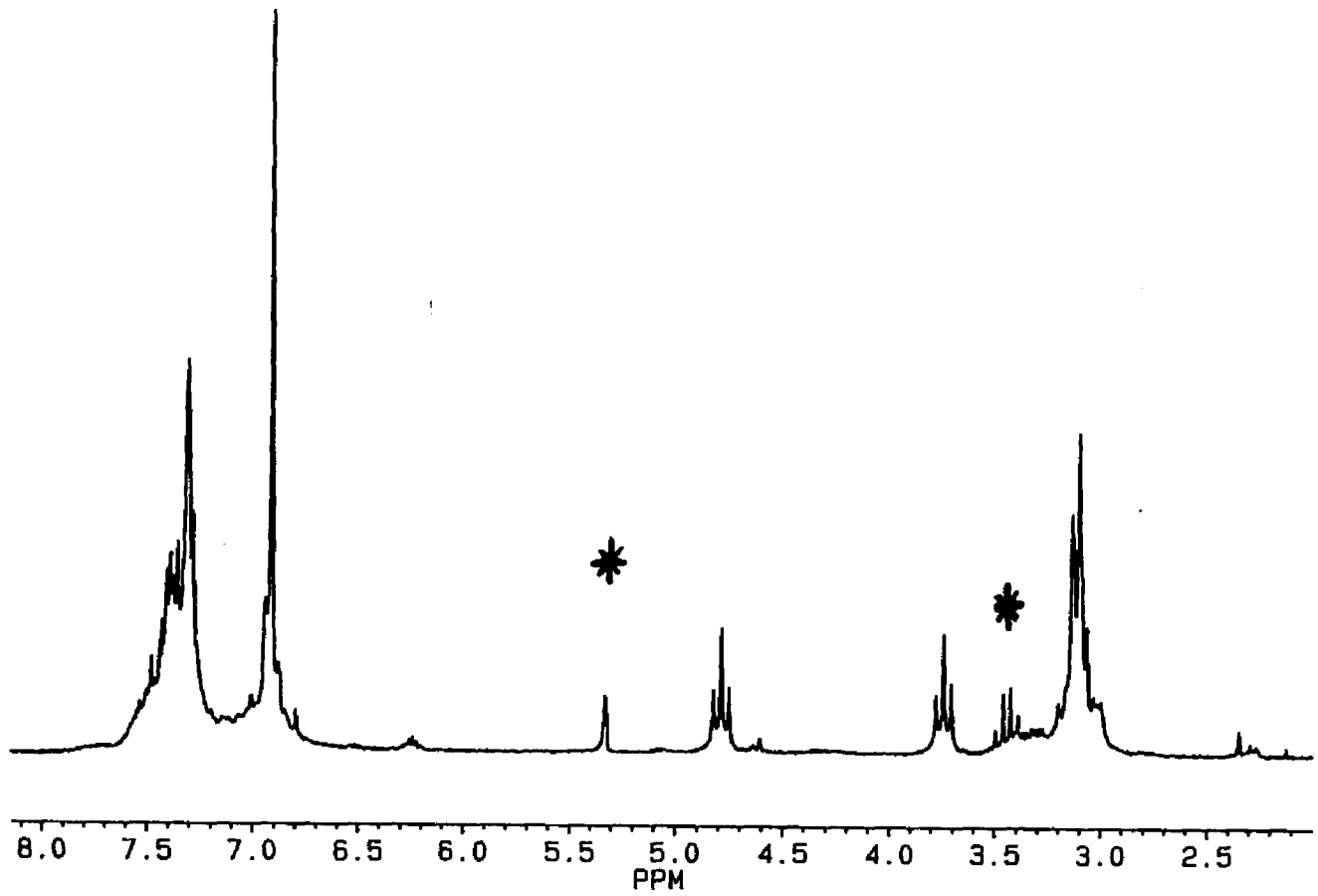

Figure B-7: The ^{1}H NMR of $[Ph(H)PCH_2]_2$-*p*-C_6H_4 in d_6-benzene (200.13 MHz). Astericked peaks are solvent impurities.

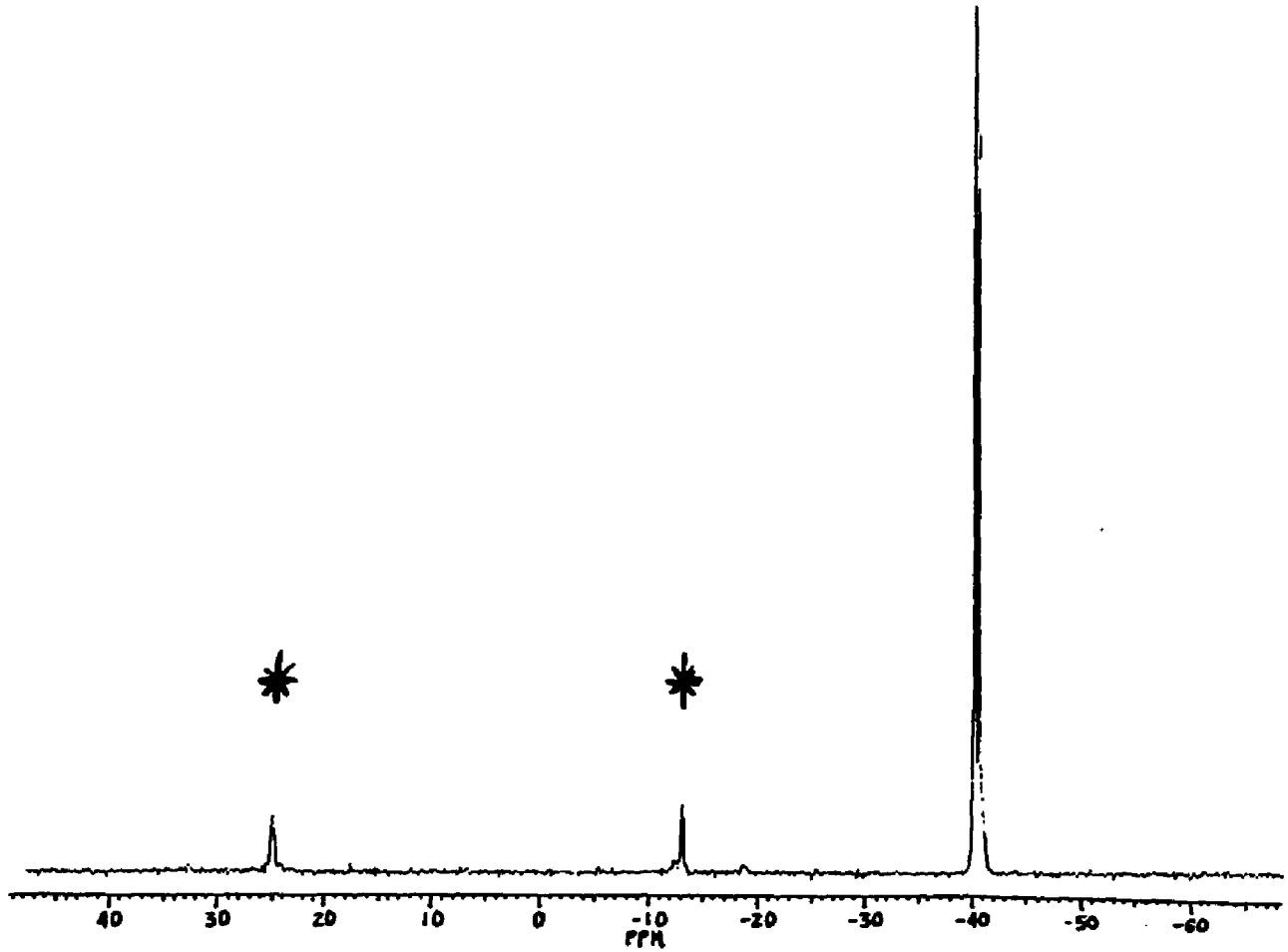

Figure B-8: The ^{31}P NMR of $[Ph(H)PCH_2]_2$-*p*-C_6H_4 in d_6-benzene (40.48 MHz). Asterisked peaks are impurities.

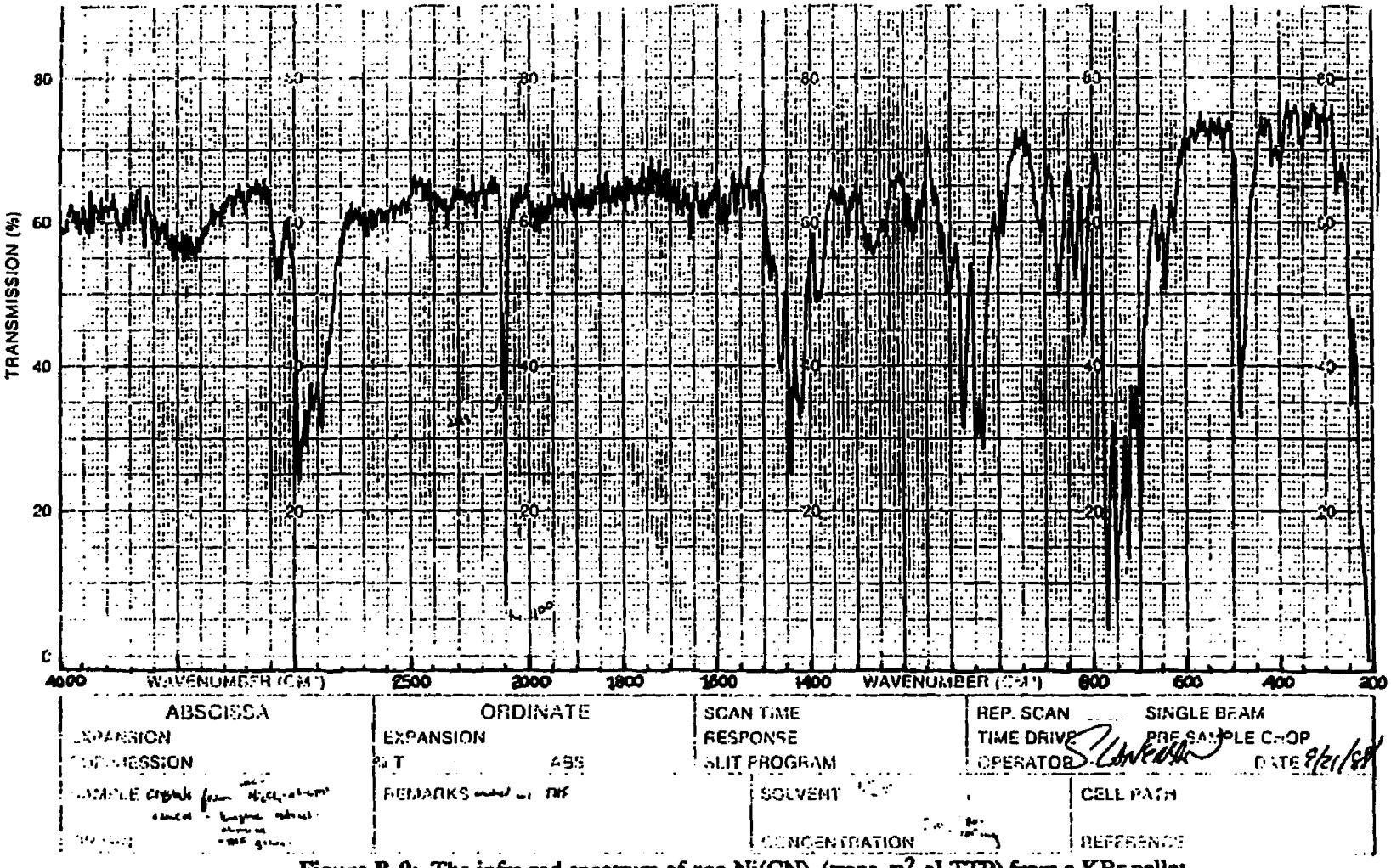

Figure B-9: The infra red spectrum of *rac*-Ni(CN)$_2$(trans, η^2-eLTTP) from a KBr pellet.

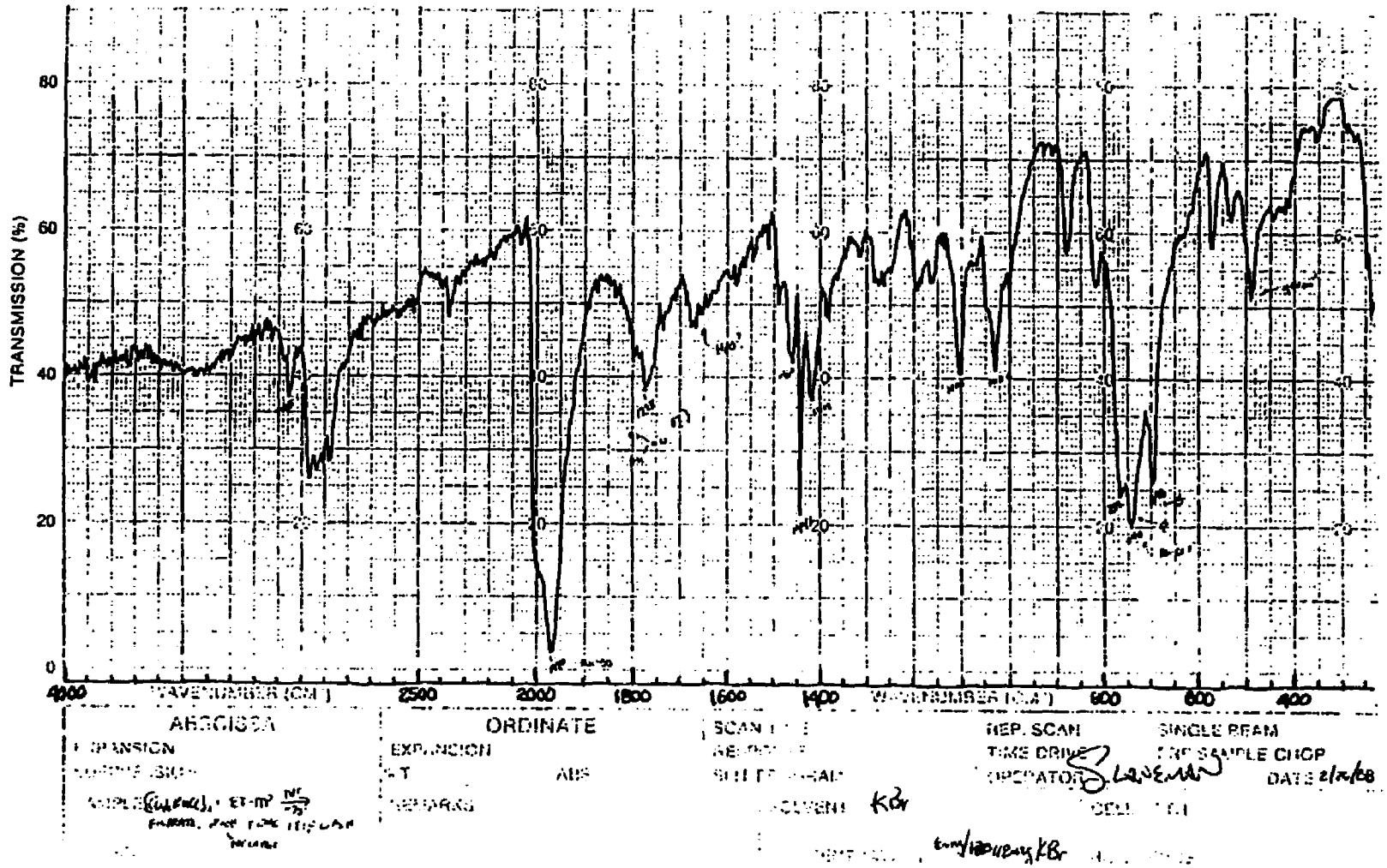

Figure B-10: The infra red spectrum of $Rh_2Cl_2(CO)_2$(eLTTP) from a KBr pellet.

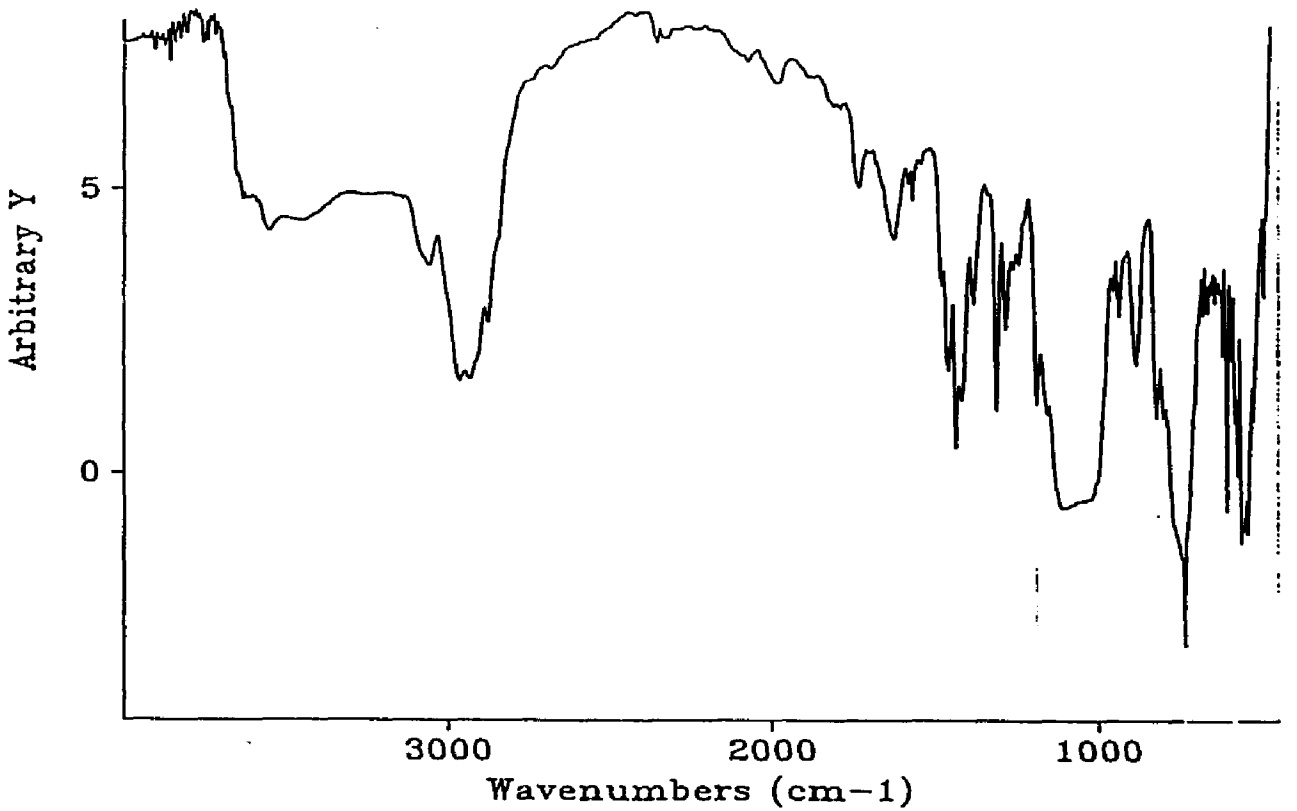

Figure B-11: The infra red spectrum of $[Rh_2(NBD)_2(eLTTP)]\ 2BF_4$ from a powder.

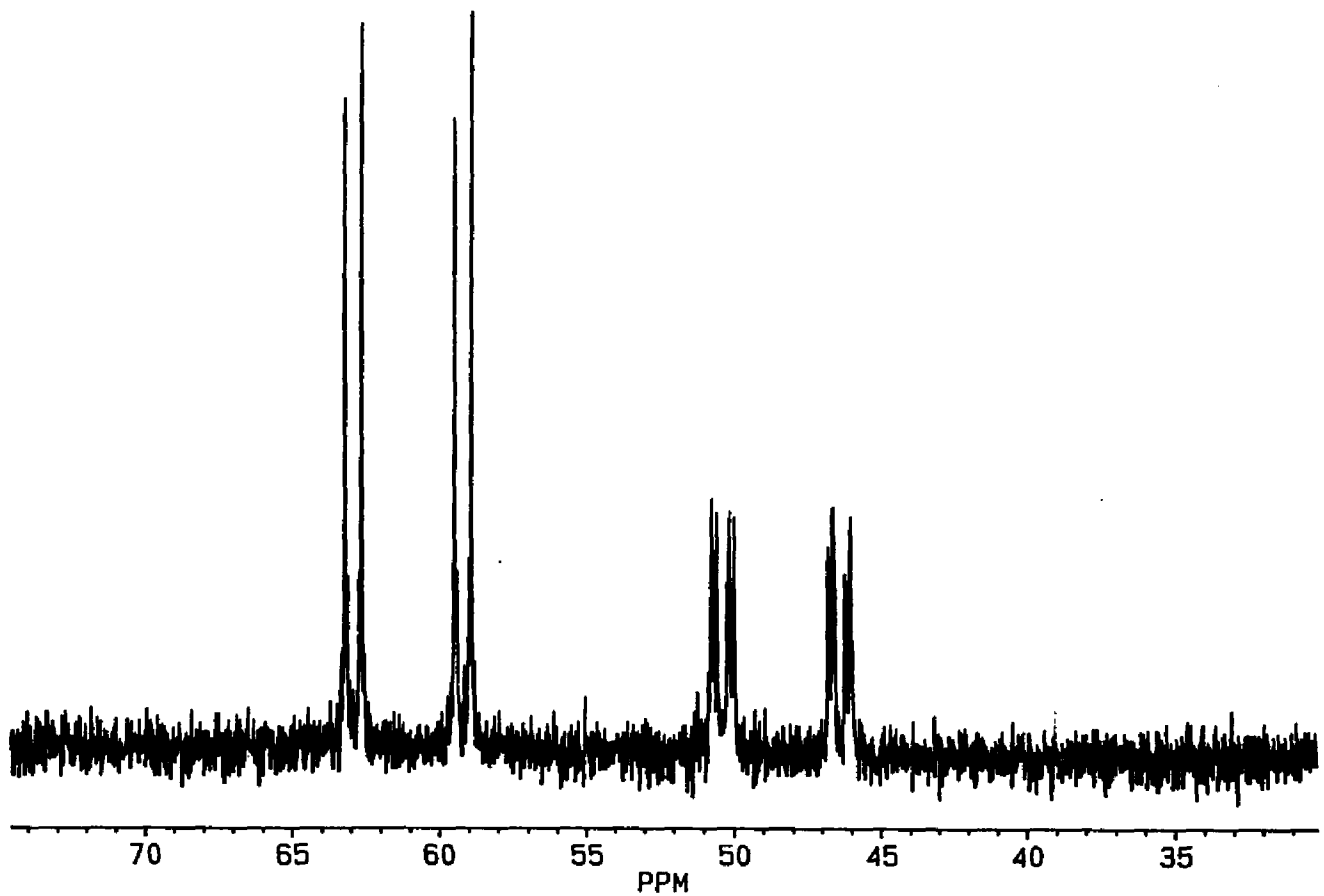

Figure B-12: The $^{31}P\{^{1}H\}$NMR of *rac*-$[Rh_2(NBD)_2(eLTTP)]$ $2BF_4$ in d_6-acetone (40.48 MHz).

VITA

Scott Anthony Laneman was born in St. Louis, Missouri on March 3, 1963. He graduated from Pattonville Senior High in Maryland Heights, Missouri, in June 1981. In August of 1981 he attended Southeast Missouri State University where he received a Bachelor of Science Degree in chemistry in May 1985.

In June of 1985, he went to Washington University in St. Louis to pursue his Doctor of Philosophy. In June of 1986, he followed his advisor to Louisiana State University, where he is now a candidate for the degree of Doctor of Philosophy in the department of chemistry.

He married Miriam Ruth Belice in August 1987 and has no children.

DOCTORAL EXAMINATION AND DISSERTATION REPORT

Candidate: Scott Anthony Laneman

Major Field: Chemistry

Title of Dissertation: The Synthesis, Characterization, and Reactivities of Metal Tetratertiaryphosphine Complexes.

Approved:

Major Professor and Chairman

Dean of the Graduate School

EXAMINING COMMITTEE:

Date of Examination:

July 17, 1990